Application of Concentrated Solar Radiation to Chemical Looping Combustion

Seyed Mehdi Jafarian

Thesis submitted for the degree of Doctor of Philosophy

School of Mechanical Engineering

Faculty of Engineering, Computer & Mathematical Sciences

The University of Adelaide, Australia

March 2014

Table of contents

Abstract

The novel concept of the application of the Oxygen Carrier (OC) particles in a Chemical Looping Combustion (CLC) system for diurnal storage of the concentrated solar thermal energy is presented here. Two innovative configurations of Hybrid Solar CLC (Hy-Sol-CLC) systems for continuous base-load power generation are proposed and assessed. The systems seek to take the key features of a CLC system that are desirable for a hybrid solar GTCCs; notably the production of an industrially pure stream of CO_2, inherent chemical and sensible heat storage, relatively low temperature of the fuel reactor relative to that of the air reactor and the potential to operate the fuel and air reactors at different pressures.

In the first proposed configuration, three reservoirs have been added to a conventional CLC system to allow storage of the OC particles, while a cavity solar receiver has been chosen for the fuel reactor. In this Hy-Sol-CLC system the flow rates of the fuel and OC particles were considered to be constant. The calculations demonstrated that the solar thermal energy can be stored using CLC components. However, this configuration is limited to a low solar share of about 6.5% when averaged over the whole day. Besides, the variations in fuel reactor temperature, owing to the diurnal variations of the input concentrated solar thermal energy, might result in damage to the OC particles.

The second Hy-Sol-CLC system addresses the limitations associated with the first configuration. In this system, as for the first one, a cavity solar reactor has been chosen for the fuel reactor while two reservoirs have been added to a conventional CLC for the storage of OC particles. A direct air-particle heat

exchanger has been also proposed to provide independent control of the temperature of the OC particles in the air reactor from those stored in the storage reservoirs. In this process the operating temperature of the solar fuel reactor is controlled through varying the flow rates of fuel and OC particles proportional to the variations in the input concentrated solar thermal energy. This hybrid cycle is estimated to achieve a solar share of up to 60% when averaged over the whole day. The performance of this hybrid system in a GTCC cycle was evaluated with and without the application of an after-burner. The after-burner was added to further increase the gas turbine inlet temperature. The calculations predict a first law efficiency of 50.0% for the cycle employing the after-burner, compared with 44.0% for that without the after-burner. However, this higher thermal efficiency is achieved at the cost of decreasing the solar share from 60.0%, without the after-burner, to 41.4% with it.

Applicability of the combinations of natural gas, CO and H_2, as fuel with the oxides of Co, Cu, Fe, Mn and Ni, as oxygen carriers in the proposed Hy-Sol-CLC system was also evaluated. The calculations demonstrated that, from all of the assessed metal-based oxygen carriers, only the pairs of CoO/Co, NiO/Ni and Fe_2O_3/Fe_3O_4 are potentially suitable for use in a Hy-Sol-CLC system working with natural gas. However, none of these materials allow any significant chemical storage of solar energy for the oxidation of CO and H_2.

An unsteady-state model of an OC particle exposed to high intensity solar heat flux was also developed to provide the fundamental knowledge required for the selection of an efficient solar cavity reactor for the Hy-Sol-CLC systems. The model was validated against the available data in the literature. The numerical

analysis demonstrated that the application of direct heat transfer is desirable. However, it must be combined with a high convective cooling to avoid excessive heating rates, which would result in overheating of the particles.

Declaration

I certify that this work contains no material which has been accepted for the award of any other degree or diploma in my name, in any university or other tertiary institution and, to the best of my knowledge and belief, contains no material previously published or written by another person, except where due reference has been made in the text. In addition, I certify that no part of this work will, in the future, be used in a submission in my name, for any other degree or diploma in any university or other tertiary institution without the prior approval of the University of Adelaide and where applicable, any partner institution responsible for the joint-award of this degree.

I give consent to this copy of my thesis when deposited in the University Library, being made available for loan and photocopying, subject to the provisions of the Copyright Act 1968.

The author acknowledges that copyright of published works contained within this thesis resides with the copyright holder(s) of those works.

I also give permission for the digital version of my thesis to be made available on the web, via the University's digital research repository, the Library Search and also through web search engines, unless permission has been granted by the University to restrict access for a period of time.

Seyed Mehdi Jafarian Date

Acknowledgment

I would not have been able to complete this journey without the aid, support and contribution of many people.

I would firstly like to acknowledge the support given to me by my supervisors Dr. Maziar Arjomandi and Professor Graham (Gus) Nathan who helped me in all time of my research and writing of this thesis. I thank Dr. Arjomandi for his patience, support and guide through up and down times of my PhD thesis. I thank Prof. Nathan for his motivation, enthusiasm, immense and comprehensive knowledge in the field of energy and combustion which were essential for my understanding and development of the proposed hybrid CLC system.

I would like to acknowledge Adelaide Scholarship International (ASI) for their financial support. I would also like to thank the current and former staffs of the School of Mechanical Engineering and Centre for energy Technology (CET).

I am deeply and forever indebted to my parents who are passed away. I am also extremely grateful to my brothers, Hadi and Mohammad and my lovely sister, Sara, and my Aunts specially, Homa Seraj, and my Uncles specially, Mahmood Jafarian, whose love and support led me to this point.

Finally, I would like to express my special gratitude and thank to Pegah for being the most loving, patient and understanding wife for over this long period.

CHAPTER 1

INTRODUCTION

CHAPTER 1

1.1. Background

The recent increase in the atmospheric concentration of greenhouse gases, mainly due to anthropogenic emissions, is widely linked to the simultaneous increase in the global mean temperature [1, 2]. The most abundant greenhouse gases in the Earth's atmosphere are: water vapour (H_2O), carbon dioxide (CO_2), methane (CH_4), oxides of nitrogen (N_2O, NO…), ozone (O_3) and Chlorofluorocarbons (CFCs). Methane and CFCs have higher green-house gas effect per their unit mass than CO_2 [3]. However, CO_2 has the major contribution to the global warming, because of its larger amount in the atmosphere [4]. The concentration of CO_2 in the atmosphere has increased significantly from 280 ppm in the pre-industrial times to 396 ppm in 2013 [3, 5], which is mainly due to the dependency on the fossil fuel for energy production [3]. Furthermore, the investigations performed by the Energy Information Administration (EIA) within the U.S. Department of Energy (DOE) have demonstrated that the consumption of fossil fuels will increase by around 27% over the next 20 years [1]. However, if no action is taken, the world could be around 4 °C warmer by the end of this century than it was at the beginning of industrial revolution [6]. This temperature raise would have serious impacts on sea level rise, water supplies security and agriculture. To assure that the increase in mean global temperature is less than 2 °C, which is believed as the limit to prevent the most catastrophic changes on earth [7, 8], the CO_2 concentration in the atmosphere must not exceed 450 ppm. This means that the concentration of CO_2 must not increase more than 15% over today's concentration [8]. However; at present, despite the urgent need to decrease the CO_2 emission, fossil fuels account for more than 80% of the world

energy demand [3, 9], which is mainly because of their low cost, availability, high energy density, existing reliable technology and established position worldwide [2]. Therefore, there is need to develop novel technologies that enable reduction in CO_2 emissions into the atmosphere, while also mitigating the significant economic and/or political advantages that favour the business-as-usual technologies. There are three options to reduce total CO_2 emissions, to reduce the energy consumption (including increasing the efficiency of the energy conversion and/or utilization systems), to switch to non-fossil fuel energy sources such as solar energy, wind energy and biomass and finally Carbon Capture and Storage (CCS) [10].

The sun as the world's primary source of energy with a surface temperature of about 5800 K and a solar radiosity of 63 MW/m^2 is an unlimited source for high temperature heat [11]. It is also freely available and has no impacts on the ecology. However, solar energy is inherently intermittent, distributed unequally over the earth and highly diluted owing to the sun-to-earth geometrical constraint, to the extent that terrestrial solar irradiance at maximum is about 1 kW/m^2 [11]. Optical concentrator devices enable high solar radiative fluxes with relatively low thermal losses [12]. They use large reflective surfaces to collect and concentrate the incident solar radiation into a solar receiver [13], in which the high temperature heat can be utilized either to drive the endothermic reactions [14, 15] or to generate electricity through e.g. steam/gas turbines or Stirling engine [16-19]. The development of the utility-scale Concentrated Solar Thermal (CST) power plants worldwide shows that it has potential to achieve cost-competitive power generation, especially in arid regions where direct sunlight is abundant

[20]. This is because CST can dispatch power round-the-clock through either incorporating Thermal Energy Storage (TES), when enough solar thermal energy is available during the day time [11, 21], and/or hybridizing with fossil fuels [22].

Currently sensible TES systems, using molten salt as storage medium, are the only commercially viable method in large scale CST plants [22, 23]. Nevertheless, they have a number of significant disadvantages and typically increase the capital cost of a solar thermal plant by 10–20%, depending on the amount of storage [24, 25]. They also require large quantities of salt and two correspondingly large storage tanks. The size and solidification potential of these systems are disadvantages that increase their cost [26]. Besides, in these systems heat is stored at temperatures of around 565-600°C, while it is released at lower temperatures of around 540 °C [22, 27] which are suitable only for inefficient Rankine cycles. Moreover, the temperature drop associated with storage and release of the concentrated solar thermal energy in these systems, lowers the exergy efficiency of the CST Plant. Hence, new options for the storage of solar thermal energy are required to improve the efficiency of the power generation in CST power plants and consequently reduce the costs.

Hybrids of CST and fossil-fuelled technologies are also receiving growing attention owing to the complementary nature these two energy sources and their potential to lower the cost of solar energy [22]. Solar thermal power offers low net greenhouse gas emissions but suffers from high cost, due largely to the intermittent nature of the resource, while the combustion of fossil fuels offers high availability and low fuel cost, but at the expense of high CO_2 emissions [28]. Advantages of hybrids include greater ease in mitigating the intermittent solar

resource, sharing of infrastructure, and increased efficiency [7, 29-32]. Hybrids with Rankine cycles are now commercially available [33]. However, these commercially available hybrid solar cycles are limited both to a low solar share, typically less than 10%, and thermal efficiency, less than around 40% [29, 34]. Therefore, new hybrid systems are required enabling both a high solar share and more efficient power generation cycles based on gas turbine combine cycles (GTCC).

As mentioned above, CCS is a promising approach to mitigate anthropogenic CO_2 emissions to the atmosphere. It also enables the reduction of other pollutants e.g. NO_x, SO_x and particulate matter. The Intergovernmental Panel on Climate Change (IPCC) has shown that CCS can account for 19% of the world total CO_2 emission reduction needed this century to stabilise the climate change at a reasonable cost [2]. Thus far four classes of CCS technologies have been proposed: pre-combustion, post-combustion, oxi-fuel combustion and Chemical Looping Combustion (CLC). However, different economic assessments performed by the CO_2 Capture Project, CCP, [35] and by the International Panel on Climate Change, IPCC, [2] have shown that CLC is among the best of the these options for low cost CO_2 capture. Hence, interest in CLC systems is growing. In the CLC process a solid oxygen carrier (OC) is used to transfer oxygen from the air to the fuel to avoid direct contact between the fuel and air. The oxygen carries are typically particles composed of the metal oxides as active component and the inert materials as binder. A CLC system consists of two separate reactors; an air reactor and a fuel reactor. During the CLC operation, OC particles in the fuel reactor are reduced through oxidation of the fuel and

transferred to the air reactor, where they are oxidised by the air to produce metal oxide. The metal oxide is then returned to the fuel reactor and the process is repeated. Hong *et al.* [36-38] was a pioneer in identifying that the solid OCs in the CLC systems offer to solar thermal technology a form of high temperature chemical storage. They proposed a number of hybrid solar CLC (Hy-Sol-CLC) systems in which, advantageously, concentrated solar thermal energy is converted to chemical energy at a lower temperature than that it is released and used for power generation. However, in these Hy-Sol-CLC systems the application of OC particles for diurnal solar thermal energy storage was not reported. Furthermore, their proposed hybrids suffer from a low solar share or cycle thermal efficiency. Therefore the principle objective of this thesis is to develop a novel Hy-Sol-CLC process in which the concentrated solar thermal energy is stored using the CLC components and used for a dispatchable power generation. The proposed Hy-Sol-CLC system also aims to enable a high solar share and thermally efficient power generation to decrease the costs of both CST and CCS technologies. Such a hybrid solar CLC system not only offers potential to address the challenge of the intermittency of solar energy but also presents the opportunity of combining the advantages of CLC and CSP in a unit solar hybrid power plant.

1.2. Aims

The specific aims of the thesis were defined as follows:

- to determine the feasibility of the hybridization of a CLC system with CST and the application of the OC particles for TES;

- to identify the potential of storing solar thermal energy as chemical and sensible heat using OC particles in a CLC system;
- to explore novel configurations of the Hy-Sol-CLC with which a high solar share and thermal efficiency can be achieved and to explore the fundamental knowledge required for the design and operation of such a system;
- to explore the performance of the proposed Hy-Sol-CLC in a Gas Turbine Combined Cycle (GTCC);
- to identify the parameters that best describe the performance of the Hy-Sol-CLC system;
- to explore potential fuel and OC particles for the Hy-Sol-CLC systems;
- to explore the behaviour of an OC particle exposed to high radiation heat flux.

1.3. Thesis outline

The thesis is presented in eight chapters, the sequence of which highlights the chronology of the knowledge development and research undertakings to meet the defined aims. The first Chapter, which is the introduction, gives an overview of the subject and specifies briefly the gap in knowledge. The principle objective and the aims of the thesis are also defined in this Chapter. Chapter 2 provides a comprehensive literature review and explains the gap in knowledge as well as the importance of the research in more details. The main body of the thesis, Chapters 3 to 7, is a collection of five manuscripts that have been published, or are currently under review. These publications present the progress made in the course of this study and explain the achievements of this research. Finally, the conclusions of the research performed in addition to some basic recommendations for the future works are given in the Chapter 8. In the following paragraphs the content of each chapter and the alignment of the research with the specified aims are explained.

Chapter 2 provides a critical review of the literature both related to the CST and CCS technologies. The emphasis of the chapter is on the state of the art in CLC, TES and Hy-Sol-CLC systems. The research gap in each section has been identified.

The research was started by looking at the potentials of the CLC systems for hybridisation with CST and different possible configurations of the Hy-Sol-CLC. Chapter 3 is the first of five journal publications. In this chapter the basic concept of the application of the OC particles in a CLC system for diurnal storage of the concentrated solar thermal energy is described. The chapter also presents the

configuration of the first proposed Hy-Sol-CLC process. This system was designed to achieve a base-load power generation despite the variations in the input concentrated solar thermal energy. The validated mathematical simulation required for the analysis of the system in addition to the parameters used for the assessment of the operation of the Hy-Sol-CLC systems have been also presented in this chapter. Furthermore, the advantages and disadvantages of the system have been identified in detail. The calculations showed the solar share achieved using this configuration is relatively low, at about 6.5% when averaged over the whole day. In addition, the operating temperature of the solar fuel reactor increases uncontrolled in response to the variation in input concentrated solar thermal energy. It was also demonstrated that these limitations are only associated with the present configuration of the Hy-Sol-CLC. Therefore, another Hy-Sol-CLC process was proposed to overcome these issues. This process is discussed in the next chapter.

Chapter 4 is the second of five journal publications which presents the second proposed Hy-Sol-CLC system. The calculations demonstrated that this system is preferred significantly over the first proposed Hy-Sol-CLC system in terms of solar share and the viability to control the solar fuel reactor operating temperature. A high solar share of around 60% as well as a controlled temperature of the fuel reactor was calculated for this system. A comprehensive sensitivity analysis is also presented here to assess the effect of different operating conditions on the performance of the system. Due to better thermal performance of this Hy-Sol-CLC system, it was selected for further investigations in the next two chapters.

Chapter 5, which is the third of the five journal publications, presents the operation of the proposed Hy-Sol-CLC system, described in Chapter 4, in a hybrid solar GTCC cycle. The chapter also evaluates the performance of the Hy-Sol-CLC GTCC with and without the application of an after-burner. Furthermore, a comprehensive sensitivity analysis is presented to evaluate the effects of various operating conditions.

Chapter 6 is the fourth of the five journal publications and aims to identify the potential fuels and oxygen carrier combinations applicable in the Hy-Sol-CLC systems with the purpose of achieving a higher solar share and better system performance. In this chapter a thermal analysis of the Hy-Sol-CLC system, described in Chapter 4, is presented to identify the energetic performance of various combinations of the fuel and the oxygen carriers. Three fuels in combination with the oxides of five different metals, as oxygen carriers, were assessed. The possibility and the advantages/disadvantages of the application of each combination of the mentioned fuels and oxygen carriers are presented here.

The investigations presented in former Chapters demonstrated that the solar fuel reactor is a key component in the Hy-Sol-CLC systems. Hence, Chapter 7 is allocated to the development of the fundamental knowledge required for design and operation of a cavity solar fuel reactor. This chapter is the final publication of this thesis in which an un-steady-state mathematical model is presented to calculate the temperature variations during the conversion of an OC particle exposed to high intensity solar heat flux as a function of time. The validation of the model against reported experimental and theoretical data is presented. This model was used to study the effect on the particle conversion and maximum

temperature of various operating parameters i. e. particle size, external heat and mass transfer resistance, radiation heat flux intensity, composition and temperature of the surrounding gas.

Finally Chapter 8 lists the conclusions from this research along with recommendations for further development of the concept toward commercialisation step.

1.4. Publications and Patents arising from this thesis

The research discussed in this thesis has led to the generation of five journal and two peer reviewed conference papers. The journals in which the papers are published or submitted are three of the best in the fields of Energy and Chemical Engineering. In addition, the proposed Hy-Sol-CLC system has been patented by the Adelaide Research and Innovation Centre. The Australian Provisional Patent Application has been also added to the thesis through Appendix A.

Journal papers:

- **M. Jafarian,** M. Arjomandi, G. J. Nathan, "A hybrid solar and chemical looping combustion system for solar thermal energy storage". Applied Energy, (2012), vol: 103, p: 671-678.
- **M. Jafarian**, M. Arjomandi, G. J. Nathan, "The influence of high intensity solar radiation on the temperature and reduction of an oxygen carrier particle in hybrid chemical looping combustion". Chemical Engineering Science, (2013), vol: 95, p: 331-342.

- **M. Jafarian**, M. Arjomandi, G. J. Nathan, "A hybrid solar chemical looping combustion system with a high solar share". Applied Energy, (2014), vol: 126, p: 69-77.
- **M. Jafarian**, M. Arjomandi, G. J. Nathan, "The energetic performance of a novel hybrid solar thermal & chemical looping combustion system". Applied Energy, (2014), (Under review).
- **M. Jafarian**, M. Arjomandi, G. J. Nathan, "Influence of the type of the type of oxygen carriers on the performance of a hybrid solar chemical looping combustion system". Energy& Fuels, (2014), vol: 28, issue: 5, p: 2914–2924.

Peer review conference papers

- **M. Jafarian**, M. Arjomandi, G. J. Nathan, "Modelling the influence of high intensity radiation flux on particle performance in a hybrid solar chemical looping combustion reactor". Dec 6-7, 2012, Australian Solar Council's academic conference, Swinburne University, Melbourne, Victoria, Australia.
- **M. Jafarian**, M. Arjomandi, G. J. Nathan, "Application of Chemical Looping for Solar Thermal Energy Storage". Proceedings of the Australian Combustion Symposium Nov 29 to Dec 1, 2011, the University of Newcastle, Newcastle, NSW, Australia, p: 231-235.

Patent

- **M. Jafarian,** M. Arjomandi, G. J. Nathan. A hybrid solar and chemical looping combustion system, Provisional Patent Application No. 2013903807, Adelaide Research and Innovation Pty. Ltd.; 2013 [Priority Date: 02.10.2013]. 2013**.**

1.5. Format

The thesis has been submitted as a portfolio of the publications according to the formatting requirements of The University of Adelaide. The printed and online versions of this thesis are totally identical. The online version of the thesis is available as a PDF. The PDF version can be viewed in its correct fashion with the use of Adobe Reader 9.

References

[1] Figueroa JD, Fout T, Plasynski S, McIlvried H, Srivastava RD. Advances in CO_2 capture technology-The U.S. Department of Energy's Carbon Sequestration Program. International Journal of Greenhouse Gas Control. 2008;2:9-20.

[2] Carbon Dioxide Capture and Storage: Special Report of the Intergovernmental Panel on Climate Change: Cambridge University Press; 2005.

[3] He F, Han T, Hong H, Jin H. Solar thermochemical hybrid trigeneration system with CO_2 capture using dimethyl ether-fueled chemical-looping combustion. ASME 2011 5th International Conference on Energy Sustainability. Washington, DC, USA2011. p. 1651-60.

[4] Yamasaki A. An overview of CO_2 mitigation options for global warming-empasizing CO_2 sequestration options. Journal of Chemical Engineering of Japan. 2003;36:361-75.

[5] Trends in Atmospheric Carbon Dioxide. 2013.

[6] InternationalElectricityChiefExecutiveSummit. Road-map for a low-carbon power sector by 2050. 2009.

[7] Nataly Echevarria Huaman R, Xiu Jun T. Energy related CO_2 emissions and the progress on CCS projects: A review. Renewable and Sustainable Energy Reviews. 2014;31:368-85.

[8] Adanez J, Abad A, Garcia-Labiano F, Gayan P, de Diego LF. Progress in chemical-looping combustion and reforming technologies. Progress in Energy and Combustion Science. 2012;38:215-82.

[9] Liu W, King D, Liu J, Johnson B, Wang Y, Yang Z. Critical material and process issues for CO_2 seperation from coal-powered plants. JOM Journal of the Minerals, Metals and Materials Society. 2009;61:36-44.

[10] Yang H, Xu Z, Fan M, Gupta R, Slimane RB, Bland AE, et al. Progress in carbon dioxide separation and capture: A review. Journal of Environmental Sciences. 2008;20:14-27.

[11] Romero M, Steinfeld A. Concentrating solar thermal power and thermochemical fuels. Energy & Environmental Science. 2012;5:9234-45.

[12] Winter CJ, Sizmann RL, Vant-Hull LL. Solar power plants: fundamentals,

technology, systems, economics: Springer-Verlag; 1991.

[13] Rabl A. Active Solar Collectors and Their Applications: Oxford University Press, USA; 1985.

[14] Piatkowski N, Wieckert C, Weimer AW, Steinfeld A. Solar-driven gasification of carbonaceous feedstock-a review. Energy & Environmental Science. 2011;4:73-82.

[15] Steinfeld A. Solar thermochemical production of hydrogen–a review. Solar Energy. 2005;78:603-15.

[16] Kronberger B, Johansson E, Löffler G, Mattisson T, Lyngfelt A, Hofbauer H. A two-compartment fluidized bed reactor for CO_2 capture by chemical-looping combustion. Chemical Engineering & Technology. 2004;27:1318-26.

[17] Hischier I, Leumann P, Steinfeld A. Experimental and numerical analyses of a pressurized air receiver for solar-driven gas turbines. Journal of Solar Energy Engineering. 2012;134.

[18] Ahmadi MH, Sayyaadi H, Dehghani S, Hosseinzade H. Designing a solar powered Stirling heat engine based on multiple criteria: Maximized thermal efficiency and power. Energy Conversion and Management. 2013;75:282-91.

[19] Ruelas J, Velázquez N, Cerezo J. A mathematical model to develop a Scheffler-type solar concentrator coupled with a Stirling engine. Applied Energy. 2013;101:253-60.

[20] Concentrated solar power heats up. Emerging Energy Research (EER); 2006.

[21] Romero M, González-Aguilar J. Energy and Power Generation Handbook: Established and Emerging Technologies. In: Rao KR, editor: American Society of Mechanical Engineers; 2011.

[22] Kolb GJ. Economic evaluation of solar-only and hybrid power towers using molten-salt technology. Solar Energy. 1998;62:51-61.

[23] Robak CW, Bergman TL, Faghri A. Economic evaluation of latent heat thermal energy storage using embedded thermosyphons for concentrating solar power applications. Solar Energy. 2011;85:2461-73.

[24] Group SLLC. Assessment of parabolic trough and power tower solar technology cost and performance forecasts. Chicago, Illinois: National Renewable Energy Laboratory (NREL); 2003.

[25] Gil A, Medrano M, Martorell I, Lázaro A, Dolado P, Zalba B, et al. State of the art on high temperature thermal energy storage for power generation. Part 1-Concepts, materials and modellization. Renewable and Sustainable Energy Reviews. 2010;14:31-55.

[26] Mills D. Advances in solar thermal electricity technology. Solar Energy. 2004;76:19-31.

[27] Dunham MT, Iverson BD. High-efficiency thermodynamic power cycles for concentrated solar power systems. Renewable and Sustainable Energy Reviews. 2014;30:758-70.

[28] Nathan GJ, Battye DL, Ashman PJ. Economic evaluation of a novel fuel-saver hybrid combining a solar receiver with a combustor for a solar power tower. Applied Energy. 2014;113:1235-43.

[29] Hybridisation of fossil fuel energy generation in Australia. Asutralian Renewable Energy Agancy (ARENA); 2013.

[30] Kribus A, Zaibel R, Carey D, Segal A, Karni J. A solar-driven combined cycle power plant. Solar Energy. 1998;62:121-9.

[31] Schwarzbözl P, Buck R, Sugarmen C, Ring A, Marcos Crespo MJ, Altwegg P, et al. Solar gas turbine systems: Design, cost and perspectives. Solar Energy. 2006;80:1231-40.

[32] Buck R, Brauning T, Denk T, Pfander M, Schwarzbozl P, Tellez F. Solar-hybrid gas turbine-based power tower systems (REFOS). Journal of Solar Energy Engineering. 2002;124:2-9.

[33] Schunk LO, Steinfeld A, Haeberling P, Wepf S, Wuillemin D, Meier A. A receiver-reactor for the solar thermal dissociation of zinc oxide. Journal of Solar Energy Engineering. 2008;130:021009-.

[34] Barigozzi G, Bonetti G, Franchini G, Perdichizzi A, Ravelli S. Thermal performance prediction of a solar hybrid gas turbine. Solar Energy. 2012;86:2116-27.

[35] McGovern RK, Smith WJ. Optimal concentration and temperatures of solar thermal power plants. Energy Conversion and Management. 2012;60:226-32.

[36] Hong H, Jin H. A novel solar thermal cycle with chemical looping combustion. International Journal of Green Energy. 2005;2:397-407.

[37] Hong H, Jin H, Liu B. a novel solar-hybrid gas turbine combined cycle with inherent CO_2 separation using chemical-looping combustion by solar heat source. Journal of Solar Energy Engineering. 2006;128:275-84.

[38] Hong H, Han T, Jin H. a low temperature solar thermochemical power plant with CO_2 recovery using methanol-fueled chemical looping combustion. Journal of Solar Energy Engineering. 2010;132:031002.

CHAPTER 2

LITERATURE REVIEW

2.1. Concentrated solar thermal (CST)

Concentrated Solar Thermal (CST) systems use reflective surfaces to concentrate solar radiation incident on a large area into a small area that is called focal point [1]. The concentrated solar radiation is then converted to heat either to ultimately generate electricity through a heat engine, which is typically a steam turbine, or to drive an endothermic reaction. At present, there are four available CST technologies at commercial and pilot scales, namely parabolic trough (PT) collectors, parabolic dish (PD) collectors, linier Fresnel (LF) reflector systems and central receivers (CR) [2-4]. Figure 1 shows a schematic representation of these systems.

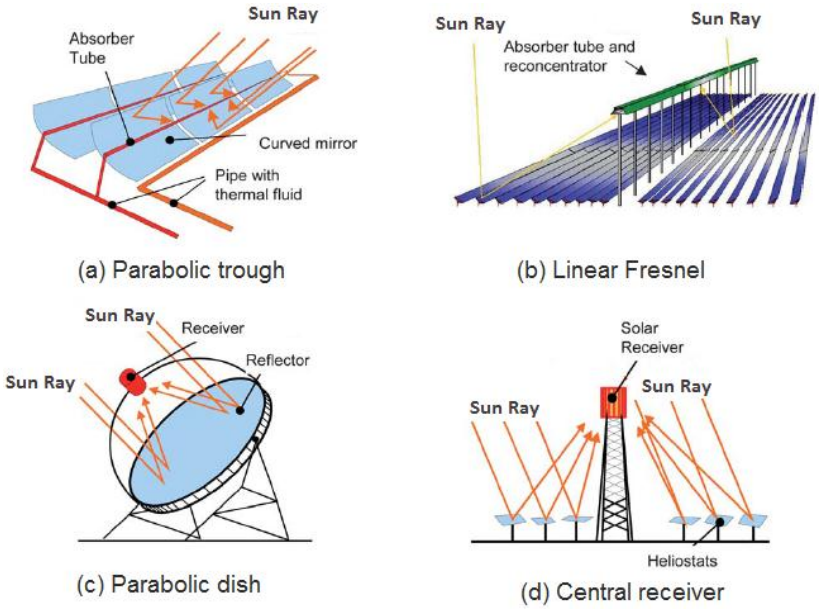

Figure 2.1. Schematic representation of (a) parabolic trough, (b) linear Fresnel, (c) parabolic dish and (d) central receiver technologies, adopted from [1].

As shown in Figure 2.1, a PT collector is a 2-D concentrating system comprising a curved trough focusing sunrays onto an absorber tube that is

mounted at its focal line. The concentrators are controlled to track the movement of the sun [4]. LF systems are also 2-D concentrating systems in which thin, long segments of reflectors are utilised to focus sunlight into a fixed absorber located at a common focal point of the reflectors. As for PTs, here also the reflectors are mirrors that can follow the sun on a single or dual axis regime. However, the application of flat plate mirrors makes them cheaper to manufacture than PTs. Usually a concentration ratio of around 30-80 and a thermal fluid temperature of around 500 °C can be achieved using PT and LF collectors, which is well suited for the steam Rankine cycles [1, 5]. (The concentration ratio is defined as the projected reflection surface area divided by the projected receiver aperture area [6].)

A DE system comprises of a stand-alone parabolic reflector that concentrates sunrays into a receiver positioned at the focal point of the reflector. Typically, each dish works independently and produces a power capacity of 5-25 kW which is appropriate for a usual Stirling engine or a Brayton mini-turbine. In this arrangement, a large number of DEs is required to be installed in a large scale plant [5]. Normally, a concentration ratio of 100-3000 and an operating temperature of 150-1500 °C can be achieved using DEs [1].

Central receivers (CR), also known as Solar Power Towers (SPT), are one of the most recently developed CST technologies [5]. In this system, as shown in Figure 2.1, a field of sun tracking reflectors, called heliostat field, reflects and concentrates the sun rays into a central receiver which is typically positioned on top of a central tower. The concentration ratio of these systems is typically in the range of 150-1500. Various working fluids such as molten salts, superheated or

saturated steam and pressurised air can be used and heat to temperatures of 500-2000 °C [1]. Advantageously, the temperature range achievable with these systems is well-matched to gas GTCCs which are more efficient than Rankine steam turbines.

The available energy technology roadmap presented by the International Energy Agency (IEA) predicts that CST can be a competitive option for base-load power generation by 2025-2030 in the arid region where the sun light is abundant [7]. However, the intermittent nature and low intensity of solar radiation are major barriers to achieving economic viability. To compensate for the intermittent resource and to improve the economic viability of CST plants, compared with the conventional fossil-fuel based power generation plants, CST plants require either storage capacity or back up power generator to continue electricity supply when sunlight is below a threshold [8]. The CST plants equipped with backup systems are called hybrids. Hybridisation of the CSTs with fossil fuel-based power plants can also increase their efficiency which in turn reduces their costs and enables them to compete economically with fossil fuelled based power plants which ultimately enables the CST power plants to penetrate into the electricity market [1].

2.2. Solar thermal energy storage (TES)

Energy storage (ES) is the storage of some form of energy that can be drawn upon at a later time to perform some useful operation [9]. Solar thermal energy can be stored as sensible heat, latent heat, heat of chemical reactions or combination of these methods [9]. Sensible heat thermal energy storage (TES)

stores energy by raising the temperature of a solid or liquid without any phase change, latent heat TES stores energy through change in phase of materials referred to as Phase Change Materials (PCM), and chemical TES relies on the energy absorbed in endothermic and released in exothermic chemical reactions [10, 11].

2.2.1. Sensible TES

Sensible thermal energy can be stored by solids and liquids. The amount of the sensible energy stored per unit volume of a storage medium depends both on the energy density of the storage medium and the temperature lift. Therefore energy density is an important parameter in the selection of the materials for sensible TES. A suitable storage medium also requires [12]:

- to have chemical and mechanical stability during the large number of charge/discharge cycles;
- to provide a high heat transfer rate in charge/discharge processes;
- to have a low thermal expansion;
- to provide a high storage temperature.

Different solid materials have been proposed for sensible TES, e. g. recycled materials, concrete, rock and metals [13-15], in which a Heat Transfer Fluid (HTF) is used for the charging/discharging the storage medium. The main drawbacks of these systems are typically the conductive resistance of the storage materials, which limits the heat transfer rate during the charge and discharge processes, and the complexity and heat losses associated with the application of

the HTF. In addition, the thermal stresses, associated with the material thermal expansion, can lead to technical and operational problems [15, 16].

Sensible TES using molten salt is currently the only commercially viable method being widely used in large-scale CST plants [17, 18]. Other liquids, e.g. synthesis oil and liquid sodium, have been also proposed. However, the operating temperature of the synthesis oil is typically limited to around 400 °C and the system pressurization for further increasing the operating temperature is costly [19, 20]. Besides, their energy density is typically lower than that of molten salts. Liquid sodium can provide a high heat transfer rate and is used as HTF in nuclear power plants. However, the energy density of liquid sodium is usually lower than those of molten salts [9]. In a typical arrangement, the system consists of two storage tanks and a solar receiver. Molten salt at a temperature of around 300 °C from the first (cold storage) tank is pumped to the solar receiver, where it is heated to around 600 °C and delivered to the second (hot storage) tank. The stored hot fluid is then used for steam generation [21]. The benefit of molten salt systems in addition to simplicity is that heat transfer during both charging and discharging occurs through forced convection and therefore is not a controlling factor for the heat transfer in the system [17]. However, molten salt systems typically increase the capital cost of a solar thermal plant by around10-20%, depending on the amount of storage [22]. They also require large quantities of salt and two correspondingly large storage tanks. The size and solidification potential of these systems are disadvantages that increase the costs [3]. Besides, the operating temperature of the molten salt systems is limited to around 600 °C, which in turn imposes limitations on the thermodynamic efficiency of the solar power stations.

This is because an appropriate temperature difference between the molten salt and the steam is required in the heat exchangers to keep a high rate of heat transfer, which typically limits the maximum operating temperature of the power cycle to the range 300 to 550 °C [21]. Beside in all sensible TES systems, the reduction in the temperature at which the heat is released relative to that at which it is stored results in the loss of exergy within the TES process. Hence, it is desirable to seek for new alternatives storage mediums to decrease the disadvantages of the sensible TES systems.

2.2.2. Latent heat TES

The applicable changes in materials phase for latent heat TES vary from solid-solid, liquid-vapour and solid-liquid transitions. However, the solid-liquid phase change is usually preferred over the liquid-vapour transition, due to its low volumetric expansion, and over the solid-solid transition, due to its higher latent heat [17]. Storage systems based on phase change (PCM) materials are considered to be an efficient alternative to sensible TES systems, because not only changing the phase of PCMs is nearly an isothermal process but also enables a higher energy density than that of sensible TES [23-25]. However, despite the large number of PCMs proposed for high temperature TES, e. g. NaCl [26], Li_2CO_3 [17], $MgCl_2$ [9], LiF [26], $NaCO_3$-$BaCO_3$/MgO [9], it is not still available for large scale CST systems. Because, most of the PCMs have a low thermal conductivity of the storage medium, which leads to a low charge and discharge rates, and suffer from the solid deposition on heat transfer surfaces [27].

2.2.3. Chemical TES

Chemical TES is the least investigated and developed storage technology [28], though it has potential to provide a higher energy density than both sensible and latent TES techniques [9]. In this process solar thermal energy is first used to derive an endothermic reaction and then the stored heat is released subsequently in an exothermic reaction. The stored heat can be released at a constant and even higher temperature than the stored energy, provided that heat is removed at a rate that would prevent self-heating/cooling [29]. These advantages make chemical TES an appropriate alternative that can be applied in higher energy efficient processes than sensible and latent heat TES technologies [30, 31]. The most important requirements of a chemical TES system are the reversibility of both the endothermic/exothermic reactions at an appropriate temperature level with an adequate reaction rate, high heat capacity, cycling stability, low cost, having low parasitic losses due to side reactions, being environmentally benign and the possibility to providing fast heat transfer in to and out from the endothermic/exothermic reactors [32].

A large number of reactions have been proposed and investigated for chemical TES including thermochemical water-splitting [33], the catalytic dissociation of ammonia [34] or reforming of methane [35] and decomposition reactions including that of calcium hydroxide [36, 37] and metal carbonates [32]. However, chemical TES have not yet been extensively developed at scale in industrial applications [38]. This is because the proposed systems typically suffer from poor cyclic performance of the reactants and the technical issues due to the impact of transient solar radiation on large chemical process facilities that typically operate

at steady-state. Furthermore, chemical TES requires additional reactors to be introduced to the system, relative to conventional power generation systems, which in turn increases both the costs and complexity.

In conclusion, new technologies are required to be identified in which the endothermic and exothermic reactions are an integral component of the process, enabling high temperature storage at low cost.

2.3. Hybrid solar power plants

Integration of CST into the thermal cycles of a fuel combustion power plant is known as solar hybridisation and is considered to be an attractive alternative to decrease the costs of power generation from CST [21]. Advantages of hybrids are: (a) lower or no TES required; (b) sharing infrastructure with the existing or new combustion power plants without disrupting their operations [39], degrading their performance or requiring extensive modifications; (c) reducing the CO_2 emissions from combustion power plants by either power boosting, through increasing the generation capacity, or fuel saving, through decreasing the fuel consumption [21]. The main disadvantage of the hybrid CST systems is that their level of greenhouse gas mitigation is lower than that of standalone CST power cycles.

Here the state-of-the-art in solar hybrid power cycles is presented through three sections: (a) hybrid solar steam power plants, (b) hybrid Brayton (Gas turbine) cycles and finally (c) hybrid solar combined cycles.

The performance of the reviewed cycles have been compared mostly based on three parameters including, solar hybrid cycle thermal efficiency (or first law efficiency), Solar share and solar to electrical efficiency (or incremental solar to

electrical efficiency). The cycle thermal efficiency is the ratio of the net power generated by the cycle to the net power input to the power cycle from both fuel and solar thermal energy sources [40]. Solar share is the contribution of the solar load in the total heating load [41]. The solar share can be calculated instantaneously or based on an average over a certain period of time such as 24 hours. The solar to electrical efficiency is the ratio of power generated by the hybrid cycle compared with a pure fossil-based power plant to the input solar thermal energy to the hybrid system [40]. It is worth noting that, the input solar thermal energy to the system should be calculated considering the efficiencies of the heliostat field and solar receivers.

2.3.1. Hybrid solar steam power plants

A simple steam power plant, known also as Rankine cycle, consists of four sections: a pump, a boiler, a turbine and a condenser. Schematic representation of this cycle is shown in Figure 2.2. Firstly, water is compressed by the pump to a high pressure. The compressed fluid is then heated and subsequently vaporised in the boiler by a heat source. In the next step the produced high pressure and temperature working fluid is expanded and used to drive a turbine to produce mechanical work. Finally, the working fluid is cooled back to its initial state within a condenser. The thermal efficiency of a Rankine cycle increases either as the pressure and hence the vaporization temperature in the boiler is increased or the pressure and hence the temperature within the condenser is decreased [42]. However, these conditions raise the capital cost of the plants. Thus in practice the Rankine cycles seldom operate at temperatures above 600 °C or pressure higher

than 100 bar. It is worth noting that this temperature range is suited to molten salt TES systems [43, 44]. The condensation temperature in the condenser is also controlled by the cooling medium, which depends on the power plant location geography. The thermal efficiency of a simple steam Rankine cycles is typically less than 30 % [42].

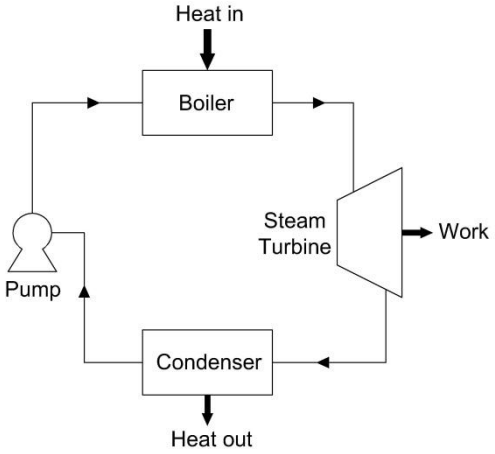

Figure 2.2. Schematic configuration of a simple steam Rankine cycle adopted from [42].

In most of the modern power plants the simple Rankine cycle is modified to improve the cycle thermal efficiency. In these modified cycles the condensed water from the condenser, rather than being pumped directly back to the boiler, is first heated in several stages by the steam taken from turbine in some intermediate stages of expansion. These modified Rankine cycles are known as regenerative Rankine cycles and can achieve a thermal efficiency of 37-42% [45, 46].

Solar hybridisation of steam power plants was first proposed by Zoschak and Wu [47] in 1975. They studied seven methods for the application of the concentrated solar thermal energy as a supplementary heat source in an 800 MW

fossil fuelled steam power plant. In these cycles, solar radiation is first concentrated onto an absorber which is mounted on a tower by an array of flat mirrors. The heat absorbing methods considered were heating of feed water, evaporation of water, superheating of steam, combined evaporation and superheating, reheating of steam, preheating of air required for the combustion and finally combined air and feed water heating. They found that combined evaporation and super heating can be the preferred method due to its high utilization of solar energy, relatively low indicated capital cost and moderate complexity of design and operation. Kolb [21] pioneered in identifying the economic benefits of hybrids between solar thermal energy and Rankine cycles through assessment of various hybrid and solar-only configurations for molten salt power towers. Solar hybridisation of a 210 MW coal-fired power plant was studied by Pai [48]. In this regenerative Rankine hybrid cycle solar thermal heat was used to reheat the condensed water, instead of extracting steam from the turbine in different stages of expansion. A fuel saving of 24.5 % during the period of insolation was estimated to be achieved. Deng [49] proposed a solar and coal-fired steam power plant with secondary air pre-heating. An instantaneous solar share of about 5% and a solar to electrical efficiency of 24.1% was predicted for this hybrid power cycle. Another 200 MW solar aided coal-fired power generation cycle was proposed by Yang *et al.* [50]. In this cycle also concentrated solar thermal heat in the temperature range of 100-260 °C was utilised to preheat the feedwater in a regenerative Rankine cycle. The cycle was estimated to achieve a maximum solar to electrical efficiency of 36.5% for solar heat at 260 °C.

Supercritical steam Rankine cycles can achieve higher thermal efficiency than subcritical steam power cycle. This is because of their higher operating temperature and less exergy loss within their supercritical boilers, which is due to the better match of temperature profile and avoiding the heating at constant temperature. The efficiency of these cycles is typically around 45% [51, 52]. However, when the steam temperature exceed 627 °C high quality nickel allows are required which in turn increases the costs [53]. Yan *et al.* [54] studied the energy and economic benefits of the hybridising a range of subcritical, critical and super critical coal-fired power plants with solar heat in the temperature range from 90 to 260 °C. In their proposed cycles solar thermal energy was utilised to reheat the feedwater. They found that a fuel saving of up to 20% can be achieved, when solar thermal energy is available. They also showed that the benefits of solar hybridisation varies for different steam extracted positions and different power plants. Besides, as the power plant gets larger the benefits of solar hybridisation increases. Organic Rankine cycles have also been proposed typically for temperatures less than 370 °C [55]. However, their thermal efficiency is low and in the range of 10-20% [56, 57].

Solar hybrid Rankine cycles are now commercially available. However, these hybrid technologies are limited to a low solar share of typically less than 15%, while averaged over a long time such as a day [58, 59], and to the relatively low efficiency of the Rankine cycle, which limits their relevance either to the retrofitting with existing power stations. Furthermore, the number of opportunities for such a retro-fit is quite limited, due to the need to satisfy a range of other

conditions including good solar resource, sufficient space and suitable plant characteristics [59].

2.3.2. Hybrid Brayton cycles

In a Brayton cycle, as shown in Figure 2.3, air at ambient conditions is first drawn into a compressor, in which it is pressurised, typically to 5-30 bar, and consequently heated [60]. The pressurised and heated air is then introduced into a combustion chamber where the fuel is burned and the temperature of the pressurised air is further increased. Finally, the high pressure and temperature flue gas is passed through a gas turbine, expanding to the atmospheric pressure and thus producing power [60].

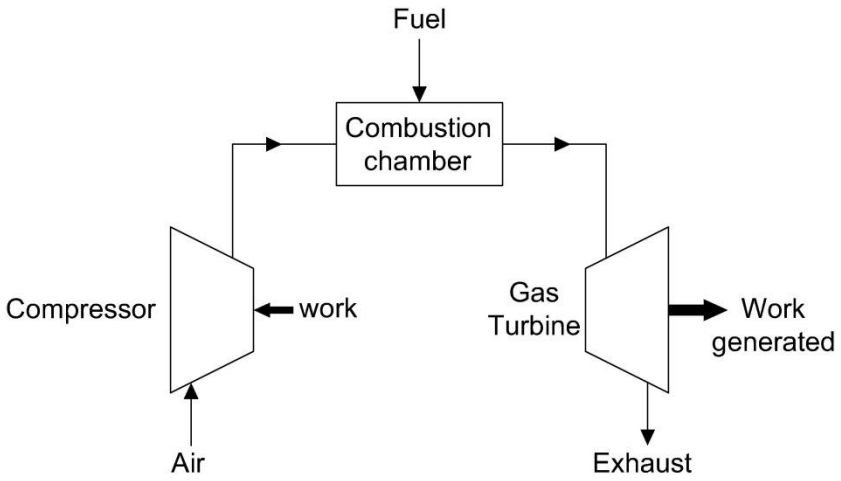

Figure 2.3. Schematic configuration of a simple Brayton cycle adopted from [42].

The operating temperature of the commercially available gas turbines is around 1250 °C [61] and is anticipated to increase to 1700 in foreseeable future [62]. The thermal efficiency of simple Brayton cycle is typically higher than that of a simple

steam Rankine cycles due to its higher operating temperature. Therefore, higher solar to electrical efficiencies can be achieved using Brayton cycles, when hybridised with the concentrated solar thermal energy, relative to hybridised simple Rankine cycles.

In a hybrid solar gas turbine both the concentrated solar thermal energy and the combustion of the fuel are used to increase the temperature of the pressurised air before introduction to the gas turbine [63]. Typically, the concentrated solar thermal energy is first used to preheat the pressurised air coming from the compressor, within a pressurised solar receiver, and then the heated air goes through an after-burner to further heat. The after-burner is also used to compensate for fluctuating solar input and to keep the power cycle working when solar thermal heat is not available [46]. In a such hybrid solar gas turbine system the solar share increases with the temperature of the output pressurised air from the solar receiver [64]. Therefore a key component of a hybrid solar Brayton cycle is the solar receiver, where the concentrated solar radiation is absorbed and transferred to the pressurised air.

Various configurations of the pressurised solar receivers have been proposed based on direct or indirect heating concepts. In direct heating configurations, concentrated solar thermal radiation is either absorbed by the high pressure gas directly or by a surface which is exposed to it, while in indirect heating concept the working fluid is not directly exposed to either the solar radiation or the surface heated by it. In this method, concentrated solar thermal energy is first absorbed on a surface and then is transferred though a conductive medium to a second surface on which heat is mainly transfer to pressurised air by convection. Outlet air

temperatures of up to 1300 °C have been achieved [41, 65, 66] using direct heating concepts owing to its high heat transfer rate [60]. However, these solar receivers require a transparent window which is vulnerable to high pressure, especially when the window size increases. It has been also demonstrated that the application of a window also imposes serious technical construction and operating problems owing to special requirements in optical properties, mechanical strength, high diurnal variable working temperature of the receiver, sealing, cooling and stress-less installation [66-68]. In indirect-irradiated solar receivers the need for the window is eliminated by using an appropriate heat transfer medium. However, this achieved at the cost of conduction-limited heat transfer rates through the solar absorber walls [69, 70], as described above. Consequently, the disadvantages are associated with the restrictions imposed by the material of construction such as resistance to thermal shocks, thermal conductivity and inertness to oxidation by air [60]. Recently, a high temperature indirect pressurised air solar receiver prototype has been developed by Hischier *et al.* [60] that can achieve a maximum outlet temperature of around 1060 °C at an absolute operating pressure of 5 bar and an average incident solar heat flux of 4360 W/m^2 to yield a thermal efficiency of 36%. However, the peak thermal efficiency obtained by this system was 77% at an outlet temperature of 553 °C. This novel solar receiver has not been demonstrated in commercial scale and its thermal efficiency is low due to high re-radiation heat losses.

Supercritical Brayton cycles have been also demonstrated to potentially offer high efficiencies, because in the supercritical region, fluid shows heat transfer characteristics and compressibility like liquids. This in turn results in low

compression work required and more efficient regenerative heat exchangers [71]. Several cycles have been proposed [71-73] but have not been demonstrated at commercial scale.

2.3.3. Hybrid solar combined cycles

Significant effort has been expended for the development of efficient single cycles. However, it has been widely accepted that thermal efficiencies above 50% require the implementation of the gas turbine combined cycles [74, 75]. A gas turbine combined cycle, GTCC, comprises a principal high-temperature Brayton cycle (topping) and one or more lower-temperature Rankine cycles (bottoming) which are driven by the heat released from the topping cycle. A schematic representation of the system is shown in Figure 2.4. Typically natural gas or syngas (produced from coal) are used in these systems. In the former case a gasification step is also required, prior to the combustion chamber, for the production of syngas from coal. Hence, a combined cycle with a gasification step is usually called Integrated Gasification Combined Cycle (IGCC).

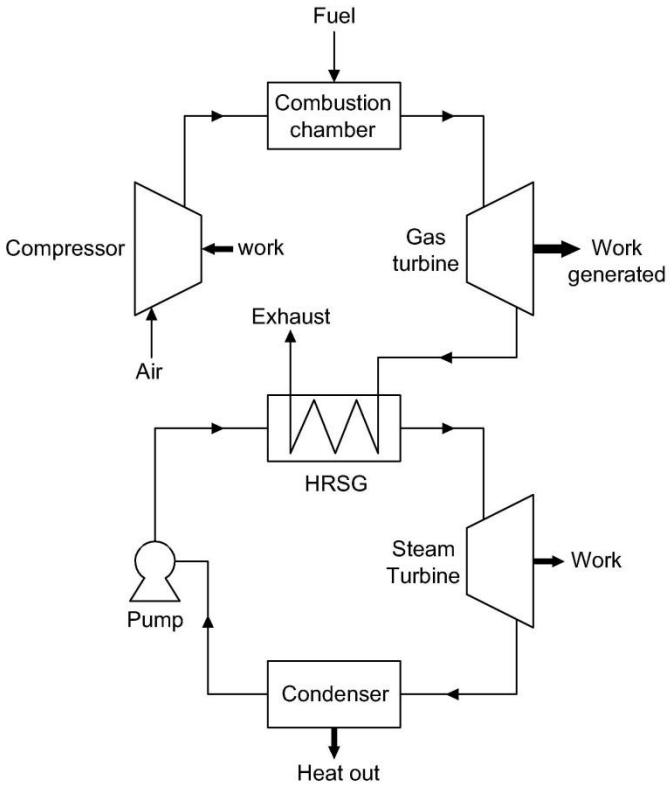

Figure 2.4. Schematic configuration of a gas turbine combine cycle. The outlet stream from the gas turbine is used for more steam generation through Heat Recovery Steam Generator (HRSG).

Solar thermal energy is typically incorporated into the GTCCs either through a pressurised solar receiver in the gas turbines section or, as a supplementary heat source, into the bottoming Rankine cycle. In the first configuration concentrated solar thermal energy is used to preheat the air before going through the combustion chamber of the gas turbine (Sec 1.2.2) [63, 76], while in the second configuration a solar field is used to either increase the steam generation, power boosting, or to decrease the fuel consumption, fuel saving (Sec 1.2.1). These cycles are known as integrated solar combined cycles (ISCC) or hybrid solar GTCC. The solar hybrid GTCC enables the optimum harnessing of the highly

concentrated solar thermal irradiation [77]. Furthermore, the high efficiency of the GTCCs can lead to lower capital cost of solar collector fields due to less heliostat/receiver area required [40]. One of the earliest studies on hybrid GTCCs was performed by Oda and Hashem [78] in 1987 where three different hybrid GTCC configurations incorporating solar thermal energy, both for preheating of compressed air and supplemental heat to the bottoming Rankine cycles, were compared. Their cycles were limited to a thermal efficiency of around 30%. The Sacramento Municipal Utility District and the National Renewable Energy Technology (NREL) led a conceptual assessment of a 30 MW_e hybrid CC power plant which utilises nitrate-salt solar tower along with a salt/air heat exchanger to heat the pressurised air during the peak solar insolation condition [79]. This hybrid plant is estimated to achieve a peak solar share of 27%. Segel and Epstain [80] optimised a solar hybrid CC with the aim of achieving the maximum overall efficiency of the major components of the system namely, the heliostat field and tower, receiver and the secondary optics and finally the power block. They found that the efficiency of the hybrid CC varies from 35% for a solar receiver of 1000 K to 55% for a receiver temperature of 2000 K. However, a receiver temperature of 2000 K seems to be unrealistic at the present state-of-the-art in pressurised solar receivers. A hybrid CC with wet gas turbine technology was studied by Kakaras *et al.* [81]. In this cycle solar thermal energy is used to evaporate the water injected into the compressed air before it goes through the combustion chamber. They showed that the efficiency of the hybrid cycle is increased. However, the cycle is not likely to be implemented in large scale due to increased costs. Li and Yang [82] proposed a solar hybrid GTCC with DSG system with a

maximum thermal efficiency of 53% and an instantaneous solar share of 27.8%. They found that using solar thermal heat for evaporation of feedwater is superior to that to be used for sensible heating purposes. (The parabolic trough can either produce steam directly, which is called Direct Steam Generation (DSG), or through heating an intermediate HTF which is later used for steam generation [76]). Montes *et al*. [83] studied the annual operation of a hybrid GTCC system in which solar heat was incorporated to preheat and generate steam in bottoming cycle for two different pressures. Annual simulations were conducted for two sites: Almería and Las Vegas. They found that even though both locations are suitable for placing a solar thermal power plant, the beneficence of the coupling solar field-combined cycle is more evident in the Las Vegas due to its very hot and dry climate.

In conclusion, despite the large number of proposed configurations of the solar hybrid CCs, they suffer mostly from both the low solar share and the technical issues associated with the high pressure solar receivers, as described in Section 1.2.2. Furthermore, these hybrids use conventional combustion technologies, which burn the carbon-base fuel in air and release the diluted CO_2 with N_2 into the atmosphere. Carbon Capture and Storage (CCS) is an alternative to decrease the CO_2 emission from these hybrid systems. However, CCS imposes around 25% efficiency penalty on the gross plant energy output of steam Rankine power cycles [84]. This energy penalty is even larger for the gas turbines (either Brayton cycle or GTCC) than it is for boilers, because of the greater nitrogen dilution, even though the GTCC is otherwise more efficient. Hence there is a need for new

hybrid technologies that enable the efficient hybridisation of GTCCs with concentrated solar thermal energy as well as low cost capture of CO_2 emissions.

2.4. Carbon Capture and Storage (CCS)

The motivation behind the development of CCS is to minimize the effect of CO_2 emission on global climate change, while keeping the low cost carbon-based infrastructure [85]. Carbon capture and storage consists of three main steps: capturing CO_2 at the generation point such as power plants, compressing it to a concentrated fluid and finally either reserving it in safe and secure places such as oil reservoirs and mineral deposits [86, 87] or reusing it [88, 89]. Of these three stages, carbon capture is the most energy consuming step. Hence, substantial research endeavours globally to improve the efficiency of this step. There are four ways for CO_2 capture: 1. pre-combustion, (2) oxi-fuel combustion, (3) post-combustion and (4) chemical looping combustion (CLC) [87, 90, 91]. In the following sections a brief description of each technology is provided.

2.4.1. Pre-combustion

In pre-combustion CO_2 capture, CO_2 is recovered before the fuel is burned. In this process the hydrocarbon fuel is first reformed to produce a mixture of CO and H_2. The CO is then further oxidised to CO_2 through water-gas shift reaction ($CO + H_2O \leftrightarrow CO_2 + H_2$). The CO_2 so produced is then separated using adsorption, absorption or membrane separators [87, 92, 93] to generate industrially pure H_2, which is subsequently combusted with air in the power plants.

Pre-combustion carbon capture can decrease the energy conversion efficiency of the Integrated Gasification Combined Cycles (IGCC) by 13-24% [94-96]. This efficiency loss is mainly due to the large steam consumption through water-gas shift reaction, heating and cooling required within the CO_2 separation and power consumption for CO_2 compression. It also increases the cost of electricity generation by around 25-45% [94-97].

2.4.2. Post combustion separation

Post-combustion is a downstream process for the separation of CO_2 from the flue gas after being produced in the combustion. Several post-combustion gas separation technologies have been proposed, such as absorption [98-100], adsorption [101, 102], cryogenic separation [103], membrane separation [104, 105] and micro algal bio fixation [106, 107]. Among these technologies absorption using amines, e. g. Mono Ethanol Amine (MEA), is a well-established technology primarily being developed and used as a potential economic source of CO_2, mainly for enhanced oil recovery (EOR) operations, but the primary driver was not the greenhouse mitigation [108]. In this process the flue gas is first cooled and treated to remove the solid impurities before being fed to the absorption column. Within the absorption column MEA is used to remove the CO_2 by chemical reactions. The CO_2-rich solution is then transferred to a stripper column in which the MEA is heated to release dissolved CO_2. Finally the separated CO_2 is compressed and the recovered MEA is sent back to absorption column [96]. The energy-intensive nature of this system results in 21-42% decrease in the thermal efficiency of the power cycle when retrofitted into the existing power plants [97,

109]. Various investigations also demonstrated that a 90% CO_2 capture using MEA leads to around 40-70% increase in the cost of power generation [109, 110].

2.4.3. Oxy-fuel combustion

In oxy-fuel combustion almost pure oxygen is used for fuel combustion, instead of air. This results in a high concentration of CO_2 in the flue gas [91]. Oxy-fuel flames have a higher temperature than air flames due to elimination of N_2 from the oxidant gas. Typically, a fraction of the flue gas is recycled to the combustor to moderate the temperature and the rest is cooled down to remove the produced water [111]. Consequently, high temperatures of the flue gas are possible, which is important in term of cycle efficiency, besides the thermal NO_x formation is suppressed. However, the main disadvantage of the process is an efficiency loss of around 20-35% in production of pure oxygen required, which is usually provided by an air-separation unit (ASU) [96]. A novel chemical looping air separation technology has been recently proposed by Moghtaderi *et al.* [112] for pure O_2 production with low energy penalty. However, this technology is at its early stages of development yet and has not been demonstrated at pilot scale.

2.5. Chemical looping combustion (CLC)

The concept of CLC was first proposed by Lewis and Gilland [113] in 1954 for the production of pure CO_2. Later the CLC was suggested as a novel system for decreasing the irreversibilities associated with conventional combustion systems [114-116]. Finally; in 1994, Ishida and Jin [116] proposed it for CO_2 separation with minimum energy loss. In this system a metal oxide, such as and

oxygen carrier (OC), is used to provide oxygen for fuel oxidation to avoid direct contact between the fuel and air [84, 85]. The OCs are typically solid particles comprised of an active and an inert. Other configurations e. g fixed bed oxygen carriers have been also reported in literature.

The schematic representation of the CLC concept is shown in Figure 2.5. The system consists of two separate reactors, an air reactor and a fuel reactor. During the CLC operation, oxygen carriers (OC) in the fuel reactor reduce through oxidation of the fuel and migrate to the air reactor where they are oxidised by the oxygen from the air. The metal oxides so produced are then transferred back to the fuel reactor and the process continues. CLC can be categorised as either the pre-combustion or oxy-combustion. Because, carbon of the fuel is first separated within the fuel reactor (pre-combustion), then the reduced metal oxide is oxidised by air within the air reactor (oxy-combustion) [96].

If the composition of the fuel and metal oxide are expressed as $C_nH_{2m}O_p$ and Me_aO_b, respectively, the reactions within the fuel and air reactors can be expressed as:

Fuel reactor:

$$C_nH_{2m}O_p + \left(\frac{m+2n-p}{b-ah/g}\right)Me_aO_b \rightarrow \left(\frac{m+2n-p}{b-ah/g}\right)\frac{a}{g}Me_gO_h + mH_2O + nCO_2 \quad (2.1)$$

Air reactor:

$$\frac{1}{2}(2n+m-P)O_2 + \left(\frac{m+2n-p}{b-ah/g}\right)\frac{a}{g}Me_gO_h \rightarrow \left(\frac{m+2n-p}{b-ah/g}\right)Me_aO_b \quad (2.2)$$

The summation of these two reactions is the oxidation of fuel with oxygen:

$$C_nH_{2m}O_p + \frac{1}{2}(2n+m-p)O_2 \rightarrow n\,CO_2 + mH_2O. \quad (2.3)$$

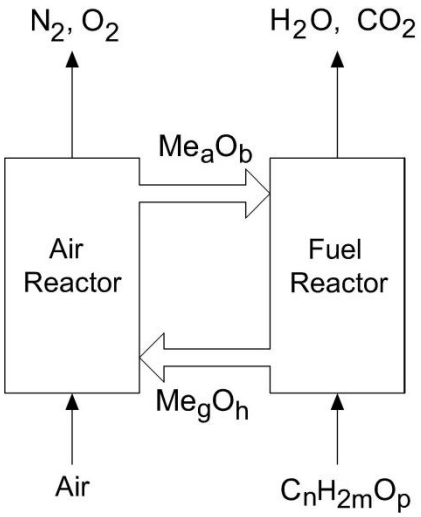

Figure 2.5. Schematic representation of chemical looing combustion. The oxygen carriers are reduced and oxidised alternatively within the fuel and air reactors, respectively. The H_2O so produced can be separated from the fuel reactor output gas stream through a condensation process.

In CLC process, as shown in Figure 2.5, the outlet stream from the fuel reactor consists of mainly of H_2O and CO_2. Thus, it is possible to obtain almost industrially pure CO_2 through condensation of water without any energy loss. In addition, because in a CLC system air and fuel are carried through different reactors, the possibility of NO_x formation is greatly decreased [117]. Nevertheless, several irreversibilities occur due mainly to incomplete fuel conversion, heat losses, attrition and deactivation of the OC particles.

Furthermore, the restrictions associated with both the physical properties of the particles and the operation of the system impose restrictions on the maximum operating temperature achievable for power generation, which in turn result in decreased efficiency of CLC-based power generation cycles [118, 119].

Various economic assessments carried out by the CO_2 Capture Project, CCP, [120] and by the International Panel on Climate Change IPCC [121], have shown that CLC is among the best of the options available for low cost CO_2 capture from combustion. Hence, the interest in CLC systems is growing. So far around 3500 hours of operational experiments in continuous plants of different sizes has been reported [85] and several pilot scale plants have been demonstrated [85, 122, 123]. Considering that this technology is around than 10 years old, this development can be considered very successful.

2.5.1. Thermal Energy Storage (TES) as an inherent part of Chemical Looping Combustion (CLC)

In a CLC system the oxidation of the reduced oxygen carriers, within the air reactor, (Eq. 2.2) is always an exothermic reaction. However, the reduction of the oxygen carriers with fuel, inside the fuel reactor, (Eq. 2.1) can be either exothermic or endothermic depending on the type of fuel and the metal oxide used. In the CLC processes, for those combinations of fuel and metal oxide that react endothermically, the required heat for fuel oxidation is provided by the exothermic oxidation of metal oxides in the air reactor [124] and is transferred to the fuel reactor by means of the hot oxygen carriers, coming from the air reactor, and/or through the direct contact between the fuel and the air reactors [124]. This

results in a temperature difference between the air and fuel reactors [125]. Consequently, if the required energy within the fuel reactor can be provided from an external source such as concentrated solar thermal energy rather than the air reactor, the output from the CLC-based power plant will increase. In addition, it provides the possibility of chemical TES for concentrated solar thermal energy. Solar energy can be also stored within the OC particles as sensible heat. Therefore CLC offers to solar thermal energy the potential for sharing the infrastructure and consequently decreasing the capital costs.

2.5.2. Solar hybridisation of Chemical Looping Combustion (CLC) systems

Solar hybridization of CLC with concentrated solar thermal energy was first proposed by Hong and Jin [126] in 2005. Their proposed Hybrid Solar Chemical Looping Combustion Gas Turbine Combined Cycle (Hy-Sol-CLC GTCC) is shown in Figure 2.6. The process comprises two sections: (a) the CLC reactors, which allow the integration of the solar thermal energy and (b) the combined cycle with CO_2 recovery and separation. In the first section, CH_4 is preheated by the exhaust stream from the turbine GT1 and is fed to the fuel reactor, where it reacts with NiO using solar heat to produce CO_2 and H_2O at a temperature of 530 °C. Then the solid Ni particles are transported to the air reactor where they are oxidized with pressurized and preheated air to make a hot gas stream of N_2 and O_2 at a temperature of 1200 °C. In the second section, the exhaust gas streams from the oxidation and reduction reactors are used to drive two gas turbines called "GT1" and "GT2". Finally, the CO_2 and H_2O in the exhaust stream, as shown in Figure 2.6, are separated in a condenser.

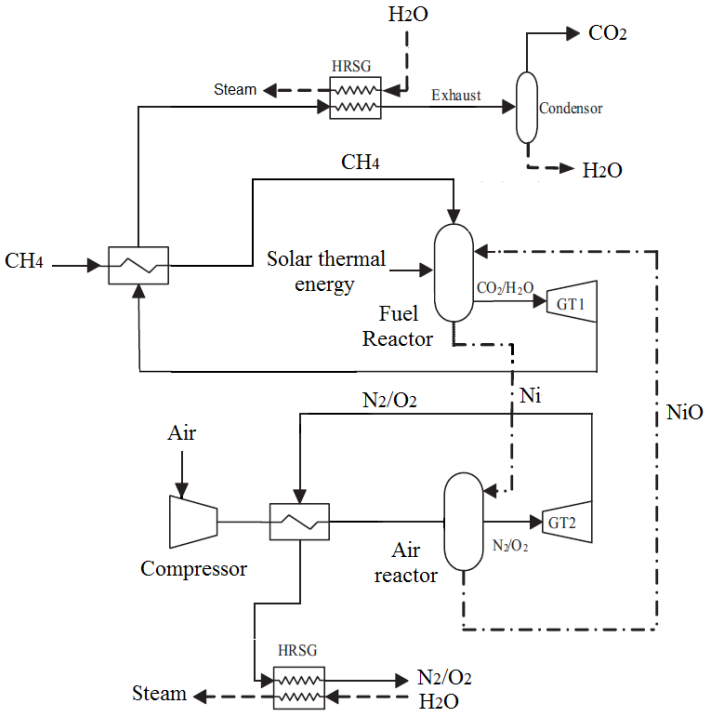

Figure 2.6. Simplified flow diagrams of the solar thermal cycle with CLC proposed by Hong *et al*. [126], adopted from [126]. Solar energy is used both to preheat the inlet CH_4 and to derive the endothermic reaction of NiO and CH_4. Turbines GT1 and GT2 are applied to produce power.

It was shown that the exergy efficiency of this Hy-Sol-CLC process, shown in Figure 2.6, would be about 4 percentage points higher than that of a conventional GTCC and the cycle can achieve an instantaneous solar share of around 16.0%, while solar thermal energy is available [126]. This hybrid power cycle was modified by Hong *et al*. [127] in 2006, as shown in Figure 2.7. In the former proposed process, NiO and CH_4 are also used as the oxygen carrier and fuel, respectively, and the same operating temperatures for the fuel and air reactors were considered. However, in this system a gas-solid heat exchanger is added to the process to further heat the exhaust stream from the fuel reactor and,

consequently, to enhance the gas turbine GT2 efficiency. Two steam turbines are also proposed for power generation from the steam generated by the heat recovered from output streams within the Heat Recovery Stream Generators (HRSG). Other parts of this process are similar to the system shown in Figure 2.3. The operation of this Hy-Sol-CLC GTCC has been also compared with that of a conventional solar hybrid GTCC, in which concentrated solar thermal energy, as supplementary heat source, is used in the bottoming regenerative Rankine cycle. Hong *et al*. [127] showed that the Hy-Sol-CLC GTCC can achieve a net solar to electrical efficiency of 31.8% which is around 7.4 percentage points higher than that of the assessed solar hybrid GTCC. However, this is achieved at the cost of decreasing the instantaneous solar thermal share from 28.6% for the conventional hybrid solar GTCC to 18.65% for the Hy-Sol-CLC GTCC.

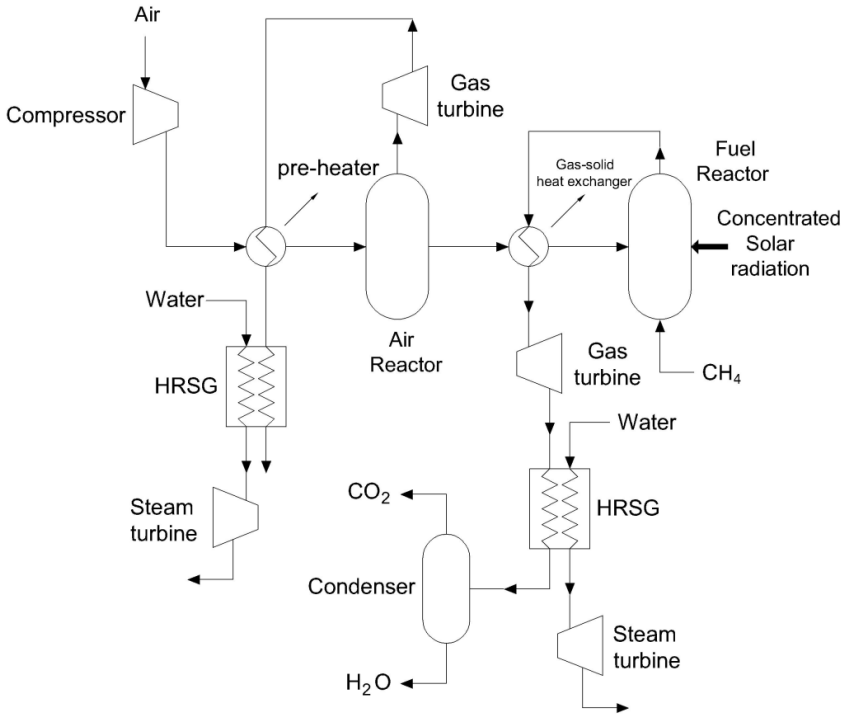

Figure 2.7. The Flow diagram for the solar hybrid systems proposed by Hong *et al*. [127]. The solar thermal energy is used to drive the reaction between NiO and CH_4. The outlet streams from the reduction and oxidation reactions are utilised for power generation through two gas turbines. Two heat recovery steam generators along with steam turbines have been also applied to increase the cycle efficiency.

More recently, Hong *et al.* [128] reported another Hy-Sol-CLC GTCC integrating methanol-fuelled CLC with low temperature solar thermal energy at 200 °C. This process is shown in Figure 2.8 and also employs two main sections. In the first section methanol is evaporated and introduced into a reduction reactor in which it reacts with Fe_2O_3, as oxygen carrier, producing FeO, CO_2 and H_2O. The heat required for both the evaporation of methanol and its endothermic reaction with Fe_2O_3 is provided by solar thermal energy at a temperature of 200

°C. The FeO produced is then oxidized in the oxidation reactor to produce a high temperature gas stream at 1000 °C. In the second section, to enhance the efficiency of the gas turbine, the hot gas stream so produced from oxidation reactor is further heated to 1400 °C through combustion of methanol in an after-burner prior to introduction to a gas turbine. A HRSG and a steam Rankine cycle were also utilised to increase the efficiency of the power cycle. They also modelled a conventional hybrid solar GTCC. And showed that this Hy-Sol-CLC GTCC can achieve a solar to electrical efficiency of 22.3% which is around 6.0 point percentages more than that of the considered conventional solar hybrid GTCC. However, the instantaneous solar share of the hybrid system is decrease from 24.9 to 15.54% using the CLC-based hybrid system.

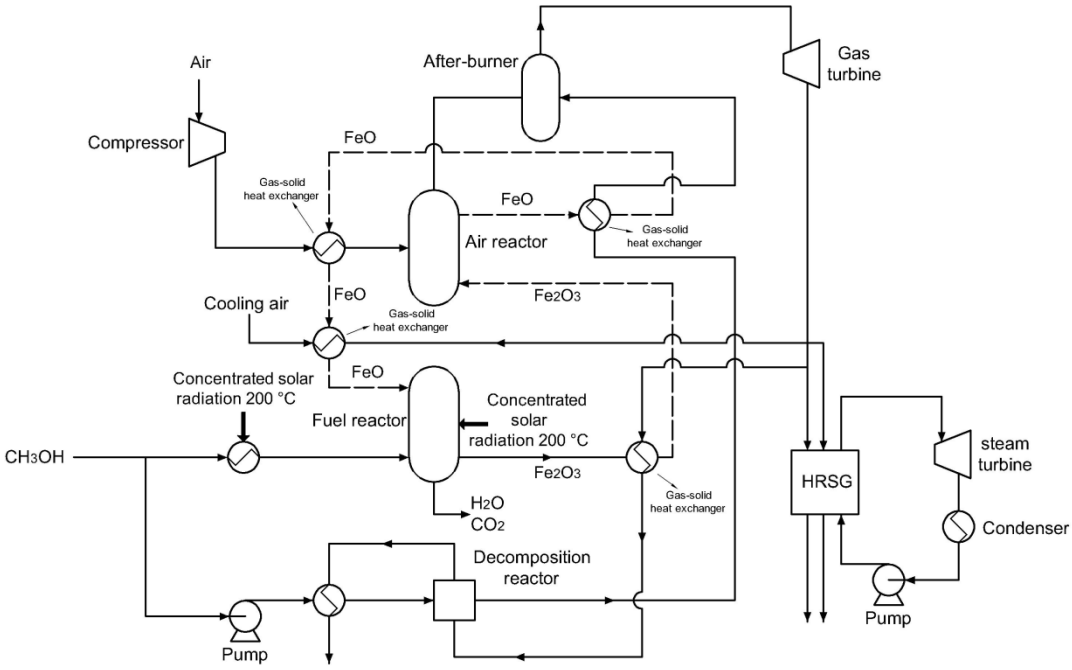

Figure 2.8. Flow diagram of a solar-hybrid thermal cycle with methanol fuelled chemical looping combustion adopted from [128]. The after-burner is used to further the temperature of hot stream produced in the air reactor. The outlet streams from both turbines are used to produce more power through a heat recovery steam generator and a bottoming Rankine cycle.

In all of these hybrids solar GTCCs concentrated solar thermal energy is mainly used as a heat source to provide either the heat of endothermic reactions of the fuel and oxygen carriers or the energy to preheat the reactants. Therefore, advantageously in this cycle solar thermal energy is converted to chemical energy at a lower temperature than that at which it is released. This favourably not only reduces the re-radiation losses from the solar receivers but also increases the solar to electrical efficiency of the cycles. However, the solar share in these cycles has not been assessed considering the impact of diurnal, cloud induced and seasonal transience in solar insolation. Over these much larger time scales the solar share

of these processes would be significantly lower than those reported, which only examine instantaneous performance when solar energy completely satisfies the process thermal demand.

In conclusion, to the best of our knowledge, no previous investigation has assessed or proposed the application of OC particles within a CLC system for diurnal solar thermal energy storage. Such a solar hybrid system offers not only the potential to address the challenge of the intermittency of solar thermal energy but also presents the opportunity to reduce the cost of storage for solar thermal energy through sharing the infrastructure. Therefore, one of the aims of this thesis is to investigate the novel concept of Hy-Sol-CLC systems in which solar thermal energy can be stored diurnally with a high solar share and solar to electrical efficiency, using CLC system components.

2.5.3. Oxygen carrier materials

The large scale utilization of CLC depends on the availability of suitable oxygen carriers [129]. A suitable oxygen carrier should satisfy the following criteria [129-132]:

- withstand a large number of oxidation and reduction reaction cycles with a high reactivity to fully combust the hydrocarbon fuels.
- have a good capability for fluidization with resistance to agglomeration.
- have a high melting point, active surface area, particles pore volume, and mechanical resistant to friction.
- be environmentally benign and economically viable.

Several investigations have shown that the oxides of transition metals Ni, Cu, Co, Fe and Mn are good oxygen carrier candidate given their favourable reductive/oxidative thermodynamics [84, 133, 134]. These are often doped with an inert e. g. $NiAl_2O_4$, Al_2O_3, TiO_2, MgO and yttria-stablized zirconium (YSZ) with a view to increasing their reactivity and durability during the reactions [131, 133]. The combinations of these active and inert materials have been the subject of many experimental and numerical studies. The reactivity and mechanical strength of 240 samples of potential oxygen carriers composed of 40-80 % Cu, Mn and Ni oxides as active metal solids and Al_2O_3, sepiolite, SiO_2, TiO_2, or ZrO_2 as inert using CH_4 as fuel was investigated by Adanez *et al.* [135]. They showed that for Cu-based oxygen carriers SiO_2 and TiO_2 are the best inert binders while for Fe-based oxygen carriers Al_2O_3 and ZrO_2 are more suitable. They also demonstrate that the OC particles prepared with the oxides of Mn and Ni behave more efficiently with ZrO_2 and TiO_2, respectively, than other assessed inert materials. Approximately, 300 different oxygen carriers based on the oxides of Ni, Fe, Mn and Cu, as active components, and Al_2O_3, sepiolite, SiO_2, TiO_2 and ZrO_2, as inert, were assessed by Mattisson *et al*. [136]. They found that a high reactivity can be achieved with Mn, Fe and Cu oxygen carriers and these cheaper and more environmental friendly metal oxides may be better candidates than Ni which is more expensive. An inclusive thermal investigation of various oxygen carriers based on the oxides of Ni, Cu, Fe, Mn, Co, W and sulphates of Ba and Sr for three fuels; namely, CH_4, CO and H_2, was reported by Jerndal *et al*. [130]. They used HSC Chemistry software for their equilibrium calculation. The oxygen carriers were analysed for their ability to convert the fuel to the combustion products CO_2

and H_2O, stability in air and the melting temperatures of the solid material. They showed that only a few of these potential oxygen carriers, based on Cu, Fe and Mn, can achieve complete conversion of the fuel. They also showed that the oxides of Ni, W, BaS and SrS are highly promising, even though their reactions with fuels are not fully completed. The favorable reduced/oxidized pairs were investigated further considering the possible carbon, sulphide and sulphate formation in the fuel reactor. They found that the fuel needs to be de-sulphurised prior to being oxidized by Ni and Co, to avoid formation of sulphates and/or sulphides, while it is necessary to have some sulphur in the fuel to prevent decomposition of the $BaSO_4$ and $SrSO_4$ in the fuel reactor.

In the following section an overview of each type of the metal oxides is presented.

2.5.3.1. Co-based oxygen carriers

Cobalt oxide is a potential oxygen-carrier because of its high oxygen transport capacity. Nevertheless, it is expensive relative to other possible metal oxides and there are some environmental concerns about its applications [84, 85]. Three main oxidation states; namely, Co_3O_4, CoO and Co, can be involved in the reduction/oxidation reactions of Co. However, Co_3O_4 is unstable above 950 °C and decomposes to CoO. Therefore, only the reduction of CoO to Co is applicable in CLC systems [85] although this reaction is not favourable in terms of fuel conversion efficiency and decreases the fuel conversion efficiency [85, 137]. Hence, little work has been reported on this type of materials. Jin *et al.* [138] developed Co-based OC particles using Yttria-stabilised zirconia (YSZ) as inert.

Good reactivity and low carbon deposition was observed. A similar test was performed by Mattisson *et al*. [139] using γ-Al_2O_3 as inert.

2.5.3.2. Cu-based oxygen carriers

Cu-based oxygen carriers have a high oxygen transfer capacity with no thermodynamic limitations for the complete conversion of fuels [134, 137]. They are also highly reactive with Al_2O_3, SiO_2, sepiolite, TiO_2 and ZrO_2, regardless of the preparation method used [139-141]. Furthermore, copper is cheaper than other materials used for CLC such as Ni and Co [142-144]. However, the main concern regarding the application of Cu-based oxygen carriers for CLC systems is associated with the agglomeration problem, which is due to the low melting point of Cu (1085 °C) [139, 145].

2.5.3.3. Fe-based oxygen carriers

Iron is not only environmentally benign but also one of the cheapest metals available [84, 85]. In addition, iron oxides are thermodynamically quite favorable for the complete conversion of fuel to CO_2 and H_2O [137]. As a result, despite the low oxygen transport capability of Fe-based metal oxides, they are considered as an attractive oxygen carrier for CLC systems. Different oxidation states can be found for iron; namely, Fe_2O_3, Fe_3O_4, FeO and Fe. However, only the transformation from hematite (Fe_2O_3) to magnetite (Fe_3O_4) can be used in industrial CLC systems [125] because further reduction of Fe_3O_4 to FeO and/or Fe leads to both agglomeration problems in the bed [146] and to a decrease in the purity of CO_2 obtained [111, 137]. Several, investigations have demonstrated that

Fe-based oxygen carriers have adequate reactivity with natural gas and specially syngas both at atmospheric [125, 133, 147, 148] and pressurized conditions [149]. The application of natural mineral iron oxides, as ore, [150-152] and synthesis particles using different support materials e. g. Al_2O_3, $MgAl_2O_4$, TiO_2 and SiO_2, have been also investigated in detail [147, 153-156].

2.5.3.4. Mn-based oxygen carriers

Manganese is a non-toxic and cheap metal with an oxygen transport capacity higher than that of iron [85]. As with Fe, Mn also has several oxidation states; namely, MnO_2, Mn_2O_3, Mn_3O_4 and MnO [157]. The highest oxidised manganese, MnO_2, decomposes to Mn_2O_3 at around 773 K, whereas Mn_2O_3 is thermodynamically stable in air at temperatures lower than 1173 K. At temperatures below 1100 K, MnO can be oxidized to Mn_2O_3 in air. Additionally, Mn_3O_4 is the only form of Mn oxides that is stable in air at temperatures higher than 1073 K [157, 158]. It has been demonstrated that pure manganese has as a low reactivity in reaction with coal and methane [159]. The reactivity also does not improve using Al_2O_3, SiO_2, TiO_2 and $NiAl_2O_4$ as support [135], which is due to the production of highly irreversible and non-reactive phases between the active and inert materials. The reactivity of particles supported with ZrO_2 has been also investigated and very high conversion efficiencies have been achieved.

2.5.3.5. Nickel-based oxygen carriers

Ni-based oxygen carriers, as both bulk and supported with inert binders, have been the most extensively analysed materials in the literature. Early experimental

works were done in either thermo-gravimetric analyzers (TGA) or fixed bed reactors in Japan [160, 161]. These studies demonstrated that the NiO reduction reaction is fast enough to be employed in practice, the fuel oxidation reaction is nearly completed and that the soot formation or carbon deposition on the particles did not appear to be a major problem if the oxidation reaction was carried out at a high enough temperature [162]. However, typically the performance of pure NiO decreases in the repeated reduction/oxidation cycles, which is due to the agglomeration of the particles [163]. Therefore, supported NiO/Ni oxygen carrier particles by inerts, e.g. Al_2O_3, $NiAl_2O_4$, $MgAl_2O_4$, MgO, ZrO_2, bentonite and sepiolite, are preferred and receiving growing attention [93, 133, 164-169].

Among different proposed support materials, the oxygen carriers supported by AL_2O_3 has been studied more comprehensively [84, 85]. This is due to their low attrition rates during the operation in the fluidized beds, high thermal stability, low carbon deposition and no agglomeration problems [164, 170-173]. However, the side reaction of NiO and Al_2O_3 leads to the production of spinal component $NiAL_2O_4$ [93, 164, 174, 175], which has poor reactivity for CLC systems [164, 165]. The application of $NiAl_2O_4$ as support has been also investigated by several researchers. Johansson *et al.*[176] investigated the performance of the OC particles composed of $NiAl_2O_4$ and NiO, with a mass ratio of 6 to 4, for the combustion of CH_4 in a 10 kW CLC prototype for 100 h. Possible chemical and physical property changes were studied. They showed not only no major changes had occurred but also the used OC particles were harder than fresh ones and had a similar reactivity to the gaseous fuel. In addition, the composition of the particles had remained unchanged, indicating that no irreversible reactions had occurred

within the particles. Similar experiments were performed by Linderholm *et al.* [177] for the combustion of natural gas using an oxygen carrier consisting of 60 wt% NiO and 40 wt% $NiAl_2O_4$ in a 10 kW CLC reactor system for 160 h of operation. The results were in agreement with those presented by Johansson *et al*. [176] and a total particle life time of 4500 h was estimated based on the attrition rate measured. Estimated life time of 40000 h and 33000 for the OC particles composed of NiO/Al_2O_3 and $NiO/(NiAl_2O_4+MgAl_2O_4)$, respectively, have been also reported in literature [85, 178].

2.5.3.6. Complex metal oxides

Complex mixed metal oxides have been also proposed to be used as oxygen carrier in CLC systems in order to improve the particles reactivity, stability, mechanical strength and to decrease the carbon deposition, the cost of oxygen carrier preparation and the use of toxic metals [85]. The investigations have been performed either by mixing different active metal oxides into the same particle or mixing different oxygen-carriers composed by single metal oxides [85]. Jin *et al.* [138] studied the synergetic combination of NiO and CoO supported by Yttria-stabilized zirconia (YSZ). A great performance was achieved in the fuel conversion, high reactivity and avoidance of carbon deposition. The behavior of a number of $Ni\text{-}Cu/Al_2O_3$ in increasing the efficiency of fuel conversion during the CLC operation working at high temperatures was studied by Adanez *et al.* [179]. They found that the presence of NiO stabilizes the CuO and allows working at 950 °C. It was also shown that the addition of CuO to Ni-based oxygen carriers improves their efficiency in fuel conversion. The same results were reported by

Johansson *et al.* [180] for mixed Fe and Ni oxygen carriers. The Fe-Mn mixed oxides were studied by Lambert *et al.* [181] to assess the cooperative effect in between the two metals. They found that these mixed oxides, depending on their synthesis technique, show a lower oxygen transfer capacity than that of Ni. In addition to bimetallic and mixed oxides oxygen carriers, other more complex oxygen carriers with pervoskite structure have been also proposed [182, 183]. Nevertheless, the long term operation of these materials in CLC reactors is mostly unknown [85].

To summarise, although several metal oxides with a variety of fuels have been proposed and tested for application in CLC systems, the potential advantages and disadvantages of these alternative oxygen carriers and inert materials for use in a Hy-Sol-CLC system have not been investigated yet. Besides, hybridisation of CLC with solar thermal energy introduces more limitations and characteristics in the performance of the OC particles.

2.6. Configuration of the Chemical Looping Combustion (CLC) reactors

Efficient operation of a CLC process depends on:

- appropriate contact between the oxygen carriers and the gas phase through both the oxidation and reduction reactions;
- high conversion efficiency of fuel oxidation to CO_2 and H_2O;
- adequate conversion of solids in both of the oxidation and reduction reactions;

- efficient transfer of the oxygen carriers between the oxidation and reduction reaction zones with restricted gas leakage;
- consistent and reliable operation of both the fuel and air reactors as well as long term operation of oxygen carriers.

To achieve these criteria, different CLC reactor configurations have been proposed, which can be mainly categorised as interconnected fluidised bed and fixed bed configurations [184, 185].

2.6.1. Interconnected fluidized bed reactors

The majority of the CLC plants existing worldwide use the two interconnected fluidized bed reactors [85, 186], one as a fuel reactor, in which the fluidised OC particles are reduced via fuel (reaction 2.1), and the other as air reactor, in which the fluidised reduced OC particles are oxidised by oxygen from air (reaction 2.2) [85]. Schematic representation of these systems is shown in Figure 2.9. During the CLC operation the OC particles are pneumatically transported between the air and fuels reactors. Typically, loop seal devices have been also applied to avoid the leakage of the gas between the fuel and air reactors. This design has the following main advantages [187-189]:

- high heat and mass transfer coefficients within the fuel and air reactors due to the perfect mixing of the particle;
- homogeneous and nearly uniform temperature distribution within both reactors;
- continuous production of a hot gas stream for power generation.

The major drawbacks of the interconnected fluidised bed reactors are related to [186, 190, 191]:

- problems associated with the sufficient particle circulation between the fuel and air reactors;
- the gas leakage between the fuel and air reactors, which leads to decreased CO_2 separation efficiency;
- the pressure drop throughout the reactors;
- the separation of the OC particles from the gas streams;
- the attrition and agglomeration of the OC particle due to the collisions within the fluidised bed reactors at high temperature;
- the gas leakage between the reactors.

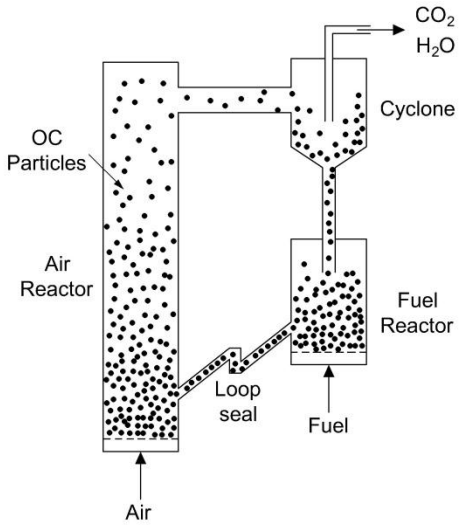

Figure 2.9. Schematic view of two interconnected fluidized bed, adopted from [85]. A high velocity riser is used to provide the required elevation for the particles to circulate through the system. The fuel reactor is a low velocity fluidised bed.

A variety of interconnected fluidized bed reactors have been proposed varying typically on the sealing technique used and the control of the solid circulation between the two fluidised bed reactors. One of the earliest designs was proposed by Lyngfelt *et al*. [134] in 2001. Their system comprises a low velocity bubbling fuel reactor, a high velocity riser air reactor, a cyclone for the separation of the OC particles and two gas seals. In this system the gas velocity in the riser air reactor provides the driving force for the circulation of particles between the two reactors beds. The high velocity riser is devoted to the air reactor due to the higher flow rate of air than that of fuel. Later a 10 kW_{th} CLC prototype based on this design was built and run by Lyngfelt *et al*. [187] in 2004, using nickel-based OC particles and natural gas as fuel. A combustion efficiency of 99.5% was achieved during a total operation time of more than 100 h with no sign of gas leakage between the air and fuel reactors. This CLC system was then used by Linderholm *et al*. [177] to study application of the OC particles consisting of 60% NiO and 40% $NiAl_2O_4$ for 160 h of operation. During these experiments the operating temperature of the air reactor was kept constant at 1000 °C while the operating temperature of the fuel reactor varied in the range of 660-950 °C. A nearly complete conversion of fuel, approximately 99%, as well as no indication of decrease in reactivity of the OC particles was seen during the test period. Similar experiments in a 10 kW_{th} CLC system with the interconnected fluidised bed reactors were performed by Adanez *et al*. [192] for 200 h. These experiments were the first long time demonstration of the application of the Cu-based OC particles in a CLC system. Similarly, no serious leakage of gas was found. They demonstrated that the fuel conversion efficiency is mostly affected by both the

temperature of the fuel reactor and the oxygen carrier to fuel ratio. Ryu *et al*. [193] reported results of a 50 kW_{th} CLC system for the combustion of CH_4 using two types of OC particles based on the oxides of nickel and cobalt. They found that the nickel-based OC particles provide higher conversion efficiency than cobalt-based OC particles. Several experiments with different OC particles in a two interconnected circulating fluidised bed reactors were performed by ALSTOM Power Boilers [194] to study the attrition behaviour of the OC particles. Forero *et al.* [195] tested Cu-based OC particles in a 500 W_{th} CLC using syngas as fuel. Their atmospheric CLC system comprises two interconnected bubbling fluidized bed reactors that were separated by a loop seal and a cyclone. A riser and a solid valve were also added to the system to improve the control of the circulation of the OC particles between the bubbling fuel and air reactors. A nearly full conversion of fuel was achieved during the experiments and after 40 h of operation, significant sign of agglomeration, attrition, and carbon deposition was not found. De Diego *et al.* [142] used a bubbling fluidised bed as the air reactor in a 10 kW_{th} CLC prototype. In their CLC system a separated riser was proposed after the air reactor. A loop-seal was also proposed. A good reactivity of the Cu-based OC particles was found with no agglomeration during 100 h of operation. A dual circulating air and fuel reactors were used in a 120 KW_{th} CLC developed by Kolbitsch *et al*. [123, 196] and Proll *et al*. [197-199]. In this system both air and fuel reactors operate in the turbulent regime, improving the gas and solid contact within the reactors. The system was fed with either natural gas or mixtures of CH_4, CO, H_2, and higher hydrocarbons. Ilmenite, which is a natural iron titanium ore, and a designed Ni-based particle were used as oxygen carrier. In

all cases assessed the fuel was almost fully converted to CO_2 and H_2O. They also succeeded in controlling of the solid flow rate through the system based on the aeration rate in the air reactor, independent of the fuel reactor operating conditions. A CLC system with two-compartment fluidized bed reactors was proposed by Kronberger *et al*. [200]. The system comprises two adjacent fluidised bed reactors, which are separated by a vertical wall. A downcomer and a slot were also used to circulate the OC particles between the air and fuel reactors. In this system the air reactor has a high velocity causing the particles to be thrown into a down comer, where they are directed to the fuel reactor. This results in a higher pressure in the fuel reactor, pushing the particles back into the air reactor through the slot. This system suffers from a high leakage of gas between the fuel and air reactors, which in turn decreases the performance of the CLC in separation of CO_2 from flue gases, even though its simple configuration can decrease the capital costs. Operation of a pressurised CLC has been reported by Wang *et al*. [201]. The system maximum operating temperature is 950 °C and the pressure was maintained at 0.3 MPa during the 15 h experiment. The reactivity of four potential oxygen carrier particles composed of Fe_2O_3/CuO, as active metal oxides, supported on $MgAl_2O_4$ was assessed. However, the maximum fuel conversion reached was 92.3%. Combustion of the solid fuels in the interconnected fluidised bed reactors has been also investigated by many researchers. In these systems, typically the solid fuel is first gasified and then the produced syngas is oxidised by the OC particles [202-204].

2.6.2. Fixed bed reactors

To avoid the problems associated with the separation of gas and particles and to minimize the gas leakage between the fuel and air reactors, a concept of dynamically operated packed bed reactor was proposed by Noorman *et al.* [191, 205, 206]. In this concept, as shown schematically in Figure 2.10, the solid oxygen carriers are stationary in a fixed bed reactor and are alternately exposed to reducing/oxidizing conditions through periodic switching of the fuel and air streams.

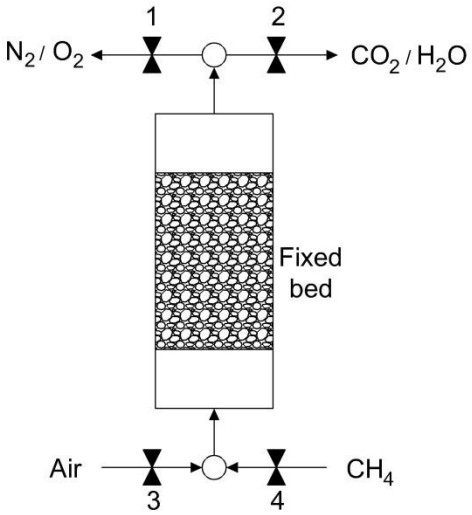

Figure 2.10. Schematic representation of a periodically operated packed bed reactor taken from [191, 205, 206]. The valves 1-4 are used to periodically switch the fuel and air streams.

The advantages of this system is that the separation of solid and gas phases is intrinsically avoided, is that the reactor design can be much more compact and is that a nearly complete fuel conversion can be achieved while the oxygen carriers are used over the entire range of their oxidation state [191, 205, 206].

Disadvantage of the system includes the need for complicated control systems both to switch the fuel and air streams and to provide the inert gases, as a purge stream, in between the gas switching times. Furthermore, changing the oxidizing condition to the reducing one can lead to a large temperature drop within the fixed bed [191, 205, 206], which in turn causes thermal shocks and increases the long term operational and maintenance costs.

The rotating bed reactor is a kind of modified packed bed reactor [186]. The concept is shown schematically in Figure 2.11. In this reactor, the oxygen carrier particles are fixed in a doughnut shaped fixed bed reactor. The reactor rotates, when fuel and air streams are introduced radially outward through the reactor. Between the fuel and air sectors an inert gas e. g. steam or N_2 is fed to avoid the mixing of reacting gases and explosion. The main advantages of this design are both the continuous operation and the compactness of the design. However, the main drawback is associated with the gas leakage and dilution between fuel and air streams [186, 207].

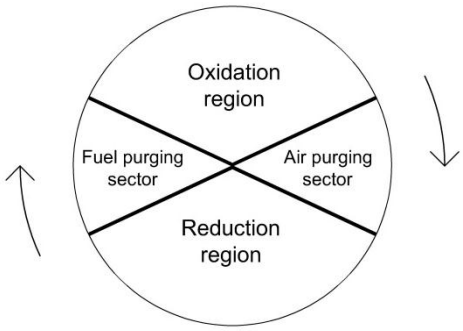

Figure 2.11. Schematic representation of a rotating fixed bed reactor taken from [186, 207]. The reactor rotates while the air and fuels gases are fed radially. An inert gas section is also applied in between the oxidation and reduction sectors to avoid the fuel and air mixing.

In conclusion, even though the operation of the CLC systems in lab scale prototypes has been demonstrated, further investigations are required for their demonstration in pilot plant and commercial scales. In addition, none of the aforementioned concepts of CLC reactors have been especially designed for Hy-Sol-CLC systems. The solar fuel reactor of a Hy-Sol-CLC system, in addition to the efficient operation in the CLC cycle, should also provide the capability for efficient harnessing of the concentrated solar thermal energy. Therefore, further investigation is required to develop the principle knowledge required for the design and operation of the efficient hybrid solar fuel reactors for the Hy-sol-CLC systems.

2.7. Solar reactors

Previous investigations have demonstrated that the cavity-type solar reactor configurations are the most appropriate configuration for harnessing highly

concentrated solar radiation [208]. Thus far a wide range of solar cavity solar reactors have been proposed which can be categorized by those that directly [209-211] or indirectly [212, 213] utilize the concentrated solar heat to drive the endothermic reactions. The reactors have been also categorised as those that are oriented horizontally [210, 214, 215] or vertically [212, 216] to incoming concentrated sunlight.

In direct absorption reactors concentrated solar thermal energy is directly introduced to the reaction site. Therefore, a transparent window is required [1], which is vulnerable to high pressures and/or harsh environments [68, 217]. In indirect solar reactor either an intermediate heat transfer fluid or a conductive separating medium is used between the solar radiation absorption surface and the chemical reactions sites. As a result, the need for transparent window is eliminated [1, 217]. However, the disadvantages are mainly associated with the limitations in the maximum operating temperature, thermo-physical properties of heat transfer mediums, resistance to thermal shocks, inertness and suitability for transient operation [217]. Direct heating can achieve more efficient heat transfer rates than that of indirect heating, due to the elimination of heat losses and thermal resistances in conduction and convection mechanisms, which is advantages in term of system efficiency [217].

In conclusion, despite the large number of proposed direct and indirect solar reactors [210, 218-220], none of these are well suited to the Hy-Sol-CLC processes. This is mainly because of the fact that previous solar reactors have been proposed for other processes such as solar gasification [218, 221] and solar ZnO dissociation [211, 222] in which particles are consumed within the reactor, in

contrast to the Hy-Sol-CLC processes in which the OC particles are regenerated for reuse. Therefore, there is a need for further analysis to better understand the detailed characteristics of existing direct and indirect heated reactors and to develop the fundamental knowledge required for the design and operation of efficient solar reactors for Hy-Sol-CLC systems.

References

[1] Romero M, Steinfeld A. Concentrating solar thermal power and thermochemical fuels. Energy & Environmental Science. 2012;5:9234-45.

[2] Romero M, González-Aguilar J. Energy and Power Generation Handbook: Established and Emerging Technologies. In: Rao KR, editor: American Society of Mechanical Engineers; 2011.

[3] Mills D. Advances in solar thermal electricity technology. Solar Energy. 2004;76:19-31.

[4] Zhang HL, Baeyens J, Degrève J, Cacères G. Concentrated solar power plants: Review and design methodology. Renewable and Sustainable Energy Reviews. 2013;22:466-81.

[5] Barlev D, Vidu R, Stroeve P. Innovation in concentrated solar power. Solar Energy Materials and Solar Cells. 2011;95:2703-25.

[6] Meng L, Bilton AM, You Z, Dubowsky S. Adaptive heliostat solar arrays using shape-optimized compliant mirrors. ASME Proceedings | 36th Mechanisms and Robotics Conference; 2012. p. 331-40.

[7] Technology Roadmap: Concentrating Solar Power. 2010.

[8] Duffie JA, Beckman WA. Solar Engineering of Thermal Processes: Wiley; 2006.

[9] Gil A, Medrano M, Martorell I, Lázaro A, Dolado P, Zalba B, et al. State of the art on high temperature thermal energy storage for power generation. Part 1-Concepts, materials and modellization. Renewable and Sustainable Energy Reviews. 2010;14:31-55.

[10] M. N. Azpiazu, J. M. Morquillas, A. Vazquez. Heat recovery from a thermal energy storage based on the Ca(OH)2/CaO cycle. Applied Thermal Engineering. 2003;23:733-41.

[11] A. Sharma, V. V. Tyagi, C. R. Chen, D. Buddhi. Review on thermal energy storage with phase change materials and applications. Renewable and Sustainable Energy Reviews. 2009;13:318-45.

[12] Cabeza LF. 3.07 - Thermal Energy Storage. In: Sayigh A, editor. Comprehensive Renewable Energy. Oxford: Elsevier; 2012. p. 211-53.

[13] Py X, Calvet N, Olives R, Meffre A, Echegut P, Bessada C, et al. Recycled material for sensible heat based thermal energy storage to be used in concentrated solar Thermal Power Plants. Journal of Solar Energy Engineering. 2011;133:031008.

[14] Herrmann U, Kearney DW. Survey of thermal energy storage for parabolic trough power plants. Journal of Solar Energy Engineering. 2002;124:145-52.

[15] Laing D, Steinmann W-D, Tamme R, Richter C. Solid media thermal storage for parabolic trough power plants. Solar Energy. 2006;80:1283-9.

[16] Laing D, Bahl C, Bauer T, Lehmann D, Steinmann W-D. Thermal energy storage for direct steam generation. Solar Energy. 2011;85:627-33.

[17] Kuravi S, Trahan J, Goswami DY, Rahman MM, Stefanakos EK. Thermal energy storage technologies and systems for concentrating solar power plants. Progress in Energy and Combustion Science. 2013;39:285-319.

[18] Robak CW, Bergman TL, Faghri A. Economic evaluation of latent heat thermal energy storage using embedded thermosyphons for concentrating solar power applications. Solar Energy. 2011;85:2461-73.

[19] Yang Z, Garimella SV. Thermal analysis of solar thermal energy storage in a molten-salt thermocline. Solar Energy. 2010;84:974-85.

[20] Price H, Lupfert E, Kearney D, Zarza E, Cohen G, Gee R, et al. advances in parabolic trough solar power technology. Journal of Solar Energy Engineering. 2002;124:109-25.

[21] Kolb GJ. Economic evaluation of solar-only and hybrid power towers using molten-salt technology. Solar Energy. 1998;62:51-61.

[22] Group SLLC. Assessment of parabolic trough and power tower solar technology cost and performance forecasts. Chicago, Illinois: National Renewable Energy Laboratory (NREL); 2003.

[23] Tamme R, Laing D, Steinmann W-D. Advanced thermal energy storage technology for parabolic trough. Journal of Solar Energy Engineering. 2004;126:794-800.

[24] Morrison DJ, Abdel-Khalik SI. Effects of phase-change energy storage on the performance of air-based and liquid-based solar heating systems. Solar Energy. 1978;20:57-67.

[25] Ghoneim AA. Comparison of theoretical models of phase-change and sensible heat storage for air and water-based solar heating systems. Solar Energy. 1989;42:209-20.

[26] Mehling H, Cabeza L. Phase change materials and their basic properties. In: Paksoy H, editor. Thermal Energy Storage for Sustainable Energy Consumption: Springer Netherlands; 2007. p. 257-77.

[27] Couto Aktay KS, Tamme R, Müller-Steinhagen H. Thermal conductivity of high-temperature multicomponent materials with phase change. Int J Thermophys. 2008;29:678-92.

[28] Glatzmaier G. Summary Report for Concentrating Solar Power Thermal Storage Workshop: New Concepts and Materials for Thermal Energy Storage and Heat-Transfer Fluids. NREL; 2011.

[29] Harries DN, Paskevicius M, Sheppard DA, Price TEC, Buckley CE. Concentrating solar thermal heat storage using metal hydrides. Proceedings of the IEEE. 2012;100:539-49.

[30] S. M. Hasnain. Review on sustainable thermal energy storage technologies, Part II: cool thermal storage 1998.

[31] A. Gil, M. Medrano, I. Martorell, a. Lázaro, P. Dolado, B. Zalba, et al. State of the art on high temperature thermal energy storage for power generation. Part 1-Concepts, materials and modellization. Renewable and Sustainable Energy Reviews. 2010;14:31-55.

[32] Schaube F, Wörner A, Tamme R. High temperature thermochemical heat storage for concentrated solar power using gas–solid reactions. Journal of Solar Energy Engineering. 2011;133:031006-.

[33] Kodama T, Gokon N. Thermochemical cycles for high-temperature solar hydrogen production. Chemical Reviews. 2007;107:4048-77.

[34] Lovegrove K, Luzzi A, Soldiani I, Kreetz H. Developing ammonia based thermochemical energy storage for dish power plants. Solar Energy. 2004;76:331-7.

[35] Fedders H, Höhlein B. Operating a pilot plant circuit for energy transport with hydrogen-rich gas. International Journal of Hydrogen Energy. 1982;7:793-800.

[36] Samms JAC, Evans BE. Thermal dissociation of $Ca(OH)_2$ at elevated pressures. Journal of Applied Chemistry. 1968;18:5-8.

[37] Schmidt P. On the design of a reactor for high temperature heat storage by means of reversible chemical reactions KTH; 2011.

[38] Agyenim F, Hewitt N, Eames P, Smyth M. A review of materials, heat transfer and phase change problem formulation for latent heat thermal energy storage systems (LHTESS). Renewable and Sustainable Energy Reviews. 2010;14:615-28.

[39] Kaniyal AA, Nathan GJ, Pincus JJ. The potential role of data-centres in enabling investment in geothermal energy. Applied Energy. 2012;98:458-66.

[40] Sheu EJ, Mitsos A, Eter AA, Mokheimer EM, Habib MA, Al-Qutub A. a review of hybrid solar–fossil fuel power generation systems and performance metrics. Journal of Solar Energy Engineering. 2012;134:041006.

[41] Buck R, Brauning T, Denk T, Pfander M, Schwarzbozl P, Tellez F. Solar-hybrid gas turbine-based power tower systems (REFOS). Journal of Solar Energy Engineering. 2002;124:2-9.

[42] Smith JM, Van Ness H, Abbott MM. Introduction to Chemical Engineering Thermodynamics: McGraw-Hill Education; 2005.

[43] Buck R, Barth C, Eck M, Steinmann W-D. Dual-receiver concept for solar towers. Solar Energy. 2006;80:1249-54.

[44] Dersch J, Geyer M, Herrmann U, Jones SA, Kelly B, Kistner R, et al. Trough integration into power plants—a study on the performance and economy of integrated solar combined cycle systems. Energy. 2004;29:947-59.

[45] Dunham MT, Iverson BD. High-efficiency thermodynamic power cycles for concentrated solar power systems. Renewable and Sustainable Energy Reviews. 2014;30:758-70.

[46] Barigozzi G, Bonetti G, Franchini G, Perdichizzi A, Ravelli S. Thermal performance prediction of a solar hybrid gas turbine. Solar Energy. 2012;86:2116-27.

[47] Zoschak RJ, Wu SF. Studies of the direct input of solar energy to a fossil-fueled central station steam power plant. Solar Energy. 1975;17:297-305.

[48] Pai PR. Augmentation of thermal power stations with solar energy. Sadhana. 1991;16:59-74.

[49] Deng S. Hybrid solar and coal-fired steam power plant based on air preheating. Journal of Solar Energy Engineering. 2013;136:021012-.

[50] Yang Y, Yan Q, Zhai R, Kouzani A, Hu E. An efficient way to use medium-or-low temperature solar heat for power generation–integration into conventional power plant. Applied Thermal Engineering. 2011;31:157-62.

[51] Tsiklauri G, Talbert R, Schmitt B, Filippov G, Bogoyavlensky R, Grishanin E. Supercritical steam cycle for nuclear power plant. Nuclear Engineering and Design. 2005;235:1651-64.

[52] Forsberg CW, Peterson PF, Zhao H. High-temperature liquid-fluoride-salt closed-brayton-cycle solar power towers. Journal of Solar Energy Engineering. 2006;129:141-6.

[53] Wheeldon JM. Engineering and Economic Evaluation of 1300F Series Ultra-Supercritical Pulverized Coal Power Plants: Phase 1, 1015699. 2008.

[54] Yan Q, Hu E, Yang Y, Zhai R. Evaluation of solar aided thermal power generation with various power plants. International Journal of Energy Research. 2011;35:909-22.

[55] Hung TC, Shai TY, Wang SK. A review of organic rankine cycles (ORCs) for the recovery of low-grade waste heat. Energy. 1997;22:661-7.

[56] Madhawa Hettiarachchi HD, Golubovic M, Worek WM, Ikegami Y. Optimum design criteria for an organic Rankine cycle using low-temperature geothermal heat sources. Energy. 2007;32:1698-706.

[57] Manolakos D, Kosmadakis G, Kyritsis S, Papadakis G. On site experimental evaluation of a low-temperature solar organic Rankine cycle system for RO desalination. Solar Energy. 2009;83:646-56.

[58] Ordorica-Garcia G, Delgado AV, Garcia AF. Novel integration options of concentrating solar thermal technology with fossil-fuelled and CO_2 capture processes. Energy Procedia. 2011;4:809-16.

[59] Hybridisation of fossil fuel energy generation in Australia. Asutralian Renewable Energy Agancy (ARENA); 2013.

[60] Hischier I. Developement os a pressurized receiver for solar-driven gas turbine: ETH ZURICH; 2011.

[61] Bhargava RK, Bianchi M, Pascale A, Negri di Montenegro G, Peretto A. gas turbine based power cycles- a state-of-the-art review. in: cen k, chi y, wang f, editors. challenges of power engineering and environment: Springer Berlin Heidelberg; 2007. p. 309-19.

[62] Chyu MK. recent advances in turbine heat transfer-with a view of transition to coal-gas based systems. Journal of Heat Transfer. 2012;134:031006-.

[63] Schwarzbözl P, Buck R, Sugarmen C, Ring A, Marcos Crespo MJ, Altwegg P, et al. Solar gas turbine systems: Design, cost and perspectives. Solar Energy. 2006;80:1231-40.

[64] Nathan GJ, Battye DL, Ashman PJ. Economic evaluation of a novel fuel-saver hybrid combining a solar receiver with a combustor for a solar power tower. Applied Energy. 2014;113:1235-43.

[65] Karni J, Rubin R, Sagie D, Fiterman A, Kribus A, Doron P. The DIAPR: a high-pressure, high-temperature solar receiver. Journal of Solar Energy Engineering. 1997;119:74-8.

[66] Pritzkow WEC. Pressure loaded volumetric ceramic receiver. Solar Energy Materials. 1991;24:498-507.

[67] Posnansky M, Pylkkänen T. Development and testing of a volumetric gas receiver for high-temperature applications. Solar Energy Materials. 1991;24:204-9.

[68] Ávila-Marín AL. Volumetric receivers in solar thermal power plants with central receiver system technology: a review. Solar Energy. 2011;85:891-910.

[69] Jarvinen PO. Solar-heated-air receivers. Solar Energy. 1977;19:139-47.

[70] Strumpf HJ, Kotchick DM, Coombs MG. High-Temperature Ceramic Heat Exchanger Element for a Solar Thermal Receiver. Journal of Solar Energy Engineering. 1982;104:305-9.

[71] Angelino G. perspectives for the liquid phase compression gas turbine. Journal of Engineering for Gas Turbines and Power. 1967; 89:229-36.

[72] Iverson BD, Conboy TM, Pasch JJ, Kruizenga AM. Supercritical CO_2 Brayton cycles for solar-thermal energy. Applied Energy. 2013;111:957-70.

[73] Moisseytsev A, Sienicki JJ. Investigation of alternative layouts for the supercritical carbon dioxide Brayton cycle for a sodium-cooled fast reactor. Nuclear Engineering and Design. 2009;239:1362-71.

[74] Marrero IO, Lefsaker AM, Razani A, Kim KJ. Second law analysis and optimization of a combined triple power cycle. Energy Conversion and Management. 2002;43:557-73.

[75] Kehlhofer R. Combined Cycle Gas and Steam Turbine Power Plants: PennWell Publishing Company; 1999.

[76] Rovira A, Montes MJ, Varela F, Gil M. Comparison of heat transfer fluid and direct steam generation technologies for integrated solar combined cycles. Applied Thermal Engineering. 2013;52:264-74.

[77] McGovern RK, Smith WJ. Optimal concentration and temperatures of solar thermal power plants. Energy Conversion and Management. 2012;60:226-32.

[78] Oda SD, Hashem HH. A case study for three combined cycles of a solar-conventional power generation unit. Solar & Wind Technology. 1988;5:263-70.

[79] Price H, Whitney D, Beebe B. SMUD Kokhala Power tower study. San Antonio, Texas: Proceedings of the International Solar Energy Conference; 1996. p. 273–6.

[80] Segal A, Epstein M. Optimized working temperatures of a solar central receiver. Solar Energy. 2003;75:503-10.

[81] Kakaras E, Doukelis A, Leithner R, Aronis N. Combined cycle power plant with integrated low temperature heat (LOTHECO). Applied Thermal Engineering. 2004;24:1677-86.

[82] Li Y, Yang Y. Thermodynamic analysis of a novel integrated solar combined cycle. Applied Energy. 2014;122:133-42.

[83] Montes MJ, Rovira A, Muñoz M, Martínez-Val JM. Performance analysis of an Integrated Solar Combined Cycle using Direct Steam Generation in parabolic trough collectors. Applied Energy. 2011;88:3228-38.

[84] Hossain MM, de Lasa HI. Chemical-looping combustion (CLC) for inherent CO_2 separations-a review. Chemical Engineering Science. 2008;63:4433-51.

[85] Adanez J, Abad A, Garcia-Labiano F, Gayan P, de Diego LF. Progress in Chemical-Looping Combustion and Reforming technologies. Progress in Energy and Combustion Science. 2012;38:215-82.

[86] Gibson-Poole CM, Edwards S, Langford RP, Vakarelov b. Review of geological storage opportunities for carbon capture and storage (CCS) in Victoria-Summary Report. Cooperative Research Centre for Greenhouse Gas Technologies; 2007.

[87] Pires JCM, Martins FG, Alvim-Ferraz MCM, Simões M. Recent developments on carbon capture and storage: An overview. Chemical Engineering Research and Design. 2011;89:1446-60.

[88] Fagerlund J, Nduagu E, Romão I, Zevenhoven R. CO_2 fixation using magnesium silicate minerals part 1: Process description and performance. Energy. 2012;41:184-91.

[89] Slotte M, Romão I, Zevenhoven R. Integration of a pilot-scale serpentinite carbonation process with an industrial lime kiln. Energy. 2013;62:142-9.

[90] Gibbins J, Chalmers H. Carbon capture and storage. Energy Policy. 2008;36:4317-22.

[91] Olajire AA. CO_2 capture and separation technologies for end-of-pipe applications– A review. Energy. 2010;35:2610-28.

[92] Blomen E, Hendriks C, Neele F. Capture technologies: Improvements and promising developments. Energy Procedia. 2009;1:1505-12.

[93] Mendes D, Mendes A, Madeira LM, Iulianelli A, Sousa JM, Basile A. The water-gas shift reaction: from conventional catalytic systems to Pd-based membrane reactors-a review. Asia-Pacific Journal of Chemical Engineering. 2010;5:111-37.

[94] Kanniche M, Bouallou C. CO_2 capture study in advanced integrated gasification combined cycle. Applied Thermal Engineering. 2007;27:2693-702.

[95] Damen K, Troost Mv, Faaij A, Turkenburg W. A comparison of electricity and hydrogen production systems with CO_2 capture and storage. Part A: Review and selection of promising conversion and capture technologies. Progress in Energy and Combustion Science. 2006;32:215-46.

[96] Fan L-S, Zeng L, Wang W, Luo S. Chemical looping processes for CO_2 capture and carbonaceous fuel conversion- prospect and opportunity. Energy & Environmental Science. 2012;5:7254-80.

[97] Woods MC, Capicotto PJ, Haslbeck JL, Kuehn NJ, Matuszewski M, Pinkerton LL, et al. Cost and Performance Baseline for Fossil Energy Plants. National Energy Technology Laboratory; 2007.

[98] Hagewiesche DP, Ashour SS, Al-Ghawas HA, Sandall OC. Absorption of carbon dioxide into aqueous blends of monoethanolamine and N-methyldiethanolamine. Chemical Engineering Science. 1995;50:1071-9.

[99] Ma'mun S, Svendsen HF, Hoff KA, Juliussen O. Selection of new absorbents for carbon dioxide capture. Energy Conversion and Management. 2007;48:251-8.

[100] Bai H, Yeh AC. Removal of CO_2 greenhouse gas by ammonia scrubbing. Industrial & Engineering Chemistry Research. 1997;36:2490-3.

[101] Menard D, Py X, Mazet N. Development of thermally conductive packing for gas separation. Carbon. 2003;41:1715-27.

[102] Burchell TD, Judkins RR. A novel carbon fiber based material and separation technology. Energy Conversion and Management. 1997;38, Supplement:S99-S104.

[103] Meratla Z. Combining cryogenic flue gas emission remediation with a CO_2/O_2 combustion cycle. Energy Conversion and Management. 1997;38, Supplement:S147-S52.

[104] Bounaceur R, Lape N, Roizard D, Vallieres C, Favre E. Membrane processes for post-combustion carbon dioxide capture: A parametric study. Energy. 2006;31:2556-70.

[105] Corti A, Fiaschi D, Lombardi L. Carbon dioxide removal in power generation using membrane technology. Energy. 2004;29:2025-43.

[106] Kwak K-O, Jung S-J, Chung S-Y, Kang C-M, Huh Y-i, Bae S-O. Optimization of culture conditions for CO2 fixation by a chemoautotrophic microorganism, strain YN-1 using factorial design. Biochemical Engineering Journal. 2006;31:1-7.

[107] Benemann JR. Utilization of carbon dioxide from fossil fuel-burning power plants with biological systems. Energy Conversion and Management. 1993;34:999-1004.

[108] Rao AB, Rubin ES. A Technical, Economic, and environmental assessment of amine-based CO_2 capture technology for power plant greenhouse gas control. Environmental Science & Technology. 2002;36:4467-75.

[109] Rubin ES, Chen C, Rao AB. Cost and performance of fossil fuel power plants with CO_2 capture and storage. Energy Policy. 2007;35:4444-54.

[110] Davison J. Performance and costs of power plants with capture and storage of CO_2. Energy. 2007;32:1163-76.

[111] Figueroa JD, Fout T, Plasynski S, McIlvried H, Srivastava RD. Advances in CO_2 capture technology-The U.S. Department of Energy's Carbon Sequestration Program. International Journal of Greenhouse Gas Control. 2008;2:9-20.

[112] Moghtaderi B. Application of chemical looping concept for air separation at high temperatures. Energy & Fuels. 2009;24:190-8.

[113] Lewis WK, Gilliland ER. Production of pure carbon dioxide. 1954.

[114] Richter Horst J, Knoche Karl F. Reversibility of combustion processes. efficiency and costing: American Chemical Society; 1983. p. 71-85.

[115] Richter HJ, Knoche KF. Reversibility of combustion processes. ACS Symposium1983. p. 71-85.

[116] Ishida M, Zheng D, Akehata T. Evaluation of a chemical-looping-combustion power-generation system by graphic exergy analysis. Energy. 1987;12:147-54.

[117] Ishida M, Jin H. A novel chemical-looping combustor without NO_x formation. Industrial & Engineering Chemistry Research. 1996;35:2469-72.

[118] Wolf J, Anheden M, Yan J. Comparison of nickel- and iron-based oxygen carriers in chemical looping combustion for CO2 capture in power generation. Fuel. 2005;84:993-1006.

[119] Consonni S, Lozza G, Pelliccia G, Rossini S, Saviano F. Chemical-looping combustion for combined cycles with CO_2 capture. Journal of Engineering for Gas Turbines and Power. 2006;128:525-34.

[120] Thomas DC, Benson SM. Carbon dioxide capture for storage in deep geologic formations: results from the CO_2 capture project: CPL Press; 2005.

[121] Metz B. Carbon Dioxide Capture and Storage: Special Report of the Intergovernmental Panel on Climate Change: Cambridge University Press; 2005.

[122] Kolbitsch P, Bolhàr-Nordenkampf J, Pröll T, Hofbauer H. Comparison of two Ni-Based oxygen carriers for chemical looping combustion of natural gas in 140 kW continuous looping operation. Industrial & Engineering Chemistry Research. 2009;48:5542-7.

[123] Kolbitsch P, Bolhàr-Nordenkampf J, Pröll T, Hofbauer H. Operating experience with chemical looping combustion in a 120 kW dual circulating fluidized bed (DCFB) unit. International Journal of Greenhouse Gas Control. 2010;4:180-5.

[124] Adánez J, Dueso C, de Diego LF, García-Labiano F, Gayán P, Abad A. methane combustion in a 500 W_{th} chemical-looping combustion system using an impregnated Ni-based oxygen carrier. Energy & Fuels. 2008;23:130-42.

[125] Abad A, Adánez J, García-Labiano F, de Diego LF, Gayán P, Celaya J. Mapping of the range of operational conditions for Cu-, Fe-, and Ni-based oxygen carriers in chemical-looping combustion. Chemical Engineering Science. 2007;62:533-49.

[126] Hong H, Jin H. A Novel Solar Thermal cycle with chemical looping combustion. International Journal of Green Energy. 2005;2:397-407.

[127] Hong H, Jin H, Liu B. A novel solar-hybrid gas turbine combined cycle with inherent CO_2 separation using chemical-looping combustion by solar heat source. Journal of Solar Energy Engineering. 2006;128:275-84.

[128] Hong H, Han T, Jin H. A low temperature solar thermochemical power plant with CO_2 recovery using methanol-fueled chemical looping combustion. Journal of Solar Energy Engineering. 2010;132:031002.

[129] M. M. Hossain, H. I. de Lasa. Chemical-looping combustion (CLC) for inherent CO_2 separations-a review. Chemical Engineering Science. 2008;63:4433-51.

[130] E. Jerndal, T. Mattisson, A. Lyngfelt. Thermal analysis of chemical-looping combustion. Chemical Engineering Research and Design. 2006;84:795-806.

[131] A. Lyngfelt, B. Leckner, T. Mattisson. A fluidized-bed combustion process with inherent CO_2 separation; application of chemical-looping combustion. Chemical Engineering Science. 2001;56:3101-13.

[132] P. Gayán, C. Dueso, A. Abad, J. Adanez, L. F. de Diego, F. García-Labiano. NiO/Al_2O_3 oxygen carriers for chemical-looping combustion prepared by impregnation and deposition-precipitation methods. Fuel. 2009;88:1016-23.

[133] Adánez J, de Diego LF, García-Labiano F, Gayán P, Abad A, Palacios JM. Selection of oxygen carriers for chemical looping combustion. Energy & Fuels. 2004;18:371-7.

[134] Lyngfelt A, Leckner B, Mattisson T. A fluidized-bed combustion process with inherent CO_2 separation; application of chemical-looping combustion. Chemical Engineering Science. 2001;56:3101-13.

[135] J. Adanez, L. F. de Diego, F. Garcia-Labiano, P. Gayan, A. Abad. Selection of oxygen carriers for chemical looping combustion. Energy & Fuel 2004;18:371-7.

[136] Mattisson T, García-Labiano F, Kronberger B, Lyngfelt A, Adánez J, Hofbauer H. Chemical looping combustion using syngas as fuel. International Journal of Greenhouse Gas Control. 2007;1:158-69.

[137] Jerndal E, Mattisson T, Lyngfelt A. Thermal analysis of chemical-looping combustion. Chemical Engineering Research and Design. 2006;84:795-806.

[138] Jin H, Okamoto T, Ishida M. Development of a novel chemical-looping combustion: synthesis of a looping material with a double metal oxide of CoO−NiO. Energy & Fuels. 1998;12:1272-7.

[139] Mattisson T, Järdnäs A, Lyngfelt A. Reactivity of some metal oxides supported on alumina with alternating methane and oxygenapplication for chemical-looping combustion. Energy & Fuels. 2003;17:643-51.

[140] de Diego LF, García-Labiano F, Adánez J, Gayán P, Abad A, Corbella BM, et al. Development of Cu-based oxygen carriers for chemical-looping combustion. Fuel. 2004;83:1749-57.

[141] Chuang SY, Dennis JS, Hayhurst AN, Scott SA. Development and performance of Cu-based oxygen carriers for chemical-looping combustion. Combustion and Flame. 2008;154:109-21.

[142] De Diego LF, GarcI´a-Labiano F, Gayán P, Celaya J, Palacios JM, Adánez J. Operation of a 10 kWth chemical-looping combustor during 200 h with a CuO-Al_2O_3 oxygen carrier. Fuel. 2007;86:1036-45.

[143] Cao Y, Pan W-P. Investigation of chemical looping combustion by solid fuels. 1. process analysis. Energy & Fuels. 2006;20:1836-44.

[144] Cao Y, Casenas B, Pan W-P. Investigation of chemical looping combustion by solid fuels. 2. redox reaction kinetics and product characterization with coal, biomass, and solid waste as solid fuels and CuO as an oxygen carrier. Energy & Fuels. 2006;20:1845-54.

[145] Cho P, Mattisson T, Lyngfelt A. Comparison of iron-, nickel-, copper- and manganese-based oxygen carriers for chemical-looping combustion. Fuel. 2004;83:1215-25.

[146] Cho P, Mattisson T, Lyngfelt A. Defluidization conditions for a fluidized bed of iron oxide-, nickel oxide-, and manganese oxide-containing oxygen carriers for chemical-looping combustion. Industrial & Engineering Chemistry Research. 2005;45:968-77.

[147] Mattisson T, Johansson M, Lyngfelt A. Multicycle reduction and oxidation of different types of iron oxide particlesapplication to chemical-looping combustion. Energy & Fuels. 2004;18:628-37.

[148] Johansson M, Mattisson T, Lyngfelt A. Investigation of Fe_2O_3 with $MgAl_2O_4$ for Chemical-Looping Combustion. Industrial & Engineering Chemistry Research. 2004;43:6978-87.

[149] García-Labiano F, Adánez J, de Diego LF, Gayán P, Abad A. Effect of pressure on the behavior of copper-, iron-, and nickel-based oxygen carriers for chemical-looping combustion. Energy & Fuels. 2005;20:26-33.

[150] Tian H, Siriwardane R, Simonyi T, Poston J. Natural ores as oxygen carriers in chemical looping combustion. Energy & Fuels. 2013;27:4108-18.

[151] Song T, Shen T, Shen L, Xiao J, Gu H, Zhang S. Evaluation of hematite oxygen carrier in chemical-looping combustion of coal. Fuel. 2013;104:244-52.

[152] Song T, Wu J, Zhang H, Shen L. Characterization of an Australia hematite oxygen carrier in chemical looping combustion with coal. International Journal of Greenhouse Gas Control. 2012;11:326-36.

[153] Abad A, Mattisson T, Lyngfelt A, Johansson M. The use of iron oxide as oxygen carrier in a chemical-looping reactor. Fuel. 2007;86:1021-35.

[154] Scott SA, Dennis JS, Hayhurst AN, Brown T. In situ gasification of a solid fuel and CO_2 separation using chemical looping. AIChE Journal. 2006;52:3325-8.

[155] Ku Y, Wu H-C, Chiu P-C, Tseng Y-H, Kuo Y-L. Methane combustion by moving bed fuel reactor with Fe_2O_3/Al_2O_3 oxygen carriers. Applied Energy. 2014;113:1909-15.

[156] Bayham SC, Kim HR, Wang D, Tong A, Zeng L, McGiveron O, et al. Iron-based coal direct chemical looping combustion process: 200-h continuous operation of a 25-kWth subpilot unit. Energy & Fuels. 2013;27:1347-56.

[157] Zafar Q, Abad A, Mattisson T, Gevert B, Strand M. Reduction and oxidation kinetics of $Mn_3O_4/Mg–ZrO_2$ oxygen carrier particles for chemical-looping combustion. Chemical Engineering Science. 2007;62:6556-67.

[158] Stobbe ER, de Boer BA, Geus JW. The reduction and oxidation behaviour of manganese oxides. Catalysis Today. 1999;47:161-7.

[159] Siriwardane R, Tian H, Richards G, Simonyi T, Poston J. Chemical-looping combustion of coal with metal oxide oxygen carriers. Energy & Fuels. 2009;23:3885-92.

[160] Ishida M, Jin H. A novel combustor based on chemical-looping reactions and its reaction kinetics. Journal of Chemical Engineering of Japan. 1994;27:296-301.

[161] Ishida M, Jin H. A new advanced powergeneration system using chemical-looping combustion. Energy. 1994;19:415–9.

[162] Hatanaka T, Matsuda S, Hatano H. A new-concept gas-solid combustion system "MERIT" for high combustion efficiency and low emissions. Energy Conversion Engineering Conference, 1997 IECEC-97, Proceedings of the 32nd Intersociety1997. p. 944-8 vol.2.

[163] Jin H, Ishida M. A new type of coal gas fueled chemical-looping combustion. Fuel. 2004;83:2411-7.

[164] Gayán P, Dueso C, Abad A, Adanez J, de Diego LF, García-Labiano F. NiO/Al_2O_3 oxygen carriers for chemical-looping combustion prepared by impregnation and deposition-precipitation methods. Fuel. 2009;88:1016-23.

[165] Villa R, Cristiani C, Groppi G, Lietti L, Forzatti P, Cornaro U, et al. Ni based mixed oxide materials for CH_4 oxidation under redox cycle conditions. Journal of Molecular Catalysis A: Chemical. 2003;204–205:637-46.

[166] Kuusik R, Trikkel A, Lyngfelt A, Mattisson T. High temperature behavior of NiO-based oxygen carriers for chemical looping combustion. Energy Procedia. 2009;1:3885-92.

[167] Shen L, Wu J, Xiao J. Experiments on chemical looping combustion of coal with a NiO based oxygen carrier. Combustion and Flame. 2009;156:721-8.

[168] Mattisson T, Johansson M, Lyngfelt A. The use of NiO as an oxygen carrier in chemical-looping combustion. Fuel. 2006;85:736-47.

[169] Baek J-I, Kim J-W, Lee JB, Eom TH, Ryu J, Ryu CK, et al. Effects of Support on the Performance of NiO-Based Oxygen Carriers. Oil Gas Sci Technol – Rev IFP Energies nouvelles. 2011;66:223-34.

[170] Sedor KE, Hossain MM, de Lasa HI. Reduction kinetics of a fluidizable nickel–alumina oxygen carrier for chemical-looping combustion. The Canadian Journal of Chemical Engineering. 2008;86:323-34.

[171] Sedor KE, Hossain MM, de Lasa HI. Reactivity and stability of Ni/Al_2O_3 oxygen carrier for chemical-looping combustion (CLC). Chemical Engineering Science. 2008;63:2994-3007.

[172] Son SR, Kim SD. Chemical-Looping Combustion with NiO and Fe_2O_3 in a Thermobalance and Circulating Fluidized Bed Reactor with Double Loops. Industrial & Engineering Chemistry Research. 2006;45:2689-96.

[173] Baek J-I, Ryu J, Lee JB, Eom T-H, Kim K-S, Yang S-R, et al. Highly attrition resistant oxygen carrier for chemical looping combustion. Energy Procedia. 2011;4:349-55.

[174] Ryu H-J, Lim N-Y, Bae D-H, Jin G-T. Carbon deposition characteristics and regenerative ability of oxygen carrier particles for chemical-looping combustion. Korean J Chem Eng. 2003;20:157-62.

[175] Cho P, Mattisson T, Lyngfelt A. Carbon Formation on nickel and iron oxide-containing oxygen carriers for chemical-looping combustion. Industrial & Engineering Chemistry Research. 2005;44:668-76.

[176] Johansson M, Mattisson T, Lyngfelt A. Use of $NiO/NiAl_2O_4$ particles in a 10 kw chemical-looping combustor. Industrial & Engineering Chemistry Research. 2006;45:5911-9.

[177] Linderholm C, Abad A, Mattisson T, Lyngfelt A. 160 h of chemical-looping combustion in a 10 kW reactor system with a NiO-based oxygen carrier. International Journal of Greenhouse Gas Control. 2008;2:520-30.

[178] Shulman A, Linderholm C, Mattisson T, Lyngfelt A. High Reactivity and Mechanical Durability of $NiO/NiAl_2O_4$ and $NiO/NiAl_2O_4/MgAl_2O_4$ Oxygen Carrier Particles Used for more than 1000 h in a 10 kW CLC Reactor. Industrial & Engineering Chemistry Research. 2009;48:7400-5.

[179] Adánez J, García-Labiano F, de Diego LF, Gayán P, Celaya J, Abad A. Nickel−Copper Oxygen Carriers To Reach Zero CO and H_2 Emissions in Chemical-Looping Combustion. Industrial & Engineering Chemistry Research. 2006;45:2617-25.

[180] Johansson M, Mattisson T, Lyngfelt A. Creating a synergy effect by using mixed oxides of iron- and nickel oxides in the combustion of methane in a chemical-looping combustion reactor. Energy & Fuels. 2006;20:2399-407.

[181] Lambert A, Delquié C, Clémeneçon I, Comte E, Lefebvre V, Rousseau J, et al. Synthesis and characterization of bimetallic Fe/Mn oxides for chemical looping combustion. Energy Procedia. 2009;1:375-81.

[182] Readman JE, Olafsen A, Larring Y, Blom R. $La_{0.8}Sr_{0.2}Co_{0.2}Fe_{0.8}O_{3-\delta}$ as a potential oxygen carrier in a chemical looping type reactor, an in-situ powder X-ray diffraction study. Journal of Materials Chemistry. 2005;15:1931-7.

[183] Rydén M, Lyngfelt A, Mattisson T, Chen D, Holmen A, Bjørgum E. Novel oxygen-carrier materials for chemical-looping combustion and chemical-looping reforming; $La_xSr_{1-x}Fe_yCo_{1-y}O_{3-\delta}$ perovskites and mixed-metal oxides of NiO, Fe_2O_3 and Mn_3O_4. International Journal of Greenhouse Gas Control. 2008;2:21-36.

[184] Rifflart S, Hoteit A, Yazdanpanah MM, Pelletant W, Surla K. Construction and operation of a 10 kW CLC unit with circulation configuration enabling independent solid flow control. Energy Procedia. 2011;4:333-40.

[185] Yazdanpanah MM, Hoteit A, Forret A, Delebarre A, Gautheir T. Experimental investigation on a novel chemical looping combustion configuration. Oil Gas Sci Technol-Rev IFP Energies nouvelles. 2011;66:265-75.

[186] Zhao Z, Chen T, Ghoniem AF. Rotary Bed Reactor for Chemical-Looping Combustion with Carbon Capture. Part 1: Reactor Design and Model Development. Energy & Fuels. 2012;27:327-43.

[187] Lyngfelt A, Kronberger B, Adanez J, Morin JX, Hurst P. The grace project. developement ofoxygen carriers for chemical looping combustion. design and operation of a 10 kw chemical looping combustor. 7'th International Conference on Greenhouse Gas Control Technologies. Vancouver, Canada, 2004.

[188] García-Labiano F, de Diego LF, Adánez J, Abad A, Gayán P. Temperature variations in the oxygen carrier particles during their reduction and oxidation in a chemical-looping combustion system. Chemical Engineering Science. 2005;60:851-62.

[189] Johansson E, Mattisson T, Lyngfelt A, Thunman H. Combustion of syngas and natural gas in a 300 w chemical-looping combustor. Chemical Engineering Research and Design. 2006;84:819-27.

[190] Johansson E, Lyngfelt A, Mattisson T, Johnsson F. Gas leakage measurements in a cold model of an interconnected fluidized bed for chemical-looping combustion. Powder Technology. 2003;134:210-7.

[191] Noorman S, van Sint Annaland M, Kuipers. Packed bed reactor technology for chemical-looping Combustion. Industrial & Engineering Chemistry Research. 2007;46:4212-20.

[192] Adánez J, Gayán P, Celaya J, de Diego LF, García-Labiano F, Abad A. Chemical looping combustion in a 10 kWth prototype using a CuO/Al_2O_3 oxygen carrier: effect of operating conditions on methane combustion. Industrial & Engineering Chemistry Research. 2006;45:6075-80.

[193] Ryu H-J, Bae D-H, Jin G-T. Effect of temperature on reduction reactivity of oxygen carrier particles in a fixed bed chemical-looping combustor. Korean J Chem Eng. 2003;20:960-6.

[194] Mattisson T, Adanez J, Proell T, Kuusik R, Beal C, Assinkf J, et al. Chemical-looping combustion CO_2 ready gas power. Energy Procedia. 2009;1:1557-64.

[195] Forero CR, Gayán P, de Diego LF, Abad A, García-Labiano F, Adánez J. Syngas combustion in a 500 W_{th} chemical-looping combustion system using an impregnated Cu-based oxygen carrier. Fuel Processing Technology. 2009;90:1471-9.

[196] Kolbitsch P, Pröll T, Bolhar-Nordenkampf J, Hofbauer H. Characterization of chemical looping pilot plant performance via experimental determination of solids conversion. Energy & Fuels. 2009;23:1450-5.

[197] Pröll T, Rupanovits K, Kolbitsch P, Bolhàr-Nordenkampf J, Hofbauer H. Cold flow model study on a dual circulating fluidized bed (DCFB) system for chemical looping processes. Chemical Engineering & Technology. 2009;32:418-24.

[198] Pröll T, Kolbitsch P, Bolhàr-Nordenkampf J, Hofbauer H. A novel dual circulating fluidized bed system for chemical looping processes. AIChE Journal. 2009;55:3255-66.

[199] Pröll T, Mayer K, Bolhàr-Nordenkampf J, Kolbitsch P, Mattisson T, Lyngfelt A, et al. Natural minerals as oxygen carriers for chemical looping

combustion in a dual circulating fluidized bed system. Energy Procedia. 2009;1:27-34.

[200] Kronberger B, Johansson E, Löffler G, Mattisson T, Lyngfelt A, Hofbauer H. A two-compartment fluidized bed reactor for CO_2 capture by chemical-looping combustion. Chemical Engineering & Technology. 2004;27:1318-26.

[201] Wang S, Wang G, Jiang F, Luo M, Li H. Chemical looping combustion of coke oven gas by using Fe_2O_3/CuO with $MgAl_2O_4$ as oxygen carrier. Energy & Environmental Science. 2010;3:1353-60.

[202] Linderholm C, Lyngfelt A, Dueso C. Chemical-looping combustion of solid fuels in a 10kW reactor system using natural minerals as oxygen carrier. Energy Procedia. 2013;37:598-607.

[203] Linderholm C, Lyngfelt A, Cuadrat A, Jerndal E. Chemical-looping combustion of solid fuels – Operation in a 10kW unit with two fuels, above-bed and in-bed fuel feed and two oxygen carriers, manganese ore and ilmenite. Fuel. 2012;102:808-22.

[204] Markström P, Linderholm C, Lyngfelt A. Chemical-looping combustion of solid fuels – Design and operation of a 100 kW unit with bituminous coal. International Journal of Greenhouse Gas Control. 2013;15:150-62.

[205] Noorman S, Gallucci F, van Sint Annaland M, Kuipers JAM. Experimental investigation of chemical-looping combustion in packed beds: a parametric study. Industrial & Engineering Chemistry Research. 2011;50:1968-80.

[206] Noorman S, van Sint Annaland M, Kuipers JAM. Experimental validation of packed bed chemical-looping combustion. Chemical Engineering Science. 2010;65:92-7.

[207] Dahl IM, Bakken E, Larring Y, Spjelkavik AI, Håkonsen SF, Blom R. On the development of novel reactor concepts for chemical looping combustion. Energy Procedia. 2009;1:1513-9.

[208] Diver RB. Receiver/Reactor Concepts for Thermochemical Transport of Solar Energy. Journal of Solar Energy Engineering. 1987;109:199-204.

[209] Nikulshina V, Gebald C, Steinfeld A. CO2 capture from atmospheric air via consecutive CaO-carbonation and $CaCO_3$-calcination cycles in a fluidized-bed solar reactor. Chemical Engineering Journal. 2009;146:244-8.

[210] Schunk LO, Steinfeld A, Haeberling P, Wepf S, Wuillemin D, Meier A. A receiver-reactor for the solar thermal dissociation of zinc oxide. Journal of Solar Energy Engineering. 2008;130:021009-.

[211] Müller R, Haeberling P, Palumbo RD. Further advances toward the development of a direct heating solar thermal chemical reactor for the thermal dissociation of ZnO(s). Solar Energy. 2006;80:500-11.

[212] Osinga T, Frommherz U, Steinfeld A, Wieckert C. Experimental investigation of the solar carbothermic reduction of ZnO using a two-cavity solar reactor. Journal of Solar Energy Engineering. 2004;126:633-7.

[213] Melchior T, Perkins C, Weimer AW, Steinfeld A. A cavity-receiver containing a tubular absorber for high-temperature thermochemical processing using concentrated solar energy. International Journal of Thermal Sciences. 2008;47:1496-503.

[214] Kräupl S, Steinfeld A. Operational performance of a 5-kW solar chemical reactor for the Co-production of Zinc and syngas. Journal of Solar Energy Engineering. 2003;125:124-6.

[215] Maag G, Zanganeh G, Steinfeld A. Solar thermal cracking of methane in a particle-flow reactor for the co-production of hydrogen and carbon. International Journal of Hydrogen Energy. 2009;34:7676-85.

[216] Piatkowski N, Wieckert C, Steinfeld A. Experimental investigation of a packed-bed solar reactor for the steam-gasification of carbonaceous feedstocks. Fuel Processing Technology. 2009;90:360-6.

[217] Steinfeld A. Solar thermochemical production of hydrogen-a review. Solar Energy. 2005;78:603-15.

[218] Z'Graggen A, Haueter P, Trommer D, Romero M, de Jesus JC, Steinfeld A. Hydrogen production by steam-gasification of petroleum coke using concentrated solar power-II Reactor design, testing, and modeling. International Journal of Hydrogen Energy. 2006;31:797-811.

[219] Koepf E, Advani SG, Steinfeld A, Prasad AK. A novel beam-down, gravity-fed, solar thermochemical receiver/reactor for direct solid particle decomposition: Design, modeling, and experimentation. International Journal of Hydrogen Energy. 2012;37:16871-87.

[220] Chueh WC, Falter C, Abbott M, Scipio D, Furler P, Haile SM, et al. High-flux solar-driven thermochemical dissociation of CO_2 and H_2O using nonstoichiometric ceria. Science. 2010;330:1797-801.

[221] Gokon N, Ono R, Hatamachi T, Liuyun L, Kim H-J, Kodama T. CO_2 gasification of coal cokes using internally circulating fluidized bed reactor by concentrated Xe-light irradiation for solar gasification. International Journal of Hydrogen Energy. 2012;37:12128-37.

[222] Steinfeld A, Brack M, Meier A, Weidenkaff A, Wuillemin D. A solar chemical reactor for co-production of zinc and synthesis gas. Energy. 1998;23:803-14.

CHAPTER 3

A HYBRID SOLAR AND CHEMICAL LOOPING COMBUSTION SYSTEM FOR SOLAR THERMAL ENERGY STORAGE

Statement of Authorship

Title of Paper	A hybrid solar and chemical looping combustion system for solar thermal energy storage
Publication Status	⦿ Published, ○ Accepted for Publication, ○ Submitted for Publication, ○ Publication style
Publication Details	M. Jafarian, M. Arjomandi, G. J. Nathan, "A hybrid solar and chemical looping combustion system for solar thermal energy storage". Applied Energy, (2012), vol: 103, p: 671-678.

Author Contributions

By signing the Statement of Authorship, each author certifies that their stated contribution to the publication is accurate and that permission is granted for the publication to be included in the candidate's thesis.

Name of Principal Author (Candidate)	Seyed Mehdi Jafarian		
Contribution to the Paper	Developed ideas. performed simulations and calculations, interpreted data, wrote manuscript and acted as corresponding author.		
Signature		Date	05/06/2014.

Name of Co-Author	Maziar Arjomandi		
Contribution to the Paper	Supervised development of work, helped in developing ideas, data interpretation and manuscript evaluation.		
Signature		Date	05.06.2014

Name of Co-Author	Graham Nathan		
Contribution to the Paper	Supervised development of work, helped in developing ideas, data interpretation and manuscript evaluation.		
Signature		Date	5/6/14

Name of Co-Author			
Contribution to the Paper			
Signature		Date	

Applied Energy 103 (2013) 671–678

Contents lists available at SciVerse ScienceDirect

Applied Energy

journal homepage: www.elsevier.com/locate/apenergy

A hybrid solar and chemical looping combustion system for solar thermal energy storage

Mehdi Jafarian *, Maziar Arjomandi, Graham J. Nathan

School of Mechanical Engineering, The University of Adelaide, SA 5005, Australia
Centre for Energy Technology, The University of Adelaide, SA 5005, Australia

HIGHLIGHTS

- A novel solar–CLC hybrid system is proposed which integrates a CLC with solar thermal energy.
- The oxygen carrier particles are used as storage medium for thermal energy storage.
- A solar cavity reactor is proposed for fuel reactor.
- The absorbed solar energy is stored in the particles to produce a base heat load.

ARTICLE INFO

Article history:
Received 16 March 2012
Received in revised form 5 July 2012
Accepted 15 October 2012
Available online 11 November 2012

Keywords:
Hybrid system
Chemical looping combustion
Thermal energy storage
Solar reactor
Power generation

ABSTRACT

A novel hybrid of a solar thermal energy and a chemical looping combustion (CLC) system is proposed here, which employs the oxygen carrier particles in a CLC system to provide diurnal thermal energy storage for concentrated solar thermal energy. In taking advantage of the chemical and sensible energy storage systems that are an inherent part of a CLC system, this hybrid offers potential to achieve cost effective, base load power generation for solar energy. In the proposed system, three reservoirs have been added to a conventional CLC system to allow storage of the oxygen carrier particles, while a cavity solar receiver has been chosen for the fuel reactor. The performance of the system is evaluated using ASPEN PLUS software, with the model being validated using independent simulation result reported previously. Operating temperature, solar efficiency, solar fraction, exergy efficiency and the fraction of the solar thermal energy stored for a based load power generation application are reported.

1. Introduction

The utilization of renewable energy sources such as solar radiation is a potential approach to reduce the carbon dioxide emissions from power generation. However at present, the combined contributions of solar, geothermal and wind meet only 0.4% of the global energy demand, while fossil fuels account for about 80% [1,2]. Concentrated solar thermal power, CSP, technology is under development and is considered to have potential to achieve cost-competitive power generation, especially in arid regions where direct sunlight is abundant [3]. However, the intrinsic low intensity and intermittent nature of solar radiation are major barriers to achieving economic viability. To compensate for the intermit resource, CSP plants require either supporting generation (from auxiliary sources, the network or as a hybrid) or storage capacity to continue electricity supply when sunlight is below a threshold [4]. It is well known that the addition of thermal storage has the potential to increase economic viability to a CSP power plant [4], but storage is one of the least developed components of CSP plants and also adds to the capital cost [5]. New options to reduce the cost of storage are therefore needed.

Thermal energy storage, TES, can utilize chemical energy (the heat of reaction), sensible heat, latent heat or a combination of these methods [6]. Sensible TES, implies a change in the temperature of the storage medium without any phase change. Latent heat TES involves a phase change, while chemical TES involves an endothermic chemical reaction. Currently, sensible heat TES technology is the only commercially viable method for storing solar thermal energy in large scale CSP plants [7]. In these systems molten salt is the most developed storage medium [8]. While sensible TES can add value to a solar thermal plant by allowing it to sell power when the price is high, current approaches also have some significant disadvantages. Molten salt systems typically increase the capital cost of a solar thermal plant by 10–20%, depending on the amount of storage [9]. They also require large quantities of salt and two correspondingly large storage tanks. The size and

* Corresponding author at: School of Mechanical Engineering, The University of Adelaide, Adelaide, SA 5005, Australia. Tel.: +61 8 8303 5460.
E-mail address: mehdi.jafarian@adelaide.edu.au (M. Jafarian).

0306-2619/$ - see front matter

Nomenclature

A_{ap}	solar fuel reactor aperture area (m^2)
A_{coll}	collector area (m^2)
CR	mean flux concentration ratio
E_{xi}	exergy efficiency ith stream (kJ/mol)
E_{xs}	solar energy exergy (kJ/mol)
LHV_{CH_4}	lower heating value CH_4 (kJ/mol)
I	normal insolation beam (W/m^2)
$\dot{n}_i$	molar flow rate ith (mol/min)
$q_{ap,min}$	minimum aperture input solar thermal heat flux required (W/m^2)
$\dot{Q}_{ap}$	aperture input solar thermal power (W)
$\dot{Q}_{coll}$	normalized incoming power from collector (kJ/mol)
$\dot{Q}_{s,in}$	solar thermal power (W)
$\dot{Q}_{s,r}$	reradiated thermal power (W)
T_{FR}	fuel reactor temperature (K)
$T_{FR,0}$	fuel reactor temperature without solar thermal energy (K)

Greek letters

α_{eff}	effective absorptance
ΔH_i	total stream enthalpy change (kJ/mol)
ε_{eff}	effective absorptance
ς	oxygen added ratio
η_{abs}	absorption efficiency
η_{coll}	collector system optical efficiency
σ	Stephan–Boltzmann constant ($W/(m^2\,k^4)$)
$\chi_{loss,rad}$	total fraction of solar input energy reradiated
χ_{sol}	thermal solar share
$\chi_{sol,AR,out}$	total fraction of solar input energy added to air reactor output stream
$\chi_{sol,FR,out}$	total fraction of solar input energy added to fuel reactor output stream
$\chi_{st,ch}$	chemical storage fraction
$\chi_{st,sen}$	sensible heat storage fraction
$\chi_{sol,st}$	solar fraction stored

Subscripts

abs	absorption
ap,o	solar fuel reactor aperture open
ap,c	solar fuel reactor aperture close
coll	collector
ex	exergy
in	input
out	output
part	particle

solidification potential of the these systems are disadvantages that increase cost [10]. Besides, in this systems heat is stored at temperatures of ~840 K, while it is released at lower temperatures ~820–570 K [8]. This lowers the isentropic efficiency in comparison to latent or chemical storage, where heat can be stored and released at almost the same temperatures. Hence, it is desirable to seek alternative approaches that have potential to lower the cost of TES.

CLC is a technology under development to provide inherent capability for CO_2 capture in the combustion of a hydrocarbon fuel. The CLC process is based on the indirect transfer of oxygen from the air to the fuel by means of a solid oxygen carrier particle to avoid direct contact between the fuel and air. A CLC system consists of two separate reactors; an air reactor and a fuel reactor. Within the CLC process, oxygen carriers in the fuel reactor are reduced through oxidation of the fuel and transferred to the air reactor, where they are oxidized by the air to produce metal oxide. The metal oxide is then returned back to the fuel reactor and the process is repeated [11–14]. A comprehensive review of CLC systems, reporting the main advantages of this technology up to 2010, has been published recently by Adanez et al. [15]. Solar energy could potentially be stored as chemical energy, through the endothermic fuel oxidation reaction, or as sensible heat, either in the un-reacted metal oxide itself or in the inert material added to oxygen carriers to increase their reactivity and durability. The apparent synergy between the CLC and solar thermal systems suggests that there may be economic advantages in combining them to also enable the storage of solar thermal energy. However, no assessment of this has been reported previously.

The hybridization of a CLC power cycle with solar thermal energy was first proposed by Hong and Jin [16]. In their process solar thermal energy was used as a heat source to drive the endothermic reaction of NiO and CH_4. This cycle was modified by Hong et al. [17] in 2006 to achieve a higher thermal efficiency. More recently, Hong et al. [18] also reported a hybrid cycle integrating methanol-fuelled CLC with low temperature solar thermal energy at 200 °C. These investigations identified an important advantage of hybrid solar–CLC systems, in that solar energy can be converted to chemical energy at low temperatures and released at a higher temperature. However, to our knowledge, no previous investigation has proposed or assessed the application of oxygen carrier particles within a CLC system for diurnal solar thermal energy storage. Such a solar hybrid system offers not only the potential to address the challenge of the intermittency of solar energy but also presents the opportunity to reduce the cost of storage for solar thermal power. Therefore, the aim of this current work is to investigate this novel concept of a solar–CLC hybrid system in which solar thermal energy is stored using CLC system components.

2. Conceptual design

Fig. 1 presents the configuration of the solar–CLC hybrid process considered here. The system is designed to produce a steady power output despite an intermittent solar thermal energy input, using CLC process components (oxygen carrier particles and reactors of fuel and air). In this hybrid system, concentrated solar thermal energy from the heliostat field is captured and stored by the oxygen carrier particles, here NiO, within the fuel reactor at a relatively low temperature and is then released into the air reactor at a higher temperature. The NiO is used to convert CH_4 into CO_2 and H_2O with high efficiency. As noted above, the metal oxide (e.g. NiO) in oxygen carrier particles for a CLC system is typically mixed with an inert material [12,15,19]. However, since the present aim is to assess only the feasibility of a solar–CLC hybrid process, we follow Hong et al. [16,17] in adopting the simplifying assumption that the NiO oxygen carrier particles are pure.

The process consists of two CLC reactors and three particle storage reservoirs. The NiO is reduced within the fuel reactor by an endothermic reaction with CH_4 ($4NiO + CH_4 \rightarrow 4Ni + CO_2 + 2H_2O$), while Ni is reacted exothermically with oxygen in the air reactor ($4Ni + O_2 \rightarrow 4NiO$). The three additional reservoirs are added to a conventional CLC system, both to store solar thermal energy and to allow particles to be fed to the air reactor at a constant temperature despite the variations in the input of concentrated solar thermal energy. This is achieved with a constant mass flow rate of

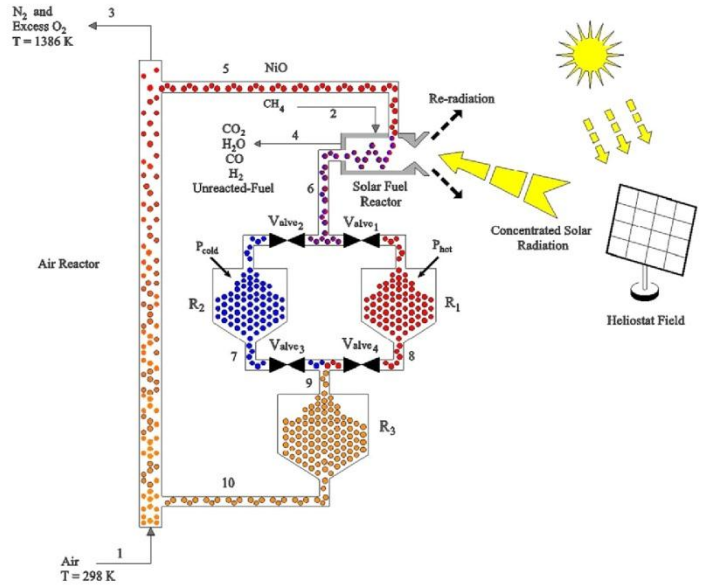

Fig. 1. The configuration of the solar–CLC hybrid system assessd here to provide storage of solar thermal energy. Resrvoirs R_1 and R_2 are used to store the hot and cold particles, respectively, produced with and without the addition of solar thermal energy. The hot and cold particles are then mixed and stored in R_3 to provide a constant temperature feed to the air reactor.

oxidizer. The reduced particles produced in the fuel reactor are stored in reservoir R_1 for the case that their temperature is further increased by solar thermal energy, and in reservoir R_2 for the case without the addition of solar energy.

The fuel reactor must be capable of operating with or without the input of solar radiation, which is best achieved by adapting solar reactors or receivers. Previous work has showed that the cavity-type reactor configurations are the most suitable configuration for harnessing highly concentrated solar radiation [20]. One possible approach to achieve this is to adapt the Solar Vortex Reactor of Z'Graggen et al. [21] to allow the fuel reactions to occur in the same vessel in which the solar energy is introduced, without any need for an extra component in the solar–CLC hybrid system. The present analysis is based on this device. The aperture of the device must be modified to allow it to be closed when the input from solar energy is below the losses through the aperture to avoid excessive heat losses. For the present paper, it is assumed that this modification is feasible, without undertaking a detailed design.

Concentrated solar radiation is introduced into the Solar Fuel Reactor when the solar flux is sufficient to exceed losses, to contribute to the fuel oxidation reaction energy and to provide additional sensible heating of the particles, shown as "P_{hot}" in Fig. 1. These are stored in the reservoir R_1. When solar energy is not available, the solar cavity reactor aperture is closed and the metal oxide particles are reduced by means of their sensible heat following conventional operation of CLC fuel reactor to produce the "P_{cold}" metal oxide particles shown in Fig. 1. These are stored in Reservoir R_2. The stored cold and hot particles from R_1 and R_2, respectively, are then mixed and stored in Reservoir R_3. This allows the input temperature of the oxygen carrier particles to the air reactor, Stream 9, to be maintained constant despite the variations in input solar energy, so as to achieve a constant temperature at the output from the air reactor, line 3 in Fig. 1, for base-load power generation.[1]

3. Methodology of investigation

Simulation of the proposed solar–CLC hybrid system was performed using ASPEN PLUS software with the compositions of products being taken into account by the Gibbs minimization method with the assumption of ideal gas behavior. The gaseous product from the fuel reactor is also assumed to have the following components: CH_4, H_2O, CO_2, CO and H_2. It is also assumed that the system operates at atmospheric pressure. The dynamic performance of the plant due to a time-varying solar input was simulated by a pseudo steady state approximation based on the hourly averaged profile of the solar irradiance. To calculate a reservoir temperature, it is assumed that all stored particles within it are well mixed to a uniform temperature at each time step. Several parameters are defined and calculated to assess the operation of the system.

Radiative heat losses are accounted for through the solar energy absorption efficiency, η_{abs}, which is defined as the net ratio of solar energy absorbed by the solar reactor to the solar power input through the solar cavity's aperture, $\dot{Q}_{s,in}$. For a completely insulated solar cavity fuel reactor with no heat losses through conduction and convection, the solar efficiency is given by [22]:

$$\eta_{abs} = \frac{\alpha_{eff}\dot{Q}_{ap} - \varepsilon_{eff}A_{ap}\sigma T_{FR}^4}{\dot{Q}_{s,in}}, \quad (1)$$

[1] To facilitate the transport of particles between the reactors by gravity, reservoirs R_1 and R_2 can be positioned at a higher elevation than the reservoir R_3, while reservoir R_3 can be located at a higher elevation than the air reactor input. A high velocity through the air reactor can be used to transfer the particles to the fuel reactor during the oxidation reaction.

where α_{eff} and ε_{eff} are the effective absorptance and emittance of the cavity-receiver respectively, σ is the Stephan–Boltzmann constant, $\dot{Q}_{ap}$ is the amount of solar power intercepted by the aperture with the area of A_{ap}, and T_{FR} is the temperature of the solar cavity fuel reactor. For simplicity it is assumed that the aperture size allows capture of all incoming power from collector, so that $\dot{Q}_{ap} = \dot{Q}_{coll}$ following earlier work [22]. The incoming solar power from the concentrator normalized to input fuel molar flow rate, $\bar{\dot{Q}}_{coll}$, is calculated by the collector area, A_{coll}, the normal beam insolation, I, and the optical efficiency, η_{coll}, of the collection system [22].

$$\bar{\dot{Q}}_{coll} = \eta_{coll}\left(\frac{A_{coll}}{\dot{n}_2}\right)I. \tag{2}$$

In this equation, $\dot{n}_2$ is the input fuel molar flow rate. With this assumption and the definition of mean flux concentration ratio, $(CR = \dot{Q}_{ap}/(I \cdot A_{ap}))$ the solar absorption efficiency of the solar cavity reactor can be determined by:

$$\eta_{abs} = 1 - \frac{\varepsilon_{eff}\sigma T_{FR}^4}{\alpha_{eff} ICR}. \tag{3}$$

A value of $\eta_{abs} = 0$ indicates that the input solar thermal energy to solar fuel reactor is equal to the re-radiation through the solar reactor aperture. Hence, it is important to identify the time at which the fuel reactor aperture must be closed or opened to have a net positive gain of solar input energy. For a fuel reactor working at a temperature of $T_{FR,0}$ without solar energy, the minimum value of solar heat flux required to make a net contribution to thermal input, $q_{ap,min}$, can be calculated by setting the absorption efficiency equal to zero (Eq. (2)).

$$q_{ap,\min} = \frac{\dot{Q}_{ap,\min}}{A_{ap}} = \frac{\varepsilon_{eff}\sigma T_{FR,0}^4}{\alpha_{eff}}. \tag{4}$$

When the heat flux produced by the collector field $\left(\frac{\dot{Q}_{ap}}{A_{ap}} = I \cdot CR\right)$ is lower than $q_{ap,min}$ calculated by Eq. (4), the solar fuel reactor aperture must be closed.

The thermal solar share, χ_{sol}, which is the contribution of the input solar thermal power to the solar hybrid system performance, is calculated as follows [23]:

$$\chi_{sol} = \frac{\dot{Q}_{s,in} - \dot{Q}_{s,r}}{\dot{Q}_{s,in} - \dot{Q}_{s,r} + \dot{n}_2 LHV_{CH_4}}, \tag{5}$$

where $\dot{Q}_{s,r}$ is the reradiated power from solar reactor and LHV_{CH_4} is the lower heating value of CH_4.

To asses the solar energy stored in particles, the stored solar fraction, $\chi_{sol,st}$, is defined as:

$$\chi_{sol,st} = \frac{(\dot{n}_6\Delta H_6)_{ap,o} - (\dot{n}_6\Delta H_6)_{ap,c}}{\dot{Q}_{s,in} - \dot{Q}_{s,r}}. \tag{6}$$

In this equation ΔH_6 is the molar enthalpy of oxygen carrier particles leaving the fuel reactor and $\dot{n}_6$ is the molar flow rate of Stream 6. Subscripts "*ap,o*" and "*ap,c*" denote the condition where the solar fuel reactor aperture is opened or closed, respectively.

When operated without the solar energy input, the proposed solar hybrid CLC reverts to a conventional CLC system. That is, it operates at a lower temperature than the solar–CLC hybrid system. Therefore, the increase in the enthalpies of the air and fuel reactor output gas streams (Streams 3 and 4 in Fig. 1), caused by the introduction of solar energy to solar–CLC hybrid system, can be used to determine the thermal power added to fuel reactor output stream, $\dot{Q}_{s,out,FR}$, and air reactor output stream, $\dot{Q}_{s,out,AR}$. Total fractions of solar input energy added to the fuel reactor output gas stream, $\chi_{sol,FR,out}$, and to the air reactor output gas streams, $\chi_{sol,AR,out}$, can then be calculated by:

$$\chi_{sol,FR,out} = \frac{\int_{24\,hours}\dot{Q}_{s,out,FR}dt}{\int_{day\,time}\dot{Q}_{s,in}dt} = \frac{\int_{24\,hours}((\dot{n}_4\Delta H_4)_{sol} - (\dot{n}_4\Delta H_4)_{non-sol})dt}{\int_{day\,time}\dot{Q}_{s,in}dt}, \tag{7}$$

$$\chi_{sol,AR,out} = \frac{\int_{24\,hours}\dot{Q}_{s,out,AR}dt}{\int_{day\,time}\dot{Q}_{s,in}dt} = \frac{\int_{24\,hours}((\dot{n}_3\Delta H_3)_{sol} - (\dot{n}_3\Delta H_3)_{non-sol})dt}{\int_{day\,time}\dot{Q}_{s,in}dt}. \tag{8}$$

Here the subscribes "*sol*" and "*non-sol*" represent the operation of the solar–CLC hybrid system with and without solar energy and $\chi_{sol,AR,out}$ implies the fraction of total input solar energy that can be used for continuous power generation. Hence, the total fraction of solar input energy that is reradiated through solar fuel reactor aperture, $\chi_{loss,rad}$, is given by:

$$\chi_{loss,rad} = 1 - (\chi_{sol,FR,out} + \chi_{sol,AR,out}). \tag{9}$$

The exergy efficiency is defined as the ratio of the net output exergy to the total input exergy [24]:

$$\eta_{ex} = \frac{Ex_3 + Ex_4}{Ex_s + Ex_1 + Ex_2}. \tag{10}$$

Here Ex_s represents the exergy of the absorbed solar thermal energy and Ex_i is the exergy of stream i ($i = 1, 2, 3, 4$) shown in Fig. 1. The exergy of the absorbed solar thermal energy corresponds to the maximum work availability at the solar reactor temperature and is given by [17]:

$$Ex_s = (\dot{Q}_{s,in} - \dot{Q}_{s,r})\left(1 - \frac{T_0}{T_{FR}}\right), \tag{11}$$

where T_0 is the ambient temperature. The exergies of various streams have been calculated from previous work [25,26].

The mass flow rate of circulating oxygen carrier particles between the air and fuel reactors is calculated using the oxygen added ratio, ς, which is defined as the amount of O, added with the oxide, $\dot{m}_{O,added}$, relative to the stoichiometric amount needed for full conversion of fuel to CO_2 and H_2O, $\dot{m}_{O,stoich}$ [27]:

$$\varsigma = \frac{\dot{m}_{O,added}}{\dot{m}_{O,stoich}}. \tag{12}$$

For the present case, a value of ς equal to unity implies that the solar energy is stored entirely as chemical energy, while values greater than unity imply a combination of chemical and sensible heat storage.

The most relevant operating conditions of the solar–CLC hybrid system are summarized in Table 1. The heliostat area and the input

Table 1
Main assumptions for the solar–CLC hybrid system.

Parameter	Value
Effective absorptance [22,29]	1
Effective emittance [22,29]	1
Optical efficiency of heliostat filed (%) [30]	65
Mean flux concentration ratio	2000
Normalized fuel molar flow rate ($mol/mol_{CH_4,in}$)	1
Air mass flow ($mol/mol_{CH_4,in}$)	23.8
Input fuel pressure (atm)	1
Input air pressure (atm)	1
Input fuel temperature (°C)	25
Input air temperature (°C)	25
Normalized Heliostat area to input fuel mass flow $\left(\frac{m^2}{mol_{CH_4,in}/s}\right)$	450
Fuel reactor pressure (atm)	1
Air reactor pressure (atm)	1
Oxygen added ratio	2

fuel and air mass flow rates are normalized by the input fuel mass flow rate. The input solar energy to solar fuel reactor is calculated based on normalized heliostat area given in Table 1 and direct normal irradiance data for Port Augusta, South Australia [28].

4. Validation

Model validation was performed by repeating the calculations of the fuel and air reactor of Hong et al. [16,17] with the same input parameters. The results of these calculations are shown in Tables 2 and 3. It can be seen that two models agree to within 6%. The differences between the present model and that of Hong et al. [16,17] are attributed to the different polynomial equations used in each to calculate the heat capacity of Ni. The polynomial used by Hong et al. [16,17] employs the ASPEN PLUS software database, which is appropriate for the temperatures in the range of 25–358 °C. However the fuel and air reactors in their proposed hybrid system are at 530 °C and 1200 °C, respectively, which consequently leads to a small error in the calculated values of Ni heat capacity and corresponding reactions enthalpies. In contrast, the present model has modified the ASPEN PLUS data base using Perry's Handbook data [31] to match the present temperature range.

5. Results and discussion

The compositions and normalized flow rates of the various streams of the solar–CLC hybrid system are given in Table 4. In this table $\dot{n}_i$ is the flow rate of stream i.

Table 2
Comparison of the predictions of the present fuel reactor model with the simulation results reported by Hong et al. [16,17] for the purpose of validation.

Input parameter	Value		
Operating pressure (bar)	15.0		
Input CH_4 temperature (°C)	15.0		
Input CH_4 molar flow rate (mol/s)	1.0		
Input NiO temperature (°C)	530.0		
Input NiO molar flow rate (mol/s)	4.0		
Absorbed solar thermal energy (kW)	183.4		
Calculated value	Hong et al. [16,17]	Present model	Difference%
Fuel reactor temperature (°C)	530.0	562.0	6.0
ΔH_{530} (kJ/mol)[a]	158.0	150.0	5.0

[a] ΔH_{530} is the CH_4 and NiO reaction enthalpy change at 530 °C.

Table 3
Comparison of the predictions of the present air reactor model with the simulation results reported by Hong et al. [16,17] for the purpose of validation.

Input parameter	Value		
Operating pressure (bar)	15.0		
Input air temperature (°C)	530.0		
Input air molar flow rate (mol/s)	37.8		
Input Ni temperature (°C)	530.0		
Input Ni molar flow rate (mol/s)	4.0		
Calculated value	Hong et al. [16,17]	Present model	Difference %
Fuel reactor temperature (°C)	1200.0	1195.0	0.4
$\Delta H'_{1200}$ (kJ/mol)[a]	−959.0	−934.0	2.7

[a] $\Delta H'_{1200}$ is the Ni and O_2 reaction enthalpy change at 1200 °C.

While the particles in fuel reactor input stream (Stream 5 in Fig. 1) comprise only NiO, the fuel reactor output stream (Stream 6 in Fig. 1) contains a mixture of Ni and NiO in equal proportions by mol fraction. The calculations show that the fuel is approximately fully converted to CO_2 and H_2O, while the mole fractions of the products CO, H_2 and unreacted CH_4 are less than 0.01 and 0.001, respectively. The flow rates of Streams 7, 8 and 9 are not given in this table because they are used only once a day to transfer the particles from reservoir R_1 and R_2 to reservoir R_3. The simulation also predicts the total stored energy in the particles, normalized by the *LHV* of the input fuel, LHV_{CH_4}, to be 31078 (kg/MW), 26297 (kg/MW) and 57376 (kg/MW) for the reservoirs R_1, R_2 and R_3, respectively.

Fig. 2 presents the variation of the temperature of the reservoirs, streams and reactors with hours of the day for the hourly average solar insolation of Port Augusta, South Australia [28]. While the air reactor operating temperature and consequently its outputs streams (Streams 3 and 5 in Fig. 1) are constant at 1386 K, the temperatures of the fuel reactor and its output streams (Streams 4 and 6 in Fig. 1) change due to variations of the solar energy. The fuel reactor temperature increases from 981 K at 5:30 to a maximum of 1300 K at 12:30, corresponding to solar noon, and then it decreases again to 981 K at 19:30.

As shown in Fig. 2, the temperature of reservoir R_2 is constant at 981 K due to the constant temperature of stored particles between 20:30 and 5:30. The temperatures of reservoir R_1 and the fuel reactor both equal 990 K at 6:30. However, between 6:30 and 18:30 the temperature of reservoir R_1 increases from 990 K at 6:30 to 1216 K at 16:30 and then decreases to 1186 K at 18:30. This is due to the drop in temperature of the particles from the fuel reactor, which lowers the equilibrium temperature of reservoir R_1 after 16:30. The temperature of R_1 remains constant during the night time between 19:30 and 5:30. The temperatures of reservoir R_3 and Stream 9 are successfully controlled to the constant value of 1102 K by the mixing of Streams 7 and 8.

Fig. 2 shows that, when solar energy is not introduced to the fuel reactor (between 00:30 to 05:30 and 19:30 to 23:30) its calculated temperature is 981 K. Therefore the minimum heat flux required to provide a positive net contribution of solar input to fuel reactor is 52.5 kW/m^2 (Eq. (4)). The average annual normal irradiance in Port Augusta, South Australia, at 5:30 and 19:30 are 0.5 W/m^2 and 19.2 W/m^2, respectively [28]. Therefore at these hours the solar heat flux produced by the heliostat field with the considered mean flux concentrated ratio are 1.0 and 38.4 kW/m^2, respectively. These figures are below the minimum threshold required to make a net positive contribution to the solar fuel reactor. Hence despite the presence of solar thermal energy, the solar fuel reactor's aperture is kept closed.

To evaluate the effect of solar thermal energy in this solar–CLC hybrid system, the operating temperatures of the equivalent conventional CLC system (with the solar input set to zero) is also shown in Fig. 2. It can be seen that the application of solar thermal energy increases the operating temperature of the air and fuel reactors of the solar–CLC hybrid system relative to those of the equivalent conventional CLC system. The increase in temperature of the air reactor is constant at 45 K, while that for the fuel reactor varies diurnally from 43 K during the night time to 362 K at solar noon. Hence too, the difference in temperature between the fuel and air reactors varies diurnally, with the minimum temperature difference being 85 K, which occurs at solar noon when the fuel reactor receives the highest solar thermal energy input (Fig. 2). In contrast, the temperature difference between the fuel and air reactors of the conventional CLC system is always 402 K.

Fig. 3 presents the diurnal variations of the calculated absorption efficiency of the solar cavity fuel reactor for the present solar–CLC hybrid system. The absorption efficiency of the solar fuel

Table 4
The normalized flow rates and compositions of various streams for the solar–CLC hybrid system.

Stream number	$\dot{n}_i/\dot{n}_2$	Gas phase							Solid phase	
		y_{N_2}	y_{O_2}	y_{CO_2}	y_{H_2O}	y_{CO}	y_{H_2}	y_{CH_4}	x_{Ni}	x_{NiO}
1	23.80	0.79	0.21	0.00	0.00	0.00	0.00	0.00		
2	1.00	0.00	0.00	0.00	0.00	0.00	0.00	1.00		
3	21.80	0.86	0.14	0.00	0.00	0.00	0.00	0.00		
4	3.00	0.00	0.00	0.33	0.67	<0.01	<0.01	≪0.0001		
5	8.00								0.00	1.00
6	8.00								0.50	0.50
7									0.50	0.50
8									0.50	0.50
9									0.50	0.50
10	8.00								0.50	0.50

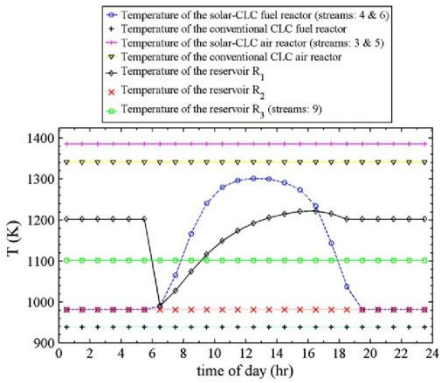

Fig. 2. The calculated temperatures of the fuel and air reactors of a conventional CLC system and the calculated hourly average variations of the corresponding temperatures of the reactors, reservoirs and streams for the solar insolation at Port Augusta, South Australia [28].

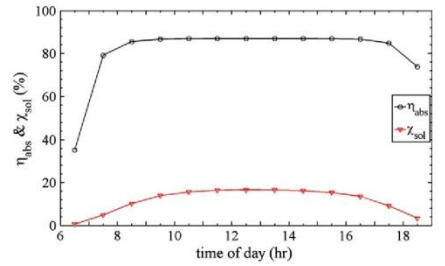

Fig. 3. The calculated hourly average variations of the solar share and fuel reactor solar absorption efficiency through the day for the solar radiation of Port Augusta, South Australia [28].

reactor increases sharply from 35.0% at 6:30 to 87.0% at 9:30 and then, despite the variations in solar irradiance [28], remains relatively constant until 16:30, after which it reduces to 74.0% at 18:30. The relatively linear behavior of the solar absorption efficiency between 9:30 and 16:30 is due to the proportional changes in solar irradiance and solar fuel reactor temperature (Eq. (4)).

The solar share of the system is also shown in Fig. 3. It increases from 0.5% at 6:30 to 16.0% at 12:30 and then decreases to 3.0% at 18:30. The slight changes of solar share between 9:30 and 16:30 are due to the increasing re-radiation losses from the solar fuel reactor aperture with operating temperature. The calculation show that the corresponding net solar share, averaged over the whole day, is 6.5%.

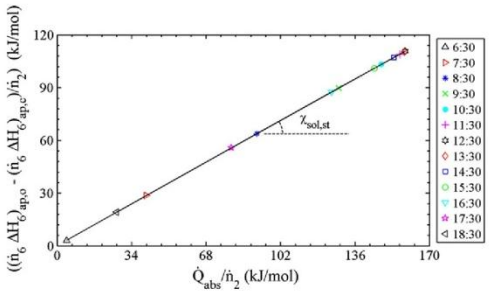

Fig. 4. The calculated variations of the stored solar thermal energy with normalized absorbed solar thermal power. (The axes are normalized to input fuel mass flow rate.)

Variations of the total heat stored in particles with the absorbed solar thermal power in the fuel reactor at different times is shown in Fig. 4. In this figure both axes are normalized to input fuel input mass flow rate. The slope of this line at each time corresponds to $\chi_{sol,st}$ as given by Eq. (6). As shown, 70.0% of the absorbed solar thermal energy in the fuel reactor is stored in the particles during the day. Consequently 30.0% of the absorbed solar energy leaves the fuel reactor with output gas stream (Stream 4 in Fig. 1).

Fig. 5 shows the diurnal variation of the solar energy introduced to the system and the heat added by the solar energy to the air and fuel reactor output gas streams (Streams 3 and 4 in Fig. 1). These parameters are normalized by the input fuel mass flow rate. As shown, while the normalized thermal power added to Stream 3 ($\dot{Q}_{s,out,AR}/\dot{n}_2$) is constant at 33.0 kJ/mol, the normalized power added to Stream 4 ($\dot{Q}_{s,out,FR}/\dot{n}_2$) increases from a night time level of 8.0 kJ/mol, to 57.0 kJ/mol at solar noon and then decreases to 16.0 kJ/mol at 18:30. Since the reaction of CH_4 and NiO without solar thermal energy is completed (Table 4), the solar energy is used here only to increase the particle temperature during the day (Fig. 2). Consequently the stored fraction of the absorbed solar energy in solar fuel reactor is stored as sensible heat in oxygen carrier particles.

The area under the curve $\dot{Q}_{s,in}$ shown in Fig. 5, corresponds to the total solar input per unit of fuel flow rate, while that under the curves $\dot{Q}_{s,out,AR}$ and $\dot{Q}_{s,out,FR}$ corresponds to the equivalent solar contribution to the air and fuel reactor output gas streams,

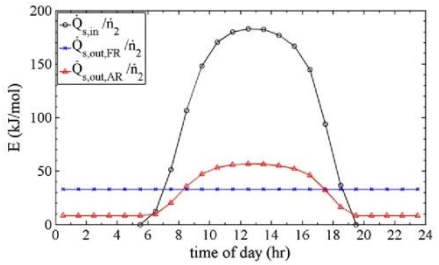

Fig. 5. The hourly average variations of the solar thermal power and the contribution of input solar power to fuel and air reactor output gas streams.

respectively. The total heat loss through re-radiation from the solar fuel reactor aperture can be calculated by subtracting the areas under both curves $\dot{Q}_{s,out,AR}$ and $\dot{Q}_{s,out,FR}$ from that under curve $\dot{Q}_{s,in}$. Based on a normalized solar thermal input of 1652 kJ s/mol for this averaged diurnal variation of solar input, 791 kJ s/mol is added to the air reactor output gas stream (Stream 3 in Fig. 1), 628 kJ s/mol is added to the fuel reactor output gas stream (Stream 4 in Fig. 1) and 233 kJ s/mol is reradiated through the solar fuel reactor aperture. Using Eqs. (7)–(9), the values of $\chi_{sol,AR,out}$, $\chi_{sol,FR,out}$ and $\chi_{loss,rad}$ are 0.48, 0.38 and 0.14, respectively. That is, the output from the air reactor ($\dot{Q}_{s,out,AR} = 32$ kJ/mol), consisting 48% of the total input solar energy, is constant and suitable for base load power generation. In addition, the base load component of the output from the fuel reactor ($\dot{Q}_{s,out,FR} = 8.3$ kJ/mol) constitutes another 12% of the total solar input. The variable component of the output from the fuel reactor constitutes 26% of the total solar input. This component could be used either for peaking power or, with additional storage, also for base load.

Fig. 6 shows the diurnal variation of the exergy efficiency of the solar hybrid system. While the exergy efficiency during the night time is fixed at 63.0%, during the day it decreases from 62.0% at 6:30 to a minimum of 59.0% at 12:30. The minimum exergy efficiency occurs at solar noon when the heat loss via re-radiation is maximum and the reactor temperature is at its peak (see Fig. 2). The exergy efficiency of the equivalent conventional CLC system (operated with zero solar energy input) is also shown in Fig. 6. It can be seen that the exergy efficiency of the solar integrated CLC system is 9.0% higher than that of a conventional CLC system at night time and is 1.0% higher at solar noon. When averaged over the 24 h day, the net increase in exergy efficiency is 7.0%.

It is well known that oxygen carrier particles become soft when the temperature of a CLC system approaches their melting point

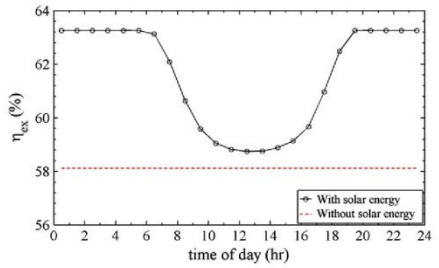

Fig. 6. The exergy efficiency of the conventional CLC system and the variations of the hourly average exergy efficiency of solar–CLC hybrid system with time of day.

[32]. Thus it is important to operate the solar–CLC hybrid system well below the particle's melting point. This generates a threshold for the operating temperature and consequently the solar share in this hybrid system. The solar share in this solar–CLC hybrid system also decreases by the re-radiation heat loss through the reactor aperture. The present solar–CLC hybrid system under these conditions achieves only a 6.5% average solar share over 24 h. This value can be increased by the application of oxygen carrier particles with a higher melting point, optimizing the operating conditions to decrease the fuel reactor temperature and/or increasing the mean flux concentration ratio of the heliostat field. The two former options decrease the heat losses by re-radiation and increase the diurnal operating time of the system.

In the present solar–CLC hybrid system, 70% of the absorbed solar thermal energy is stored in the oxygen carrier particles and the remaining is added to the fuel reactor output gas stream. Both the fuel and air reactor output gas steams can be used for power generation. However, since the fuel reactor output gas stream temperature changes with time it is undesirable to use this stream for power generation due to an unsteady power output which, in turn, would result in inefficiency of the storage systems. The storage efficiency of the system could be enhanced by optimization of the operating conditions or by a different design of the solar CLC hybrid system.

In this solar-hybrid CLC system, the stored sensible solar thermal heat is stored and released at temperatures of 1102 and 1386 K, respectively. Importantly, these temperatures are higher than those of molten salt systems and several systems proposed for solar TES [33] which offers a higher thermodynamic efficiency of power generation. Furthermore, since the stored energy in the particles is released at a higher temperature in air reactor the exergy losses associated with sensible heat storage mediums due to temperature drop are not significant in this solar hybrid system. These are significant advantageous of this system.

6. Conclusion

A novel solar–CLC hybrid system for steady base-load power production, despite diurnal fluctuations in solar input, is proposed which integrates a CLC plant with a solar thermal energy plant. The system maintains a constant operating temperature at the outlet from the air reactor despite the variations in the fuel reactor operating temperature due to the variation in solar thermal energy. The simulation predicts that 70% of the absorbed solar energy in solar fuel reactor is stored in the particles, while 14.25% of the total energy is lost due to re-radiation through solar fuel reactor aperture. The solar energy is also used efficiently, with the exergy efficiency of the proposed solar hybrid CLC being 7% higher than the reference CLC system without solar input when averaged over the 24 h day. The analysis shows that the solar thermal energy is stored as sensible heat in the oxygen carrier particles. A key limitation of the present configuration is that the solar fraction is relatively low, at about 6.5% when averaged over the whole day. However, this limit is only for the present configuration and a number of options are available to increase the solar fraction.

Acknowledgements

The authors wish to acknowledge the supportive environment of the Centre for Energy Technology in fostering research in solar thermal hybrids. The first author is grateful for the support of an Adelaide Scholarship International. The third author wishes to acknowledge the support of the Australian Research Council through a Discovery Outstanding Researcher Award.

References

[1] Liu W, King D, Liu J, Johnson B, Wang Y, Yang Z. Critical material and process issues for CO_2 separation from coal-powered plants. JOM J Min Metal Mater Soc 2009;61:36–44.
[2] Mokhtar M, Ali MT, Khalilpour R, Abbas A, Shah N, Hajaj AA, et al. Solar-assisted post-combustion carbon capture feasibility study. Appl Energy 2012;92:668–76.
[3] Concentrated Solar Power Heats Up. Emerging Energy Research (EER); 2006.
[4] Zhang Y, Smith SJ, Kyle GP, Stackhouse Jr PW. Modeling the potential for thermal concentrating solar power technologies. Energ Policy 2010;38:7884–97.
[5] Py X, Calvet N, Olives R, Meffre A, Echegut P, Bessada C, et al. Recycled material for sensible heat based thermal energy storage to be used in concentrated solar thermal power plants. J Sol Energ Eng 2011;133:031008.
[6] Koca A, Oztop HF, Koyun T, Varol Y. Energy and exergy analysis of a latent heat storage system with phase change material for a solar collector. Renew Energ 2008;33:567–74.
[7] Robak CW, Bergman TL, Faghri A. Economic evaluation of latent heat thermal energy storage using embedded thermosyphons for concentrating solar power applications. Sol Energy 2011;85:2461–73.
[8] Kolb GJ. Economic evaluation of solar-only and hybrid power towers using molten-salt technology. Sol Energy 1998;62:51–61.
[9] Group SLLC. Assessment of parabolic trough and power tower solar technology cost and performance forecasts. Chicago (IL): National Renewable Energy Laboratory (NREL); 2003.
[10] Mills D. Advances in solar thermal electricity technology. Sol Energy 2004;76:19–31.
[11] Abad A, Adánez J, García-Labiano F, de Diego LF, Gayán P, Celaya J. Mapping of the range of operational conditions for Cu-, Fe-, and Ni-based oxygen carriers in chemical-looping combustion. Chem Eng Sci 2007;62:533–49.
[12] Adánez J, Dueso C, de Diego LF, García-Labiano F, Gayán P, Abad A. Methane combustion in a 500 Wth chemical-looping combustion system using an impregnated Ni-based oxygen carrier. Energ Fuel 2008;23:130–42.
[13] Lyngfelt A, Leckner B, Mattisson T. A fluidized-bed combustion process with inherent CO_2 separation; application of chemical-looping combustion. Chem Eng Sci 2001;56:3101–13.
[14] Hossain MM, de Lasa HI. Chemical-looping combustion (CLC) for inherent separations – a review. Chem Eng Sci 2008;63:4433–51.
[15] Adanez J, Abad A, Garcia-Labiano F, Gayan P, de Diego LF. Progress in chemical-looping combustion and reforming technologies. Prog Energ Combust Sci 2012;38:215–82.
[16] Hong H, Jin H. A novel solar thermal cycle with chemical looping combustion. Int J Green Energy 2005;2:397–407.
[17] Hong H, Jin H, Liu B. A novel solar-hybrid gas turbine combined cycle with inherent CO_2 separation using chemical-looping combustion by solar heat source. J Sol Energ Eng 2006;128:275–84.
[18] Hong H, Han T, Jin H. A low temperature solar thermochemical power plant with CO_2 recovery using methanol-fueled chemical looping combustion. J Sol Energ Eng 2010;132:031002.
[19] Gayán P, de Diego LF, García-Labiano F, Adánez J, Abad A, Dueso C. Effect of support on reactivity and selectivity of Ni-based oxygen carriers for chemical-looping combustion. Fuel 2008;87:2641–50.
[20] Diver RB. Receiver/reactor concepts for thermochemical transport of solar energy. J Sol Energ Eng 1987;109:199–204.
[21] Z'Graggen A, Haueter P, Trommer D, Romero M, de Jesus JC, Steinfeld A. Hydrogen production by steam-gasification of petroleum coke using concentrated solar power—II Reactor design, testing, and modeling. Int J Hydrogen Energ 2006;31:797–811.
[22] Steinfeld A, Larson C, Palumbo R, Foley Iii M. Thermodynamic analysis of the co-production of zinc and synthesis gas using solar process heat. Energy 1996;21:205–22.
[23] Buck R, Brauning T, Denk T, Pfander M, Schwarzbozl P, Tellez F. Solar-hybrid gas turbine-based power tower systems (REFOSs). J Sol Energ Eng 2002;124:2–9.
[24] Dincer Ibrahim, Rosen MarcA. Exergy: energy, environment and sustainable development. Elsevier Science; 2007.
[25] Anheden M, Svedberg G. Exergy analysis of chemical-looping combustion systems. Energ Convers Manage 1998;39:1967–80.
[26] Morris DR, Szargut J. Standard chemical exergy of some elements and compounds on the planet earth. Energy 1986;11:733–55.
[27] Mattisson T, Johansson M, Lyngfelt A. The use of NiO as an oxygen carrier in chemical-looping combustion. Fuel 2006;85:736–47.
[28] Analysis of 10-years record Port Agusta Asutralia for Renewables SA.
[29] Steinfeld A, Kuhn P, Reller A, Palumbo R, Murray J, Tamaura Y. Solar-processed metals as clean energy carriers and water-splitters. Int J Hydrogen Energ 1998;23:767–74.
[30] Kribus A, Krupkin V, Yogev A, Spirkl W. Performance limits of heliostat fields. J Sol Energ Eng 1998;120:240–6.
[31] Perry RH, Green DW. Perry's Chemical Engineering's Handbook. New York, San Francisco, Washington, DC Auckland, Bogota, Libon, London, Madrid, Mexico City, Milan, Montreal, New Delhi, San Juan, Singapore, Sydney, Tokyo, Torento: McGraw-Hill; 1997.
[32] Jerndal E, Mattisson T, Lyngfelt A. Thermal analysis of chemical-looping combustion. Chem Eng Res Des 2006;84:795–806.
[33] Gil A, Medrano M, Martorell I, Lázaro A, Dolado P, Zalba B, et al. State of the art on high temperature thermal energy storage for power generation. Part 1-Concepts, materials and modellization. Renew Sust Energ Rev 2010;14:31–55.

CHAPTER 4

A HYBRID SOLAR CHEMICAL LOOPING COMBUSTION SYSTEM WITH A HIGH SOLAR SHARE

Statement of Authorship

Title of Paper	A hybrid solar chemical looping combustion system with a high solar share
Publication Status	⦿ Published, ○ Accepted for Publication, ○ Submitted for Publication, ○ Publication style
Publication Details	M. Jafarian, M. Arjomandi, G. J. Nathan, "A hybrid solar chemical looping combustion system with a high solar share". Applied Energy, (2014), vol: 126, p: 69–77.

Author Contributions

By signing the Statement of Authorship, each author certifies that their stated contribution to the publication is accurate and that permission is granted for the publication to be included in the candidate's thesis.

Name of Principal Author (Candidate)	Seyed Mehdi Jafarian		
Contribution to the Paper	Developed ideas, performed simulations and calculations, interpreted data, wrote manuscript and acted as corresponding author.		
Signature		Date	05/06/2014.

Name of Co-Author	Maziar Arjomandi		
Contribution to the Paper	Supervised development of work, helped in developing ideas, data interpretation and manuscript evaluation.		
Signature		Date	05.06.2014

Name of Co-Author	Graham Nathan		
Contribution to the Paper	Supervised development of work, helped in developing ideas, data interpretation and manuscript evaluation.		
Signature		Date	5-6-14

Name of Co-Author			
Contribution to the Paper			
Signature		Date	

Applied Energy 126 (2014) 69–77

Contents lists available at ScienceDirect

Applied Energy

journal homepage: www.elsevier.com/locate/apenergy

A hybrid solar chemical looping combustion system with a high solar share

Mehdi Jafarian *, Maziar Arjomandi, Graham J. Nathan

Centre for Energy Technology, School of Mechanical Engineering, The University of Adelaide, SA 5005, Australia

HIGHLIGHTS

- A novel hybrid solar chemical looping combustion system is presented.
- This hybrid CLC system integrates a CLC plant with a solar thermal energy plant.
- The oxygen carrier particles are used for chemical and sensible thermal energy storage.
- A solar cavity reactor is proposed for fuel reactor.
- The calculations show a total solar share of around 60% can be achieved.

ARTICLE INFO

Article history:
Received 11 October 2013
Received in revised form 24 February 2014
Accepted 27 March 2014
Available online 24 April 2014

Keywords:
Hybrid systems
Solar thermal energy
Chemical looping combustion
Energy storage

ABSTRACT

A novel hybrid solar chemical looping combustion (Hy-Sol-CLC) is presented, in which the oxygen carrier particles in a CLC system are employed to provide thermal energy storage for concentrated solar thermal energy. This hybrid aims to take advantage of key features of a chemical looping combustion (CLC) system that are desirable for solar energy systems, notably their inherent chemical and sensible energy storage systems, the relatively low temperature of the "fuel" reactor (to which the concentrated solar thermal energy is added in a hybrid) relative to that of the final temperature of the product gas and the potential to operate the fuel reactor at a different pressure to the heated gas stream. By this approach, it is aimed to achieve high efficiency of the solar energy, infrastructure sharing, economic synergy, base load power generation and a high solar fraction of the total energy. In the proposed Hy-Sol-CLC system, a cavity solar receiver has been chosen for fuel reactor while for the storage of the oxygen carrier particles two reservoirs have been added to a conventional CLC. A heat exchanger is also proposed to provide independent control of the temperatures of the storage reservoirs from those of solar fuel and air reactors. The system is simulated using Aspen Plus software for the average diurnal profile of normal irradiance for Port Augusta, South Australia. The operating temperature of the fuel reactor, solar absorption efficiency, solar share, fraction of the solar thermal energy stored within the solar reactor, the fractions of sensible and chemical storages and the system exergy efficiency are reported. The calculations show that a total solar share of around 60% can be achieved. Also reported is the sensitivity to the effects of key operating parameters, i.e. reservoir temperature, molar ratio of oxygen carrier particles to fuel, solar fuel reactor operating temperature and solar collector field concentration ratio.

1. Introduction

The combustion of fossil fuels over the last hundred years has led to a significant increase in CO_2 emissions, which is widely linked to the simultaneous increase in the global mean temperature [1]. However, despite the urgent need to decrease these CO_2 emissions, fossil fuels are likely to remain the dominant energy source for the short to medium term owing to their relative abundance and their established position worldwide [2]. Therefore, it is necessary to develop technologies that decrease the net CO_2 emissions from fossil fuel combustion, while also mitigating the significant economic and/or political advantages that favour the business-as-usual technologies. Two classes of technology under development to mitigate the release of CO_2 emissions are those associated with carbon capture and storage (CCS), which aims to prevent these emissions from being released to the atmosphere,

* Corresponding author. Address: School of Mechanical Engineering, The University of Adelaide, Adelaide, SA 5005, Australia. Tel.: +61 8 8303 5460.
E-mail address: mehdi.jafarian@adelaide.edu.au (M. Jafarian).

http://dx.doi.org/10.1016/j.apenergy.2014.03.071
0306-2619/

Nomenclature

A_{ap}	solar fuel reactor aperture area (m^2)
A_{coll}	area of solar collector field (m^2)
CR	mean flux concentration ratio
DNI	direct normal insolation (W/m^2)
Ex_i	exergy of ith stream (kJ/mol)
$\dot{E}x_s$	solar exergy (kW/mol)
LHV_{CH_4}	lower heating value CH_4 (kJ/mol)
$\dot{n}_i$	molar flow rate of ith stream (mol/s)
$\dot{q}_{ap,min}$	minimum aperture input solar thermal heat flux required (W/m^2)
$\dot{Q}_{ap}$	aperture input solar thermal power (W)
$\dot{Q}_{ap,min}$	minimum aperture input solar thermal power required (W)
$\dot{Q}_{coll}$	incoming power from solar collector (kJ/mol)
$\dot{Q}_F$	input fuel power (W)
$\dot{Q}_{non,st}$	non-stored power (W)
$\dot{Q}_{re-rad}$	re-radiated thermal power (W)
$\dot{Q}_{s,abs}$	absorbed solar thermal power (W)
$\dot{Q}_{s,in}$	input solar thermal power (W)
$\dot{Q}_{s,in,max}$	maximum input solar thermal power (W)
$\dot{Q}_{st}$	stored power in OC particles (W)
$Q_{st,t}$	total energy stored in OC particles (J)
T_{FR}	fuel reactor temperature (K)
T_i	temperature of stream ith (K)

Greek letters

α_{eff}	effective absorptance
ΔH_i	enthalpy of stream ith (kJ/mol)
ΔH	reaction enthalpy (kJ/mol)
ε_{eff}	effective absorptance
η_{abs}	absorption efficiency
η_{ex}	exergy efficiency
$\bar{\eta}_{coll}$	average collector system optical efficiency
σ	Stephan–Boltzmann constant ($W/m^2\,k^{-4}$)
$\emptyset$	molar ratio of oxygen carrier to fuel
$\chi_{non,st}$	non-store fraction
$\chi_{sol,t}$	thermal solar share
χ_{st}	storage fraction
$\chi_{st,ch}$	chemical storage fraction
$\chi_{st,sen}$	sensible heat storage fraction

Subscripts

abs	absorption
ap,open	solar fuel reactor aperture open
ap,close	solar fuel reactor aperture close
coll	collector
ex	exergy
in	input
out	output
F	fuel
P	particle

and renewable energy generation from sources such as solar radiation, which aims to avoid them. Most scenario analysis predict that a mix of both of these classes of energy technology will be employed in future [1,3]. Whilst these two classes of technology have been predominantly been developed independently, their hybridisation systems is now attracting growing attention, owning to its potential to combine the complementary benefits of these two different energy sources and thereby to lower the costs of greenhouse gas abatement [4].

Chemical looping combustion (CLC) is a newly proposed technology which provides inherent capability for CO_2 capture in the combustion of hydrocarbon fuels [5]. In this process, to avoid direct contact between the fuel and air, oxygen is transferred from the air to the fuel by utilisation of a solid oxygen carrier (OC). The main components of a CLC system are an air reactor and a fuel reactor. In the fuel reactor the OC particles are reduced through oxidation of the fuel. These reduced particles then are transported to the air reactor, in which they are oxidised by the air to produce metal oxide. The process is repeated by returning the metal oxide to the fuel reactor [5–8]. The oxidation of fuel within the fuel reactor can be endothermic or exothermic depending on the type of fuel and metal oxide used, while the oxidation of reduced metal oxides is always an exothermic reaction [9–11]. In the conventional CLC processes the required heat for the reaction between the fuel and oxygen carriers is provided by the exothermic oxidation of metal oxides in the air reactor [12]. This results in a temperature difference between the fuel and air reactors [12]. Consequently, if the required energy within the fuel reactor can be provided from an external source, such as concentrated solar thermal energy, the output from the CLC-based power plant will increase. In addition, this offers the possibility of the application of OC particles for chemical and/or sensible heat storage of solar thermal energy [13].

In the solar hybrid CLC systems, first proposed by Hong et al. [14–16], solar energy was proposed to provide the endothermic heat required for the reactions between the fuel and OC particles. This process advantageously converts the solar energy to chemical energy at a lower temperature than that of the exit temperature of the product gas, which favourably reduces radiation losses from the solar receiver. However, in this system the diurnal storage of the solar energy is not considered. A new hybrid solar CLC (Hy-Sol-CLC) concept in which OC particles are used as a storage medium of the concentrated solar thermal energy has recently been proposed by Jafarian et al. [13]. This hybrid system accounted for the transient nature of concentrated solar thermal energy and thereby enabled particles to be fed to the air reactor at a constant temperature, by adding three reservoirs to the conventional CLC system. A key limitation of this hybrid system is that the solar share is relatively low, at about 6.5%, based on the annually-averaged diurnal cycle. In addition, the increase in the solar fuel reactor operating temperature over that in a conventional CLC system has the potential to result in the deactivation of the OC particles and also increases the re-radiation heat loss through solar cavity reactor aperture over the case with no storage. Therefore, the aim of this current work is to investigate a novel alternative and patent-pending [17] solar-CLC hybrid system configuration that retains the base-load capability of previous system, while, both increasing the share of solar thermal energy in the system and limiting the increase in the temperature of the solar reactor due to the introduction of storage.

2. Conceptual design

Fig. 1 presents the key components of the proposed solar-CLC hybrid process [17]. In this hybrid system, concentrated solar thermal radiation from the solar collector field is captured and stored by the oxygen carrier (OC) particles within the solar fuel reactor at a constant temperature. The stored heat in the OC particles is then released in the air reactor at a higher temperature to produce a steady power output despite an intermittent solar radiation input

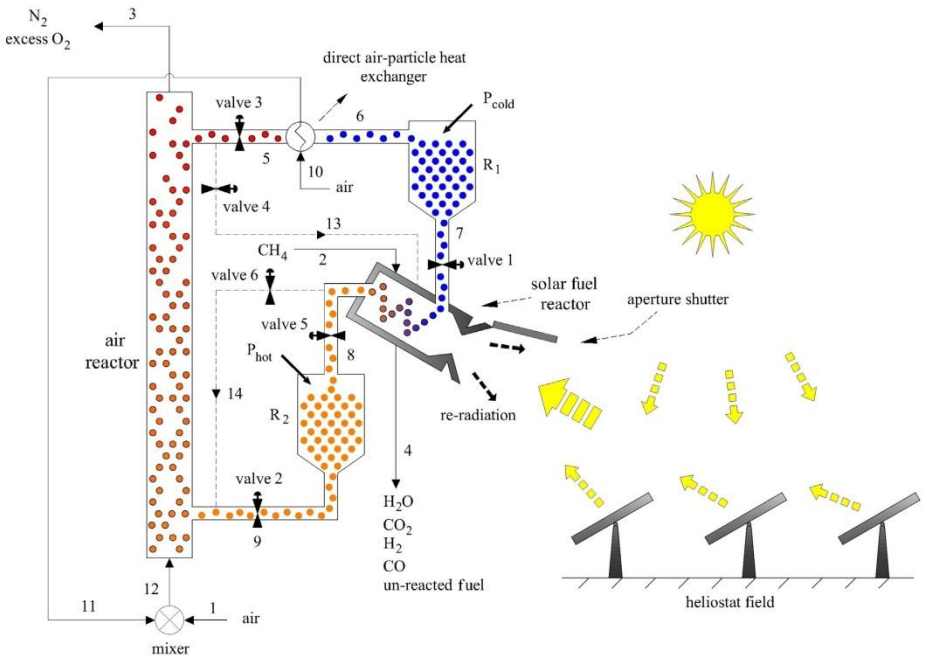

Fig. 1. The proposed solar-CLC hybrid system. Resrvoirs R_1 and R_2 are used to store the hot and cold particles produced in the solar fuel reactor and in the air reactors, respectively. A direct air-particle heat exhanger is employed to further cool the particles to the OC particle storage temperaure in resevior R_1. Valves 1 and 2 are used to control the flow rate of OC particles to the solar fuel and air reactors, respectively. The system can be also operated as a conventional CLC system using streams 13 and 14 and valves 3, 4, 5 and 6 [17].

using CLC process components (OC particles, fuel and air reactors). Methane (CH_4) is considered as fuel, being the dominant component of natural gas, and the particles tested by Johansson et al. [18] are chosen as the oxygen carrier. In these OC particles, NiO is supported by $NiAl_2O_4$ with a mass ratio of 4 to 6. These particles are selected due both to their endothermic reaction with CH_4 and appropriate performance in more than 100 h of operation in CLC prototype reactors, even though other OC particles could alternatively be considered.

The main components are the two CLC reactors, a direct air-particle heat exchanger and two particle storage reservoirs. The air reactor is operated continuously, while the fuel reactor must be designed to operate, both with and without solar energy input. One of the preferred options to achieve this is to adapt solar reactors or receivers, which are reported as the most suitable configuration for harnessing highly concentrated solar radiation [19]. A moveable aperture shutter is considered to cover the aperture and to reduce the losses when the solar insolation drops below a useful threshold. This allows the fuel oxidation reaction to occur in the same vessel, with or without concentrated solar energy, minimizing total infrastructure. Here, it is assumed that this modification is feasible without undertaking a detailed design.

When the available solar energy is sufficient to exceed the losses, the solar fuel reactor aperture is opened and the concentrated solar radiation is introduced into the solar fuel reactor to provide sensible heating of the OC particles and to drive the fuel oxidation reaction ($4NiO + CH_4 \rightarrow 4Ni + CO_2 + 2H_2O$ $\Delta H = 139$ kJ/mol_{CH_4} at $T = 750$ °C). The temperature of this reactor is kept constant by varying the flow rates of CH_4 (stream 2), and of the OC particles (stream 7). The reduced hot particles produced in the solar fuel reactor, shown as "P_{hot}" in Fig. 1, are stored in reservoir R_2. This allows the input flow rate of the oxygen carrier particles to the air reactor, stream 9, to be controlled and maintained constant despite variation in the solar energy input.

In the air reactor, the reduced OC particles react exothermically with oxygen from the air ($4Ni + 2O_2 \rightarrow 4NiO$ $\Delta H = -937139$ kJ/mol_{CH_4} at $T = 950$ °C). These particles, called P_{cold} in Fig. 1, are then stored in reservoir R_1 after being cooled by the air (stream 10) through a direct air-particle heat exchanger. This heat exchanger is added to the process, in between the air reactor and reservoir R_1, both to lower temperature of the stored OC particles in reservoir R_2 without reducing the oxidation reaction rate in the air reactor and to preheat the input air to the air reactor. Stream 1 is also used to control the operating temperature of the air reactor.

As described above, the process can also be run as a conventional CLC system, for extended periods of low solar radiation. In this mode of operation, the aperture of the solar fuel reactor is closed and the fuel reactor operates as in a conventional CLC system. In addition, the oxidised particles from the air reactor (stream 5 in Fig. 1), are transferred directly to the fuel reactor using valves 3, 4 to bypass reservoir R_1 using stream 13, where these particles are reduced using their own sensible heat. The reduced particles produced in the fuel reactor, are then introduced directly to the air reactor by means of valves 5, 6 and stream 14. Since a conventional CLC reactor does not employ an air-particle heat exchanger, this component is bypassed during the CLC-only operation. The operation of the system in conventional mode is beyond the scope of this work. However, further information can be found in [18,20].

The system can achieve a constant temperature and mass flow rate of the output from the air reactor (stream 3 in Fig. 1) with and without concentrated solar thermal energy for base-load power generation. Alternatively, it can also achieve a flexible operation (such as for load following), since the stored energy of the OC particles in the solar fuel reactor is released in the air reactor, which can be operated independently. Furthermore, the fuel reactor can be "over-sized" for those periods of high solar insolation to achieve longer term storage of solar energy in reservoir R_2 for use during periods of lower insolation. However, all of these issues are beyond the scope of the present investigation, in which we consider only the case of base-load power operation calculated from the annually averaged solar diurnal radiation profile. This is sufficient to estimate the average performance, although it does not account for all details of the long and short-term fluctuations caused by seasonal variability and cloud.

3. Methodology

Aspen Plus was used to model the performance of the proposed Hy-Sol-CLC system. The model solved the governing equations of mass and energy, simultaneously. The composition of the products was calculated by the Gibbs minimization method assuming ideal gas behaviour and the following components: CH_4, H_2O, CO_2, CO and H_2. Furthermore, to account for the dynamic performance of the Hy-Sol-CLC due to the time-varying concentrated solar thermal energy, a quasi-steady state condition based on the annually average variation of solar irradiance through the day was considered. It was also assumed that the system operates at atmospheric pressure. The physical properties of the OC particle components are available elsewhere [21].

The mass flow rate of the OC particles into the solar fuel reactor was calculated from the CH_4 flow rate, $\dot{n}_{CH_4}$, using the molar ratio of oxygen carrier particles to fuel, Ø, which is defined as the ratio of the flow rate of the OC particles introduced into the solar fuel reactor, $\dot{n}_{OC}$, to the flow rate of CH_4 [12]:

$$\phi = \frac{\dot{n}_{OC}}{4\dot{n}_{CH_4}}. \tag{1}$$

The incoming solar power from solar collector field, $\dot{Q}_{coll}$, is calculated by the direct normal insolation, DNI, and the average optical efficiency, $\bar{\eta}_{coll}$, of the collection system.

$$\dot{Q}_{coll} = \bar{\eta}_{coll} A_{coll}\,\mathrm{DNI}. \tag{2}$$

Here A_{coll} is the area of the solar collector field. For simplicity it is assumed that the receiver aperture size allows capture of all incoming power from the collector, so that $\dot{Q}_{s,in} = \dot{Q}_{coll}$ as explained in an earlier work [22].

Radiative heat losses are accounted for through the solar energy absorption efficiency, η_{abs}, which is defined as the net ratio of solar power absorbed by the solar fuel reactor, $\dot{Q}_{s,abs}$, to the solar power input through the solar cavity's aperture, $\dot{Q}_{s,in}$. This is calculated by [22]:

$$\eta_{abs} = \frac{\dot{Q}_{s,abs}}{\dot{Q}_{s,in}} = 1 - \frac{\varepsilon_{eff}\sigma T_{FR}^4}{\alpha_{eff}\,\mathrm{CR}\cdot\mathrm{DNI}}, \tag{3}$$

where ε_{eff}, α_{eff} and T_{FR} are the effective emittance, effective absorptance and the temperature of the solar cavity fuel reactor, respectively, σ is the Stephan–Boltzmann constant, DNI is the normal beam insolation and CR is the mean flux concentration ratio. A value of $\eta_{abs} = 0$ indicates that the input solar thermal energy to solar fuel reactor is equal to the re-radiation through the solar reactor aperture. Hence, it is important to identify the time at which the fuel reactor aperture must be closed or opened to have a net positive gain of solar input energy. The minimum value of solar heat flux required, $q_{ap,min}$, for a solar fuel reactor to work at a temperature of T_{FR} can be calculated by setting the absorption efficiency equal to zero (Eq. (3)) [13].

$$\dot{q}_{ap,min} = \frac{\dot{Q}_{ap,min}}{A_{ap}} = \frac{\varepsilon_{eff}\sigma T_{FR,0}^4}{\alpha_{eff}}. \tag{4}$$

When the heat flux produced by the collector field ($\mathrm{CR} = \dot{Q}_{ap}/(\mathrm{DNI}\cdot A_{ap})$) is lower than $q_{ap,min}$ calculated by Eq. (4), the solar fuel reactor aperture must be closed. For the present annually averaged daily radiation profile, the fuel and OC particles flow are stopped during these periods. Since in the considered case except the solar fuel reactor all of the process components work continuously, it is considered that the cooling within the fuel reactor due to intermittent operation does not affect the process operation significantly. As a result, the start up and shut down losses associated with the intermitted operation of the fuel reactor are neglected. It should also be noted that the fuel reactor does not need to be off for all times that the aperture is closed, but that the system can revert to conventional CLC operation when the storage capacity of the reservoirs reaches a lower threshold.

The total thermal solar share, $\chi_{sol,t}$, which is the contribution of the input solar thermal power to the solar hybrid system performance, [23] is calculated as follows:

$$\chi_{sol,t} = \frac{\int_{t_{ap,open}}^{t_{ap,close}} (\dot{Q}_{s,in} - \dot{Q}_{re-rad})\,dt}{\int_{t_{ap,open}}^{t_{ap,close}} (\dot{Q}_{s,in} - \dot{Q}_{re-rad})dt + \int_{t_{ap,open}}^{t_{ap,close}} (\dot{n}_{CH_4}\mathrm{LHV}_{CH_4})\,dt}, \tag{5}$$

where $\dot{Q}_{s,in}$ is the solar power input through the solar aperture, $\dot{Q}_{re-rad}$ is the reradiated power from solar reactor and LHV_{CH_4} is the lower heating value of CH_4. Subscripts "*ap,open*" and "*ap,close*" denote the condition where the solar fuel reactor aperture is opened or closed, respectively, and so when the fuel reactor operates with solar energy. However, the fuel reactor can also operate in conventional CLC mode, during periods of extended cloud, although such flows of methane are not considered here.

From the total input power into the solar hybrid system, comprising the absorbed solar power ($\dot{Q}_{s,abs}$) and power of fuel ($\dot{Q}_F$), a fraction is stored in particles ($\dot{Q}_{st}$), while the rest leaves the system via stream 4. The total storage fraction, χ_{st}, is defined as:

$$\chi_{st} = \frac{\int_{t_{ap,o}}^{t_{ap,close}} \dot{Q}_{st}\,dt}{\int_{t_{ap,open}}^{t_{ap,close}} \dot{Q}_{s,abs}\,dt + \int_{t_{ap,open}}^{t_{ap,close}} \dot{Q}_F\,dt} = \frac{\int_{t_{ap,open}}^{t_{ap,close}} \dot{n}_{CH_4}.\phi(\Delta H_8 - \Delta H_7)\,dt}{\int_{t_{ap,open}}^{t_{ap,close}} (\dot{Q}_{s,in} - \dot{Q}_{re-rad})\,dt + \int_{t_{ap,open}}^{t_{ap,close}} (\dot{n}_{CH_4}\mathrm{LHV}_{CH_4})\,dt}. \tag{6}$$

The numerator of this equation indicates the total amount of energy stored in the OC particles in reservoir R_2, $Q_{st,t}$ for the whole operation time of the solar fuel reactor. The non-stored fraction of input energy, $\chi_{non,st}$, that leaves the fuel reactor via stream 4 (see Fig. 1) can be calculated by:

$$\chi_{non,st} = 1 - \chi_{st}, \tag{7}$$

The stored energy in OC particles comprises of both chemical and sensible heat. Therefore, to distinguish the fractions of sensible and chemical stored energy, the sensible heat stored fraction, $\chi_{st,sen}$, is defined as the ratio of the sensible stored heat in both the metal oxide and the inert materials to the total heat stored in the metal oxide particles. The sensible and chemical storage fractions can be calculated by:

$$\chi_{st,sen} = \frac{\int_{t_{ap,open}}^{t_{ap,close}} \int_{T_7}^{T_8} (\dot{n}_{ox,ex}C_{p,ox} + \dot{n}_{Inert}C_{p,Inert})\,dT\,dt}{\int_{t_{ap,open}}^{t_{ap,close}} \dot{n}_{CH_4}.\phi(\Delta H_8 - \Delta H_7)\,dt}, \tag{8}$$

$$\chi_{st,ch} = 1 - \chi_{st,sen}. \tag{9}$$

Here, $\dot{n}_{ox,ex}$ is the flow rate of excess metal oxides leaving the solar fuel reactor (stream 8 in Fig. 1), $\dot{n}_{inert}$ is the flow rate of inert materials (stream 7 or 8 in Fig. 1) and $C_{p,ox}$ and $C_{p,inert}$ are the heat capacities of metal oxide and inert materials, respectively.

The exergy efficiency is defined as the ratio of the net output exergy to the total input exergy [24]:

$$\eta_{ex} = \frac{\int_{t_{op,open}}^{t_{op,close}} (\dot{n}_3 Ex_3 + \dot{n}_4 Ex_4)\, dt}{\int_{24\ hours} (\dot{E}x_s + \dot{n}_1 Ex_1 + \dot{n}_2 Ex_2 + \dot{n}_{10} Ex_{10})\, dt}. \quad (10)$$

Here Ex_i and $\dot{n}_i$ are the molar exergy and molar flow rate of stream i (i = 1, 2, 3, 4, 10), respectively, and $\dot{E}x_s$ is the exergy of the absorbed solar thermal power, shown in Fig. 1. The exergy of the absorbed solar thermal power is given by [15]:

$$\dot{E}x_s = (\dot{Q}_{s,in} - \dot{Q}_{s,r})\left(1 - \frac{T_0}{T_{FR}}\right), \quad (11)$$

where T_0 is the ambient temperature. The exergies of different components have been calculated from previous works [25,26]. The input air exergy is ignored since it is at ambient conditions.

The key operating conditions of the solar-CLC hybrid system are presented in Table 1. The solar energy added to the solar fuel reactor is calculated based on the direct normal irradiance data for Port Augusta, South Australia [27] and the solar collector optical efficiency given in Table 1. The results are relative to the average maximum solar power input to solar fuel reactor, $\dot{Q}_{s,in,max}$, for Port Augusta, South Australia [27], which occurs at 12:30.

The Aspen Plus model was validated by repeating the calculations of the Hong et al. [14,15] with the same input parameters, as reported in our previous work [13]. The sensitivity of the model to variation of the parameters listed in Table 1 was also assessed to detect those variables with the greatest influence on the system operation.

4. Results and discussion

The temperature, composition and average flow rates of each stream relative to the maximum solar power input to the solar fuel reactor are shown in Table 2. Since the operating temperature of the solar fuel reactor is considered to be constant at 750 °C, the temperature of the stored particles in reservoir R_1 is also 750 °C. While the input particles to the fuel reactor input stream (stream 7 in Fig. 1) comprise of NiO and $NiAl_2O_4$, the fuel reactor output stream (stream 8 in Fig. 1) contains a mixture of Ni, NiO and $NiAl_2O_4$. The equilibrium calculations predict that the fuel is approximately fully converted to CO_2 and H_2O, while the mole fractions of CO, H_2 and un-reacted CH_4 in the outlet stream from the fuel reactor (stream 4 in Fig. 1) are less than 0.01 and 0.001, respectively. The simulations also predict the total mass of stored particles to be 46.550 kg/$kW_{s,max}$ and 44.96 kg/$kW_{s,max}$ for reservoirs R_1 and R_2, respectively, where the symbol $kW_{s,max}$ is the maximum solar power input to the reactor based on the annually averaged profile, i.e. at solar noon. The difference between the relative weights per unit of solar heat in reservoirs R_1 and R_2 is attributed to the difference in the masses of reduced and oxidised OC particles. The flow rates of input air (stream 1 in Fig. 1) and cooling air (stream 10 in Fig. 1) per unit of maximum solar heat are constant at 4.23 mol/MJ and 15.33 mol/MJ, respectively. However, the flow rates of CH_4 and OC particles per unit of maximum heat flux (stream 2, 4, 7 and 8) must change with the solar energy heat flux to achieve a constant operating temperature in the fuel reactor.

Fig. 2 presents the calculated diurnal variations of the average CH_4 flow rate (stream 2 in Fig. 1) relative to the maximum solar power input to solar fuel reactor, $\dot{n}_{CH_4}/\dot{Q}_{s,in,max}$, for the hourly average solar insolation of Port Augusta, South Australia [27]. As shown, $\dot{n}_{CH_4}/\dot{Q}_{s,in,max}$ increases from a minimum of 1.52×10^{-2} mol/MJ at 6:30 to a maximum of 7.8×10^{-1} mol/MJ at 12:30, when the solar insolation is at its maximum, and then decreases to 1.2×10^{-1} mol/MJ at 18:30 when the fuel reactor aperture is closed. The area under the curve shown in Fig. 2 corresponds to the total relative CH_4 consumption over the whole solar day and is 6.92 mol/$MW_{s,max}$. The minimum required threshold of the concentrated solar radiation heat flux with the considered mean flux concentration ratio and operating temperature of the solar fuel reactor is 31.05 kW/m^2, which is exceeded between 6:30 to 18:30 for this annually averaged insolation [27].

Fig. 3 presents the average diurnal variation of the calculated absorption efficiency, η_{abs}, of the solar cavity fuel reactor for the present hybrid-CLC system. It can be seen that η_{abs} increases sharply from 0.27 at 6:30 to 0.95 at 12:30 and then decreases to 0.75 at 18:30. However, η_{abs} varies little during the period 10:30 to 16:30, since the solar flux varies little during this period [27]. Hence too, $\dot{n}_{CH_4}$ varies little during this period as shown in Fig. 2.

Fig. 4 presents the calculated average diurnal variations of the normalized absorbed solar power, $\dot{Q}_{s,abs}/\dot{Q}_{s,in,max}$; input fuel power, $\dot{Q}_F/\dot{Q}_{s,in,max}$, and the heat lost through re-radiation from the solar fuel reactor aperture, $\dot{Q}_{re\text{-}rad}/\dot{Q}_{s,in,max}$. Since it is assumed that the fuel reactor operates at a constant temperature of 750 °C, the normalized heat loss through re-radiation form solar fuel reactor aperture to maximum solar heat is constant at 5×10^{-2}. The normalized absorbed solar power in solar fuel reactor per maximum solar heat increases from 1.8×10^{-2} at 6:30 to 95×10^{-2} at 12:30 and then decreases to 15×10^{-2} at 18:30, when the aperture is closed. The normalized power of the fuel shows the same trend. It increases from an initial value of 1.2×10^{-2} at 6:30 to reach a peak value of 62.8×10^{-2} at 12:30 and then decreases to a final value of 1×10^{-1} at 18:30.

The calculated average diurnal variations of the normalized stored power in OC particles, $\dot{Q}_{st}/\dot{Q}_{s,in,max}$; the non-stored power (stream 4 in Fig. 1), $\dot{Q}_{non,st}/\dot{Q}_{s,in,max}$; and the power added to the air in the air reactor (stream 3 in Fig. 1), $\dot{Q}_{out,3}/\dot{Q}_{s,in,max}$; are also

Table 1
Main assumptions for the hybrid solar-CLC system.

Parameter	Reference operating conditions	Variation range	Source
Effective absorptance (α_{eff})	1		[22,28]
Effective emittance (ε_{eff})	1		[22,28]
Optical efficiency of solar collector filed (%)	65		[29]
Mean flux concentration ratio	2000	500–8000	
Solar fuel reactor temperature (°C)	750	550–950	[18]
Air reactor temperature (°C)	950		[18]
Reservoir R_1 (°C)	100	100–750	
Input fuel and air pressures (atm)	1		
Input fuel and air temperatures (°C)	25		
Fuel air reactors pressure (atm)	1		
Molar ratio of oxygen carrier particles to fuel (Ø)	2.5	1–4.5	
Approach temperature in direct air-particle heat exchanger (°C)	100		

Table 2
Temperature, composition and relative flow rate of different streams per unit of maximum solar heat input to solar fuel reactor of the solar-CLC hybrid system.

Stream no.	$\dot{n}_i/\dot{Q}_{s,in,max}$ (mol/MJ)	T (°C)	Gas phase							Solid phase		
			y_{N_2}	y_{O_2}	y_{CO_2}	y_{H_2O}	y_{CO}	y_{H_2}	y_{CH_4}	x_{NiO}	x_{Ni}	$x_{NiAl_2O_4}$
1	4.23	25	0.79	0.21	0.0	0.0	0.0	0.0	0.0			
2	Variable	25	0.0	0.0	0.0	0.0	0.0	0.0	1.0			
3	16.82	950	0.87	0.13	0	0	0	0	0			
4	Variable	750	0	0	0.33	0.67	<0.01	<0.01	<0.001			
5	4.72	950								0.61	0	0.39
6	4.72	100								0.61	0	0.39
7	Variable	100								0.61	0	0.39
8	Variable	750								0.37	0.24	0.39
9	4.72	750								0.37	0.24	0.39
10	15.3	25	0.79	0.21	0.0	0.0	0.0	0.0	0.0			
11	15.3	850	0.79	0.21	0.0	0.0	0.0	0.0	0.0			
12	19.6	683	0.79	0.21	0.0	0.0	0.0	0.0	0.0			

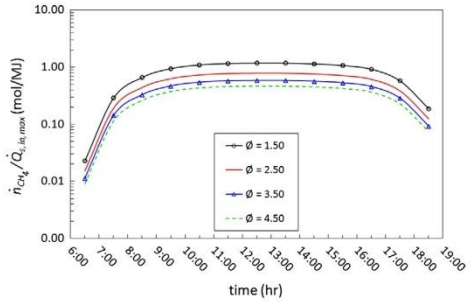

Fig. 2. The calculated average diurnal variations of the CH_4 flow rate per maximum solar power input, shown as $\emptyset = 2.5$, for the reference case given in Table 1 and the radiation of Port Augusta, South Australia [27]. Calculated sensitivity of the diurnal fuel flow rate relative to the maximum solar power input for four molar ratio of oxygen carrier particles to fuels.

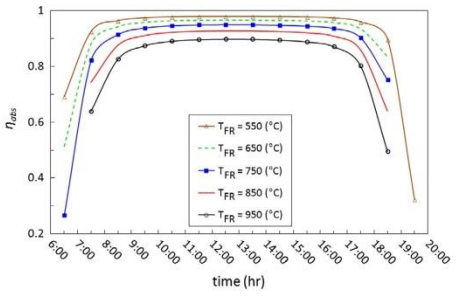

Fig. 3. The calculated absorption efficiency of the solar fuel reactor (shown as T_{FR}= 750 °C) and the calculated sensitivity of the solar fuel reactor absorption efficiency to the operating temperature of the solar fuel reactor for the reference operating conditions given in Table 1 and the average diurnal solar radiation of Port Augusta, South Australia [27].

shown in Fig. 4. As shown, $\dot{Q}_{st}/\dot{Q}_{s,in,max}$ increases from an initial value of 0.029 at 6:30 to a peak of 1.51 at 12:30 and then decreases to 0.24 at t = 18:30. As expected, $\dot{Q}_{non,st}/\dot{Q}_{s,in,max}$ shows the same trend. It increases from 1.38×10^{-3} at t = 6:30 to 0.071 at t = 12:30 and then decreases to 0.011 at t = 18:30. These trends are attributed to the increase in the inlet flow-rates of CH_4, shown in Fig. 2, and of OC particles with concentrated solar input heat. In contrast, $\dot{Q}_{non,st}/\dot{Q}_{s,in,max}$ is constant at 0.55.

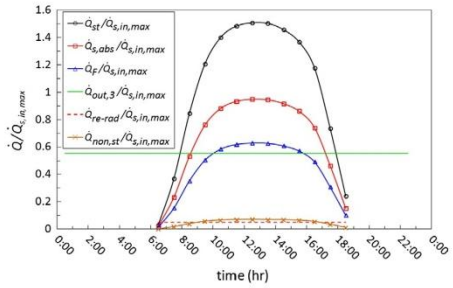

Fig. 4. The calculated normalized hourly average variations of the absorbed solar radiation in the fuel reactor, the input power of the fuel, the stored power in OC particles, the heat loss through re-radiation from solar fuel reactor aperture and the power added to air within the air reactor to the maximum solar power input to fuel reactor for the reference operating conditions given in Table 1 and the average solar insolation at Port Augusta, South Australia [27].

The area under the curves $\dot{Q}_{s,abs}/\dot{Q}_{s,in,max}$ and $\dot{Q}_F/\dot{Q}_{s,in,max}$, shown in Fig. 4, corresponds respectively to the total solar energy absorbed in solar fuel reactor and the total fuel energy input relative to the maximum solar input. Similarly, that under $\dot{Q}_{st}/\dot{Q}_{s,in,max}$ and $\dot{Q}_{non,St}/\dot{Q}_{s,in,max}$ correspond to the relative total energy stored in OC particles and total energy that leaves the fuel reactor. Using Eqs. (5)–(9), the values of $\chi_{sol,t}$, χ_{st}, $\chi_{non\text{-}st}$, $\chi_{st,sen}$ and $\chi_{st,ch}$ are 0.60, 0.95, 0.05, 0.46 and 0.54, respectively. A solar share of 0.60 means the CO_2 produced per unit of heat generated in this hybrid-system is 60% less than that of a conventional, non-solar CLC system. The area under the curve $\dot{Q}_{out,3}/\dot{Q}_{s,in,max}$ is the total heat added to the air in the air reactor, stream 3 in Fig. 1, which is equal to the total heat stored in the OC particles. That is, from the total net input energy to the system, comprising both fuel and absorbed solar energy, 95.0% is released at constant temperature and flow rate; hence it is suitable for base load power generation. Eq. (10) predicts an exergy efficiency of 0.63 for the solar hybrid CLC system under these conditions.

4.1. Effect of reservoir R_1 temperature

The average diurnal variation of the fuel flow rate per unit of maximum solar power input to the fuel reactor, $\dot{n}_{CH_4}/\dot{Q}_{s,in,max}$, is presented for different temperatures of the reservoir R_1, T_{R_1}, in Fig. 5. As mentioned before, this temperature is controlled by the direct air-particle heat exchanger. The total CH_4 required are equal to the area under the curves in Fig. 5. It can be seen that the value of $\dot{n}_{CH_4}$ required to maintain a constant temperature within the

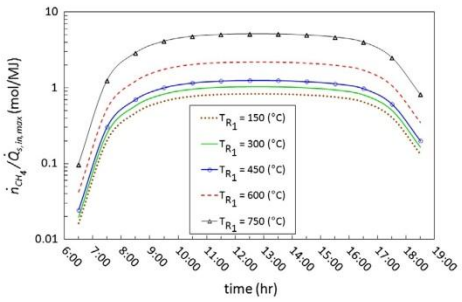

Fig. 5. The calculated sensitivity to variations in temperature of reservoir R_1 of the CH_4 flow rate per maximum solar power input to solar fuel reactor for the reference conditions (Table 1) and the average solar insolation at Port Augusta, South Australia [27].

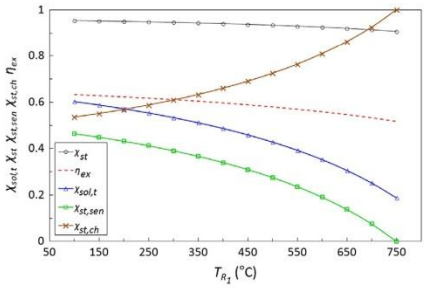

Fig. 6. The calculated sensitivity to variations in the temperature of the reservoir R_1 of the total solar share, the storage fraction, the sensible heat storage fraction, the chemical storage fraction and the exergy efficiency of the solar hybrid CLC system for the reference conditions (Table 1) and the average solar insolation at Port Augusta, South Australia [27].

solar fuel reactor increases with T_{R_1}. For example, for $T_{R_1} = 150$ °C the total CH_4 required is 7.36 mol/MJ while it is 45.4 mol/MJ for $T_{R_1} = 750$ °C. This is because more solar energy can be absorbed with a lower particle inlet temperature to the reactor and demonstrates the benefit of introducing the air-particle heat exchanger (stream 10 in Fig. 1) to lower this temperature.

Fig. 6 shows the calculated sensitivity of $\chi_{sol,t}$, χ_{st}, $\chi_{st,sen}$ and $\chi_{st,ch}$ to the variations in temperature of reservoir R_1, T_{R_1}. As can be seen, $\chi_{st,sen}$ decreases with T_{R_1} from 0.46 at $T_{R_1} = 100$ °C to 0.0 at $T_{R_1} = 750$ °C, when the inlet temperature of the input OC particles to the solar fuel reactor is equal to its operating temperature. Self-evidently, the temperature differential between the input OC particles and that of the fuel reactor limits the capacity for sensible heat storage in the OC particles. Since the chemical energy stored by the particles requires the consumption of methane, this consumption limits the solar fraction, so that the storage of further solar energy can only be achieved by sensible heat energy storage. (Note also that the solar heat absorbed by the fuel reactor is independent of the particle inlet temperature, depending only on reactor temperature). Hence too, more heat leaves the reactor through stream 4 as non-stored heat. Together these effects explain why $\chi_{sol,t}$ and χ_{st} decrease with T_{R_1} from 0.60 and 0.95 at $T_{R_1} = 100$ °C to 0.91 and 0.19 at $T_{R_1} = 750$ °C, respectively. The predicted variation of the solar hybrid system exergy efficiency, η_{ex}, with T_{R_1} is also shown in Fig. 6 and is calculated to decrease from 0.63 at $T_{R_1} = 100$ °C to 0.52 at $T_{R_1} = 750$ °C. This is attributed to the increase in CH_4 flow rate to the system with T_{R_1} (Fig. 5), which is associated with an increase in the fuel exergy to the system (Eq. (10)) and a decrease in the sensible storage fraction. However, due to the physical limitations of the OC particles the operating temperature of the air reactor is held constant at 950 °C, which in turn limits the exergy released to the air reactor (Eq. (10)).

4.2. Effect of molar ratio of oxygen carrier particles to fuel (Ø)

Fig. 2 also presents the calculated sensitivity to the variations in Ø of the fuel flow rate per maximum solar power input to solar fuel reactor. It can be seen that $\dot{n}_{CH_4}/\dot{Q}_{s,in,max}$ decreases by a factor of about 3 as Ø is increased from 1 to 4.5. For example, a total of 14.1 mol CH_4 is required per MJ of maximum solar power input for Ø = 1.0, while it is 4.13 mol/$MJ_{s,max}$ for Ø = 4.50. This is due to the increased thermal mass, and hence sensible heat storage that accompanies excess particles, although presumably kinetic issues will introduce additional benefits. This highlights the benefits of employing an excess of oxygen carrier particles.

Fig. 7 presents the sensitivity of the predicted $\chi_{sol,t}$, χ_{st}, $\chi_{st,sen}$ and $\chi_{st,ch}$ to variations in Ø. As noted above, the input solar energy to the solar fuel reactor is independent of the inlet temperature, so that increasing Ø increases the sensible heat required to heat the particles, and hence $\chi_{st,sen}$. Consequently $\chi_{st,ch}$ is reduced, lowering the consumption of CH_4 flow (Fig. 2), while $\chi_{sol,t}$ increases. For example, $\chi_{sol,t}$ is increased from 0.43 to 0.72 as Ø is increased from 1.0 to 4.5, and $\chi_{st,sen}$ is increased simoltaneously from 0.21 to 0.62. Commonsurate with this is a decrease in $\chi_{st,ch}$ from 0.79 to 0.38. In addition, decreasing the flow rate of CH_4 (with an increase in Ø) lowers the flow rate of gases leaving the solar fuel reactor (stream 4 in Fig. 1), which also increases χ_{st}. For example, while χ_{st} is 0.93 for Ø = 1.0 it is 0.97 for Ø = 4.50.

The sensitivity of the exergy efficiency of the hybrid system to variations in Ø is also depicted in Fig. 7. This shows that the exergy efficiency of the system increases with Ø. For example increasing Ø from 1 to 4.50 raises η_{ex} from 0.58 to 0.67. This is attributed to the reduction of both the CH_4 flow rate and $\chi_{st,ch}$ with increasing Ø as shown in Figs. 7 and 8, respectively.

4.3. Effect of solar fuel reactor temperature

The calculated sensitivity of the solar fuel reactor absorption efficiency to the solar fuel reactor temperature is also shown in Fig. 3. As expected, η_{abs} decreases with an increase in T_{FR}. This is caused by the increase in the re-radiation heat loss through the reactor aperture with T_{FR}. Moreover, the drop in η_{abs} is more significant at lower T_{FR} than at high values due to nonlinear relation between temperature and re-radiation heat loss. For instance, increasing T_{FR} from 550 °C to 650 °C decreases the maximum η_{abs},

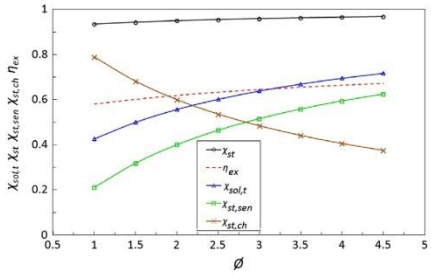

Fig. 7. The calculated sensitivity to variation in molar ratio of oxygen carrier particles to fuel of the total solar share, storage fraction, sensible heat storage fraction, chemical heat storage fraction and exergy efficiency of the solar hybrid CLC system for the reference conditions (Table 1) and the average solar insolation at Port Augusta, South Australia [27].

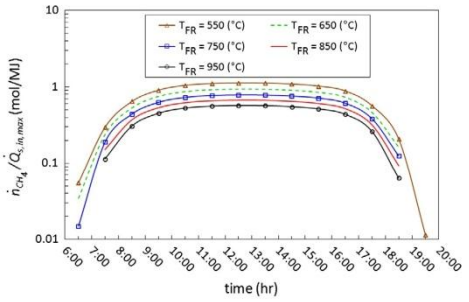

Fig. 8. The calculated sensitivity to the solar fuel reactor operating temperature of the fuel flow rate per maximum solar power input to the solar fuel reactor for the reference conditions given in Table 1 and the average solar insolation at Port Augusta, South Australia [27].

at t = 12:30, by 0.60%, while this drop is 1.71% for the increase from 900 °C to 950 °C. The temperature of the fuel reactor also affects the operating duration of the fuel reactor. As shown in Fig. 3, the average daily operating time of the solar fuel reactor is 13 h for T_{FR} = 550 °C, and 11 h for T_{FR} = 950 °C.

The predicted sensitivity of the relative CH_4 flow rate, $\dot{n}_{CH_4}/\dot{Q}_{s,in,max}$, to the variations in T_{FR} is shown in Fig. 8. It can be seen that the total daily CH_4 flow rate i.e. the area under the curve $\dot{n}_{CH_4}/\dot{Q}_{s,in,max}$, decreases with an increase in T_{FR}. For example, $\dot{n}_{CH_4}/\dot{Q}_{s,in,max}$ = 10.1 mol/$MJ_{s,max}$ at T_{FR} = 550 °C, while it is 4.95 mol/$MJ_{s,max}$ at T_{FR} = 950 °C. This is because the amount of sensible heat storage increases with the temperature difference between the OC particles in reservoir R_1 and the fuel reactor.

The sensitivity to variations in solar fuel reactor temperature of the predicted $\chi_{sol,t}$ and χ_{st} is shown in Fig. 9. Importantly, even though η_{abs} decreases with an increase in T_{FR}, the solar share increases with it. For example, $\chi_{sol,t}$ increases from 0.52 to 0.66 as T_{FR} is increased from 550 °C to 950 °C. This is due to the increase in sensible heat storage associated with the decrease of the CH_4 flow rate with T_{FR}, described above (Fig. 8). However, χ_{st} is not strongly sensitive to T_{FR}, varying by only 1.33% over the temperature range considered, so that $\chi_{st,sen}$ increases with T_{FR} while $\chi_{st,ch}$ decreases with it. Finally, it can be seen that the exergy efficiency of the system, decreases slightly from 0.65 to 0.62 as T_{FR} is increased from 550 °C to 950 °C. This is attributed to increase in re-radiation heat losses through the aperture of the solar fuel reactor with T_{FR} (Fig. 3).

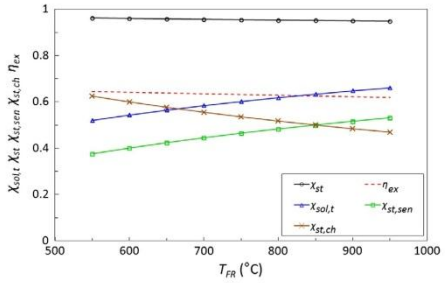

Fig. 9. The calculated sensitivity to the variations in the solar fuel reactor operating temperature of the total solar share, storage fraction, sensible and chemical heat storage fraction and the exergy efficiency of the solar hybrid CLC system for the reference conditions (Table 1) and the average solar insolation at Port Augusta, South Australia [27].

4.4. Effect of concentration ratio

The sensitivity of the calculated absorption efficiency of the fuel reactor to the variations in the concentration ratio of the solar collector field, CR, is depicted in Fig. 10. As expected, η_{abs} increases with the CR. However, this effect of CR is more significant at low values of CR than at high ones. For example, doubling the CR from 500 to 1000 increases the peak absorption efficiency (at t = 13:30) by 12.4% in contrast to a 1.29% increase for doubling CR from 4000 to 8000. Since the minimum threshold of the required heat flux for the solar fuel reactor operation decreases with CR (Eq. (3)), the operating duration time of the solar fuel reactor also increases with CR. As shown, the average operating time of the solar fuel reactor is 12 h for CR = 500 and 14 h for CR = 8000.

Fig. 11 presents the calculated variations of CH_4 flow rate with CR. It can be seen that this flow rate increases with CR, consistent with the increase in η_{abs} with CR (Fig. 11). Also as above, this increase is more significant as CR is decreased due both to the nonlinearity of η_{abs} with CR (Fig. 10), and to the dependence of operating time on CR.

Fig. 12 shows the sensitivity of the calculated $\chi_{sol,t}$, χ_{st}, $\chi_{st,sen}$, $\chi_{st,ch}$ and η_{ex} to the CR. Importantly, all of these parameters are found independent of CR. This is attributed to the control strategy for the reactor, in which the reactor is controlled at constant temperature by proportional variations of the flow rates of fuel and OC particles to the absorbed solar thermal heat within the solar fuel

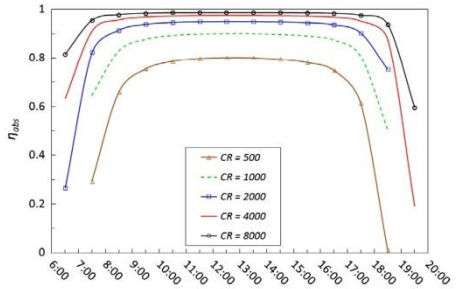

Fig. 10. The calculated sensitivity to solar collector field concentration ratio of the solar fuel reactor absorption efficiency for the reference conditions given in Table 1 and the average solar insolation at Port Augusta, South Australia [27].

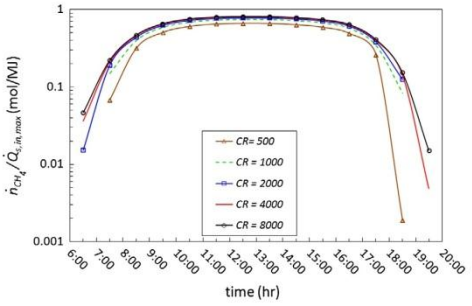

Fig. 11. The calculated sensitivity of the fuel flow rate per maximum solar power input to solar fuel reactor to solar collector field mean flux concentration ratio for the reference conditions (Table 1) and the average solar insolation at Port Augusta, South Australia [27].

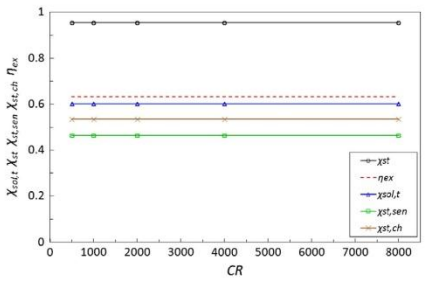

Fig. 12. The calculated sensitivity to the mean flux concentration ratio of the solar collector of the total solar share, the storage fraction, the sensible heat storage fraction, the chemical heat storage and the exergy efficiency of the solar hybrid CLC system operated to achieve constant reactor temperature for the reference conditions given in Table 1 and the average solar insolation at Port Augusta, South Australia [27].

reactor. Nevertheless, it should be noted that the total solar energy that can be extracted from the process increases with CR, due both to the lowering of the threshold of DNI at which solar energy can be absorbed by the reactor and to the increased absorption efficiency of the solar fuel reactor with increasing CR.

5. Conclusion

The proposed solar-CLC hybrid system is estimated to achieve a solar fraction of up to 60% while providing sufficient storage to achieve continuous base-load power generation, for the average diurnal fluctuations in solar radiation. This result assumes the availability of a solar fuel reactor suitable for intermittent operation with low start-up and shut-down losses, which is yet to be demonstrated at scale. On this basis, and with the assumption listed in Table 1, the system is modelled to achieve a constant operating temperature and flow rate at the outlet from the air reactor despite the variations in the flows to fuel reactor associated with the variable solar input. For the reference operating conditions considered, the simulation predicts that 95% of the total input energy to solar fuel reactor, from the CH_4 and the absorbed solar energy, is stored in the particles as chemical and sensible energy, while 7.14% of the total input solar energy is lost due to re-radiation through solar fuel reactor aperture. At the highest solar fraction of 60%, 46% of the total heat is stored as sensible heat and 54% as chemical heat. The sensitivity analysis found that:

- The sensible storage fraction and the exergy efficiency of the system decrease with an increase in particle storage temperature in reservoir R_1. However, the total energy stored in the OC particles in reservoir R_2 increases with it.
- The total heat stored in particles in reservoir R_2 decreases with an increase in the molar ratio of oxygen carrier particles to fuel, while, the exergy efficiency and sensible heat storage fraction in OC particles increases with it.
- An increase in solar fuel reactor operating temperature increases the solar share and sensible heat storage fraction. However, it decreases the total heat stored in reservoir R_2.
- The exergy efficiency, total storage fractions and sensible heat storage fraction remain constant with an increase in the solar collector mean flux concentration ratio. However, the total heat stored in reservoir R_2 and the solar absorption efficiency increase with it.

Acknowledgements

The first author is grateful for the support of an Adelaide Scholarship International. The third author wishes to acknowledge the support of Australian Research Council through a Discovery Outstanding Researcher Award.

Reference

[1] Carbon Dioxide Capture and Storage: Special Report of the Intergovernmental Panel on Climate Change: Cambridge University Press; 2005.
[2] García-Labiano F, de Diego LF, Adánez J, Abad A, Gayán P. Temperature variations in the oxygen carrier particles during their reduction and oxidation in a chemical-looping combustion system. Chem Eng Sci 2005;60:851–62.
[3] IEA. Technology roadmap – concentrating solar power. International Energy Agency; 2010a.
[4] Kolb GJ. Economic evaluation of solar-only and hybrid power towers using molten-salt technology. Sol Energy 1998;62:51–61.
[5] Adanez J, Abad A, Garcia-Labiano F, Gayan P, de Diego LF. Progress in chemical-looping combustion and reforming technologies. Prog Energy Combust Sci 2012;38:215–82.
[6] Abad A, Adánez J, García-Labiano F, de Diego LF, Gayán P, Celaya J. Mapping of the range of operational conditions for Cu-, Fe-, and Ni-based oxygen carriers in chemical-looping combustion. Chem Eng Sci 2007;62:533–49.
[7] Lyngfelt A, Leckner B, Mattisson T. A fluidized-bed combustion process with inherent CO_2 separation; application of chemical-looping combustion. Chem Eng Sci 2001;56:3101–13.
[8] Hossain MM, de Lasa HI. Chemical-looping combustion (CLC) for inherent separations—a review. Chem Eng Sci 2008;63:4433–51.
[9] Adánez J, de Diego LF, García-Labiano F, Gayán P, Abad A, Palacios JM. Selection of oxygen carriers for chemical looping combustion. Energy Fuels 2004;18:371–7.
[10] Jerndal E, Mattisson T, Lyngfelt A. Thermal analysis of chemical-looping combustion. Chem Eng Res Des 2006;84:795–806.
[11] Jerndal E, Mattisson T, Lyngfelt A. Investigation of different $NiO/NiAl_2O_4$ particles as oxygen carriers for chemical-looping combustion. Energy Fuels 2009;23:665–76.
[12] Adánez J, Dueso C, de Diego LF, García-Labiano F, Gayán P, Abad A. Methane combustion in a 500 Wth chemical-looping combustion system using an impregnated Ni-based oxygen carrier. Energy Fuels 2008;23:130–42.
[13] Jafarian M, Arjomandi M, Nathan GJ. A hybrid solar and chemical looping combustion system for solar thermal energy storage. Appl Energy 2013;103:671–8.
[14] Hong H, Jin H. A novel solar thermal cycle with chemical looping combustion. Int J Green Energy 2005;2:397–407.
[15] Hong H, Jin H, Liu B. A novel solar-hybrid gas turbine combined cycle with inherent CO_2 separation using chemical-looping combustion by solar heat source. J Sol Energy Eng 2006;128:275–84.
[16] Hong H, Han T, Jin H. A low temperature solar thermochemical power plant with CO_2 recovery using methanol-fueled chemical looping combustion. J Sol Energy Eng 2010;132:031002.
[17] Jafarian M, Nathan GJ, Arjomandi M. A hybrid solar and chemical looping combustion system, Provisional Patent Application No. 2013903807, Adelaide Research and Innovation Pty. Ltd.; 2013 [Priority Date: 02.10.2013].
[18] Johansson M, Mattisson T, Lyngfelt A. Use of $NiO/NiAl_2O_4$ particles in a 10 kW chemical-looping combustor. Ind Eng Chem Res 2006;45:5911–9.
[19] Diver RB. Receiver/reactor concepts for thermochemical transport of solar energy. J Sol Energy Eng 1987;109:199–204.
[20] Yazdanpanah MM, Forret A, Gauthier T, Delebarre A. Modeling of CH_4 combustion with $NiO/NiAl_2O_4$ in a $10kW_{th}$ CLC pilot plant. Appl Energy 2014;113:1933–44.
[21] Barin I. Thermochemical data of pure substances: VCH; 1993.
[22] Steinfeld A, Larson C, Palumbo R, Foley Iii M. Thermodynamic analysis of the co-production of zinc and synthesis gas using solar process heat. Energy 1996;21:205–22.
[23] Buck R, Brauning T, Denk T, Pfander M, Schwarzbozl P, Tellez F. Solar-hybrid gas turbine-based power tower systems (REFOS). J Sol Energy Eng 2002;124:2–9.
[24] Dincer Ibrahim, Rosen Marc A. Exergy: energy, environment and sustainable development. Elsevier Science; 2007.
[25] Sayin C, Hosoz M, Canakci M, Kilicaslan I. Energy and exergy analyses of a gasoline engine. Int J Energy Res 2007;31:259–73.
[26] Anheden M, Svedberg G. Exergy analysis of chemical-looping combustion systems. Energy Convers Manage 1998;39:1967–80.
[27] Analysis of 10-years record Port Agusta Asutralia for Renewables SA.
[28] Steinfeld A, Kuhn P, Reller A, Palumbo R, Murray J, Tamaura Y. Solar-processed metals as clean energy carriers and water-splitters. Int J Hydrogen Energy 1998;23:767–74.
[29] Kribus A, Krupkin V, Yogev A, Spirkl W. Performance limits of heliostat fields. J Sol Energy Eng 1998;120:240–6.

CHAPTER 5

THE ENERGETIC PERFORMANCE OF A NOVEL HYBRID SOLAR THERMAL & CHEMICAL LOOPING COMBUSTION PLANT

Statement of Authorship

Title of Paper	The energetic performance of a novel hybrid solar thermal & chemical looping combustion system
Publication Status	○ Published, ○ Accepted for Publication, ◉ Submitted for Publication, ○ Publication style
Publication Details	M. Jafarian, M. Arjomandi, G. J. Nathan, "The energetic performance of a novel hybrid solar thermal & chemical looping combustion system". Applied Energy, (2014), (Under review).

Author Contributions

By signing the Statement of Authorship, each author certifies that their stated contribution to the publication is accurate and that permission is granted for the publication to be included in the candidate's thesis.

Name of Principal Author (Candidate)	Seyed Mehdi Jafarian		
Contribution to the Paper	Developed ideas. performed simulations and calculations, interpreted data, wrote manuscript and acted as corresponding author.		
Signature		Date	05/06/2014.

Name of Co-Author	Maziar Arjomandi		
Contribution to the Paper	Supervised development of work, helped in developing ideas, data interpretation and manuscript evaluation.		
Signature		Date	05.06.2014

Name of Co-Author	Graham Nathan		
Contribution to the Paper	Supervised development of work, helped in developing ideas, data interpretation and manuscript evaluation.		
Signature		Date	5.6.14

Name of Co-Author			
Contribution to the Paper			
Signature		Date	

The energetic performance of a novel hybrid solar thermal & chemical looping combustion plant

Mehdi Jafarian [1], Maziar Arjomandi, Graham J. Nathan

Centre for Energy Technology, School of Mechanical Engineering,

The University of Adelaide, S.A. 5005, Australia

Abstract

The overall energetic performance of a gas turbine combined cycle powered by a hybrid cycle between a solar thermal and a chemical looping combustion (CLC) system firing methane is reported for two configurations. In one case, the outlet from the air reactor is fed directly to a gas turbine, while in the other an after-burner, also firing methane, is added to increase the gas turbine inlet temperature. The cycle is simulated using Aspen Plus software for the average diurnal profile of normal irradiance for Port Augusta, South Australia. The first law efficiency, total solar absorption efficiency, average and peak fractional power boosts, total solar share, net solar to electrical efficiency, fraction of pressurised CO_2, incremental CO_2 avoidance and the exergy efficiency for both cycles are reported. The calculations predict a first law efficiency of 50.0% for the cycle employing an after-burner, compared with 44.0% for that without the after-burner. However, this is achieved at the cost of decreasing the solar share from 60.0%, without the

[1] Corresponding author: School of Mechanical Engineering, The University of Adelaide, Adelaide, SA 5005, Australia.
Phone: (+61) 8 8303 5460
Email: mehdi.jafarian@adelaide.edu.au

after-burner, to 41.4% with it. Also reported is the sensitivity analysis of performance to variations in key operating parameters. The sensitivity analysis shows that further improvements to the performance of the cycle are possible.

Keywords: hybrid systems; solar energy; chemical looping combustion; combine cycles; power generation

1. Introduction

Hybrids of concentrated solar thermal energy and chemical looping combustion (CLC) systems are receiving growing attention, due to their potential to lower the cost of greenhouse gas abatement by harnessing the complementary strengths of two technologies to mitigate their limitations [1, 2]. Solar thermal power offers low net greenhouse gas emissions but suffers from high cost, due largely to the intermittent nature of the resource, while fossil fuels offer continuous power, but at the expense of high CO_2 emissions. Although CLC was originally developed to provide an industrially pressurised CO_2 stream for sequestration or reuse, it has also recently been shown to offer the potential to store thermal energy in a novel hybrid between these two technology concepts [1]. Jafarian *et al*. [2, 3] also calculated this hybrid to achieve an outlet temperature of 950 °C with continuous operation, a 60.0% solar share and an industrially pure and pressurised stream of CO_2 exhaust gas. However, the thermodynamic performance of this for power generation has yet to be assessed. Therefore the overall aim of this paper is to determine the full cycle performance of this hybrid

solar-CLC system, both with and without the potential use of an after-burner to increase gas turbine inlet temperature, and so cycle efficiency, at the cost of a decreased solar share.

Chemical Looping Combustion (CLC) is a new technology under development to provide inherent capability for CO_2 capture from the combustion of a hydrocarbon fuel. The process employs a metal oxide as an "oxygen carrier", to enable the indirect transfer of oxygen from the air to the fuel. This enables the fuel and air to be kept in two separate reactors, an air reactor and a fuel reactor which, in turn, prevents the CO_2 product from the fuel reactor from being diluted with the N_2 from air. During the CLC operation, the oxygen carrier in the fuel reactor is reduced by oxidation of the fuel in the fuel reactor, while it is oxidised in the air reactor. Particles have now been developed that are mechanically robust, enabling them to be cycled many times between the two reactors to provide a continuous process [4-6]. The potential to hybridise CLC systems with concentrated solar thermal energy was first identified by Hong *et al.* [7-9]. In their three hybrids solar-CLC systems, the solar energy was proposed to be used to provide either sensible heat for preheating reactants or the endothermic heat of reaction between the fuel and oxygen carrier (OC) particles. These processes have the advantage over the direct heating of air by solar radiation that the temperature of the reactor in which the solar energy is converted to chemical energy, is lower than the final temperature of the outlet air. However, these systems do not provide any storage of the solar energy. To demonstrate the potential to also achieve thermal energy storage by hybridising CLC with concentrated solar thermal energy, Jafarian *et al*. [1] proposed a hybrid CLC system that also employs the OC particles as a storage

medium. In this concept, three reservoirs were added to a conventional CLC system to provide storage of the OC particles, while a cavity solar receiver was chosen as the fuel reactor. This hybrid also offers shared infrastructure, which can potentially lower the capital and operating costs. However, it is limited to a low total solar share of about 6.5%. Moreover, since in this system the flow rates of fuel and OC particles are considered to be constant, the operating temperature of the cavity fuel reactor changes with the intensity of the concentrated solar thermal radiation, which has the potential to damage the OC particles [10]. To address these limitations, another hybrid CLC concept has been proposed more recently by Jafarian *et al*. [2, 3], in which two reservoirs are utilized to store the OC particles in a CLC system, also with a cavity solar receiver for the fuel reactor. In this system the operating temperature of the fuel reactor is proposed to be constant by varying the flow rates of fuel and OC particles in response to the variations in the input concentrated solar radiation. As with the earlier solar-CLC hybrids, the stored heat in the OC particles is released in the air reactor to achieve a higher outlet temperature than that of the solar reactor. This system also achieves shared infrastructures, but has the important advantage over the earlier systems in achieving an estimated solar fraction of 60%, averaged over the whole 24 hour day. It also provides a continuous output for base-load power, determined from the annually-averaged solar day, and has the capacity to revert to conventional CLC operation in the event of an extended period of cloud cover. The operation of conventional CLC systems in power cycles has been studied before. For example, Wolf et al. [11] estimated a thermal efficiency of 53% for an 800 MW natural gas-fired combined cycle integrating a CLC, operating at 1200 °C and 13 bar. Naqvi et

al. [12] calculated a net plant efficiency of 52.2% for a natural gas-fired combined cycle, where the combustion chamber of the gas turbine was replaced with the CLC reactors. They also estimated an efficiency of 40.1% for a CLC-integrated steam turbine [13]. Peltola et al. [14] performed a preliminary design of a 100 MW_{th} CLC-based steam power plant using a dual circulating fluidised bed reactor for gaseous fuels and found the net cycle efficiency to be 42.8%, without the purification and compression of CO_2. However, the thermodynamic efficiency of the Hy-Sol-CLC in a hybrid solar-CLC power plant cannot be derived readily from such previous studies of the conventional CLC power generation cycles because of the significant differences in the sources of input thermal energy, process configuration and operating conditions [2, 3]. Therefore, the first aim of the current work is to investigate the thermodynamic performance of the hybrid solar-CLC system proposed by Jafarian *et al*. [2, 3] when employed for continuous base-load power generation in a GTCC.

In CLC systems, the operating temperature of the air reactor typically does not exceed 1000-1200 °C, depending on the type of OC carrier particles used and the operating conditions [4]. This is significantly less than the inlet temperature of the state of the art in commercially available gas turbines, which is currently around 1250 °C [15] and is anticipated to increase up to ~1700 °C in the foreseeable future [16]. Similarly, the current temperature to which pressurised air can be heated by concentrated solar radiation is also limited to about 1000 °C [17]. One well known approach to increase the temperature of pressurised air from a solar receiver to a turbine is to employ an after-burner [18-20]. A similar approach has also been proposed for conventional CLC gas turbine systems [11, 21, 22]. This

approach requires additional fuel, so that the increase in the efficiency of the solar hybrid system will come at the expense of a decreased solar fraction. Therefore, the second aim of this work is to evaluate the advantages and disadvantages of the use of an after-burner, particularly in regard to cycle efficiency and solar share for the hybrid solar-CLC system.

2. **Power generation cycles**

The configuration of the proposed hybrid solar-CLC (Hy-Sol-CLC) Gas Turbine Combined Cycle (GTCC) is shown in Fig. 1. The cycle comprises of two main sections: (i) a hot gas generator and (ii) a combined power generation. The concentrated solar thermal radiation from the solar collector field is captured and stored within the solar fuel reactor of the hybrid-CLC section by the oxygen carrier (OC) particles. Both sensible and chemical heat stored in the OC particles are then released in the air reactor at a higher temperature to produce a steady stream of hot gas (stream 3) despite an intermittent solar radiation input. The operation of this section has been described in detail by Jafarian *et al.* [2, 3]. However, an air compressor is added to the present cycle to pressurize the air reactor (through streams 11, 12, 1 & 5 shown in Fig. 1) for delivery to the gas turbine. An air heat ex-changer is also proposed to cool the pressurised air before being introduced to the direct air-particle heat ex-changer to cool the OC particles. A loop-seal is employed between the direct air-particle heat exchanger and reservoir R_1 to allow the particles to be transferred from the high pressure air-reactor to the atmospheric-pressure of reservoir R_1 and the fuel reactor. The valve

between resevoir R_2 and the air reactror shown by Jafarian *et al.* [2, 3] has also been replaced with a loop-seal/valve, to transfer the particles to the pressurised air reactor from reservoir R_2 at a controlled flow rate. That is, the use of a loop-seal and a loop-seal/valve are proposed as a means to allow the air reactor to be pressurised while the fuel reactor is at atmospheric pressure, following other related processes [23-25]. The detailed design of the loop-seal and loop-seal/valves is beyond the scope of this work. It is worth noting that, in addition to making provision for heat storage, the use of the two reservoirs makes it technically easier to operate the air and fuel reactors at different pressures than is the case for a conventional CLC system. This is significant because the difference in the operating pressures of the fuel and air reactors can lead to gas leakage in conventional CLC systems, lowering the efficiency of CO_2 separation [4, 26]. The potential to operate the solar (fuel) reactor at a much lower pressure than the air reactor is highly desirable for solar reactors, since it significantly reduces the risk of damage to transparent windows, which are a critical component of the most efficient solar reactors and are vulnerable to high pressures and/or harsh environments [27, 28]. Operation at atmospheric pressure allows to its thickness to be minimized for efficient transmission of solar energy [17].

The after-burner can be used to increase the temperature of the pressurised outlet stream from the air reactor. Under conditions in which the excess oxygen from the air reactor is not sufficient to burn all of the fuel supplied to the after-burner, supplementary pressurised air is provided by the air compressor (stream 13 in Fig. 1). The flow rate of air in each stream is adjusted using valves V_4, V_5 and V_6. The cycle can also operate without the after-burner, using valves V_2 and

V_3, in which case the outlet air stream from the air reactor is directly introduced to the gas turbine.

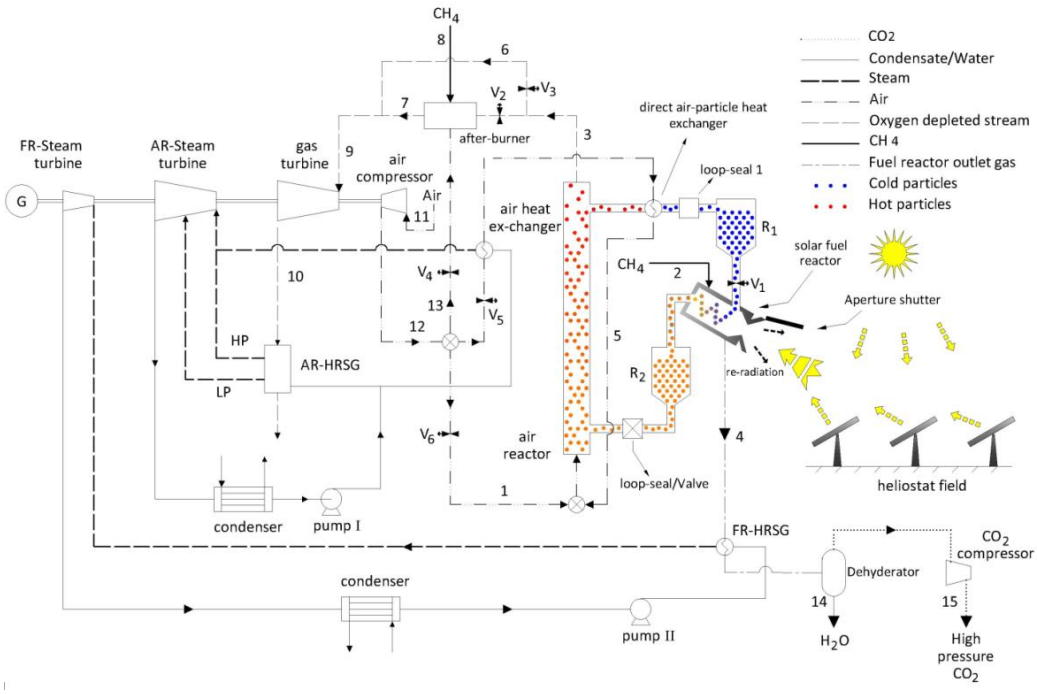

Fig. 1. The proposed hybrid solar-CLC combined cycle. Resrvoirs R_1 and R_2 are used to store the hot and cold particles from the solar fuel and air reactors, respectively. A direct air-particle heat ex-changer is employed to further cool the particles to the OC particle storage temperaure in resevior R_1 [2, 3]. The hot and pressurised stream leaving the air reactor, stream 3, is used to generate power by means of a three-stage gas turbine. The heat recovered through the heat recovery steam generators (AR-HRSG and FR-HRSG) is also utilized to produce additional power with the gas and steam turbines (AR and FR). The AR-Steam turbine has two stages, the high pressure, HP, and low pressure LP, respectively. An after-burner is optionally used to increase the temperature to the gas turbine inlet using valve V_2 and V_3 [3].

Fig. 1 also presents the power generation side of the plant, in which hot gases (stream 9) from the air reactor directly (stream 6) or after overheating in the after-burner (stream 7) is passed through a three-stage gas turbine and then through a heat recovery steam generator, AR-HRSG, (stream 10) to power a two-stage AR-Steam turbine. The hot gas stream from the fuel reactor (stream 4) is also used for power generation through a heat recovery steam generator (FR-HRSG) and FR-Steam turbine. Here the prefixes "AR" and "FR" indicate the air and fuel reactors, respectively. The AR-HRSG and AR-Steam turbines are inspired from those proposed by Naqvi *et al.* [12]. Finally, the CO_2-rich stream (stream 4 in Fig. 1), cooled down by the FR-HRSG, is fed to the CO_2 dehydration and compression process. This compression represents only a small parasitic loss of approximately 1.6% and 2.6%, respectively, for the cycles with and without the integration of the after-burner, respectively. Obviously, these losses could be decreased with multi-step compression and inter-cooling. Another possible option to the use of a small FR-HRSG together with the compression of the CO_2 for transport and geological sequestration, is to instead employ mineral sequestration of CO_2. One such process involves the endothermic conversion of magnesium silicate to magnesium hydroxide before the exothermic carbonation reaction with CO_2 to produce a stable magnesium carbonate [29, 30]. Here, the enthalpy in the hot CO_2 (stream 15) has potential to drive this process. However, the detailed assessment of these other options is beyond the scope of the present investigation.

The reference cycle, against which the S-CLC combined cycle is compared, is shown in Fig. 2. This comprises only a Gas Turbine Combined Cycle, GTCC, which uses the same amount of fuel as the hybrid Sol-CLC cycle. For each

comparison, the reference cycle is considered to operate at a temperature and pressure of 1250 °C and 15 bar, respectively.

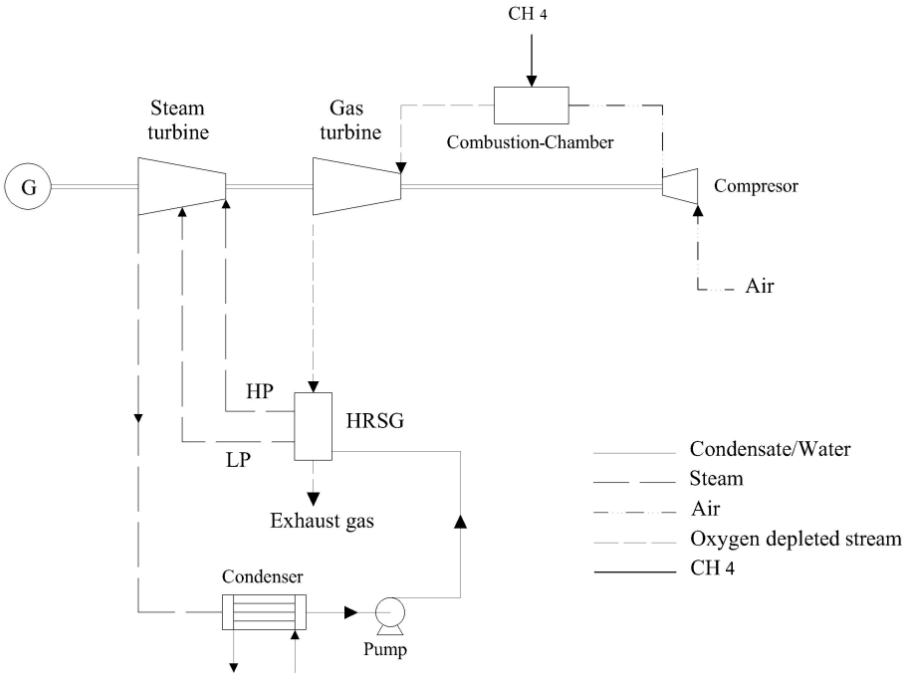

Fig. 2. The configuration of the reference combined gas turbine considered here. The pressurised hot stream produced in the air Compressor and the Combustion-chamber is used to produce power through a three-stage gas turbine. The steam turbine has two-stages, consistent with the hybrid solar CLC system (Fig. 1), which is fed to the HRSG. This is fed through the HP and LP steam streams produced by the HRSG.

3. Methodology

Simulations of the proposed Hy-Sol-CLC cycles were performed using Aspen Plus software. The model solves the governing equations of mass and energy, simultaneously. The Gibbs minimization method, with an R-Gibbs reactor, was used to calculate the equilibrium product compositions from the fuel and air reactors. The following gas phase components were considered: N_2, O_2, CH_4, H_2O, CO_2, CO and H_2. To account for departures in fluid from ideal gas behaviour of up to ~ 6%, the Peng–Robinson's equation of state was used to calculate the fluid properties. The power produced or consumed by the turbines, compressors and pumps was calculated with assumed isentropic efficiencies [31], shown in Table 1. Furthermore, to account for the dynamic performance of the Hy-Sol-CLC owing to diurnal variations of the concentrated solar thermal energy, a quasi-steady state condition based on annually averaged variations of solar irradiance through the day was considered.

The mass flow rate of the OC particles fed to the solar fuel reactor was calculated from the molar ratio of oxygen carrier particles to fuel, $\emptyset$ [32]:

$$\phi = \frac{\dot{n}_{OC}}{4\dot{n}_{CH_4}}. \qquad (1)$$

Here $\dot{n}_{CH_4}$, is the molar flow rate of CH_4 introduced into the solar fuel reactor and $\dot{n}_{OC}$, is that of the oxygen carrier particles.

The incoming solar heat flux to solar collector, $\dot{Q}_{coll}$, was calculated by the direct normal insolation, *DNI*, and the average optical efficiency, $\overline{\eta}_{coll}$, of the

collection system, which is assumed to be 65.0% (Table 1) following earlier work [7].

$$\dot{Q}_{coll} = \overline{\eta}_{coll} A_{coll} DNI . \quad (2)$$

For simplicity it is assumed that the receiver aperture is sized to capture all of the incoming power from the collector, so that $\dot{Q}_{s,in} = \dot{Q}_{coll}$, also following earlier work [33].

Radiative heat losses are accounted for through the total solar energy absorption efficiency, $\eta_{abs,tot}$, which is defined as the ratio of net solar power absorbed by the solar reactor to the net diurnal solar power input through the solar reactor's aperture, as follows:

$$\eta_{abs,tot} = \frac{\int_{ap,open}^{ap,close} \dot{Q}_{s,abs} dt}{\int_{ap,open}^{ap,close} (\dot{Q}_{s,abs} + \dot{Q}_{re-rad}) dt}, \quad (3)$$

where $\dot{Q}_{s,abs}$ and $\dot{Q}_{re-rad}$ are the concentrated solar thermal heat absorbed within the solar reactor and the heat re-radiated through the solar reactor aperture, respectively. Subscripts "*ap,open*" and "*ap,close*" denote the condition in which the solar fuel reactor aperture is opened or closed, respectively, noting that the fuel reactor operates with both solar and chemical energy. In addition:

$$\dot{Q}_{s,abs} = \dot{Q}_{s,in} (1 - \frac{\varepsilon_{eff} \sigma T_{FR}^4}{\alpha_{eff} CR\, DNI}), \quad (4)$$

$$\dot{Q}_{re-rad} = \dot{Q}_{s,in} \frac{\varepsilon_{eff} \sigma T_{FR}^4}{\alpha_{eff} \, CR \, DNI}. \quad (5)$$

Here $\dot{Q}_{s,in}$ is the solar power input through the solar aperture, α_{eff} and ε_{eff} are the effective absorptance and emittance of the cavity-receiver respectively, σ is the Stephan-Boltzmann constant, T_{FR} is the temperature of the solar cavity fuel reactor and *CR* is the mean flux concentration ratio.

The first law efficiency, η, of the hybrid system is calculated by [34]:

$$\eta = \frac{\int_{24\ hours} ((\dot{W}_{GT} - \dot{W}_{c,air}) + (\dot{W}_{AR,ST} - \dot{W}_{Pump_I}))dt + \int_{t_{ap,open}}^{t_{ao,close}} (\dot{W}_{FR,ST} - \dot{W}_{Pump_{II}} - \dot{W}_{c,CO_2}))dt}{\int_{t_{ap,open}}^{t_{ap,close}} ((\dot{Q}_{s,abs} + \dot{Q}_{re-rad}) + (\dot{n}_{F,R} LHV_{CH_4}))dt + \int_{24hours} (\dot{n}_{F,AB} \, LHV_{CH_4})dt}. \quad (6)$$

Here LHV_{CH_4} is the lower heating value of CH_4, $\dot{n}_{F,FR}$ is the CH_4 flow rate into the solar fuel reactor (stream 2 in Fig. 1), $\dot{n}_{F,AB}$ is the CH_4 flow rate into the after-burner (stream 8 in Fig. 1), $\dot{W}_{GT}$ is the power produced by gas turbine, $\dot{W}_{c,air}$ is the power required for air compression, $\dot{W}_{AR,ST}$ is the power produced by AR-Steam turbines, $\dot{W}_{FR,ST}$ is the power produced by FR-Steam turbines, $\dot{W}_{Pump_I}$ and $\dot{W}_{Pump_{II}}$ are the work consumed by pumps *I* and *II*, respectively and $\dot{W}_{c,CO_2}$ is the power required for the compression of CO_2.

The energy extracted from the gas turbine and the AR-Steam turbine is available continuously for the present cycle, while that from the FR-Steam turbine is only available intermittently when the fuel reactor is operating, i.e. when the *DNI* exceeds the minimum threshold [2]. This situation corresponds to a “power

boost" mode of operation over the "base load" component of the output, following the terminology of Kolb [35]. Hence, we define the fractional power boost share in terms of both the average and peak values, $\chi_{boost,av}$, and $\chi_{boost-pk}$, as the ratio of the additional net power available from the FR-Steam turbine over the total from the gas turbine and AR-Steam turbines.

$$\chi_{boost,av} = \frac{\int_{24\ hours} (\dot{W}_{FR,ST} - \dot{W}_{Pump_{II}}))dt}{\int_{24\ hours} ((\dot{W}_{GT} - \dot{W}_{c,air}) + (\dot{W}_{AR,ST} - \dot{W}_{Pump_{I}}))dt}, \tag{7}$$

$$\chi_{boost,pk} = \frac{(\dot{W}_{FR,ST} - \dot{W}_{Pump_{II}})_{at\ solar\ noon}}{((\dot{W}_{GT} - \dot{W}_{c,air}) + (\dot{W}_{AR,ST} - \dot{W}_{Pump_{I}}))_{at\ solar\ noon}}. \tag{8}$$

The total thermal solar share, $\chi_{sol,tot}$, is calculated as follows [20]:

$$\chi_{sol,tot} = \frac{\int_{t_{ap,open}}^{t_{ap,close}} (\dot{Q}_{s,in} - \dot{Q}_{re-rad})dt}{\int_{t_{ap,open}}^{t_{ap,close}} ((\dot{Q}_{s,in} - \dot{Q}_{re-rad}) + (\dot{n}_{F,FR} LHV_{CH_4}))dt + \int_{24hours} (\dot{n}_{F,AB} LHV_{CH_4})dt}. \tag{9}$$

The incremental concentrated solar to electrical efficiency, $\Delta\eta_{con\text{-}sol,elec}$, [20, 36] is given by:

$$\Delta\eta_{con-sol,elec} = \frac{\int_{24hours} (\dot{E}_{elec,hybrid} - \eta_{ref} . \dot{E}_{fuel,hybrid})dt}{\int_{24hours} \dot{Q}_s dt}, \tag{10}$$

where η_{ref} is the first law efficiency of reference cycle, $\dot{E}_{elec,hybrid}$ and $\dot{E}_{fuel,hybrid}$ are the power produced and the energy of fuel consumed by solar-hybrid CLC plants. The numerator of this equation shows the net increase in electricity generated by the solar-hybrid CLC plants compared with the equivalent pressurised fossil reference plant.

The CO_2 produced in the solar fuel reactor is industrially pure and pressurised (stream 15 in Fig. 1), while the CO_2 produced in the after-burner is released directly to the atmosphere. Since the former fraction is more valuable, the pressurised CO_2 fraction that is industrially pure is calculated separately, defined as:

$$\chi_{CO_2,pure} = \frac{\int_{ap,open}^{ap,close} \dot{n}_{CO_2,FR} dt}{\int_{ap,open}^{ap,close} \dot{n}_{CO_2,FR} dt + \int_{24hours} \dot{n}_{CO_2,AB} dt}. \quad (11)$$

In this equation $\dot{n}_{CO_2,FR}$ and $\dot{n}_{CO_2,AB}$ are the flow rates of CO_2 produced in solar fuel reactor and after-burner reactors, respectively. Obviously, the fraction of CO_2 that is emitted to the atmosphere can be calculated by:

$$\chi_{CO_2,emit} = 1 - \chi_{CO_2,pure}. \quad (12)$$

Since the pressurised and industrially pure CO_2 is presumed to not be released into atmosphere, it is not considered to be CO_2 emission from this process. Hence the incremental CO_2 avoidance, Δ_{CO_2}, from the solar hybrid CLC system is defined following Schwarzbözl *et al*. [19] as:

$$\Delta_{CO_2} = \left(\frac{\int_{24hours} \frac{\dot{E}_{elec,hybrid}}{\eta_{ref}} dt - \chi_{CO_2,emit} \int_{24hours} \dot{E}_{fule,hybrid} dt}{\int_{24hours} \frac{\dot{E}_{elec,hybrid}}{\eta_{ref}} dt}\right) f_{CO_2}. \quad (13)$$

Here f_{CO_2} is the amount of CO_2 emission per heating rate of fuel (for CH_4 f_{CO_2} = 0.055 kg/MJ). Obviously, while the cycle is working without the after-burner $\Delta_{CO_2} = f_{CO_2}$.

The exergy efficiency is defined as the ratio of the net output exergy to the total input exergy [37]:

$$\eta_{ex}=\frac{\int_{24hours}\dot{W}_t dt}{\int_{ap,o}^{ap,c}(\dot{Q}_{s,in}-\dot{Q}_{re-rad})(1-\frac{T_0}{T_{FR}})+\dot{n}_{F,FR}.Ex_F))\,dt+\int_{24hours}\dot{n}_{F,AB}.Ex_F\,dt}. \quad (14)$$

Here Ex_F represents the exergy of the fuel.

The key operating conditions of the cycles are presented in Table 1. The solar energy added to the solar fuel reactor is calculated based on the *DNI* data for Port Augusta, South Australia [38]. The results are calculated relative to the average maximum solar heat input to solar fuel reactor, $\dot{Q}_{s,in,\max}$, noting that solar noon occurs at 12:30 hours. A start up time of an hour is assumed for the FR-Steam turbine, while start up is ignored for the other turbines, since they operate continuously.

The net power produced by each cycle is calculated by:

$$\dot{W}_{n,i}=\sum\dot{W}_{gen}-\sum\dot{W}_{cons}. \quad (15)$$

In this equation, subscripts "*gen*" and "*cons*" indicate the power generated by the turbines or consumed by the compressors and/or pumps, respectively.

The Aspen Plus model was validated in our previous work [1]. The sensitivity of both cycles, with and without the after-burner, to the variations of the parameters listed in Table 1 was also assessed to detect those variables with the greatest influence on the cycle operations. A total pressure loss of 5 and 2 % was considered for the gas turbines and steam cycles, respectively. In both cycles the

fuel was assumed to be pressurised, so that no compressor is needed to pressurize it [39].

Table 1. The main assumptions employed in the cycle analysis. The solar fuel reactor in both cycles operates at the same conditions, while the air reactors operate at different pressures.

	Reference operating conditions	**Variation range**	**Source**
Solar collector field			
Optical efficiency ($\bar{\eta}_{coll}$) (%)	65		[7]
Mean flux concentration ratio	2000	500-8000	[33]
Fuel reactor			
Effective absorptance (α_{eff})	1		[33, 40]
Effective emittance (ε_{eff})	1		[33, 40]
Operating temperature (° C)	750	550-950	[41]
Operating pressure (bar)	1		
Ø	2.5	1-4.5	
Air reactor			
Operating temperature (°C)	950		[41]
Operating pressure (bar)	15	10-20	
Reservoir & HX's stream temperatures			
Reservoir R_1 temperature (°C)	100	100-750	
Reservoir R_2 temperature (°C)	750		
Minimum temperature difference between the outlet hot and cold streams form Direct air-particle heat ex-changer (°C)	100		
Minimum temperature difference between the outlet hot and cold streams form Steam generators (°C)	5		
Power cycles			
Isentropic efficiency of gas turbine	0.91		[9]
Isentropic efficiency of steam turbine	0.90		[42]
Isentropic efficiency of air compressor	0.88		[9]
Isentropic efficiency of pump	0.75		[42]
Steam pressure (HP/LP) (bar/bar)	60/5		[12]
Steam temperature (IP/LP) (°C/°C)	467/258		[12]
Mechanical efficiency of generators	0.99		[42]
Generator efficiency	0.99		[22]
Compression ratio of CO_2 compressor (bar)	120		[43]

The particles tested by Johansson *et al.* [41] are chosen as the oxygen carrier, considering several selection criteria [44]. In these OC particles, NiO is supported by $NiAl_2O_4$ with a mass ratio of 4 to 6.

4. Results and discussion

Fig. 3 presents for the annually averaged solar day the calculated average diurnal variations of the absorbed solar power within the solar fuel reactor, $\dot{Q}_{s,abs}$; the input power of fuel into solar fuel reactor, $\dot{Q}_{F,FR}$ (stream 2 in Figs. 1); the heat lost through re-radiation from the solar fuel reactor aperture, $\dot{Q}_{re-rad}$; and the input power from the fuel fed to the after-burner, $\dot{Q}_{F,AB}$, (stream 8 in Figs. 2). All of these parameters are normalized by the maximum solar power input to the fuel reactor, $\dot{Q}_{s,in,\max}$. As shown, $\dot{Q}_{F,FR}/\dot{Q}_{s,in,\max}$ varies in phase with $\dot{Q}_{s,abs}/\dot{Q}_{s,in,\max}$ showing that the flow rate of CH_4 through the fuel reactor is controlled in proportion to the net solar input. However, at the same time, the plant maintains an almost constant power output throughout the 24 hours day, with a slight increase in output with the solar resource. It can also be seen that the threshold of minimum solar flux occurs at t = 6:30 and 18:30 hours, while solar noon occurs at t = 12:30. The maximum values of $\dot{Q}_{s,abs}/\dot{Q}_{s,in,\max}$ and $\dot{Q}_{F,FR}/\dot{Q}_{s,in,\max}$ at solar noon are 95.0×10^{-2} and 62.9×10^{-2}, respectively, while $\dot{Q}_{re-rad}/\dot{Q}_{s,in,\max}$ is constant at 5.0×10^{-2} during the operation of solar reactor.

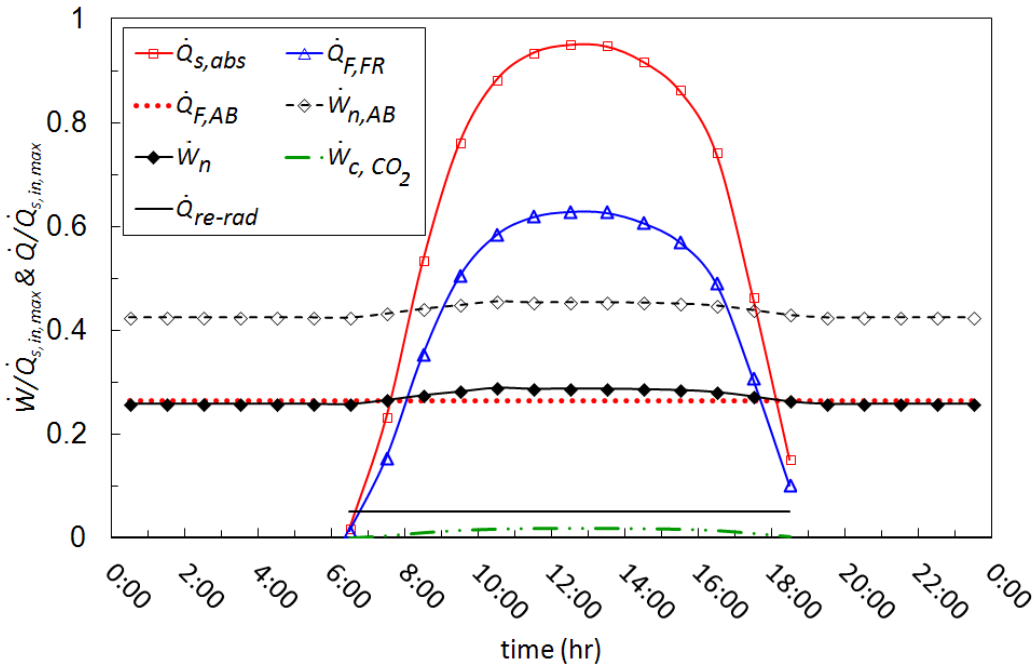

Fig. 3. The calculated normalized hourly average variations of the absorbed solar radiation in the fuel reactor, the heat loss through re-radiation from solar fuel reactor aperture, the input power of fuel into fuel reactor and after-burner, the net power produced by the hybrid combined cycle with and without after-burner and the power required for compression of CO_2 to the maximum solar input to fuel reactor for the reference operating conditions given in Table 1 and the average solar insolation at Port Augusta, South Australia [38].

Fig. 3 also shows the calculated normalised net power generated by the hybrid combined cycle with the after-burner, $\dot{W}_{n,AB}/\dot{Q}_{s,in,\max}$; that generated without it, $\dot{W}_n/\dot{Q}_{s,in,\max}$; and the power required for the compression of CO_2 produced in the fuel reactor, $\dot{W}_{c,CO_2}/\dot{Q}_{s,in,\max}$, for geological sequestration. All of these parameters are normalised to the maximum solar heat input to the solar fuel reactor. It can be

seen that the after-burner increases the net power out by 62.0%. A 4.1% increase in the net power occurs during the solar day, so that the output is not quite constant through the 24 hours. These variations, as shown in Table 2, correspond to average and peak fractional power boosts ($\chi_{boost,av}$, $\chi_{boost,pk}$) of 4.2% and 10.6%, respectively. Similarly, $\chi_{boost,av}$ is 6.90% and $\chi_{boost,pk}$ is 16.8% for the cycle not employing the after-burner, also shown in Table 2. This indicates that the application of after-burner decreases the variations in the work produced by the cycle.

Table 2 presents the total solar absorption efficiency, $\eta_{abs,tot}$; first law efficiency of the reference cycle, η_{ref}; and the first law efficiencies of the cycles with and without the after-burner, η. As expected, $\eta_{abs,tot}$ is constant for both cycles at 92.5%. This is because the solar fuel reactor in both cycles operates at the same operating conditions and is independent from the air reactor. It can be seen that, η_{ref} was estimated 57.9%. The efficiency of the hybrid cycles with and without the after-burner is calculated to be 7.9 and 13.9 percentage points lower than this respectively, although these values would reduce to 6.3 and 11.3 percentage points, respectively, where the CO_2 to be emitted to the atmosphere as is the case for the reference cycle, thereby avoiding the energy required to compress the CO_2. The other main causes for the lower efficiency of the hybrid cycles to that of reference cycle are the re-radiation heat losses through the solar fuel reactor aperture and the lower inlet gas turbine temperature for the cycle not employing the after-burner.

Table 2. Calculated first law efficiency of the reference cycle and the performance parameters for both the cycles with and without the after-burner using the operating condition given in Table 1 and the average solar insolation at Port Augusta, South Australia [38].

Parameter	Cycle with after-burner	Cycle without after-burner
$\eta_{abs,tot}$ (%)	92.5	92.5
η_{ref} (%)	57.9	57.9
η (%)	50.0	44.0
$\chi_{boost,av}$ (%)	4.2	6.9
$\chi_{boost,pk}$ (%)	10.6	16.8
$\chi_{sol,tot}$ (%)	41.4	60.0
$\Delta\eta_{con\text{-}sol,elec}$ (%)	39.4	35.4
$\chi_{CO_2,pure}$	46.8	100.0
Δ_{CO_2} (kg/MJ)	0.0357	0.055
η_{ex} (%)	57.2	54.9

Table 2 also shows the calculated solar share, $\chi_{sol,tot}$; incremental concentrated solar to electrical efficiency, $\Delta\eta_{con\text{-}sol,elec}$; fraction of pressurised CO_2, $\chi_{CO_2,pure}$; incremental CO_2 avoidance, Δ_{CO_2}, and the exergy efficiency, η_{ex}, for both cycles, with and without the after-burner. As expected, the increase in the cycle first law efficiency achieved by employing an after-burner comes with the cost of lowering $\chi_{sol,tot}$ and $\chi_{CO_2,pure}$ by around 18.6 and 53.2 percentage points, respectively. Moreover, Δ_{CO_2} decreases from 0.055kg/MJ without the integration of the after-burner to 0.033 kg/MJ with it. Importantly, even though $\chi_{sol,tot}$ decreases with the utilization of the after-burner, $\Delta\eta_{con\text{-}sol,elec}$ increases from 35.4% to 39.4% with it. This is attributed to the increase in the hybrid solar cycle first law efficiency. The calculations also show that using the after-burner increases the η_{ex} by around 2.3 percentage points.

The incorporation of post combustion carbon capture to the reference cycle leads to a ~25% decrease in the cycle's gross power output [45] and an overall first law efficiency of 43.0%. This first law efficiency is about the same as that of

the solar cycle without the after-burner. However, it is worth noting the value-adding characteristics of the present hybrid solar CLC system relative to the carbon capture integrated reference, namely the high solar share enabled by the hybrid process and the potential solar thermal energy storage feature.

4.1. Effect of air reactor operating pressure

Fig. 4 shows the sensitivity of the calculated values of η, $\eta_{con\text{-}sol,elec}$, $\chi_{sol,tot}$, $\chi_{CO_2,pure}$ and η_{ex} to the variations in the operating pressure of the air reactor, P_{AR}. As expected, η increases with an increase in P_{AR}. For example, for P_{AR} = 10 bar η is 48.9 % while it is 50.2 % for P_{AR} = 20 bar. As a result, $\Delta\eta_{con\text{-}sol,elec}$ also increases with P_{AR} from 37.4% at P_{AR} = 10 bar to 40.0% at P_{AR} = 20 bar. As P_{AR} is increased the outlet air temperature from the air compressor (stream 12 in Fig. 1) also increases. Consequently, more air is required within the air reactor to keep its temperature constant, which in turn requires more fuel in the after-burner. This explains why $\chi_{sol,tot}$ and $\chi_{CO_2,pure}$ decrease with the increasing of P_{AR} from 42.0% and 48.0% at P_{AR} = 10 bar, respectively, to 41.0% and 46.0% at P_{AR} = 20 bar. However, since most of the air required in the air reactor is supplied through stream 5, which is at constant temperature, the variations are not very significant. Hence too, Δ_{CO_2} remains relatively constant at 0.036 kg/MJ. It can also be seen that η_{ex} is also slightly sensitive to P_{AR}, increasing from 56.0 % at P_{AR} = 10 bar to 57.5 % at P_{AR} = 20 bar. This is caused by the increased efficiency of a gas turbine with operating pressure.

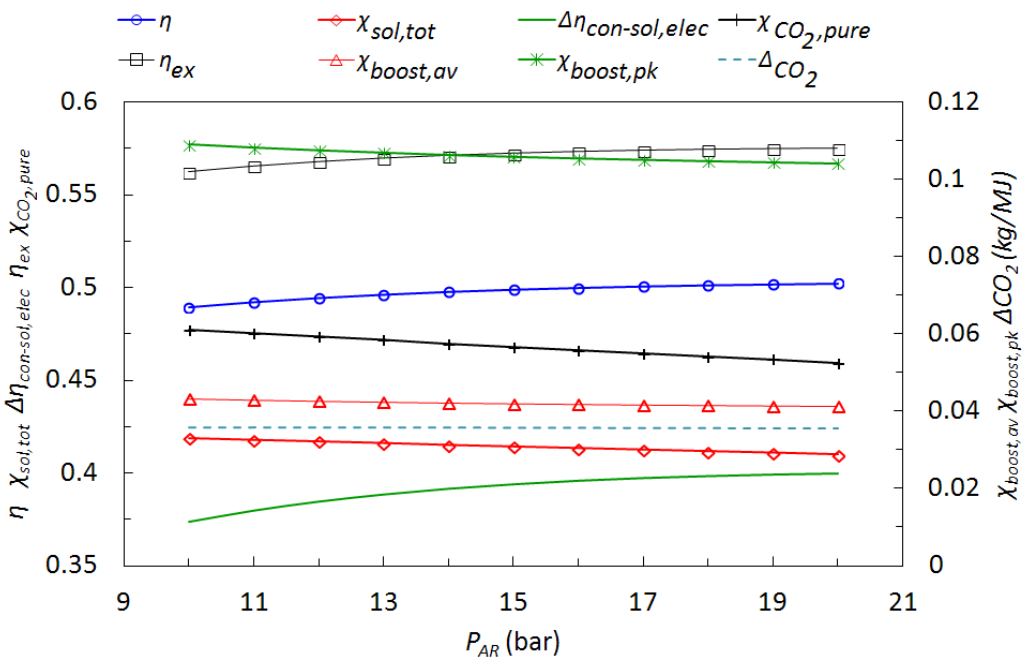

Fig. 4. Sensitivity to variations in air reactor operating pressure of the first law efficiency, total solar share, incremental concentrated solar to electrical efficiency, exergy efficiency, fraction of pressurised CO_2 , average and peak fractional power boost and the incremental CO_2 avoidance for the cycle employing the after-burner using the reference conditions given in Table 1 and the average solar insolation at Port Augusta, South Australia [38].

The sensitivity of the calculated $\chi_{boost,av}$ and $\chi_{boost,pk}$ to the variations in P_{AR} are also shown in Fig. 4. Importantly, both $\chi_{boost,av}$ and $\chi_{boost,pk}$ decrease slightly with an increase in P_{AR}. For instance, doubling P_{AR} from 10 bar to 20 bar decreases $\chi_{boost,av}$ and $\chi_{boost,pk}$ from 4.3% and 11.0%, respectively, to $\chi_{boost,av}$ = 4.1% and $\chi_{boost,pk}$ = 10.4%. This is because the power boost is derived from the waste heat generator from the fuel reactor, which is independent of the operation of the gas

turbine. Hence, increasing the pressure ratio across the gas turbine only increases the base-load component and not the boosted component.

Fig. 5 shows the calculated sensitivity of η, $\chi_{sol,tot}$, $\Delta\eta_{con\text{-}sol,elec}$, η_{ex} to the variations in P_{AR} for the cycle without the after-burner. Interestingly, η decreases marginally from 44.0% to 43.0% as P_{AR} is increased from 10 bar to 20 bar. This is due to the increase in work required to pressurise the air, given that pressurised air is then cooled by the air heat ex-changer. As expected, $\chi_{sol,tot}$ is not sensitive to P_{AR}. These trends explain why $\Delta\eta_{con\text{-}sol,elec}$ decreases with an increase in P_{AR} from 36.0% at P_{AR} = 10 bar to 34.0% at P_{AR} = 20 bar. Hence too, the exergy efficiency of the cycle, η_{ex}, also decreases by around 1.5 percentage points as P_{AR} is increased from 10 bar to 20 bar.

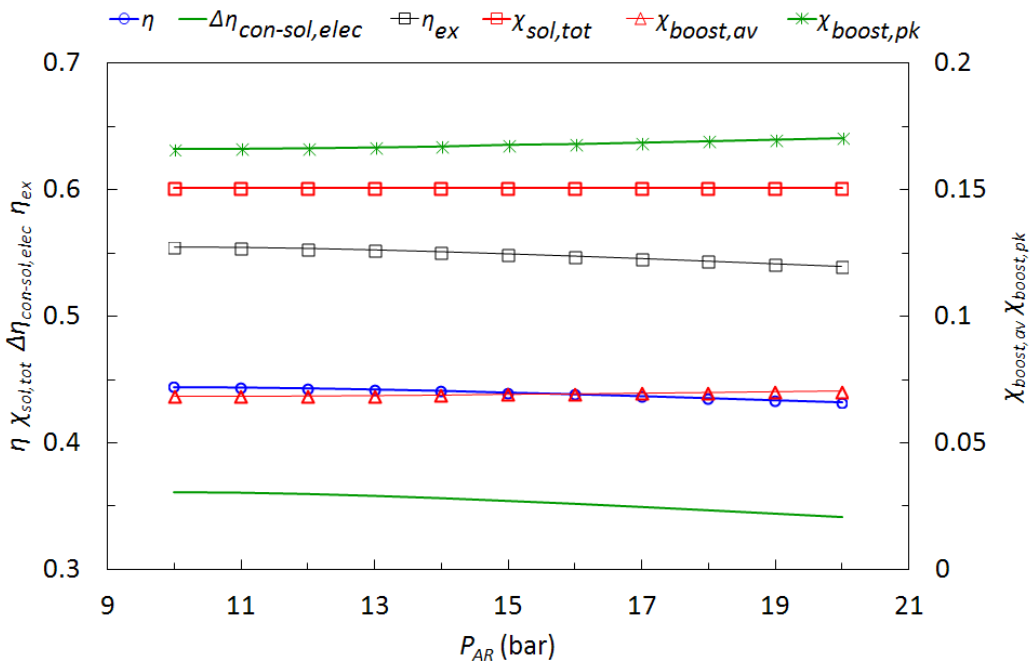

Fig. 5. Sensitivity to variations in the air reactor operating pressure of the first law efficiency, total solar share, incremental concentrated solar to electrical efficiency, exergy efficiency, average and peak fractional power boost for the cycle without the after-burner using the reference conditions given in Table 1 and the average solar insolation at Port Augusta, South Australia [38].

The calculated sensitivities of $\chi_{boost,av}$ and $\chi_{boost,pk}$ to the variations in P_{AR} for the cycle without the after-burner are also show in Fig. 5. Unlike the cycle with the after-burner, $\chi_{boost,av}$ and $\chi_{boost,pk}$ are calculated to increase from 6.8% and 16.6%, respectively, to 7.0% and 17.0%. This occurs because the increase in the work required for compression of air with an increase in P_{AR} is less than the corresponding increase in work produced by the gas turbine.

4.2. Effect of molar ratio of oxygen carrier particles to fuel

Fig. 6 illustrates the calculated sensitivity of η, $\chi_{sol,tot}$ and $\Delta\eta_{con\text{-}sol,elec}$ to the variations in the ratio of oxygen carrier particles to fuel, $Ø$, for the cycle employing the after-burner. It can be seen that $\chi_{sol,tot}$ increases by around 23.0 percentage points as $Ø$ is increased from 1.0 to 4.5. This is due to the increased thermal mass and hence sensible heat storage with $Ø$ [2]. However, the cycle efficiency decreases with $Ø$ which is attributed to the increase in the sensible storage fraction [2]. For example, for $Ø$ = 1.00, η is 52.0%, while it is 48.5% for $Ø$ = 4.50. However, since the increase in $\chi_{sol,tot}$ with $Ø$ is more significant than the decrease in η with it, the $\Delta\eta_{con\text{-}sol,elec}$ increases from 38.1% at $Ø$ = 1.0 to 40.0% at $Ø$ = 4.50. The calculations also predicted that the $\chi_{CO_2,pure}$ decreases significantly with $Ø$ by around 22.0% as $Ø$ is increased from 1.0 to 4.5 which is also arisen from the increase in the fraction of sensible heat storage with $Ø$ [2].

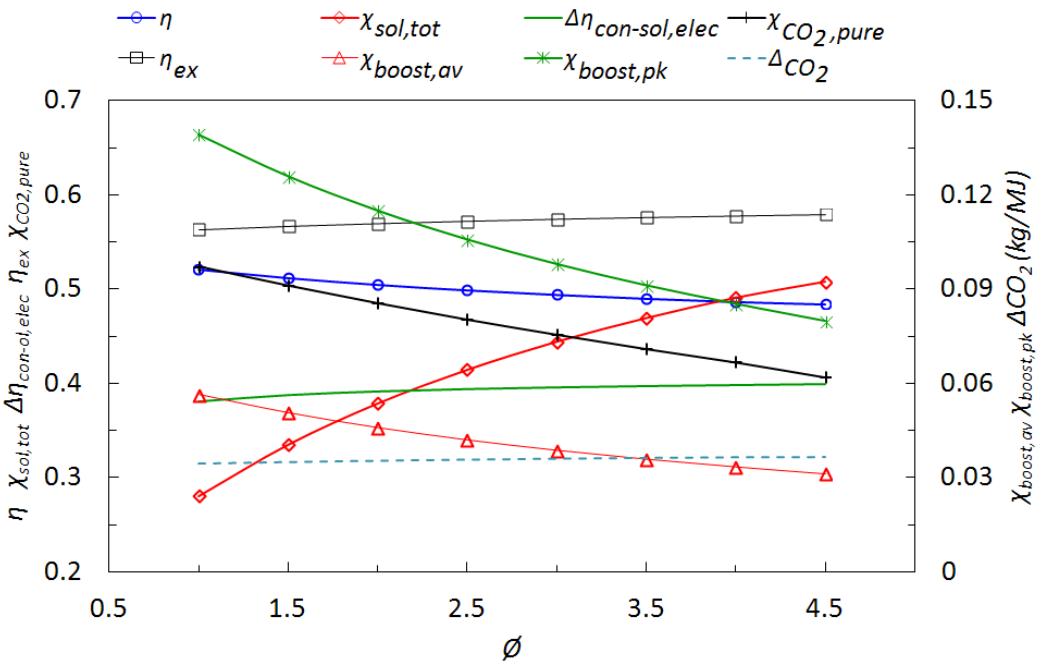

Fig. 6. Sensitivity to molar ratio of the oxygen carrier particles to fuel of the first law efficiency, total solar share, incremental concentrated solar to electrical efficiency, exergy efficiency, fraction of pressurised CO_2, average and peak fractional power boosts and the incremental CO_2 avoidance for the cycle employing an after-burner using the reference conditions given in Table 1 and the average solar insolation at Port Augusta, South Australia [38].

The calculated sensitivity of $\chi_{boost,av}$, $\chi_{boost,pk}$, Δ_{CO_2} and η_{ex} to the variations in $\emptyset$ for cycle with the after-burner is also shown in Fig. 6. As can be seen, $\chi_{boost,av}$ and $\chi_{boost,pk}$ are strongly sensitive to the variations in $\emptyset$. For instance, increasing $\emptyset$ from 1.0 to 4.5 decreases the $\chi_{boost,av}$ and $\chi_{boost,pk}$ from 5.6% and 14.0%, respectively, to 3.1% and 8.0. This is due to the increase in the fraction of sensible heat storage with $\emptyset$ [1]. The calculations also predict that Δ_{CO_2} decreases by around 6.0% over the range of $\emptyset$ considered. It is thus fairly insensitive to this

parameter. Finally, η_{ex} increases with $Ø$, which is due to the decreasing of the fraction of chemical storage with increasing of $Ø$ [2].

Fig. 7 shows the predicted sensitivity of η, $\chi_{sol,tot}$ and $\Delta\eta_{con\text{-}sol,elec}$ to the variations in $Ø$ for the cycle without the after-burner. As can be seen, η decreases by around 3.7 percentage points over the considered range of $Ø$, which is due to the increase in the sensible storage fraction with $Ø$. Hence too, $\chi_{sol,tot}$ increases with $Ø$. For instance, an increase in $Ø$ from 1.0 to 4.5, leads to an increase in $\chi_{sol,tot}$ from 42.6% to 71.7%, respectively. Importantly; as for the cycle employing an after-burner, $\Delta\eta_{con\text{-}sol,elec}$ increases with $Ø$. However, the sensitivity of $\Delta\eta_{con\text{-}sol,elec}$ to $Ø$ is greater for the cycle that does not employ an after-burner than is cycle which does. For instance, increasing $Ø$ from 1.0 to 4.5 increases $\Delta\eta_{con\text{-}sol,elec}$ by around 16.6%, compared with 4.7% for the corresponding cycle with an after-burner.

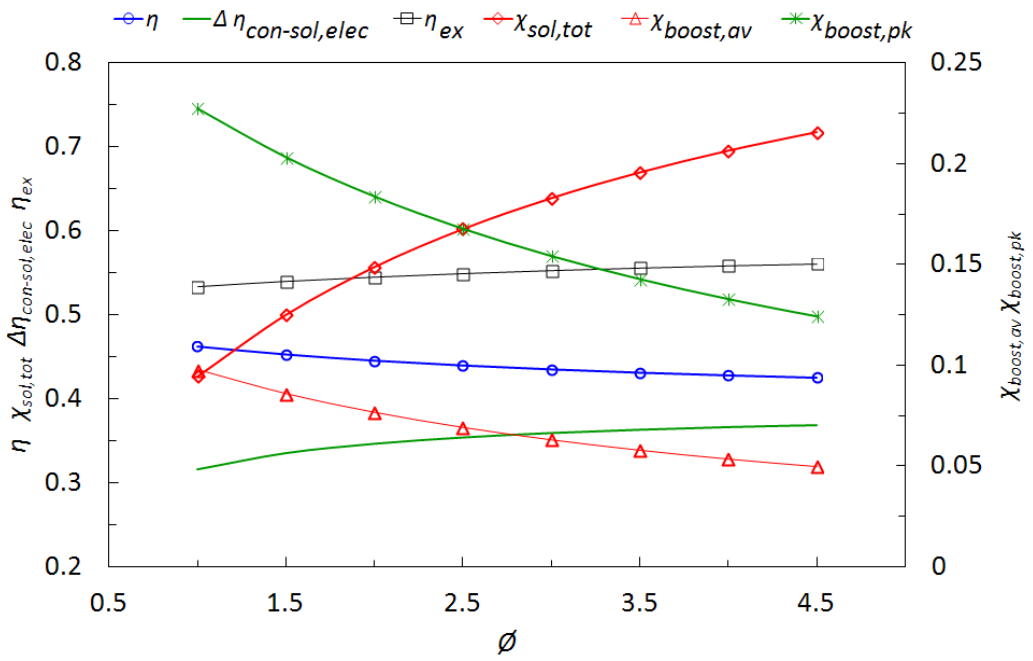

Fig. 7. Sensitivity to molar ratio of oxygen carrier particles to fuel of the first law efficiency, total solar share, incremental concentrated solar to electrical efficiency, exergy efficiency, average and peak fractional power boosts for the cycle without the after-burner using the reference conditions given in Table 1 and the average solar insolation at Port Augusta, South Australia [38].

The sensitivities of the calculated $\chi_{boost,av}$, $\chi_{boost,pk}$ and η_{ex} to the variations in Ø are also shown in Fig. 7. As for the cycle with the after-burner, $\chi_{boost,av}$, $\chi_{boost,pk}$ are found to decrease with an increase in Ø. This is attributed to the decrease in the flow rate of fuel with an increase in Ø [2]. Hence too, the exergy efficiency of the system is increased from 53.3% to 56.0% as Ø is increased from 1.0 to 4.5.

4.3.Effect of Reservoir R_1 temperature

Fig. 8 shows the sensitivity of $\chi_{sol,tot}$, $\chi_{CO_2,pure}$, η and $\Delta\eta_{con\text{-}sol,elec}$ to the variations in the temperature of the reservoir R_1, T_{R_1}, for the cycle with the after-burner. As expected, $\chi_{sol,tot}$ is strongly sensitive to T_{R_1} and decreases from 41.4% at T_{R_1} = 100 °C to 12.3% at T_{R_1} = 750 °C as the inlet temperature of the OC particles to the fuel reactor approaches to its operating temperature [2]. However, the first law efficiency of the cycle, η, is increased slightly from 50.0% to 52.5% as T_{R_1} increases from 100 °C to 750 °C. Together these effects explain why $\Delta\eta_{con\text{-}sol,elec}$ decreases considerably from 39.4% at T_{R_1} = 100 °C to 16.7% at T_{R_1} = 750 °C with the same change in T_{R_1}. Interestingly, $\chi_{CO_2,pure}$ is increased by around 30% over this range of T_{R_1}. Moreover, $\chi_{boost,av}$ and $\chi_{boost,pk}$ also increase from 4.2% and 10.6% at T_{R_1} = 100 °C to 8.1% and 19.4% at T_{R_1} = 750°C, respectively. These trends are attributed to the increase in the fraction of chemical stored energy in the OC particles with an increase in T_{R_1} [2].

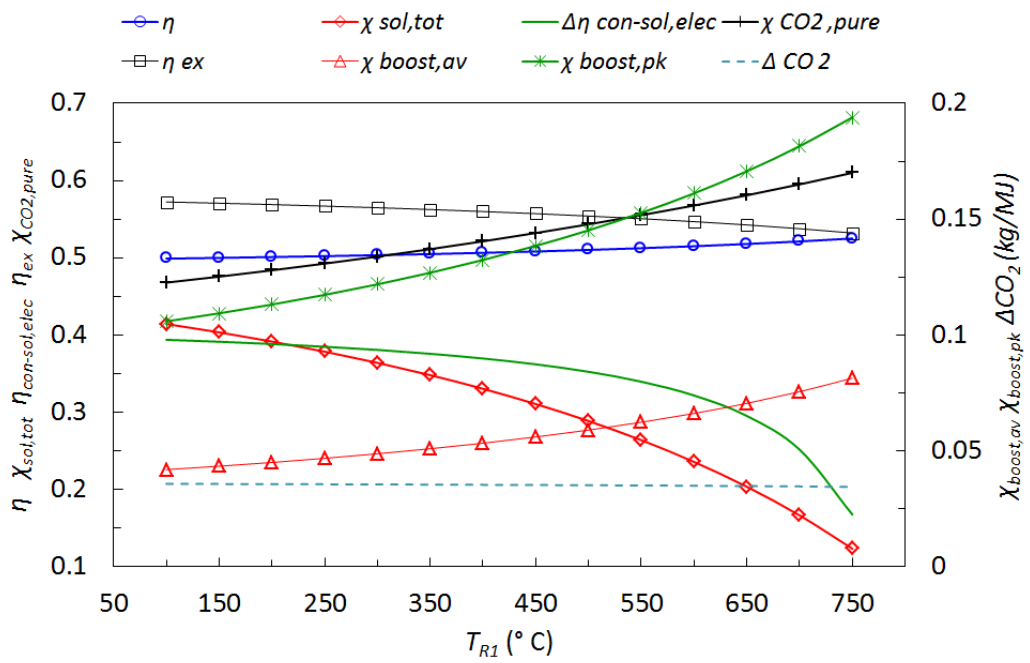

Fig. 8. Sensitivity to reservoir R_1 temperature of the first law efficiency, total solar share, incremental concentrated solar to electrical efficiency, exergy efficiency, fraction of pressurised CO_2 , average and peak fractional power boost and the incremental CO_2 avoidance for the cycle with an after-burner using the reference conditions given in Table 1 and the average solar insolation at Port Augusta, South Australia [38].

The sensitivity of the calculated Δ_{CO_2} and η_{ex} to the variations in T_{R_1} for the cycle with an after-burner is also shown in Fig. 8. Interestingly, Δ_{CO_2} is insensitive to T_{R_1} varying by only around 3.6% over the temperature range considered. Finally, it can be seen that the exergy efficiency of the system decreases from 57.2% at T_{R_1} = 100 °C to 53.2% at T_{R_1} = 750 °C. This is caused by the increase in the fraction of chemical storage with T_{R_1} [2].

Fig. 9 shows the sensitivity of η, $\chi_{sol,tot}$, $\Delta\eta_{con\text{-}sol,elec}$, η_{ex}, $\chi_{boost,av}$ and $\chi_{boost,pk}$ to the variations in temperature of reservoir R_1, T_{R_1}, for the cycle without the after-burner. As can be seen, all of the trends are fairly similar to those of cycle with the after-burner.

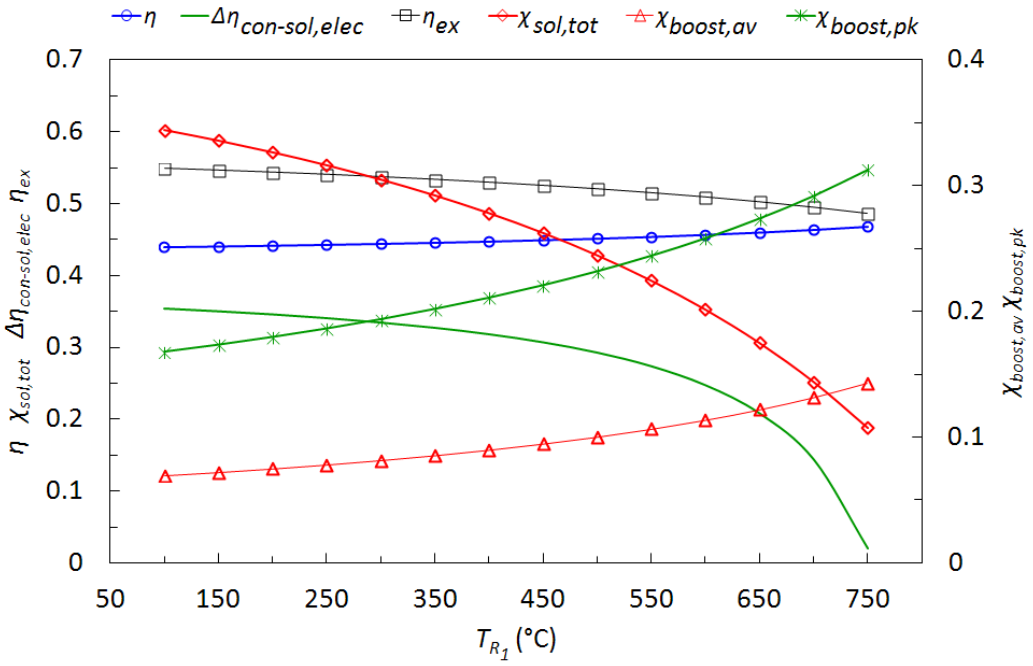

Fig. 9. Sensitivity to reservoir R_1 temperature of the first law efficiency, total solar share, incremental concentrated solar to electrical efficiency, exergy efficiency, average and peak fractional power boost for the cycle without the after-burner using the reference conditions given in Table 1 and the average solar insolation at Port Augusta, South Australia [38].

4.4. Effect of fuel reactor temperature

Fig. 10 presents the sensitivity of the predicted $\eta_{abs,tot}$, η, $\chi_{sol,tot}$, $\Delta\eta_{con\text{-}sol,elec}$ and η_{ex} to the variations in operating temperature of the solar fuel reactor, T_{FR}, for the

cycle employing the after-burner. As excepted, $\eta_{abs,tot}$ decreases with an increase in T_{FR} from 97.0% at T_{FR} = 550 °C to 85.5% at T_{FR} = 950 °C. Simultaneously η is also decreased by around 1.5 percentage points. These changes are mostly due to the increase in the re-radiation heat losses through solar fuel reactor aperture with T_{FR}. Importantly, even though $\eta_{abs,tot}$ decreases with T_{FR}, $\chi_{sol,tot}$ increases from 36.6% at T_{FR} = 550 °C to 44.8% at T_{FR} = 950 °C. This is due to the increase in sensible heat storage within the OC particles [2]. The calculations also predict that the $\Delta\eta_{con\text{-}sol,elec}$ increases slightly from 36.7% to 38.6% as T_{FR} is increased from 550 °C to 950 °C. This is attributed to the increase in the $\chi_{sol,tot}$ cycle efficiency with T_{FR}. Finally, η_{ex} is insensitive to T_{FR} changing less than 1.0 percentage point over the considered range of T_{FR}.

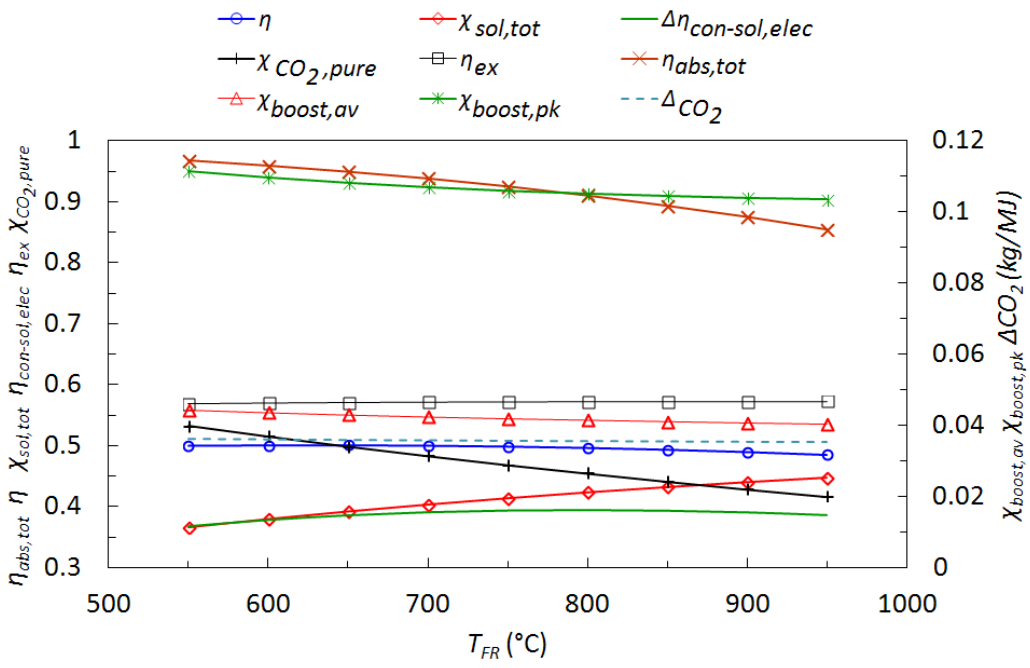

Fig. 10. Sensitivity to fuel reactor operating temperature of the solar absorption efficiency, first law efficiency, total solar share, incremental concentrated solar to electrical efficiency, exergy efficiency, fraction of pressurised CO_2, average and peak fractional power boosts and the incremental CO_2 avoidance for the cycle employing an after-burner using the reference conditions given in Table 1 and the average solar insolation at Port Augusta, South Australia [38].

The calculated sensitivity of the predicted $\chi_{CO_2,pure}$, Δ_{CO_2}, $\chi_{boost,av}$ and $\chi_{boost,pk}$ to the variations in T_{FR} for the cycle with an after-burner is also shown in Fig. 10. It can be seen that $\chi_{CO_2,pure}$ decreases with an increase in T_{FR}. For example, $\chi_{CO_2,pure}$ is 53.2% at T_{FR} = 550 °C, while it is 41.6% at T_{FR} = 950 °C. This is because of the increase in fraction of sensible heat storage in the OC particles with T_{FR} [2]. Hence too, $\chi_{boost,av}$ and $\chi_{boost,pk}$ are also decreased slightly with the increasing of

T_{FR} over the considered range. However, Δ_{CO_2} is not sensitive to T_{FR}, remaining relatively constant at 0.036 kg CO_2/MJ.

Fig. 11 depicts the calculated sensitivity of the predicted $\eta_{abs,tot}$, η, $\chi_{sol,tot}$, $\Delta\eta_{con-sol,elec}$, $\chi_{boost,av}$, $\chi_{boost,pk}$, η_{ex} and Δ_{CO_2} to variations in T_{FR} for a cycle without the after-burner. As shown, the sensitivities are similar to those of cycle employing the after-burner.

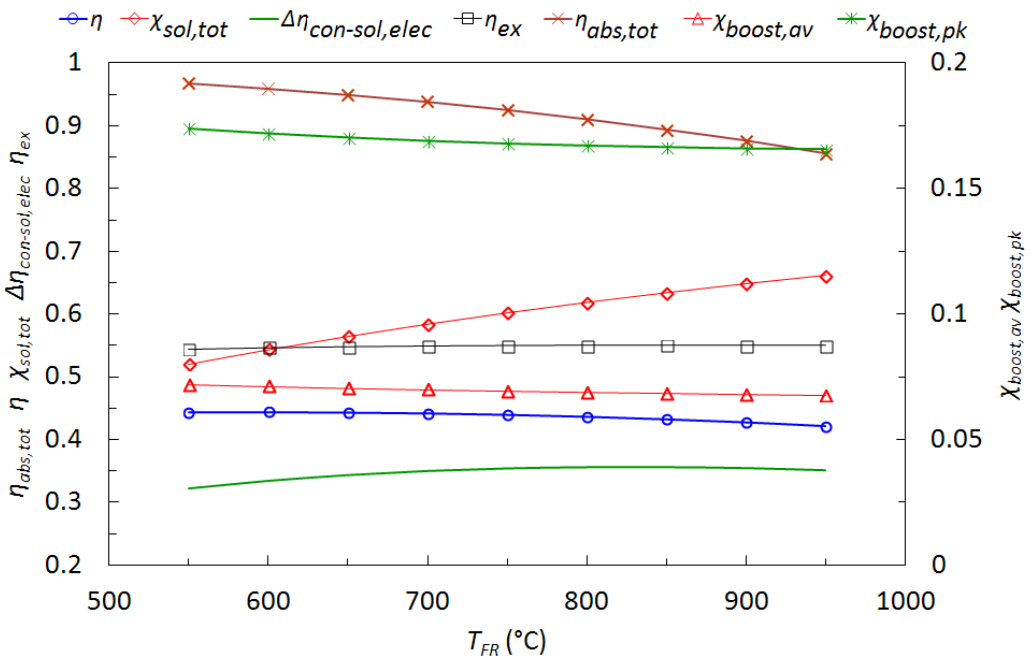

Fig. 11. Sensitivity to fuel reactor operating temperature of the solar absorption efficiency, first law efficiency, total solar share, incremental concentrated solar to electrical efficiency, exergy efficiency, average and peak fractional power boosts for the cycle without the after-burner using the reference conditions given in Table 1 and the average solar insolation at Port Augusta, South Australia [38].

4.5.Effect of concentration ratio of the solar collector field

Fig. 12 shows the calculated sensitivity of $\eta_{abs,tot}$, η and $\Delta\eta_{con\text{-}sol,elec}$ to the variations in the concentration ratio of the solar collector field, *CR*, for the cycle with the after-burner. As expected, $\eta_{abs,tot}$, η and $\Delta\eta_{con\text{-}sol,elec}$ increase with *CR* due to decrease in re-radiation heat loss through solar fuel reactor aperture. This sensitivity is greater at low values of *CR* than at high ones. For instance, an increase in *CR* from 500 to 1000 raises the $\eta_{abs,tot}$, η and $\Delta\eta_{con\text{-}sol,elec}$ by around 18.1%, 8.6% and 18.1%, respectively, in contrast to a 2.0%, 1.0% and 2.0% increase for the doubling of *CR* from 4000 to 8000 [2]. The sensitivity of the calculated $\chi_{boost,av}$, $\chi_{boost,pk}$, Δ_{CO_2} and η_{ex} to the variations in *CR* are also depicted in Fig 6. As shown, $\chi_{boost,pk}$ decreases from 11.3% at *CR* = 500 to 10.4% at *CR* = 8000 while $\chi_{boost,av}$ is generally insensitive to *CR*. Interestingly, other parameters are not sensitive to *CR*. It is also worth noting that the operation duration time of the solar fuel reactor also depends on the *CR* [2].

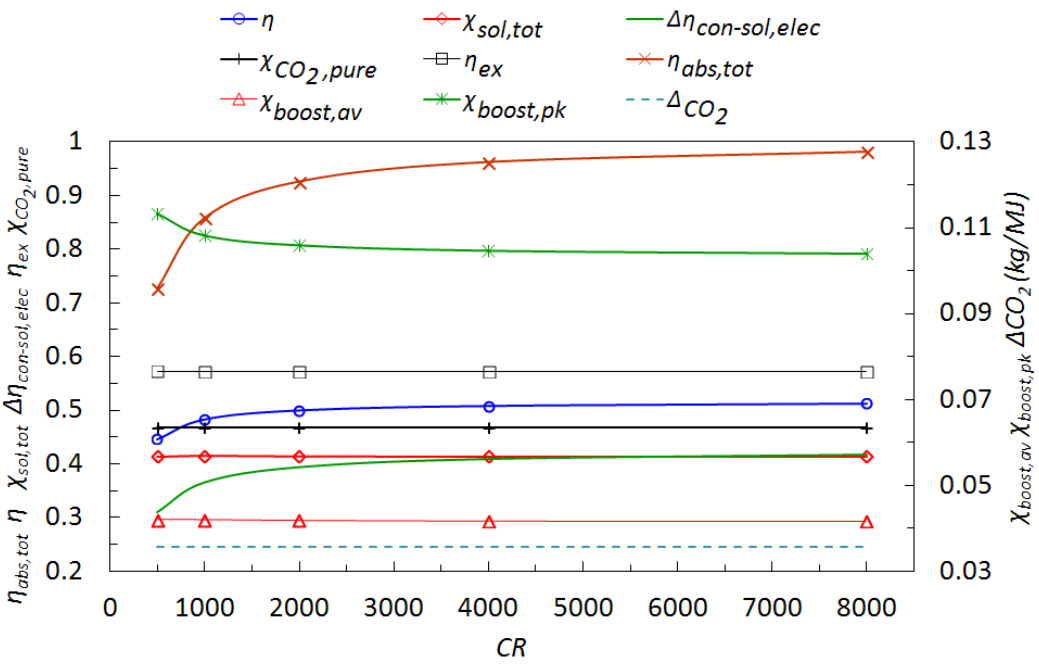

Fig. 12. Sensitivity to variations in to solar collector field concentration ratio of the solar absorption efficiency, first law efficiency, total solar share, incremental concentrated solar to electrical efficiency, exergy efficiency, fraction of pressurised CO_2, average and peak fractional power boost and the incremental CO_2 avoidance for the cycle employing an after-burner using the reference conditions given in Table 1 and the average solar insolation at Port Augusta, South Australia [38].

Fig. 13 presents the calculated sensitivity to the variations in *CR* of $\eta_{abs,tot}$, η, $\Delta\eta_{con\text{-}sol,elec}$, $\chi_{sol,tot}$, $\chi_{boostav}$, $\chi_{boost,pk}$, and η_{ex} for the cycle without the after-burner. As shown, the sensitivities are relatively similar to those of cycle employing the after-burner. However, here η is more sensitive to *CR*. For instance, η increases by around 21.2% as *CR* is increased from 500 to 8000, while this is around 14.5% for the cycle not employing the after-burner. It is worth noting that the total energy

that can be extracted from the solar radiation in both cycles is not independent from this ratio, due both to the differing thresholds of minimum solar flux and to the differing absorption efficiency of the solar fuel reactor [2].

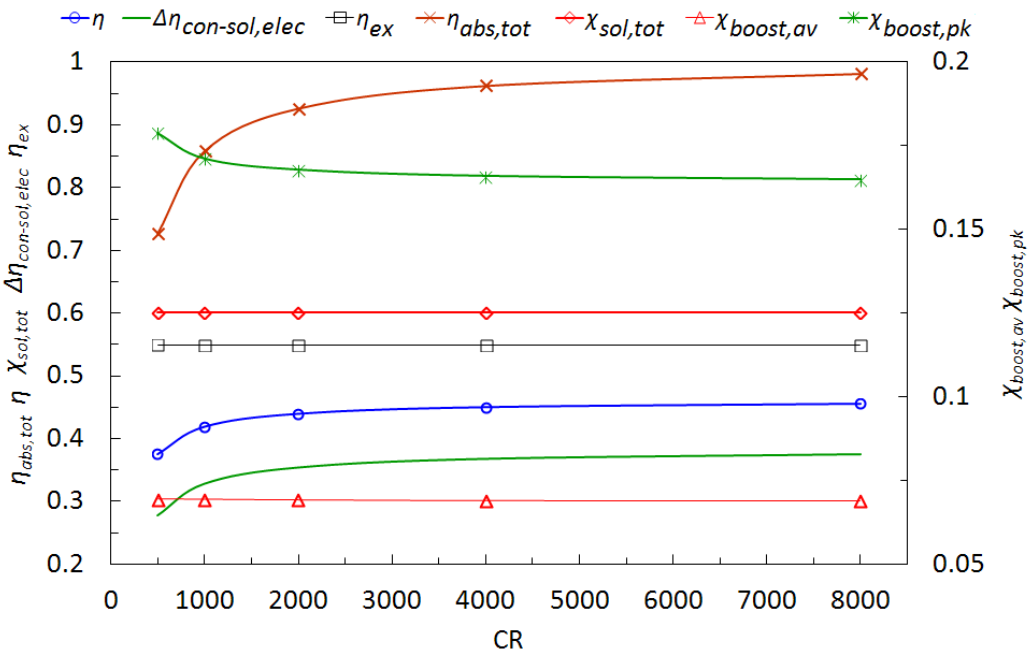

Fig. 13. Sensitivity to variations in to solar collector field concentration ratio of the solar absorption efficiency, first law efficiency, total solar share, incremental concentrated solar to electrical efficiency, exergy efficiency, average and peak fractional power boost for the cycle without the after-burner using the reference conditions given in Table 1 and the average solar insolation at Port Augusta, South Australia [38].

4.6. Effect of after-burner operating temperature

Fig. 14 shows the calculated sensitivity to the variations in after-burner temperature, T_{AB}, of $\chi_{sol,tot}$, $\chi_{CO_2,pure}$, η, ΔCO_2, $\Delta\eta_{con\text{-}sol,elec}$, $\chi_{boost,av}$ and $\chi_{boost,pk}$. Here the case of an after-burner temperature of 950 °C means that the cycle operates without it. As expected, an increase in T_{AB}, also increases η, while $\chi_{sol,tot}$, $\chi_{CO_2,pure}$ and Δ_{CO_2} all decrease, but with varying sensitivities to T_{AB}. The calculations predict that η is less sensitive to T_{AB} than are $\chi_{sol,tot}$, $\chi_{CO_2,pure}$ and Δ_{CO_2}. For example, as T_{AB} is increased from 950 °C to 1700 °C, η increases by around 23.0%, while $\chi_{sol,tot}$, $\chi_{CO_2,pure}$ and Δ_{CO_2} decrease by approximately 55.0%, 75% and 57%, respectively. Furthermore, the sensitivities of $\chi_{sol,tot}$, $\chi_{CO_2,pure}$ and Δ_{CO_2} are greater at low values of T_{AB} than at high ones. For instance, an increase in T_{AB} from 950 °C to 1000 °C decreases $\chi_{sol,tot}$, Δ_{CO_2} , $\chi_{CO_2,pure}$by around 7.0% , 8.0 % and 15.0%, respectively, in contrast to 4.0%, 3.7% and 6.0% for an increase in T_{AB} from 1650 to 1700 °C. The drop in $\chi_{sol,tot}$, $\chi_{CO_2,pure}$ and Δ_{CO_2} is only caused by the increase in fuel required in the after-burner with T_{AB}, while the increase in η with T_{AB} is due to both the increase in temperature and mass flow rate of inlet gas into the gas turbine. Significantly, $\Delta\eta_{con\text{-}sol,elec}$ also increase with T_{AB}. For example, an increase in T_{AB} from 950 °C to 1700 °C leads to around 32.0% raise in $\Delta\eta_{con\text{-}sol,elec}$. This is attributed to the increase in η with T_{AB}, as discussed above.

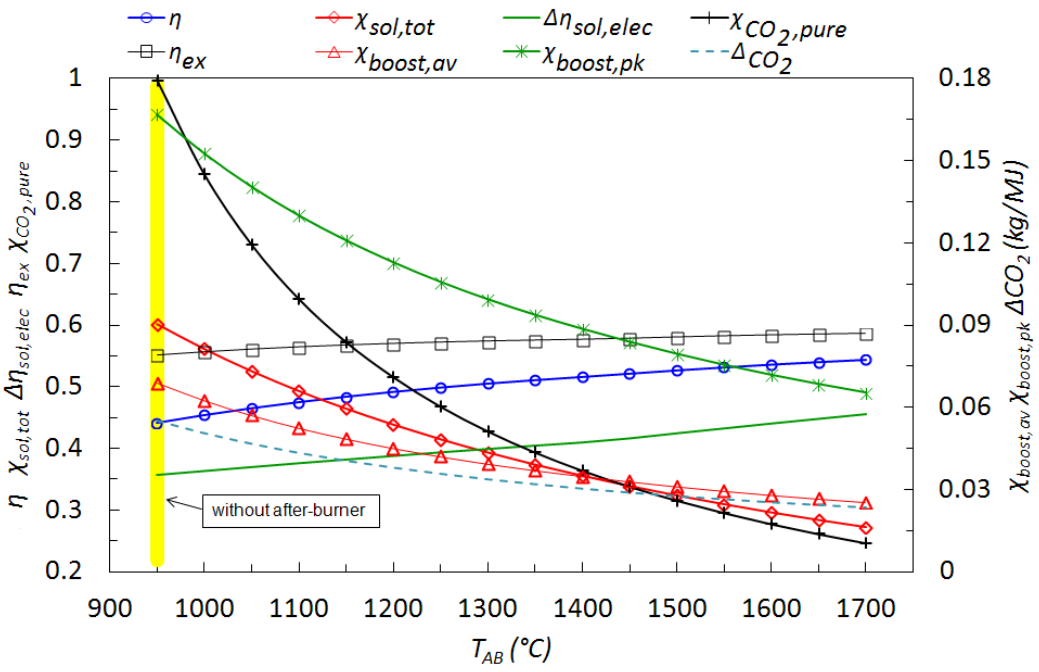

Fig. 14. Sensitivity of the first law efficiency, total solar share, incremental concentrated solar to electrical efficiency, exergy efficiency, fraction of pressurised CO_2 , average and peak fractional power boost and the incremental CO_2 avoidance to the operating temperature of the after-burner for the reference conditions given in Table 1 and the average solar insolation at Port Augusta, South Australia [38].

The sensitivities of the calculated $\chi_{boost,av}$, $\chi_{boost,pk}$ and η_{ex} to the variations in T_{AB} are also shown in Fig. 14. As shown, both $\chi_{boost,av}$ and $\chi_{boost,pk}$ decrease with T_{AB} from 6.80% and 16.70%, respectively, at T_{AB} = 950 °C to $\chi_{boost,av}$ = 2.50% and $\chi_{boost,pk}$ = 6.50% at T_{AB} = 1700 °C. As mentioned above, this is because the power generated by the capture of waste heat from the fuel reactor is independent from the operating temperature of the after-burner, while the power generated by the gas turbine and AR-Steam turbines increase with an increase in T_{AB}. Finally, it can

be seen that η_{ex} is only weakly sensitive to T_{AB} and increases from 55.0% to 58.7% as T_{AB} is increased from 950 °C to 1700 °C.

5. Conclusions

The proposed hybrid combined cycle without any supplementary heating from the after-burner is estimated to achieve a solar share of 60.0% and a first law efficiency of 44.0%, producing a pressurised and industrially pressurised CO_2 ready for reuse or storage. The incorporation of the after-burner into the cycle is found to increase the first law and the incremental concentrated solar to electrical efficiencies from 44.0% and 35.4%, respectively, to 50.0% and 39.8%, but at the dual cost of a significantly reduced solar share of 41.4% and fraction of pressurised CO_2 of 46.8%. Moreover, the incremental CO_2 avoidance is found to decrease by 35.0% with the addition of an after-burner to the cycle. The calculations also demonstrate that the exergy efficiency of the cycle increases from 54.9% to 57.2% with the introduction of the after-burner. The sensitivity analysis found that:

- Increasing the operating pressure of the air reactor from 10 to 20 bar leads to an expected increase in the first law and incremental concentrated solar to electrical efficiency of 2.6% and 6.9%, respectively, for the cycle employing the after-burner. However, this is accompanied by a corresponding 2.2% decrease in the solar share. Importantly, the solar share of the cycle without the after-burner is insensitive to the operating pressure of the air reactor, while the first law and incremental concentrated solar to electrical efficiencies decrease by around 2.8% and 5.5% over the considered pressure range.
- An increase in the molar ratio of oxygen carrier particle to the fuel increases the solar share in both cycles. However, the increase in solar

share of the cycle employing the after-burner is around 16.0% more than that of the cycle without it.

- The first law efficiency of the both cycles decreases with an increase in operating temperature of the fuel reactor. However, the incremental concentrated solar to electrical efficiency of both cycles increases with it. Moreover, in both cycles the average and peak fractional power boosts decrease with the operating temperature of the fuel reactor.
- For both cycles; the exergy efficiency, fraction of pressurised CO_2, solar share, average fractional power boosts and the incremental CO_2 avoidance are insensitive to mean flux concentration ratio of the solar collector field. However, the total absorption efficiency of the solar fuel reactor, first law efficiency and the incremental concentrated solar to electrical efficiency for both cycles, increase with it. Moreover, the peak fractional boost decreases with the increasing of mean flux concentration ratio.
- Increasing the operating temperature of the after-burner from 950 °C to 1700 °C causes an increase in the first law efficiency and the incremental concentrated solar to electrical efficiency of the hybrid solar cycle by around 23.0% and 27.0%, respectively. However, this is achieved at a considerable decrease of 54.0% in the solar share. Importantly, the exergy efficiency is quite insensitive to the gas turbine inlet temperature.

Acknowledgement

The first author is grateful for the support of an Adelaide Scholarship International. The third author wishes to acknowledge the support of Australian Research Council through a Discovery Outstanding Researcher Award. The authors also thank Dr. Woei Saw for his supporting information and comments on the paper.

Nomenclature

A_{coll}	solar collector area (m^2)
CR	mean flux concentration ratio
DNI	direct normal insolation (W/m^2)
E_{xi}	molar exergy of fuel stream (kJ/mol)
$\dot{E}_{elec,\,fuel}$	fuel consumed by the hybrid Cycle (W)
$\dot{E}_{elec,hybrid}$	power produced by the hybrid cycle (W)
LHV_{CH_4}	molar lower heating value of CH_4 (kJ/mol)
$\dot{n}_i$	molar flow rate *i*'th (mol/min)
$\dot{Q}_{coll}$	incoming power from solar collector field (kW)
$\dot{Q}_{re,rad}$	re-radiated thermal power (W)
$\dot{Q}_{s,in}$	input solar thermal power (W)
$\dot{Q}_{s,abs}$	absorbed solar thermal power (W)
$\dot{Q}_{s,in,\max}$	maximum input solar Thermal power (W)
T_{FR}	fuel reactor temperature (K)
T_i	temperature of stream *i*'th (K)
$\dot{W}_{AR,ST}$	power generated by air reactor steam turbine (W)
$\dot{W}_{c,air}$	power required for air compression (W)
$\dot{W}_{FR,ST}$	power generated by fuel reactor steam turbine (W)
$\dot{W}_{GT}$	power generated by gas turbine (W)
$\dot{W}_{pump_I}$	power consumed by pump I (W)
$\dot{W}_{pump_{II}}$	power consumed by pump II (W)

Greek letters

α_{eff}	effective absorptance
Δ_{CO_2}	incremental CO_2 avoidance
ΔH_i	total stream enthalpy change (kJ/mol)
$\Delta\eta_{con-sol,elec}$	incremental concentrated solar Electrical efficiency
ε_{eff}	effective absorptance
η	first law efficiency
$\eta_{abs,tot}$	absorption efficiency
$\overline{\eta}_{coll}$	average collector system optical efficiency
σ	Stephan-Boltzmann constant (W/m^2k^{-4})
$\emptyset$	Molar ratio of oxygen carrier particles to fuel
$\chi_{boost,av}$	average fractional power boost
$\chi_{boost,pk}$	peak fractional power boost
$\chi_{loss,rad}$	total fraction of solar input energy reradiated
$\chi_{sol,tot}$	thermal solar share
$\chi_{CO_2,pure}$	pressurised CO_2 fraction
$\chi_{CO_2,emit}$	fraction of CO_2 emitted to atmosphere
$\chi_{sol,st}$	solar fraction stored

Subscripts

abs	absorption
ap,open	solar fuel reactor aperture open
ap,close	solar fuel reactor aperture close
AB	after-burner
AR	air reactor
coll	collector
F	fuelr
FR	fuel reactor
GT	gas turbine
GTCC	gas turbine combined cycle
G	generator
in	input
oc	oxygen carrier
out	output

References

[1] Jafarian M, Arjomandi M, Nathan GJ. A hybrid solar and chemical looping combustion system for solar thermal energy storage. Applied Energy. 2013;103:671-8.

[2] Jafarian M, Arjomandi M, Nathan GJ. A solar hybrid chemical looping combustion power cycle with a high solor share. Applied Energy. 2014;126:69–77.

[3] Jafarian M, Nathan GJ, Arjomandi M. A hybrid solar and chemical looping combustion system, Provisional Patent Application No. 2013903807., Adelaide Research and Innovation Pty. Ltd.; 2013 [Priority Date: 02.10.2013]. 2013.

[4] Adanez J, Abad A, Garcia-Labiano F, Gayan P, de Diego LF. Progress in chemical-looping combustion and reforming technologies. Progress in Energy and Combustion Science. 2012;38:215-82.

[5] Abad A, Adánez J, García-Labiano F, de Diego LF, Gayán P, Celaya J. Mapping of the range of operational conditions for Cu-, Fe-, and Ni-based oxygen carriers in chemical-looping combustion. Chemical Engineering Science. 2007;62:533-49.

[6] Fan L-S, Zeng L, Wang W, Luo S. Chemical looping processes for CO_2 capture and carbonaceous fuel conversion - prospect and opportunity. Energy & Environmental Science. 2012;5:7254-80.

[7] Hong H, Jin H. A Novel solar thermal cycle with chemical looping combustion. International Journal of Green Energy. 2005;2:397-407.

[8] Hong H, Jin H, Liu B. A novel solar-hybrid gas turbine combined cycle with inherent CO_2 separation using chemical-looping combustion by solar heat source. Journal of Solar Energy Engineering. 2006;128:275-84.

[9] Hong H, Han T, Jin H. A low temperature solar thermochemical power plant with CO_2 recovery using methanol-fueled chemical looping combustion. Journal of Solar Energy Engineering. 2010;132:031002.

[10] Jafarian M, Arjomandi M, Nathan GJ. The influence of high intensity solar radiation on the temperature and reduction of an oxygen carrier particle in hybrid chemical looping combustion. Chemical Engineering Science. 2013;95:331-42.

[11] Wolf J, Anheden M, Yan J. Comparison of nickel- and iron-based oxygen carriers in chemical looping combustion for CO_2 capture in power generation. Fuel. 2005;84:993-1006.

[12] Naqvi R, Wolf J, Bolland O. Part-load analysis of a chemical looping combustion (CLC) combined cycle with CO_2 capture. Energy. 2007;32:360-70.

[13] Naqvi R, Bolland O, Brandvoll Ø, Helle K. Chemical looping combustion analysis of natural gas fired power cycles with inherent CO_2 capture. In: Proceeding of ASME turbo expo. Vienna, Austria2004.

[14] Peltola P, Ritvanen J, Tynjälä T, Hyppänen T. Model-based evaluation of a chemical looping combustion plant for energy generation at a pre-commercial scale of 100 MWth. Energy Conversion and Management. 2013;76:323-31.

[15] Bhargava RK, Bianchi M, Pascale A, Negri di Montenegro G, Peretto A. Gas Turbine Based Power Cycles - A State-of-the-Art Review. In: Cen K, Chi Y, Wang F, editors. Challenges of Power Engineering and Environment: Springer Berlin Heidelberg; 2007. p. 309-19.

[16] Chyu MK. Recent advances in turbine heat transfer-with a view of transition to coal-gas based systems. Journal of Heat Transfer. 2012;134:1-9.

[17] Hischier I, Leumann P, Steinfeld A. Experimental and numerical analyses of a pressurized air receiver for solar-driven gas turbines. Journal of Solar energy Engineering. 2012;134 (2); 021003-1.

[18] Kribus A, Zaibel R, Carey D, Segal A, Karni J. A solar-driven combined cycle power plant. Solar Energy. 1998;62:121-9.

[19] Schwarzbözl P, Buck R, Sugarmen C, Ring A, Marcos Crespo MJ, Altwegg P, et al. Solar gas turbine systems: Design, cost and perspectives. Solar Energy. 2006;80:1231-40.

[20] Buck R, Brauning T, Denk T, Pfander M, Schwarzbozl P, Tellez F. Solar-hybrid gas turbine-based power tower systems (REFOS). Journal of Solar Energy Engineering. 2002;124:2-9.

[21] Yu J, Corripio AB, Harrison DP, Copeland RJ. Analysis of the sorbent energy transfer system (SETS) for power generation and CO_2 capture. Advances in Environmental Research. 2003;7:335-45.

[22] Consonni S, Lozza G, Pelliccia G, Rossini S, Saviano F. Chemical-looping combustion for combined cycles with CO_2 capture. Journal of Engineering for Gas Turbines and Power. 2006;128:525-34.

[23] Eggers R. Industrial High Pressure Applications: Processes, Equipment, and Safety: Wiley; 2012.

[24] Yazdanpanah MM, Hoteit A, Forret A, Delebarre A, Gautheir T. Experimental investigation on a novel chemical looping combustion configuration. Oil Gas Sci Technol-Rev IFP Energies nouvelles. 2011;66:265-75.

[25] Svoboda K, Pohořelý M, Hartman M, Martinec J. Pretreatment and feeding of biomass for pressurized entrained flow gasification. Fuel Processing Technology. 2009;90:629–35.

[26] Johansson E, Lyngfelt A, Mattisson T, Johnsson F. Gas leakage measurements in a cold model of an interconnected fluidized bed for chemical-looping combustion. Powder Technology. 2003;134:210-7.

[27] Ávila-Marín AL. Volumetric receivers in solar thermal power plants with central receiver system technology: A review. Solar Energy. 2011;85:891-910.

[28] Steinfeld A. Solar thermochemical production of hydrogen–a review. Solar Energy. 2005;78:603-15.

[29] Slotte M, Romão I, Zevenhoven R. Integration of a pilot-scale serpentinite carbonation process with an industrial lime kiln. Energy. 2013;62:142-9.

[30] Khoo HH, Sharratt PN, Bu J, Yeo TY, Borgna A, Highfield JG, et al. Carbon capture and mineralization in singapore: preliminary environmental impacts and costs via LCA. Industrial & Engineering Chemistry Research. 2011;50:11350-7.

[31] Smith JM, Van Ness H, Abbott MM. Introduction to Chemical Engineering Thermodynamics: McGraw-Hill Education; 2005.

[32] Adánez J, Dueso C, de Diego LF, García-Labiano F, Gayán P, Abad A. methane combustion in a 500 W_{th} chemical-looping combustion system using an impregnated Ni-based oxygen carrier. Energy & Fuels. 2008;23:130-42.

[33] Steinfeld A, Larson C, Palumbo R, Foley Iii M. Thermodynamic analysis of the co-production of zinc and synthesis gas using solar process heat. Energy. 1996;21:205-22.

[34] Sheu EJ, Mitsos A, Eter AA, Mokheimer EM, Habib MA, Al-Qutub A. A review of hybrid solar–fossil fuel power generation systems and performance metrics. Journal of Solar Energy Engineering. 2012;134:041006.

[35] Kolb GJ. Economic evaluation of solar-only and hybrid power towers using molten-salt technology. Solar Energy. 1998;62:51-61.

[36] Hong H, Jin H, Ji J, Wang Z, Cai R. Solar thermal power cycle with integration of methanol decomposition and middle-temperature solar thermal energy. Solar Energy. 2005;78:49-58.

[37] Ibrahim Dincer, Marc A. Rosen. Exergy: Energy, Environment and Sustainable Development: Elsevier Science; 2007.

[38] Analysis of 10-years record Port Agusta Asutralia for Renewables SA.

[39] Naqvi R, Bolland O. Multi-stage chemical looping combustion (CLC) for combined cycles with CO_2 capture. International Journal of Greenhouse Gas Control. 2007;1:19-30.

[40] Steinfeld A, Kuhn P, Reller A, Palumbo R, Murray J, Tamaura Y. Solar-processed metals as clean energy carriers and water-splitters. International Journal of Hydrogen Energy. 1998;23:767-74.

[41] Johansson M, Mattisson T, Lyngfelt A. Use of $NiO/NiAl_2O_4$ particles in a 10 kW chemical-looping combustor. Industrial & Engineering Chemistry Research. 2006;45:5911-9.

[42] Gou C, Cai R, Hong H. A novel hybrid oxy-fuel power cycle utilizing solar thermal energy. Energy. 2007;32:1707-14.

[43] Notz RJ, Tönnies I, McCann N, Scheffknecht G, Hasse H. CO_2 capture for fossil fuel-fired power plants. Chemical Engineering & Technology. 2011;34:163-72.

[44] Jafarian M, Arjomandi M, Nathan GJ. Influence of the type of oxygen carriers on the performance of a hybrid solar chemical looping combustion system. Energy & Fuels. 2014;28:2914-24.

[45] Hossain MM, de Lasa HI. Chemical-looping combustion (CLC) for inherent separations-a review. Chemical Engineering Science. 2008;63:4433-51.

CHAPTER 6

INFLUENCE OF THE TYPE OF OXYGEN CARRIERS ON THE PERFORMANCE OF A HYBRID SOLAR CHEMICAL LOOPING COMBUSTION SYSTEM

Statement of Authorship

Title of Paper	Influence of the type of the type of oxygen carriers on the performance of a hybrid solar chemical looping combustion system
Publication Status	◉ Published, ○ Accepted for Publication, ○ Submitted for Publication, ○ Publication style
Publication Details	M. Jafarian, M. Arjomandi, G. J. Nathan, "Influence of the type of the type of oxygen carriers on the performance of a hybrid solar chemical looping combustion system". Energy& Fuels, (2014), vol: 28, issue: 5, p: 2914–2924.

Author Contributions

By signing the Statement of Authorship, each author certifies that their stated contribution to the publication is accurate and that permission is granted for the publication to be included in the candidate's thesis.

Name of Principal Author (Candidate)	Seyed Mehdi Jafarian		
Contribution to the Paper	Developed ideas. performed simulations and calculations, interpreted data, wrote manuscript and acted as corresponding author.		
Signature		Date	05/06/2014.

Name of Co-Author	Maziar Arjomandi		
Contribution to the Paper	Supervised development of work, helped in developing ideas, data interpretation and manuscript evaluation.		
Signature		Date	05.06.2014

Name of Co-Author	Graham Nathan		
Contribution to the Paper	Supervised development of work, helped in developing ideas, data interpretation and manuscript evaluation.		
Signature		Date	5-6-14

Name of Co-Author			
Contribution to the Paper			
Signature		Date	

Jafarian, M., Arjomandi, M. & Nathan, G.J. (2014). Influence of the Type of Oxygen Carriers on the Performance of a Hybrid Solar Chemical Looping Combustion System *Energy & Fuels*, *28*(5), 2914-2924

Chapter 7

THE INFLUENCE OF HIGH INTENSITY SOLAR RADIATION ON THE TEMPERATURE AND REDUCTION OF AN OXYGEN CARRIER PARTICLE IN HYBRID CHEMICAL LOOPING COMBUSTION

Statement of Authorship

Title of Paper	The influence of high intensity solar radiation on the temperature and reduction of an oxygen carrier particle in hybrid chemical looping combustion
Publication Status	◉ Published, ○ Accepted for Publication, ○ Submitted for Publication, ○ Publication style
Publication Details	M. Jafarian, M. Arjomandi, G. J. Nathan, "The influence of high intensity solar radiation on the temperature and reduction of an oxygen carrier particle in hybrid chemical looping combustion". Chemical Engineering Science, (2013), vol: 95, p: 331-342.

Author Contributions

By signing the Statement of Authorship, each author certifies that their stated contribution to the publication is accurate and that permission is granted for the publication to be included in the candidate's thesis.

Name of Principal Author (Candidate)	Seyed Mehdi Jafarian		
Contribution to the Paper	Developed ideas. performed simulations and calculations, interpreted data, wrote manuscript and acted as corresponding author.		
Signature		Date	05/06/2014.

Name of Co-Author	Maziar Arjomandi		
Contribution to the Paper	Supervised development of work, helped in developing ideas, data interpretation and manuscript evaluation.		
Signature		Date	05.06.2014

Name of Co-Author	Graham Nathan		
Contribution to the Paper	Supervised development of work, helped in developing ideas, data interpretation and manuscript evaluation.		
Signature		Date	5.6.14

Name of Co-Author			
Contribution to the Paper			
Signature		Date	

Chemical Engineering Science 95 (2013) 331–342

Contents lists available at SciVerse ScienceDirect

Chemical Engineering Science

journal homepage: www.elsevier.com/locate/ces

The influence of high intensity solar radiation on the temperature and reduction of an oxygen carrier particle in hybrid chemical looping combustion

Mehdi Jafarian *, Maziar Arjomandi, Graham J. Nathan

Centre for Energy Technology, School of Mechanical Engineering, The University of Adelaide, SA 5005, Australia

HIGHLIGHTS

- A model of an oxygen carrier particle exposed to radiation heat flux is presented.
- A sensitivity analysis on particle temperature and conversion time was done.
- Rate of oxygen carrier particle conversion increases with radiative heat flux.
- Convection is the dominant mechanism of particle cooling.
- Key parameters for solar hybrid CLC design are investigated.

ARTICLE INFO

Article history:
Received 16 October 2012
Received in revised form
18 February 2013
Accepted 1 March 2013
Available online 15 March 2013

Keywords:
Heat transfer
Solar energy
Modelling
Oxygen carrier particle
Solar hybrid system
Chemical looping combustion

ABSTRACT

The temperature variations during the conversion of an oxygen carrier particle exposed to high intensity solar heat flux are assessed as a function of time with an unsteady-state model. The conservation equations of energy and mass are solved simultaneously using an appropriate numerical technique, whose reliability was assessed by comparison with the available experimental and numerical data from the literature. This model was used to study the effect on the particle conversion and maximum temperature of various operating parameters i.e. particle size, external heat and mass transfer, radiation heat flux intensity, CH_4 mole fraction and surrounding temperature. The numerical results show that exposing the particle to high flux solar radiation decreases the conversion time and increases the particle temperature. The calculations indicate that a higher Nusselt number results in a lower temperature rise of the particle and a lower conversion time. The calculations also show that, convection is the dominant mechanism of particle cooling, despite the high temperature of the particle surface.

1. Introduction

Chemical Looping Combustion (CLC) is a technology under development to provide inherent capability for CO_2 capture in the combustion of hydrocarbon fuels. The CLC process is based on the indirect transfer of oxygen from the air to the fuel by means of a solid oxygen carrier (OC) particle to avoid direct contact between the fuel and air. A CLC system consists of two separate reactors; an air reactor and a fuel reactor. Within the CLC process, OC particles in the fuel reactor are reduced through oxidation of the fuel and transferred to the air reactor, where they are oxidised by the air to produce metal oxide. The metal oxide is then returned back to the fuel reactor and the process is repeated (Abad et al., 2007; Adanez et al., 2012; Hossain and de Lasa, 2008; Lyngfelt et al., 2001). While the oxidation of reduced metal oxides is always an exothermic reaction, the oxidation of fuel within the fuel reactor can be endothermic or exothermic depending on the combination of fuel and metal oxide particles (Adánez et al., 2004; Jerndal et al., 2006, 2009). In a conventional CLC process this energy is provided from the oxidation of metal oxide in the air reactor, leading to a temperature difference between the fuel and air reactors (Adánez et al., 2008). Consequently, if the required energy within the fuel reactor can be provided from an external source, such as solar thermal energy, the output from the CLC-based power plant will increase. In addition, this concept introduces the possibility of storing the solar energy in the OC particles as chemical and/or sensible heat (Jafarian et al., 2013). However, these concepts have only recently begun to be explored so that the full extent of the

* Corresponding author. Tel.: +61 8 8303 5460.
E-mail address: mehdi.jafarian@adelaide.edu.au (M. Jafarian).

0009-2509/$ - see front matter Crown Copyright © 2013 Published by Elsevier Ltd. All rights reserved.
http://dx.doi.org/10.1016/j.ces.2013.03.007

potential benefits and limitations of hybrid CLC and solar energy systems is yet to be identified.

Hong et al. (2006, 2010) and Hong and Jin (2005) were the first to propose the hybridisation of solar energy with CLC for power generation. Their cycles employ the concentrated solar radiation as a heat source to drive the endothermic oxidation reaction between the fuel and OC particles. This process converts the solar energy to chemical energy at a relatively low temperature and then releases it at a higher temperature but does not address the storage of the solar energy. More recently, to provide storage of the concentrated solar thermal energy, Jafarian et al. (2013) proposed a hybrid that employs the OC particles as a storage medium in a hybrid CLC cycle. In this system, three reservoirs were added to a conventional CLC system to allow storage of the OC particles, while a cavity solar receiver was chosen as the fuel reactor. In a solar cavity reactor the solid reactant particles are directly exposed to high flux solar irradiation, providing efficient radiative heat transfer directly to the reaction site (Z'Graggen et al., 2006). However, exposing the OC particles to high intensity solar radiation will increase their temperature, which has potential to result in damage due to melting, sintering or deactivation. Therefore, the design and optimization of a hybrid CLC-solar system require a model of the response of OC particles to high heat flux solar radiation, with which to assess these issues. The first aim of the present paper, therefore, is to develop and validate such a model.

Few previous studies reporting the numerical simulation of OC particles are available. Garcia-Labiano et al. (2005) used the Changing Grain Size Model (CGSM), together with an assumption of a 1-D variation within the particle, to predict the conversion time of an OC particle within a fluidized bed reactor. This model can be employed for either the oxidation or reduction reactions. In this model the resistance to heat and mass transfer are considered, both in the gas film and within the particle pores, together with the chemical reaction. They showed that, for particle sizes and operating conditions typical of a conventional CLC system, the increase in a particle temperature is typically only 15 °C, at most. Noorman et al. (2011) developed a 1-D numerical model of the oxygen carrier particles in which the effects of reaction kinetics and internal and external heat and mass transfer processes were incorporated in detail. They showed that the effect of Knudsen diffusion is far more important than molecular diffusion. However, to our knowledge, the behaviour of a single OC particle exposed to high heat flux solar radiation has not been investigated to date. In the light of above needs, the overall aim of this work is to investigate the effect of high radiation heat flux on the conversion and temperature variations within an OC particle during the reduction reaction, with a view to supporting the development of hybrid reactor design concepts. More specifically, the paper aims to assess the relative importance of convective and radiative components of heat transfer from particle surface at different operating conditions. It also aims to evaluate the sensitivity of both the temperature and conversion of a particle to variation in the particle size, radiative heat flux intensity, Nusselt number and surrounding gas temperature.

2. Methodology

The OC particle model of Garcia-Labiano et al. (2005) was modified to incorporate the effect of radiation at high heat fluxes on the surface of an OC particle during the reduction reaction. For the present study, Ni-40Al-FG was chosen as the oxygen carrier particle, as tested by Abad et al. (2007) and CH_4 was chosen as fuel.

2.1. Model description

A schematic representation of an OC particle exposed to high intensity radiative heat flux is shown in Fig. 1a. During the reduction of NiO, CH_4 from the surrounding bulk gas permeates through the porous solid particle to reduce NiO to Ni, while the product gases, notably H_2O and CO_2, diffuse in the reverse direction to the gas bulk (Fig. 1b). The following main assumptions are employed in the model:

1. The radius of the OC particle remains constant during the reaction.
2. The heat transfer within the particle is controlled by conduction, while that to the particle surface is controlled by both radiation and convection.
3. The reaction within the particle is limited by three steps: external diffusion of the CH_4 from the particle surrounding bulk gas to the particle surface, internal diffusion of the reactant gases through the porous of the particle and chemical reaction kinetics.
4. Gas phase radiation and absorption are negligible.
5. Only one side of the particle is exposed to concentrated solar radiation at any instant.
6. In addition to the translational motions in the three directions, z, x and y, the particle also rotates with angular velocities, $\emptyset$ and θ, respectively (Fig. 1a). Nevertheless, the rotational velocities are fast compared with the thermal response of the particle, so that the radiative heat flux is assumed to be received uniformly by the particle surface and the variations in temperature and concentration only occur only along the particle radius.
7. The gas phase temperature is constant and equal to the initial particle temperature.

The Changing Grain Size Model (CGSM) proposed initially by Georgakis et al. (1979) has been chosen to simulate the heterogeneous gas–solid reaction within an OC particle (García-Labiano et al., 2005). In this model, it is assumed that the solid porous particle comprises a cluster of smaller spherical grains, manufactured as a composite of both metal oxide and an inert blinder material, all of the same size, r_0, and uniformly mixed (García-Labiano et al., 2005). Once the reaction begins, as shown in Fig. 1c, the reactant grain radius changes and the size of the un-reacted core, r_2, shrinks. Each grain reacts following the Shrinking Core Model (SCM) (Adanez et al., 2012).

2.1.1. Energy and mass conservation equations

Of the total radiative heat incident on the particle surface, $Q_{s,t}$, a fraction is absorbed, Q_{abs}, and the rest is reflected, Q_{ref}. The radiation absorbed through the particle surface is then transferred into the particle through conduction, Q_{cond}, or is lost through re-radiation, $Q_{L,re\text{-}rad}$, and convection, $Q_{L,conv}$, from the particle surface. That is,

$$Q_{s,t} = Q_{ref} + Q_{cond} + Q_{L,re-rad} + Q_{L,conv}. \quad (1)$$

The conducted heat through the particle is utilized to drive the endothermic reaction and/or to increase the particle temperature. The unsteady state energy conservation equation and the initial and boundary conditions for the particle are given by

$$\frac{1}{r^2}\frac{\partial}{\partial r}\left(k_{eff}\, r^2 \frac{\partial T}{\partial r}\right) + r_R \Delta H_R(T) = (\rho_g \phi\, C_{p,g} + \rho_s (1-\phi)\, C_{p,s})\frac{\partial T}{\partial t}, \quad (2)$$

$$T(r,t) = T_b \quad \text{at} \quad t = 0, \quad (3)$$

$$\left.\frac{\partial T}{\partial r}\right|_{r=0} = 0 \text{ at } t \geq 0, \quad (4)$$

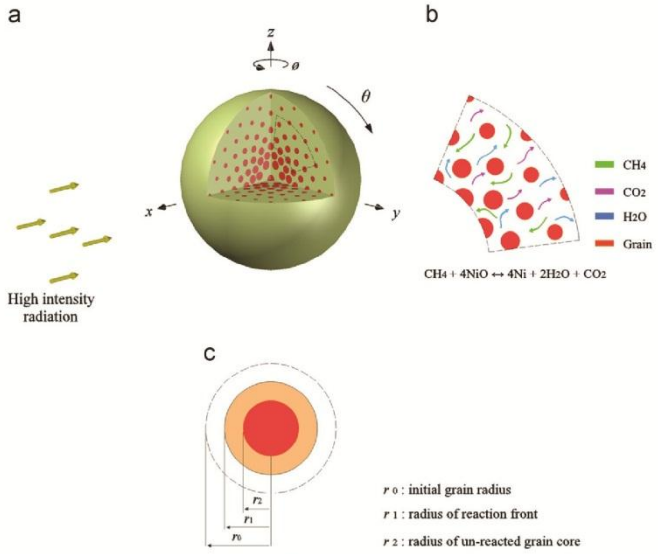

Fig. 1. (a) An oxygen carrier particle exposed to concentrated solar radiation, (b) cross section through the particle, (c) the variation of a single grain radius in the constant grain size model.

$$-k_{eff}\left.\frac{\partial T}{\partial r}\right|_{r=R_0}=\frac{Nu\,k_g}{D_p}(T_s-T_g)+\sigma\varepsilon(T_s^4-T_{srn}^4)+\frac{q_s\varepsilon}{4}\ \text{at}\ t\geq 0. \tag{5}$$

In these equations, φ, ε, ρ, $C_{p,g}$ and $C_{p,s}$, are the porosity, emissivity, density and the heat capacities of the gas and solid phases within the OC particle, respectively. In addition, T_s is the particle surface temperature, T_g is the bulk gas temperature, T_{srn} is the surrounding temperature, Nu is the Nusselt number, k_g is the surrounding gas thermal conductivity and D_p is the particle diameter. The effective thermal conductivity of the porous particle, k_{eff}, which depends on the solid and gas thermal conductivities and the porosity of the particle, was calculated by Hadley's (1986) equation. Since the composition of the particle changes with time, the emissivity of the particle is calculated for each time-step by

$$\varepsilon=\sum\chi_{v,i}\varepsilon_i, \tag{6}$$

where $\chi_{v,i}$ and ε_i are the volume fraction and emissivity of element i in the particle. The experimental data from the CRC Handbook of Chemistry and Physics (Weast, 1981) are used to calculate the emissivity of each component as a function of temperature.

The particle is cooled by convection. Hence, if the convective cooling from the particle surface is insufficient, the operation runs the risk that the particle will overheat and be subjected to particle deactivation. On this basis, to ensure a conservative approach, the reference case for the Nu number is considered to be equal to 2, as for a stationary sphere (Holman, 1999). This is the worst scenario for both heat and mass transfer. The minimum Nu number occurs when the particle Stokes number is low enough to have no gas slip velocity on the particles surface. The sensitivity to the variation of Nu is then assessed subsequently.

The reaction rate, r_R, and the heat of reaction, ΔH_R, both depend on both the temperature and the gas concentration along the radial direction within the OC particle. The mass conservation equation for the gas phase component i is

$$\frac{1}{r^2}\frac{\partial}{\partial r}\left(D_i^{eff}r^2\frac{\partial C_i}{\partial r}\right)-r_i=\varphi\frac{\partial C_i}{\partial t}. \tag{7}$$

$$r_i=\nu_i k_0\exp\left(-\frac{E}{RT}\right)C_{CH_4}^n S_r. \tag{8}$$

Here ν_i is the stoichiometric factor for the reactant i per mol of fuel and k_0 is pre-exponential factor of the chemical reaction rate constant. The specific surface area of the reactive solid, S_r, is given by (García-Labiano et al., 2005)

$$S_r=\frac{3(1-\varphi_0)}{r_0}\chi_{vol,R}. \tag{9}$$

In this equation φ_0 and $\chi_{vol,R}$ are the volume fraction of the reactant solid R in the particle and the initial porosity of the particle, respectively. The initial and boundary conditions required for the solution of this equation are as follows:

$$C_i=C_{i,b}\quad\text{at}\quad t=0, \tag{10}$$

$$\left.\frac{\partial C_i}{\partial r}\right|_{r=0}=0\ \text{at}\ t\geq 0, \tag{11}$$

$$-D_i^{eff}\left.\frac{\partial C_i}{\partial r}\right|_{r=R_0}=\frac{Sh\,D_{m,i}}{D_p}(C_{i,s}-C_{i,b})\ \text{at}\ t\geq 0, \tag{12}$$

where D_i^{eff} is the effective mass transfer of component i in solid porous particle and Sh is the Sherwood number. The random pore model proposed by Wakao and Smith (1962) was used to calculate the effective mass transfer coefficient:

$$D_i^{eff}=D\varphi^2. \tag{13}$$

The diffusion coefficient, D, was calculated by combining the contributions of molecular diffusion, $D_{m,i}$, and Knudsen diffusions, D_{Kn}:

$$D=\left(\frac{1}{D_{m,i}}+\frac{1}{D_{Kn}}\right)^{-1}. \tag{14}$$

The un-reacted core size, r_2, and the grain size, r_1, at each time were calculated from (García-Labiano et al., 2005):

$$\frac{dr_2}{dt} = -\nu_R k_0 \exp\left(-\frac{E}{RT}\right)\frac{M_{w,R}}{\rho_R} C_{CH_4}^n, \quad (15)$$

$$r_1 = (\alpha r_0^3 + (1-\alpha) r_2^3)^{1/3}, \quad (16)$$

where $M_{w,R}$ and ρ_R are the molecular weight and density of the solid reactant R and $\alpha = (V_{mol,Ni}/V_{mol,NiO})$ is the expansion factor. The local conversion at each time and location inside the particle is given by

$$X = 1 - \left(\frac{r_2}{r_0}\right)^3. \quad (17)$$

Table 1
The operating conditions chosen for the simulation of the Ni-40Al-FG oxygen carrier particle exposed to high flux solar radiation. The inert material is Al_2O_3.

Variable	Reference operating conditions	Variation range
NiO weight fraction (wt%)	60	
Active NiO weight fraction (wt%)	40	
Gas temperature (°C)	950	
CH_4 mole fraction	0.5	0.1–0.9
Particle initial temperature (°C)	950	
Surrounding temperature (°C)	950	850–1150
Particle porosity	0.36	
Particle size (μm)	200	20–800
Grain size (μm)	6.9×10^{-1}	
Pressure (atm)	1.0	
Reaction order	0.8	
Pre-exponential factor ($mol^{1-n}\ m^{3n-2}/s$)	7.1×10^{-1}	
Activation energy (kJ/mol)	78	
Concentrated solar radiation (MW/m^2)	1.5[a]	0–3
Nu	2	2–30
Sh	2	2–30

[a] The reference concentrated solar radiation flux corresponds to a mean concentration ratio of 2000 and a direct insolation of 750 W/m^2 (Steinfeld et al., 1996).

From this, the overall conversion of the OC particle, X_t, is

$$X_t = \frac{3}{R_p^3}\int_0^{R_p} Xr^2\, dr. \quad (18)$$

In this equation R_p is the radius of the OC particle.

To solve these sets of partial differential equations, the equations are discretized and solved simultaneously using the modified Gauss–Seidel iteration technique. The maximum temperature at any point within the OC particle, $T_{p,max}$, and the maximum temperature at any location and time within the OC particle, $T_{p,max,t}$, were used to investigate the possibility that sintering might occur at any point within the OC particle. The minimum temperature at any point within the OC particle, $T_{p,min,}$ was used to validate the model and calculate the temperature gradient within the particle. The total particle conversion time, $t_{conv,t}$, is also considered as the required time for full particle conversion, $X_t = 1$. The sensitivity of the model to variation of the parameters listed in Table 1 was also assessed to detect those variables with the greatest influence on the particle temperature and total conversion time.

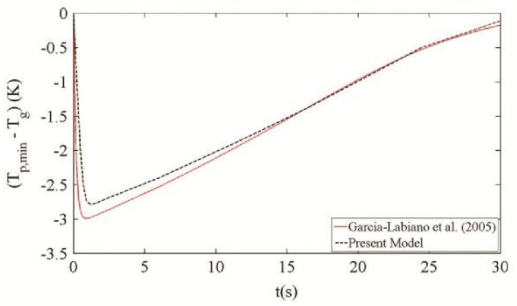

Fig. 3. Comparison of the minimum temperature change within the particle predicted by the present model with that reported by Garcia-Lebaino et al. (2005).

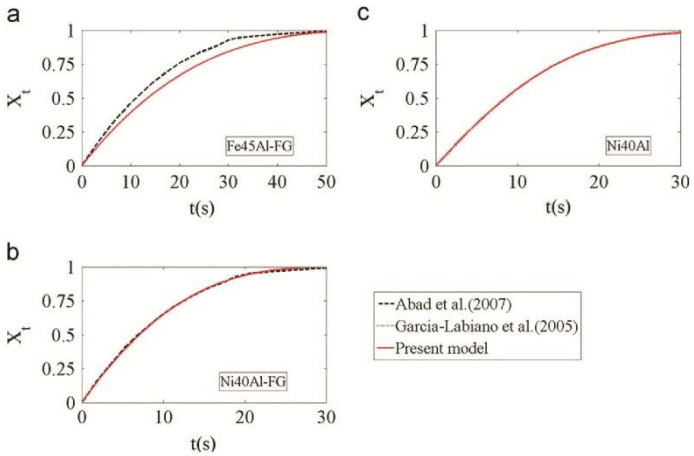

Fig. 2. (a–c) Comparison of the overall particle conversion calculated by the model with (a,b) the experimental data of Abad et al. (2007) and (c) the numerical data of Garcia-Labiano et al.(2005).

3. Model validation

Validation of the model was performed both by comparison with available experimental data and by comparison with some previous modelling. Fig. 2a–c presents a comparison of the overall solid conversion calculated by the model, with the experimental and numerical data reported by Abad et al. (2007) and Garcia-Labiano et al. (2005). As can be seen, good agreement was found between the model predictions and the experimental and numerical data, with an average deviation of less than 8% between them.

No experimental data is available for a direct validation of the temperature distribution within the oxygen carrier particles. Therefore an indirect validation was performed by comparing the temperature calculated by the present model with the numerical model proposed by Garcia-Labiano et al. (2005). This comparison is shown in Fig. 3. As can be seen, good agreement is found here also, both qualitatively and quantitatively, with the maximum difference between the minimum temperatures achieved inside the particle calculated by the present and Garcia-Labiano et al. (2005) models also being less than 8%. This small difference is attributed to minor differences in model assumptions. Therefore, this model is deemed to be suitable for investigations of the effect of various parameters on the conversion and temperature of an oxygen carrier particle.

4. Results and discussion

Fig. 4 shows the calculated variations of the maximum particle temperature and surface emissivity as a function of time for both the cases with and without a solar heat flux of 1.5 MW/m^2. For the particle exposed to q_s=1.5 MW/m^2, the maximum temperature of the particle increases rapidly to reach a peak value of 1334 K at t=0.3 s, after which it drops to an equilibrium value of 1306 K at t≈6 s. At the equilibrium temperature, the radiative heat absorbed by the particle becomes equivalent to the heat lost through convection and re-radiation from particle surface. However, without the high radiative heat flux, the maximum temperature decreases initially to around 1216 K and then increases to 1223 K at t=13.70 s. The calculations also show that, for the particle exposed to a solar heat flux the maximum and minimum temperatures occur at the particle surface and centre, respectively. As can be seen, the emissivity of both particles decreases as the reaction proceeds, which is due to the reduction of NiO to Ni at the particle surface. However, the emissivity of the particle exposed to concentrated solar energy decreases faster than that of the particle without it. This is attributed both to the increase in the rate of reduction of NiO to Ni at particle surface and to the effect of temperature on the particle surface emissivity.

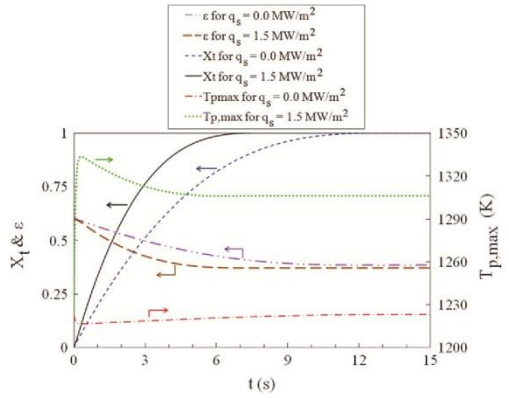

Fig. 4. Variations of the predicted particle temperature rise, surface emissivity and the overall conversion as a function of time, both with and without the addition of a radiant heat flux for the reference operating conditions given in Table 1.

Variations of the total particle conversion with time for the cases with and without a radiation heat flux of 1.5 MW/m^2 are also depicted in Fig. 4. As expected, the addition of the radiation heat flux increases the rate of reduction reaction. Consequently, the time to overall OC particle conversion (Eq. (18)) decreases from 12.80 s without radiation heat flux to 7.60 s with it. Therefore, the required residence time of particles in a solar fuel reactor is a function of the heat flux, which may change with insolation, and is generally lower than that of a conventional CLC system fuel reactor.

Variations of the calculated fraction of relative radiative heat absorbed by the particle surface as a function of time is shown in Fig. 5 relative to the total incident radiative heat, $Q_{abs}/Q_{s,t}$. It can be seen that $Q_{abs}/Q_{s,t}$ decreases from a maximum value of 60% at t=0 s to a minimum value of 37% at around t=7.1 s and remains constant thereafter. The drop in radiative heat absorption is attributed both to the change in particle surface absorptivity due to reduction of NiO to Ni and to the variation of surface material absorptivity with temperature. The mass fraction of NiO at the particle surface decreases as the reduction reaction proceeds. The absorptivity of NiO is higher than that of Ni, so that the particle absorbtivity also decreases as the reduction reaction proceeds, lowering the particle's radiative heat absorption. The drop in particle temperature (shown in Fig. 4) is also due to the fall in radiative heat absorption through the particle surface.

The calculated variations of the relative heat losses through radiation and convection from the particle surface and the heat transferred into the particle to the absorbed heat on particle surface, $Q_{L,re\text{-}rad}/Q_{abs}$, $Q_{L,conv}/Q_{abs}$ and Q_{cond}/Q_{abs}, are also depicted in Fig. 5as a function of time. The fraction of absorbed heat lost by re-radiation, $Q_{L,re\text{-}rad}/Q_{abs}$, increases dramatically at first, but to a maximum value of only 14%, which occurs when the particle is at its maximum temperature, and then decreases to 10.2% due to the reduction in the particle temperature. The fraction of absorbed heat lost through convection, $Q_{L,conv}/Q_{abs}$, also increases rapidly but to a much higher value of 77% at t=0.3 s and slowly thereafter to an asymptotic value of 90%. This shows that, despite the high temperature of the particle, the convective heat loss is the dominant heat transfer mechanism for particle cooling.

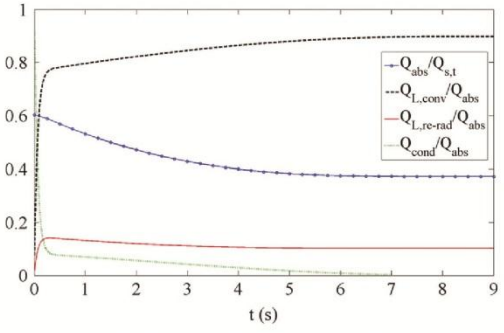

Fig. 5. Variations with time of the predicted fractions of radiative heat absorbed by the particle surface to the total radiative heat, of the heat transferred by conduction into the particle relative to the absorbed heat and of the heat lost through re-radiation and convection relative to the absorbed heat with time for a particle operating for the reference operating conditions given in Table 1.

The fraction of absorbed heat that is transferred into particle by conduction, Q_{cond}/Q_{abs}, decreases rapidly from 91.4% at $t=0$ s to 8.3% at $t=0.30$ s when the particle is at its maximum temperature, and then decreases asymptotically to 0.0 at $t=7.2$ s, which occurs when the particle is at its equilibrium final temperature. The calculations also show that only around 2.5% of the total absorbed heat was used to perform the endothermic reduction reaction.

4.1. Effect of particle size

Variations of the calculated maximum temperature at any point within an OC particle as a function of time are shown in Fig. 6 for different particle sizes. It can be seen that the results are strongly dependent on particle diameter. The maximum temperature within the smallest particle of diameter 50 μm has the highest initial rate of temperature rise, but reaches the lowest maximum value of 1159 K at $t=0.05$ s, after which it remains relatively constant at 1247 K. In contrast, the maximum temperature of the largest particle, 800 μm diameter, has the lowest initial rate of increase, but reaches the highest absolute temperature, with a double peak in the time range considered. The first peak has a temperature of 1423 K at $t=1.7$ s, while the second and final peak temperature of 1445 K occurs at $t=15$ s, which is also approximately the equilibrium temperature. This is as expected because a larger particle provides a larger surface area for radiative heat absorption. This shows that the risk of sintering is greatest for the largest particles. Hence the risk can be managed by controlling the maximum size of particles introduced to the reactor, since the risk of particle agglomeration is low if their temperature is kept below the sintering temperature, while any particle breakage will decrease the risk of sintering.

Fig. 7 presents the variation of predicted temperature gradients, $2(T_{p,max}-T_{p,min})/D_p$, within the OC particles exposed to $q_s=1.5$ MW/m^2 with time for different particle sizes. Significantly, the maximum temperature gradient is almost independent of diameter and occurs when the particle is first introduced into the reactor. Thereafter, the lower temperature gradients within the particles are strongly dependent on particle diameter, as expected. The maximum gradient is 4.8×10^4 K/m at $t=0.07$ s for the 800 μm particle and only a factor of two lower at 2.32×10^4 K/m at ~$t=0.0$ s for the 50 μm particle. In contrast the subsequent maximum temperature gradients are orders of magnitude lower, peaking at 5210 K/m at $t=5.30$ s for the 800 μm particle and only 798 K/m at $t=0.1$ s within the smallest particle of 50 μm. Interestingly, the 800 μm particle also exhibit a double peak in temperature. The maximum temperature gradients within the OC particles of diameter 50 and 800 μm correspond to a maximum temperature difference within the particle of 19.2 K and 0.58 K, respectively. In practice, the initial peak shock is likely to be lower than estimated here since the spatial distribution of heat-flux within a reactor is not uniform. Nevertheless, calculations highlight the importance of introducing the particles into a region of low heat-flux to minimise the initial shock-loading.

Fig. 8 shows the sensitivity of the heat transfer to particle size. The absorbed fraction, $Q_{abs}/Q_{s,t}$ is shown in Fig. 8a as function of time, for the different particle sizes. The same trends as found for 200 μm particle (Fig. 5) are evident. Since the initial temperature and composition of all particles is assumed to be the same, the value of $Q_{abs}/Q_{s,t}$ is 0.6 for all particle sizes at $t=0.0$ s. Interestingly, $Q_{abs}/Q_{s,t}$ decreases only quite weakly with increasing particle diameter. For example, $Q_{abs}/Q_{s,t}=47.5\%$ at $t=3.0$ s, for a particle of 50 μm, while it is still 37.50% for a particle of 800 μm at the same time. The difference is due to the higher temperature (Fig. 6) and consequently faster reduction of NiO to Ni on the surface of the larger particles. The final difference between the $Q_{abs}/Q_{s,t}$ of different particles is attributed to different particle equilibrium temperatures and consequently emissivities.

Fig. 8b shows that predicted variations of Q_{cond}/Q_{abs} increases strongly with particle size, from being insignificant for the smallest particles to become important for the largest ones. This increase arises from the greater amount of heat required for the reduction and from the slower temperature rise of the bigger particles. The double peak in particle temperature observed in Fig. 7 for 800 μm drop (1423 at $t=1.70$ s and 1413 K at $t=3.70$ s) can be explained by the decreasing the rate of radiative heat absorption on particle surface with time (Fig. 8a) and increasing the heat conducted into particle with particle size (Fig. 8b).

Fig. 8c and d shows the increased significance of convection $Q_{L,conv}/Q_{abs}$ and the decreased significance of radiant cooling $Q_{L,re\text{-}rad}/Q_{abs}$ and $Q_{L,conv}/Q_{abs}$ with decreased particle size. That is, convection is totally dominant at 94% for the smallest particles of 50 μm, while radiant cooling becomes significant for the 800 μm particles. Nevertheless, even for those largest particles, convection is still approximately double the radiant cooling, with $Q_{L,re\text{-}rad}/Q_{abs}$~0.60 and $Q_{L,conv}/Q_{abs}$~0.30. The increased rate of heat loss from particle surface through re-radiation increases with particle size is attributed to the higher temperature (Fig. 6) and surface area of the larger particles. Hence these calculations confirm the finding identical above that convection is the dominant mechanism of particle cooling and the design of the solar CLC fuel reactors should be targeted to achieve the reasonable convection heat transfer coefficient on particle surfaces.

Fig. 9 presents the sensitivity of the predicted overall particle conversion to particle diameter. Importantly, the total conversion time is not strongly sensitive to diameter, varying by only a factor of two over this size range. This weak sensitivity is desirable for a

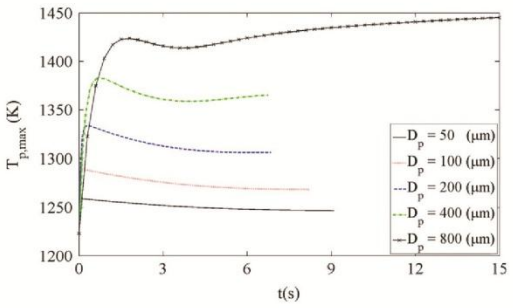

Fig. 6. Sensitivity to variations in particle size of the calculated particle maximum temperature history for $q_s=1.5$ MW/m^2.

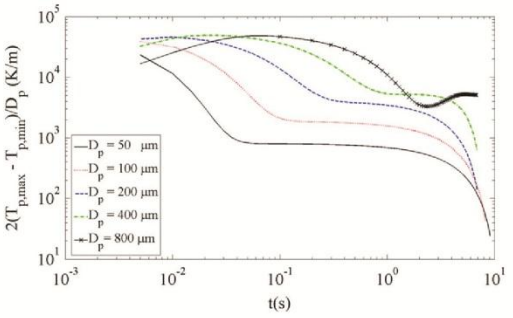

Fig. 7. Sensitivity to variations in particle size of the predicted gradient within the particle for $q_s=1.5$ MW/m^2.

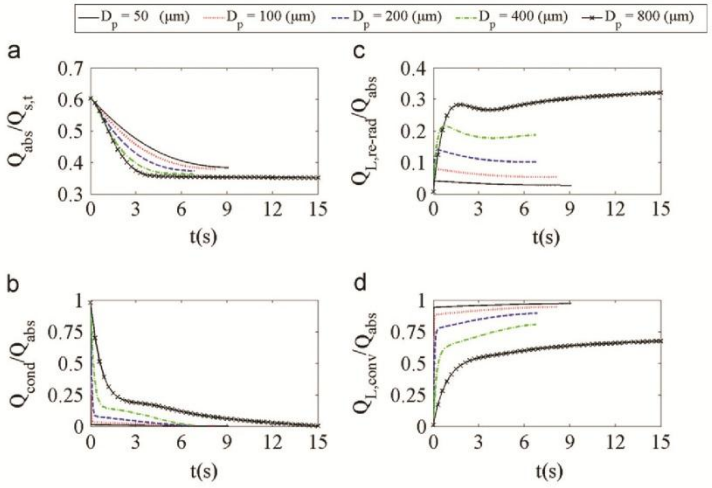

Fig. 8. Sensitivity to variations in particle diameter of the fractions (a) of radiative heat absorbed by the particle surface to the total radiative heat, (b) of the heat transferred by conduction into the particle relative to the absorbed heat and (c) of the heat lost through re-radiation and (d) convection relative to the absorbed heat for $q_s = 1.5$ MW/m^2.

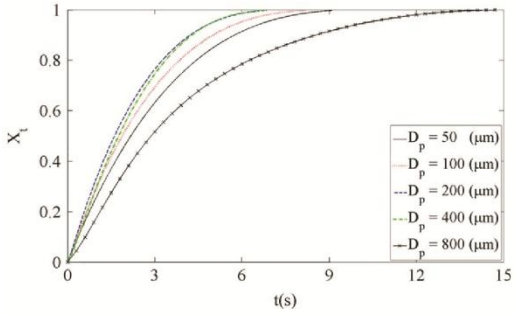

Fig. 9. Sensitivity to variations in particle size of the calculated particle overall conversion history for $q_s = 1.5$ MW/m^2.

reactor since it is difficult to accommodate a large range of reaction times in an efficient manner. Interestingly, the dependence on diameter is also complex, being slightly longer for a particle of diameter 50 μm, at 9.7 s, than the 7.75 s for a particle of diameter 200 μm. The maximum time of 16.0 s occurs for a particle of diameter 800 μm.

An explanation for the complex dependence of conversion on diameter can be found in Fig. 10 a–d, which presents the calculated conversion profile within the OC particles of sizes 50, 200, 400 and 800 μm. It can be seen that, for both the 50 and 200 μm particles, the conversion profiles within these particles are quite similar and approximately independent of radius, which implies that the extent of reaction is approximately uniform within the particle at any given time. Therefore, an increase in the particle size over this size range corresponds to an increase in the rate of reaction in response to the increase in the particle temperature with particle size (Fig. 6). However, the dependence of the conversion profile becomes evident for the particles larger than 400 μm (Fig. 10c) such that for the 800 μm particle becomes more significant (Fig. 10d). The gradients of conversion in these larger particles are attributed to the influence of gas diffusion through the particle pores, which becomes the limiting factor in the conversion rate. That is, gas diffusion does not affect the reaction rate for the particles smaller than 200 μm, but slightly affects the reaction rate for the particle of ~400 μm diameter and becomes increasingly significant with the diameter larger than this.

4.2. Effect of external mass and heat transfer

Variations of the calculated maximum particle temperature increase, $T_{p,max,t} - T_g$, and of the complete conversion time of the particle with *Nu* and *Sh* numbers are shown in Fig. 11. The highest temperature increase and the lowest complete conversion time correspond to $Nu = 2.0$ which provides the lowest external convective heat and mass transfer coefficients. The maximum particle temperature decreases strongly with an increase in *Nu* number while the particle complete conversion time increases. This shows that external mass transfer resistance does not significantly affect the reaction rate of the considered particle exposed to a radiative heat flux of $q_s = 1.5$ MW/m^2. In another words, the reaction kinetics control the rate of particle conversion. Since a higher *Nu* decreases the particle temperature, the complete conversion time of the particle increases with an increase in *Nu*. This is in complete agreement with the variation of particle conversion time with particle size discussed previously. Importantly too, the relationship is highly nonlinear so that a very large increase in *Nu* and *Sh* from the minimum of 2.0 to the maximum of 30.0 increases the reaction time by only ~58.0%, while it decreases the temperature rise by ~1052%. This has important practical implications, since it implies that can be highly advantageous to utilise a reactor that generates high convection heat transfer coefficients, since these will decrease the likelihood of particle damage.

Fig. 11 also shows that the sensitivity to *Nu* and *Sh* decreases with an increase in *Nu* and *Sh*. For example increasing the *Nu* from 2.0 to 4.0 leads to 42.7% drop in $(T_{p,max,t} - T_g)$ and 24.4% rise in $t_{conv,t}$, while increasing the *Nu* and *Sh* numbers from 20 to 22 results in only 8.85% decrease in $(T_{p,max,t} - T_g)$ and 0.36% increase in $t_{conv,t}$.

A $Nu = 2$ occurs where there is no slip velocity around the particle. This is appropriate for the solar vortex reactor, since it is desirable that the particles be convected out from chamber rather

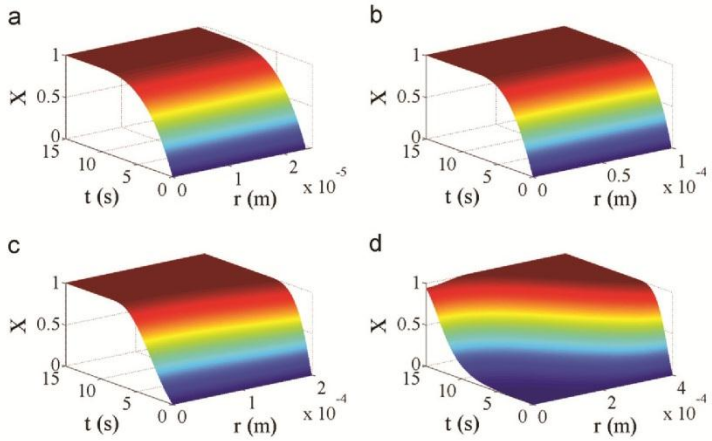

Fig. 10. Calculated internal profile of local conversion at each time for particles of diameter (a) 50 μm, (b) 200 μm, (c) 400 μm and (d) 800 μm, exposed to q_s=1.5 MW/m^2.

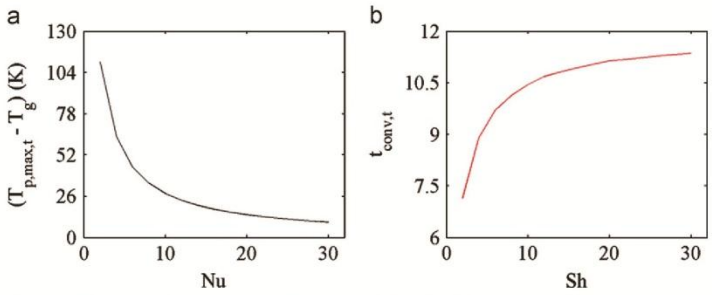

Fig. 11. (a) Predicted effect of *Nu* number on the maximum particle temperature rise. (b) Predicted effect of *Sh* number on the total particle conversion time, both for q_s=1.5 MW/m^2.

than separate the flow and adhere to the walls, as occurs in a cyclone. Furthermore, a non-slip velocity situation has been chosen previously for these kinds of solar reactors (Z'Graggen et al., 2006; Z'Graggen and Steinfeld, 2008). Fig. 11 shows that this type of reactor also results in the highest particle temperature increase, which could be a limitation for some applications, despite the short residence time required for particle complete conversion. In particular, the application of this kind of reactor for hybrid CLC systems increases the possibility of damage to the OC particles. In contrast, the environment typically established within a fluidized bed reactors, typically correspond to $4 < Nu$ and $Sh < 10$ (García-Labiano et al., 2005). This implies that the development of hybrid CLC systems would benefit from the availability of a fluidized bed reactor that can accommodate the introduction of concentrated solar radiation.

4.3. Effect of radiation intensity

The sensitivity of the calculated particle maximum temperature to radiative heat intensity is shown in Fig. 12. As expected, this sensitivity is strong, with both the maximum and equilibrium temperatures increasing with radiative heat intensity. In addition, the difference between the particle maximum and equilibrium temperatures increases with radiative heat flux intensity. For example, the peak maximum temperature of the particle exposed to q_s=0.5 MW/m^2 is 1260 K at 0.36 s, following which it reduces to an asymptotic value of 1252, which constitutes only a 0.6% reduction. However, the peak maximum temperature of the particle exposed to q_s=3.0 MW/m^2 is 1436 K at 0.26 s, which is followed by a 4% decrease to its equilibrium value of 1379 K.

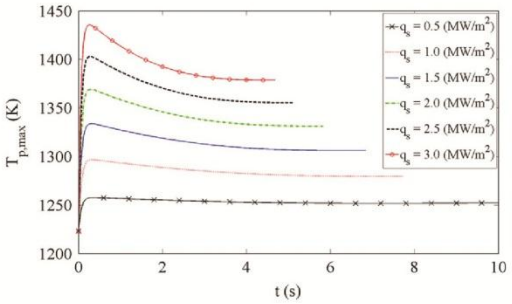

Fig. 12. Sensitivity to variations in the radiant heat flux of the calculated maximum particle temperature history.

Fig. 13 presents the sensitivity of the overall conversion to radiative heat flux intensity. As expected, the required time for complete conversion of the particle is found to decrease with increasing heat flux intensity. However, the increase is not linear,

so that a six-fold increase in heat flux intensity from 0.5 to 3.0 MW/m^2 results in less than a factor of 2 reduction in conversion time. For example, the complete conversion time for a particle exposed to qs=0.50 MW/m^2 is 10.50 s while it is 5.20 s for a particle exposed to q_s=3.0 MW/m^2. The reduction in time is due to the higher temperature increased by particle exposed to a higher radiative heat flux during the reduction reaction. Hence, while the required residence time for an OC particle decreases with solar flux, the sensitivity of this dependence is lower than that of the maximum particle temperature.

Fig. 14 presents the sensitivity of the various components of heat transfer to the radiant heat flux. The sensitivity of $Q_{abs}/Q_{s,t}$ to heat flux intensity is shown in Fig. 14a. As it can be seen, while $Q_{abs}/Q_{s,t}$ decreases with increased radiative heat flux intensity, at the final equilibrium temperature the particle absorbs an approximately equal radiative heat flux. This is due both to the increase in the rate of reduction of NiO to Ni with radiative heat flux intensity and to the effect of temperature on particle surface emissivity. For example, for a particle exposed to radiative heat flux of 0.50 MW/m^2, $Q_{abs}/Q_{s,t}$ changes from 0.60 at t=0.0 s to 0.51 at t=2.0 s, to finally approach to an equilibrium value of 0.38 at t=10.0 s. However, a particle exposed to q_s=3.0 MW/m^2 reaches $Q_{abs}/Q_{s,t}$=0.60 at t=0.0 s, followed by a $Q_{abs}/Q_{s,t}$=0.41 at t=2.0 s and a final value of 0.36 at t=5.80 s.

The sensitivity of the calculated $Q_{L,re\text{-}rad}/Q_{abs}$ and $Q_{L,conv}/Q_{abs}$ to radiative heat flux intensity is illustrated in Fig. 14b and c, respectively. These calculations show that neither $Q_{L,re\text{-}rad}/Q_{abs}$ nor $Q_{L,conv}/Q_{abs}$ are strongly sensitive to heat flux, with the influence being greatest in the heating time before the particle approaches its equilibrium temperature. Interestingly, the equilibrium values are almost independent of heat flux, despite of the considerable temperature change on particle surface with radiative heat flux intensity (Fig. 12). This is attributed to the increase of the film gas thermal conductivity and consequently convection heat transfer coefficient on particle surface with increasing particle temperature. For example, for a particle exposed to q_s=3.0 MW/m^2 at t=0.26 s, $Q_{L,re\text{-}rad}/Q_{abs}$ and $Q_{L,conv}/Q_a$ are 0.15 and 0.78, respectively. However, these are 0.12 and 0.70 for a particle exposed to q_s=0.5 MW/m^2 at t=0.36 s. As shown at the equilibrium temperature, $Q_{L,re\text{-}rad}/Q_{abs}$ is ~0.10 for both q_s=0.5 and 3.0 MW/m^2.

4.4. Effect of CH_4 mole fraction

The sensitivity to variations in the CH_4 mole fractions of the predicted variations of the overall particle conversion and maximum temperature history is illustrated in Figs. 15 and 16, respectively. The sensitivity is strong, with an order of magnitude decrease in, the total particle conversion time with an increase in CH_4 mole fraction. For example, the total particle conversion time for a particle reduced by CH_4 with a mole fraction of 0.10 is 18.2 s, while this time is 5.30 s for the particle reduced by CH_4 with a mole fraction of 0.90. Similarly, Fig. 16 shows that a higher CH_4

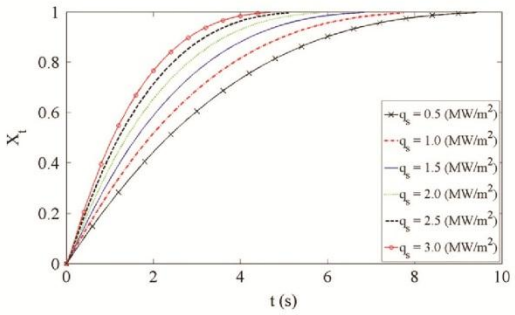

Fig. 13. Sensitivity to variations in the radiant heat flux of the calculated particle overall conversion history.

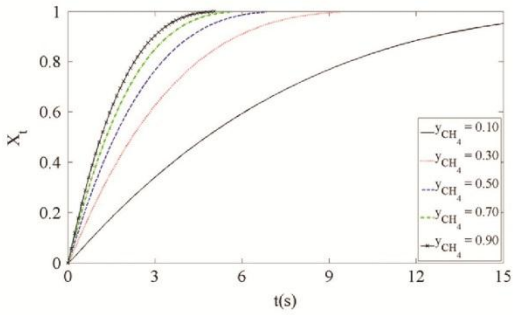

Fig. 15. Sensitivity to CH_4 mole fraction of the calculated particle overall conversion with time for q_s=1.5 MW/m^2.

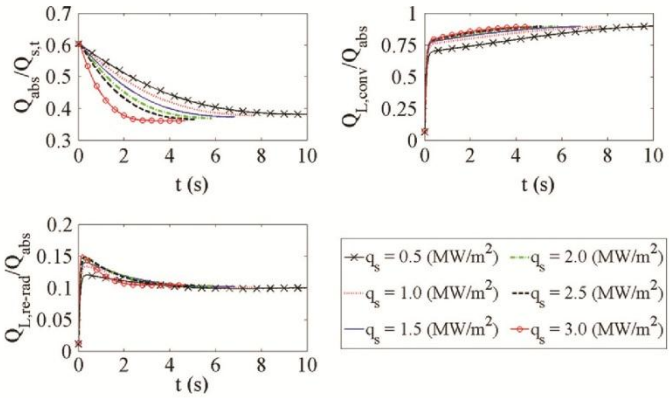

Fig. 14. Sensitivity to variations in the radiant heat flux of the predicted fractions (a) of radiative heat absorbed by the particle surface to the total radiative heat, (b) of the heat lost through re-radiation and (c) of the heat lost through convection relative to radiative heat absorbed.

mole fraction results in a lower maximum and final equilibrium temperatures. The maximum and equilibrium temperatures of particle reduction for a CH_4 mole fraction of 0.10 are 1392 and 1345 K, respectively. However, these values decrease to 1305 and 1287 K for a CH_4 mole fraction of 0.90. These lower temperatures are both due to the faster reduction of NiO to Ni at the particle surface and to the higher thermal conductivity of the surrounding gas at higher CH_4 mole fractions. It can be also seen that the effect of change in CH_4 mole fraction on total particle conversion time and particle temperature is more significant at low CH_4 concentrations than at high ones. For example, an increase in CH_4 mole fraction from 0.10 to 0.30 drops the particle full conversion time and maximum temperature by 30% and 2.5%, respectively, while, this drop is around 14% for particle conversion time and 0.9% in maximum temperature for increasing the CH_4 mole fraction from 0.70 to 0.90.

The sensitivity of the calculated history of $Q_{abs}/Q_{s,t}$ to variation in CH_4 mole fractions is shown in Fig. 17a. It can be seen that $Q_{abs}/Q_{s,t}$ is quite sensitive to the CH_4 mole fraction, while the relative significance of convective and radiant cooling are much less so. For example, $Q_{abs}/Q_{s,t}$~0.40 at $t=3.0$ s for a CH_4 mole fraction of 0.90. However, at the same time, $Q_{abs}/Q_{s,t}$ is 0.52% for a CH_4 with mole fraction of 0.10. This difference is due to the faster reduction of NiO to Ni at the particle surface for the higher CH_4 mole fraction (Fig. 15). From Fig. 17b and c it can be seen that, while $Q_{L,re\text{-}rad}/Q_{abs}$ is decreased by higher CH_4 mole fractions, and $Q_{L,conv}/Q_{abs}$ increased, these changes are relatively small in an absolute sense. The changes are attributable both to the lower particle temperature and to the increase in the surrounding gas thermal conductivity with increase in CH_4 mole fraction. In general, the calculations demonstrate that for all of the mole fractions, the impact of convection cooling of the particle surface is more than re-radiation from it.

4.5. Surrounding temperature

The sensitivity of the calculated particle maximum temperature to temperature of the surrounding environment, T_{srn}, is shown in Fig. 18. As expected, the maximum and equilibrium temperatures of the particle are sensitive to surrounding temperature. However, this sensitivity is not particularly strong, for either the maximum or equilibrium temperatures. The peak maximum temperature of the particle increases from 1323 K to

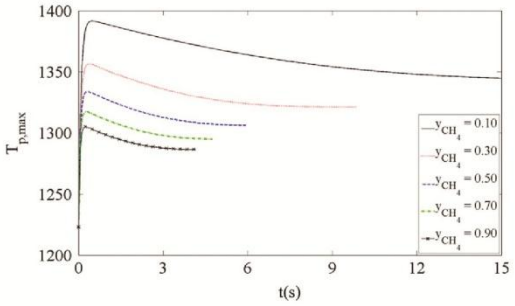

Fig. 16. Sensitivity to CH_4 mole fractions of the calculated particle maximum temperature with time for $q_s=1.5$ MW/m^2.

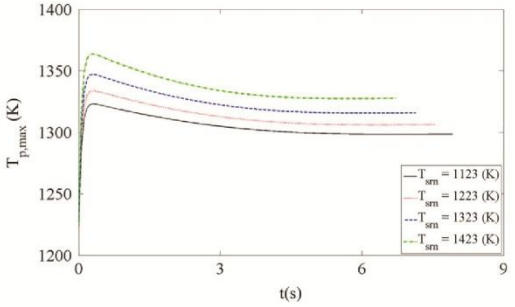

Fig. 18. Sensitivity to the surrounding temperature of the calculated particle temperature with time for $q_s=1.5$ MW/m^2.

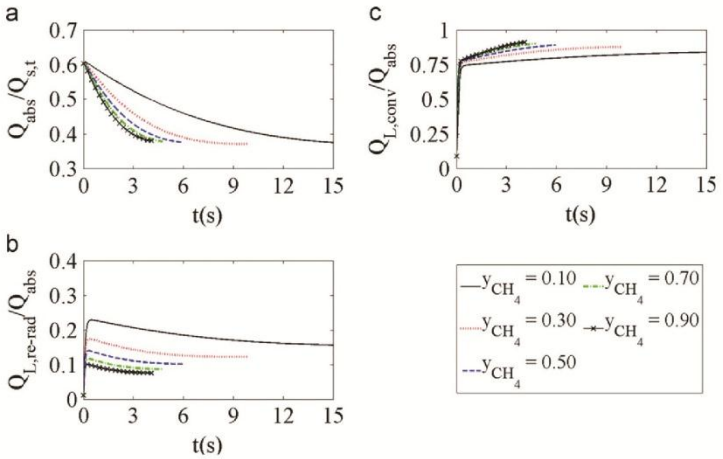

Fig. 17. Sensitivity to variations in CH_4 mole fractions of the predicted fractions (a) of radiative heat absorbed by the particle surface to the total radiative heat, (b) of the heat lost through re-radiation and (c) of the heat lost through convection relative to the radiative heat absorbed, for $q_s=1.5$ MW/m^2.

1364 K as T_{srn} is increased from 1123 K to 1423 K, while the corresponding equilibrium temperatures are 1299 and 1328 K, respectively. That is, the maximum and equilibrium temperatures increase by only 3.10% and 2.20%, respectively, despite a 27.0% rise in T_{srn}. This is attributed to the nonlinear dependence of heat transfer on the temperature difference between the particle surface and the surrounding environment.

Fig. 19 presents the sensitivity of the overall particle conversion to the surrounding temperature. As shown, the rate of particle conversion increases with surrounding temperature, which is due to the higher temperature of particle for the higher surrounding temperatures. However, over the surrounding temperature range considered, the particle conversion time is not strongly sensitive to the surrounding temperature. For example an increase in surrounding temperature from 1123 K to 1423 K decreases the conversion from 7.80 s to 6.80 s.

The sensitivity of the various components of heat transfer to the temperature of the surrounding environment is shown in Fig. 20. The sensitivity of $Q_{abs}/Q_{s,t}$ to the surrounding temperature is shown in Fig. 20a. It can be seen that $Q_{abs}/Q_{s,t}$ decreases with an increase in T_{srn}, which is related to the reduction in particle surface emissivity and increase in the rate of reduction of NiO to Ni at particle surface. However, the sensitivity of $Q_{abs}/Q_{s,t}$ to T_{srn} is not very significant. For example, $Q_{abs}/Q_{s,t}$ is 0.43 at $t=3.0$ s for a particle at $T_{srn}=1123$ K while it is 0.41 for a particle at $T_{srn}=1423$ K. At equilibrium temperature $Q_{abs}/Q_{s,t}$ for both, $T_{srn}=1123$ and $T_{srn}=1423$ K, is ~0.37. From Fig. 20b and c it can be seen that, $Q_{L,re\text{-}rad}/Q_{abs}$ and $Q_{L,conv}/Q_{abs}$ can exceed unity or achieve a negative value. A negative value of $Q_{L,re\text{-}rad}/Q_{abs}$ means that thermal energy is not lost through re-radiation, but rather, the particle is heated up by radiation heat received from the surroundings. It can be seen from Figs. 20b and 18 that, $Q_{L,re\text{-}rad}/Q_{abs}<0.0$ always occurs when $T_s<T_{srn}$. A value of $Q_{L,conv}/Q_{abs}>1.0$ means that convection is the only mechanism of particle cooling. For example, for $T_{srn}=1423$ K, $Q_{L,re\text{-}rad}/Q_{abs}$ and $Q_{L,conv}/Q_{abs}$ are −0.15 and 1.15, respectively. This means that, in addition to radiative heat being absorbed by the particle, all of the heat i.e. 15% of Q_{abs}, is lost through convection only. The calculations show that, $Q_{L,re\text{-}rad}/Q_{abs}$ and $Q_{L,conv}/Q_{abs}$ are strongly dependent on the surrounding temperature. For a particle at $T_{srn}=1423$ K, $Q_{L,re\text{-}rad}/Q_{abs}$ and $Q_{L,conv}/Q_{abs}$ are −0.10 and 1.0, respectively, at 0.30 s. However, at the same time $Q_{L,re\text{-}rad}/Q_{abs}$ is 0.22 and $Q_{L,conv}/Q_{abs}$ is 0.69 for a particle with $T_{srn}=1123$ K. Interestingly, for a particle with the minimum surrounding temperature considered at final equilibrium temperature, 81.0% of the absorbed heat is lost through convection. This reconfirms the importance of convection in the design of solar hybrid fuel reactors. It also shows that, while the particle temperature is not strongly dependent on T_{srn}, the relative significance of radiation and convection vary strongly with it.

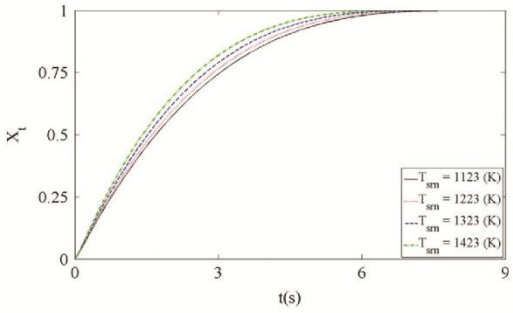

Fig. 19. Sensitivity to the surrounding temperature of the calculated particle conversion with time for $q_s=1.5$ MW/m^2.

5. Conclusion

The dynamic model of the heat transfer and reaction progress of an OC particle type Ni-40Al-FG exposed to high intensity radiation heat flux has been found to yield good agreement with the available experimental and numerical data. The key findings of the assessment of the impact of high radiant fluxes on the particle under conditions of relevance to solar-hybrid chemical looping combustion are as follows:

- The rate of conversion of an OC particle increases with particle size for $D_P<200$ μm and decreases with particle size for $D_p>200$ μm. This is attributed to the influence of gas diffusion

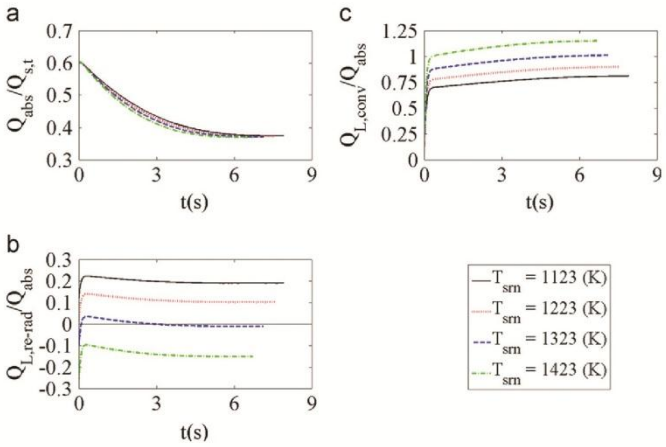

Fig. 20. Sensitivity to variations in the surrounding temperature of the predicted fractions (a) of radiative heat absorbed by the particle surface to the total radiative heat, (b) of the heat lost through re-radiation and (c) of the heat lost through convection relative to the radiative heat absorbed, for $q_s=1.5$ MW/m^2.

through the particle pores which becomes a limiting factor in the conversion rate through the larger particles.

- In general, convection is the dominant mechanism of particle cooling. However, the share of heat loss through convection and re-radiation from particle surface depends strongly on the operational conditions.
- The maximum particle temperature is strongly dependent on convective rates of heat and mass transfer, so that reactor designs with relatively high values of *Nu* and *Sh* numbers are likely to best limit the potential of high solar flux from causing damage to the particles.
- The maximum particle temperature is strongly sensitive to variations in particle diameter, radiant heat flux and composition of the surrounding gas, while the conversion time is much less sensitive to these variations.

Nomenclature

C_i	*i*th component concentration (mol/m^3)
C_p	heat capacity (J/(mol K))
D	diffusion coefficient (m^2/s)
D_i^{eff}	effective diffusion coefficient (m^2/s)
$_{DKn}$	Knudsen diffusion coefficient (m^2/s)
$D_{m,i}$	*i*th component diffusion coefficient (m^2/s)
D_p	particle diameter (m)
k_c	mass heat transfer coefficient (m/s)
k_0	pre-exponential factor coefficient (m/s)
Nu	Nusselt number
q_s	solar radiation heat flux(W/m^2)
r	radius direction
r_0	initial grain radius (m)
r_1	radius of reaction front (m)
r_2	radius of un-reacted grain core (m)
r_i	rate of reaction for reactant *i* (mol/(m^3 s))
R	gas constant (J/(mol K))
R_p	particle radius (m)
Sh	Sherwood Number
$t_{\mathrm{conv,t}}$	time required for full particle conversion (t)
T	temperature (K)
T_g	gas bulk temperature (K)
$_{Tp,max}$	maximum temperature at any location and time (K)
$T_{p,min}$	minimum temperature at any location and time (K)
$_{Tsrn}$	surrounding temperature (K)
T_s	Particle surface temperature (K)
$V_{mol,i}$	molar volume of *i*
X_t	total particle conversion

Greek letters

α	expansion factor
ΔH_R	enthalpy of reaction (J/mol)
$\Delta T_{p\text{-}g,max}$	maximum temperature difference at any point Within OC particle with gas phase (K)
ε	emissivity
ε_i	emissivity of component *i*
ν_i	stoichchiometric factor for reactant *i*
ρ_g	gas density (kg/m^3)
σ	Stephan Boltzmann constant (W/(m))^{4}K^2
φ	particle porosity
$\chi_{v,i}$	volume fraction of solid *i*

Acknowledgement

The authors are grateful to Dr. Francisco Garcia-Labiano from the Investigador Cientifico (Scientific Researcher) Instituto de Carboquimica (CSIC) for his useful discussions. This work was supported by Adelaide Scholarship International (ASI).

References

Abad, A., Adánez, J., García-Labiano, F., de Diego, L.F., Gayán, P., Celaya, J., 2007. Mapping of the range of operational conditions for Cu-, Fe-, and Ni-based oxygen carriers in chemical-looping combustion. Chem. Eng. Sci. 62, 533–549.

Adanez, J., Abad, A., Garcia-Labiano, F., Gayan, P., de Diego, L.F., 2012. Progress in chemical-looping combustion and reforming technologies. Prog. Energy Combust. Sci. 38, 215–282.

Adánez, J., de Diego, L.F., García-Labiano, F., Gayán, P., Abad, A., Palacios, J.M., 2004. Selection of oxygen carriers for chemical looping combustion. Energy Fuels 18, 371–377.

Adánez, J., Dueso, C., de Diego, L.F., García-Labiano, F., Gayán, P., Abad, A., 2008. Methane combustion in a 500 Wth chemical-looping combustion system using an impregnated ni-based oxygen carrier. Energy Fuels 23, 130–142.

García-Labiano, F., de Diego, L.F., Adánez, J., Abad, A., Gayán, P., 2005. Temperature variations in the oxygen carrier particles during their reduction and oxidation in a chemical-looping combustion system. Chem. Eng. Sci. 60, 851–862.

Georgakis, C., Chang, C.W., Szekely, J., 1979. A changing grain size model for gas–solid reactions. Chem. Eng. Sci. 34, 1072–1075.

Hadley, G.R., 1986. Thermal conductivity of packed metal powders. Int. J. Heat Mass Transfer 29, 909–920.

Holman, J.P., 1999. Heat Transfer. McGraw-Hill, Inc., New York, St. Louis, San Fransisco, Auckland, Bogota, Caracas, Hamburg, Lisbon, London, Madrid, Mexico, Milan, Montreal, New Delhi, Paris, San Jaun, Sao Paulo, Singapore, Sydney, Tokyo, Toronto.

Hong, H., Han, T., Jin, H., 2010. A low temperature solar thermochemical power plant with CO_2 recovery using methanol-fueled chemical looping combustion. J. Solar Energy Eng. 132, 031002.

Hong, H., Jin, H., 2005. A novel solar thermal cycle with chemical looping combustion. Int. J. Green Energy 2, 397–407.

Hong, H., Jin, H., Liu, B., 2006. A novel solar-hybrid gas turbine combined cycle with inherent CO_2 separation using chemical-looping combustion by solar heat source. J. Solar Energy Eng. 128, 275–284.

Hossain, M.M., de Lasa, H.I., 2008. Chemical-looping combustion (CLC) for inherent separations—a review. Chem. Eng. Sci. 63, 4433–4451.

Jafarian, M., Arjomandi, M., Nathan, G.J., 2013. A hybrid solar and chemical looping combustion system for solar thermal energy storage. Appl. Energy 103, 671–678.

Jerndal, E., Mattisson, T., Lyngfelt, A., 2006. Thermal analysis of chemical-looping combustion. Chem. Eng. Res. Design 84, 795–806.

Jerndal, E., Mattisson, T., Lyngfelt, A., 2009. Investigation of different NiO/$NiAl_2O_4$ particles as oxygen carriers for chemical-looping combustion. Energy Fuels 23, 665–676.

Lyngfelt, A., Leckner, B., Mattisson, T., 2001. A fluidized-bed combustion process with inherent CO_2 separation; application of chemical-looping combustion. Chem. Eng. Sci. 56, 3101–3113.

Noorman, S., Gallucci, F., van Sint Annaland, M., Kuipers, J.A.M., 2011. A theoretical investigation of CLC in packed beds. Part 1: particle model. Chem. Eng. J. 167, 297–307.

Steinfeld, A., Larson, C., Palumbo, R., Foley Iii, M., 1996. Thermodynamic analysis of the co-production of zinc and synthesis gas using solar process heat. Energy 21, 205–222.

Wakao, N., Smith, J.M., 1962. Diffusion in catalyst pellets. Chem. Eng. Sci. 17, 825–834.

Weast, R.C., 1981. CRC Handbook of Chemistry and Physics 61st Ed 1980-1981. Chemical Rubber.

Z'Graggen, A., Haueter, P., Trommer, D., Romero, M., de Jesus, J.C., Steinfeld, A., 2006. Hydrogen production by steam-gasification of petroleum coke using concentrated solar power–II Reactor design, testing, and modeling. Int. J. Hydrogen Energy 31, 797–811.

Z'Graggen, A., Steinfeld, A., 2008. A two-phase reactor model for the steam-gasification of carbonaceous materials under concentrated thermal radiation. Chem. Eng. Process.: Process Intensification 47, 655–662.

CHAPTER 8

CONCLUSIONS & FUTURE WORKS

CHAPTER 8

8.1.Conclusions

It can be concluded that the chemical and sensible storage systems that are an integral component of CLC, are well suited to hybridising with solar thermal power systems (as explained in Chapter 2, section of 2.4.1.). The primary contribution of the thesis is the feasibility study of a Hybrid Solar Chemical Looping Combustion (Hy-Sol-CLC) process with an estimated high solar share of ~60%, in which the oxygen carrier (OC) particles in a CLC system are employed to provide thermal energy storage for concentrated solar thermal energy. The process seeks to take advantage of the key features of the CLC systems, which are the inherent potential for sensible and chemical energy storage, the potential to operate the fuel reactor at a different pressure to the heated gas stream and the higher temperature of the product gas in the air reactor than that of the solar fuel reactor. By this approach, the re-radiation heat losses from the solar receiver are also reduced relative to a system without chemical storage, because the temperature of the solar receiver is below the maximum temperature of the power cycle. The second major contribution of the thesis is the development of the fundamental understanding required for the design and operation of the direct heated solar fuel reactor of the proposed Hy-Sol-CLC. The thesis also identifies the parameters that should be considered in the selection of the appropriate fuels and oxygen carriers for the system. The following sections outline the specific conclusions drawn from the various parts of the study.

8.1.1. How the proposed Hy-Sol-CLC system is novel

Two different configurations of the Hy-Sol-CLC were proposed and investigated for the application in power generation cycles for steady base-load power generation. In the first proposed system (shown in Figure 1, Chapter 3) the fuel reactor of a conventional CLC system was replaced with a cavity solar reactor to harness the concentrated solar thermal energy efficiently. Three reservoirs were also added to a conventional CLC system to allow storage of the OC particles. In this process, regardless of the intensity of the input concentrated solar thermal energy, the flow rates of fuel and OC particle are assumed to be constant during the system operation. Simulation of the proposed Hy-Sol-CLC system was performed by Aspen Plus software and the model was validated using available data in the literature. The analysis shows that the operating temperature of the solar fuel reactor strongly depends on the intensity of the input concentrated solar thermal energy which can lead to sintering or deactivation of the OC particles, while the operating temperature of the air reactor remains constant (Figure 2 Chapter 3). It was also shown that the variable temperature of the solar fuel reactor results in increasing of the re-radiation heat losses especially at solar noon (Figure 3 Chapter 3). Furthermore, it was estimated that the process is limited to a total solar share of 6.5%, while averaged over 24 hours.

To overcome these restrictions another Hy-Sol-CLC system (Figure 1 of Chapter 4) was proposed. In this hybrid CLC system, two reservoirs were added between the air and fuel reactors of a conventional CLC system for the storage of the OC particles. An air-particle heat exchanger was also proposed to provide independent control of the temperatures of the storage reservoirs from those of air

reactors and the solar fuel reactor. In this system the operating temperature of the solar fuel reactor is kept constant by varying the flow rates of fuel and OC particles in response to variation in the incoming concentrated solar thermal energy. The calculations show that in this cycle, despite the variations in the input solar thermal energy, a constant operating temperature of the air reactor can be achieved. In addition, the solar share achieved in this cycle is ~ 60%, averaged over the 24-hour day, which was more than any proposed hybrid solar GTCC in the state-of-the-art when the research was started. The calculations also demonstrates that due to the lower temperature of solar fuel reactor in this cycle, the re-radiation heat loss from the solar cavity fuel reactor in this cycle is lower than that of the first one. In summary, the main advantages of the proposed Hy-Sol-CLC concept are:

- combining the benefits of CST and CLC systems in a unit hybrid system;
- achieving a high level of infrastructure sharing between the solar and combustion plant;
- utilising the CLC components for chemical and sensible thermal energy storage with high energy density and high exergy efficiency;
- potential to achieve cost effective power generation relative to conventional CLC and the present CST power systems.
- lower CO_2 production compared to a conventional CLC system;
- capacity to achieve continuous, despatachable power.

Since a high solar share and a better control of temperature of the OC particle were achieved with the second cycle compared with the first one, it was selected for further investigations in the next Chapters.

8.1.2. Hy-Sol-CLC power cycle efficiency

The thermal efficiency of the selected Hy-Sol-CLC system (explained in Chapter 4) as the hot gas generator in two hybrid GTCC configurations (Figure 1, Chapter 5) was assessed. In one case, the outlet from the air reactor is fed directly to a gas turbine, while in the other an after-burner, firing the natural gas, is added to increase the gas turbine inlet temperature. The calculations predict a first law efficiency of 44% for the cycle without the after-burner compared to a first law efficiency of 50% for the cycle using the after-burner. However, this higher thermal efficiency is achieved at the cost of decreasing the solar share from 60%, without the after-burner, to 41.4% with it. The calculations also demonstrated that the exergy efficiency of the cycle increases from 54.9% to 57.2% with the utilization of the after-burner (Table 2, Chapter 5). It is worth noting that the efficiency of the solar collector field has been considered in these calculations. It was also shown that incremental concentrated solar to electrical efficiency of this Hy-Sol-CLC GTCC is 39.4% with the after-burner and 35.4% without it. It is worth noting that, to the best of our knowledge, the incremental concentrated solar to electrical efficiencies achieved by this Hy-Sol-CLC system are also higher than any proposed hybrid system in the state-of-the-art.

8.1.3. Appropriate oxygen carriers for Hy-Sol-CLC

To identify the energetic performance of various combinations of fuel and oxygen carriers in the second Hy-Sol-CLC system (explained in Chapter 4), a thermal analysis of this system was also performed (Chapter 6). Three fuels namely hydrogen, carbon monoxide (as the main components of syngas) and a sample of natural gas from Mooba-Sydney and Adelaide in combination with the oxides of five metals namely Co, Cu, Fe, Mn and Ni, were assessed. The calculations showed that none of these materials allow any considerable chemical storage of solar energy for the oxidation of syngas. However, the pairs of CoO/Co, NiO/Ni and Fe_2O_3/Fe_3O_4 are potentially suitable for use in a Hy-Sol-CLC system working with natural gas. On balance, NiO/Ni pair is likely to offer the best performance for the Hy-Sol-CLC systems fed with natural gas even though a higher solar share can be achieved with the pair of Fe_2O_3/Fe_3O_4.

The energy densities of the oxidation reactions of a sample of natural gas from Mooba-Sydney and Adelaide with the oxides of Co, Cu, Fe, Mn and Ni as well as the volumetric heat capacities of these oxides and $NiAl_2O_4$, Al_2O_3, SiO_2, TiO_2 and ZrO_2, as inert materials, were also calculated. These calculations demonstrated that more thermal energy can be stored in the unit volume of these materials as chemical and/or sensible heat than those of some proposed reactions for chemical and material for sensible heat storage in the literature.

8.1.4. Appropriate solar fuel reactor for Hy-Sol-CLC

The solar fuel reactor for the proposed Hy-Sol-CLC system is the only component that is significantly different from the fuel reactor of the conventional CLC systems. It can be either heated directly or indirectly by concentrated solar thermal energy and, advantageously, is not limited to any single heating method. In the present analysis the direct heating method, using a cavity solar fuel reactor, was selected due to its high thermal efficiency relative to the indirect heating method. The specific solar cavity reactor for this Hy-Sol-CLC system has not yet been developed, therefore a uniform temperature within the cavity solar reactor was assumed for the process analysis. To provide the fundamental knowledge for the solar cavity fuel reactor, a dynamic model of an oxygen carrier exposed to high intensity solar heat flux was also developed (Chapter 7). The un-steady state model incorporated the conservation equations of mass and energy to calculate the variations in particle temperature during the conversion. The model was validated against the available numerical and experimental data available in literature (both Figure 2 a-c and Figure 3 of Chapter 7). The numerical results show that exposing the particles to high intensity solar radiation increases the particle temperature and decreases the conversion time (Figure 4 Chapter 7), relative to an OC particle within the fuel reactor of a conventional CLC system. The calculations also show that, despite the high temperature of the particle surface, convection is the dominant mechanism of particle cooling (Figure 5 of Chapter 7). This indicates that reactor designs with relatively high values of Nu and Sh numbers are likely to best limit damage to the particles due to the high solar heat flux. Therefore, none of the developed solar cavity reactors so far are the most efficient option for the

proposed Hy-Sol-CLC system and new reactor designs are required which enables a high convective heat transfer on the OC particle surface.

8.2. Recommendations for future works

8.2.1. Solar fuel reactor

The solar fuel reactor is the main component of the Hy-Sol-CLC concept that differs from conventional CLC systems. Hence, further research is required on the design and operation of efficient solar fuel reactors. Comprehensive experimental studies are needed to determine the effect of high radiation heat flux on both the thermo-physical properties of the OC particles and the gas solid reactions. The outcomes of these investigations will provide the fundamental knowledge required for the detail simulation, optimised design and operation of the pilot and finally commercial scale solar fuel reactors.

8.2.2. Assessment of the potential benefit and/or applicability of other fuels and particles

While the combination of Ni-based OC particles with natural gas has been selected from a thorough investigation of alternative options, other alternatives remain to be explored, especially the mixed oxygen carriers, metal oxides with perovskite structures and natural ores. To meet this aim the operation of the Hy-Sol-CLC system with other fuels such as heavy oil and coke are also needed to be investigated.

8.2.3. Assessment of the hybrid chemical looping combustion configurations and applicability to other chemical looping processes

The potential benefits of adapting the Hy-Sol-CLC concept to other chemical looping processes, such as Chemical Looping Reforming (CLR) of carbonaceous fuels, remain to be evaluated. For example, Ströhle *et al.*, [1] have reported a novel CLC process in which solid carbonaceous particles are directly reacted with the OC particle in a fluidised bed and then separated with a two-stage cyclone. This process has now been demonstrated at a scale of 1MW and shown to have significant potential, even though the conversion efficiency of the ileminite OC particle was only around 60%. Importantly, the reaction with the ileminite OC particle is endothermic, so that it could be adapted for the chemical storage of solar energy. Therefore, there is a need for ongoing process analysis to continue to explore further opportunities for the Hybrid Solar Chemical Looping (Hy-Sol-CL) concept.

References

[1] Ströhle J, Orth M, Epple B. Design and operation of a 1 MW_{th} chemical looping plant. Applied Energy. 2014;113:1490-5.

EMAIL ONLY: jennifer.rudd@adelaide.edu.au

WRAYS

Contact: John King
Principal/Associate: John King

16 October 2013

Adelaide Research & Innovation Pty Ltd
PO Box 149
Rundle Mall
ADELAIDE SA 5000

Attention: Ms J Rudd

Dear Jennifer

Australian Provisional Patent Application 2013903807
Adelaide Research & Innovation Pty Ltd
A Hybrid Solar and Chemical Looping Combustion System
Our ref: 251024:JHK:lt
Your ref: T0799

In accordance with your instructions, the above application and a provisional specification have been filed at the Patent Office.

Particulars of the application are as follows:-

Application Number	2013903807
Date Lodged	2 October 2013

The official filing receipt and a copy of the specification as filed are enclosed for your records.

Please read the document titled 'Procedure Relating to Patent Applications' which is also enclosed.

International Prior Art Search

An international type search can be conducted by the Australian Patent Office in respect of your invention. An international search can be useful, particularly if no prior art searches were carried out prior to filing your provisional application, as it can help identify the novel aspects of your invention. Furthermore, if you are interested in selling, licensing or otherwise commercially dealing with your invention, a favourable international search report may make your invention more attractive to investors or commercial partners.

If you are interested in requesting an international search, please provide us with your instructions as soon as possible and preferably within ten months of the filing date of your provisional application. This will ensure the Patent Office has sufficient time to issue the report in good time prior to the deadline for filing a complete application claiming the benefit of the priority date established by your provisional application.

www.wrays.com.au

PERTH
PO Box Z5466,
St Georges Terrace, Perth,
WA 6831, Australia
T: +61 8 9216 5100
F: +61 8 9216 5199
E: wrays@wrays.com.au

SYDNEY
PO Box 1445,
North Sydney,
NSW 2059, Australia
T: +61 2 8415 6500
F: +61 2 8415 6599
E: wrays@wrays.com.au

ADELAIDE
PO Box Z5466,
St Georges Terrace, Perth,
WA 6831, Australia
T: +61 8 8212 1280
F: +61 8 9216 5199
E: wrays@wrays.com.au

BRISBANE
PO Box Z5466,
St Georges Terrace, Perth,
WA 6831, Australia
T: +61 7 3123 6002
F: +61 8 9216 5199
E: wrays@wrays.com.au

The fee for attending to the filing of the request for an International Type Search (including payment of official fees) is approximately $2800.00. Accordingly, if you wish to proceed you may give us your instructions within the ten month period mentioned above. Please note that additional costs may be incurred both in obtaining documents raised during the search and in reviewing the search results.

As an alternative, Wrays have in-house search services that can conduct an international patent search at a cost starting at $1200. The total cost of such a search reviewed and reported to you will vary depending upon the nature of the invention and the number of potentially relevant records located. However, in many circumstances, our in-house search may be more comprehensive than that offered by the Patent Office due to their time and cost constraints.

Finally, it is essential that you notify us of any change of address so that we can send you reminders in relation to the deadline for filing a complete specification.

Yours sincerely
WRAYS

John King
Principal

Encl: **Official Notification**
Specification
Procedure Relating to Patent Applications

cc: craigh@wrays.com.au
simon.firth@adelaide.edu.au